Synthesis and Characterization of Functionalized *1,8*-Diaminophosphines and Perimidines of Group 10-12 Complexes and Antimicrobial Applications

by

Fezile Siphiwe Wiseman Potwana

Thesis submitted in fulfilment of the academic requirements for the degree of

Doctor of Philosophy

School of Chemistry and Physics, University of KwaZulu-Natal, Durban

As the candidate's supervisor I have approved this thesis for submission.

Prof. Werner E. van Zyl		14 June 2017
Name	Signature	Date

June 2017

Declaration 1: Plagiarism

I, Fezile Siphiwe Wiseman Potwana, declare that the experimental work described in this dissertation was carried out at the School of Chemistry of Physics, University of KwaZulu-Natal, Westville campus, between January 2013 and June 2017, under the supervision of Professor W. E. van Zyl, and that:

1. The research reported in this thesis, except where otherwise indicated, is my original research.
2. This thesis has not been submitted for any degree or examination at any other university.
3. This thesis does not contain other persons' data, pictures, graphs or other information, unless specifically acknowledged as being sourced from other persons.
4. This thesis does not contain other persons' writing, unless specifically acknowledged as being sourced from other researchers. Where other written sources have been quoted, then:
   a. Their words have been re-written but the general information attributed to them has been referenced
   b. Where their exact words have been used, then their writing has been placed in italics and inside quotation marks, and referenced.
5. This thesis does not contain texts, graphics or tables copied and pasted from the Internet, unless specifically acknowledged, and the source being detailed in the thesis and in the references sections.

Signed

_____

Fezile Siphiwe Wiseman Potwana

Declaration 2: Publications and Presentations

Papers by F.S.W Potwana to date*

1. F.S.W. Potwana and W.E. van Zyl. Diaquabis(dimethyl sulfoxide- κO)-disaccharinatocadmium. Acta Cryst, 2011, E67, m1635.
2. F.S.W. Potwana, B.E. Shandu and W.E. van Zyl. Bis(dimethyl sulfoxide-κO)bis(saccharinato-κN)zinc(II). Acta Cryst., 2011, E67, m1665.
3. F.S.W. Potwana and W.E. van Zyl. Diaquabis(dimethyl sulfoxide-κO)bis(saccharinato-κN)-cobalt(II). Acta Cryst., 2011, E67, m1667-m1668.
4. M. Varkolu, V. Moodley, F.S.W. Potwana, S. B. Jonnalagadda, W. E. van Zyl. Esterification of levulinic acid with ethanol over bio-glycerol derived carbon–sulfonic-acid. Reac Kinet Mech Cat. , 2017, 120, 69-80.

*Above papers by the author do not pertain to this thesis. Manuscripts in preparation that pertain to this PhD thesis are listed below.

5. Synthesis and Coordination Properties of $[Ag_2(\mu\text{-}X)_2\{C_{10}H_6(1,8\text{-}NHPPh_2)_2\}_2]$ [X = Cl, Br, I] and $[Ag(C_{10}H_6(1,8\text{-}NHPPh_2)_2\}_2]PF_6$ and Antimicrobial Studies. To be submitted
6. Synthesis and Coordination Properties of Bis(amino)phosphine Complexes of Type $[Cu_2(\mu\text{-}X)_2\{C_{10}H_6(1,8\text{-}NHPR_2)_2\}_2]$ [X = Cl, Br and I, R = Ph_2 and $[(CH_3)_2CH]_2$ and $[Cu\{C_{10}H_6(1,8\text{-}NHPR_2)_2\}_2]PF_6$. Formation of Type $[Cu_4(\mu_3\text{-}Cl)_2(\mu_2\text{-}Cl)_2(O\{PPh_2\}_2)_2$ and $[Cu_4(\mu_3\text{-}I)_2(\mu_2\text{-}I)_2(O\{P[CH(CH_3)_2]_2\}_2)_2]$ Complexes *via* Oxidative Ligation. To be submitted
7. Synthesis, Characterization and Coordination Properties of Oxidized $[C1_0H_6(1,8\text{-}NHPPh_2E)_2]$ (E = S, Se and O) Bis(amino)phosphines and their Ag(I) and Cu(I) Complexes in Biological Testing. To be submitted.
8. Synthesis, Structure and Characterization of Simple Perimidinyl Derivatives: A Route to a Ligand derived from pyridinyl ketones and its Ni(II), Zn(II) and Cd(II) Metal Complexes. Compounds are tested for Antimicrobial Studies. To be submitted.

Conference Proceedings

- Assisted in the 42nd National Convention of the South African Chemical Institute (SACI) Sunday, 29 November -Friday, 4 December 2015.

Signed

……

Fezile Siphiwe Wiseman Potwana

Abstract

This thesis reports on the synthesis, characterization, molecular- and crystal structures and antimicrobial studies of bis(amino)phosphine ligands and their corresponding metal complexes. Perimidine chemistry has also been developed and the coordination mode of chelating perimidine ligands derived from *1,8*-diaminophosphines are presented.

Five bis(amino)phosphine ligands of the type $[C_{10}H_6(1,8\text{-}NHPR_2)_2]$ (R = Ph **(1)** and $(CH_3)_2(CH)_2$ **(2)**), $[C_{10}H_6(1,8\text{-}NHPPh_2E)_2]$ (E = O **(14)** and S **(15)**) and $[C_{10}H_6(1\text{-}NHPPh_2O)(8\text{-}NHPPh_2Se)]$ **(16)** were prepared by reacting *1,8*-diaminonaphthalene with chloro-phosphines in the presence of 4-dimethylaminopyridine as a catalyst in tetrahydrofuran. The ligand analysis are in agreement with the spectroscopic results and the percentage yields are in the range 50-75 %. The ^{31}P NMR spectra of the ligands showed a singlet peak in the range 23.5-57.7 ppm. Ligand **(16)** showed two ^{31}P NMR peaks which indicated that the P-donor atoms of the compound are not chemically equivalent because one P-donor atom is bonded to the Se-donor atom and the other P-donor atom is bonded to the O-donor atom. The IR spectra of the ligands showed that the ν(P-N) vibrational band occurred in the range 891-835 cm^{-1}. Ligands **(14)** and **(15)** were isolated by a single crystal X-ray crystallography. The ligands crystallized in the monoclinic system with a space group of $P2_1$ and $P2_1/n$. The DFT MO diagram and crystallography showed that the N-donor atoms in **(15)** and **(16)** possessed a pyramidalization phenomenon. The UV-Vis spectra indicated that the two absorption bands in the range ~230-318 nm were due to the intraligand $L \rightarrow L^*$ transitions. Thermogravimetric analysis showed the solid compounds were stable at room temperature and steadily decomposed in a temperature range of ~315-~520 °C.

Treatment of bis(amino)phosphine ligands with Cu(I) and Ag(I) halides resulted in several d^{10} coinage-metal complexes that was isolated and characterized. Complexes **(3-6)**, **(10)** and **(11)** of the type $[M_2(\mu\text{-}X)_2\{C_{10}H_6(1,8\text{-}NHPR_2)_2\}_2]$, where M = Cu(I) and Ag(I), respectively, were synthesized from ligands **(1)**, except **(6)** which was prepared form **(2)**. The halides bridging the two Cu(I) species were [X = Cl **(3)**, Br **(4)**, I **(5)**, Cl **(6)**, Cl **(10)** and Br **(11)**]. Complex **(12)** is a step cubane complex of the type $[Ag_4(\mu_3\text{-}I)_2(\mu_2\text{-}I)_2\{C_{10}H_6(1,8\text{-}NHPPh_2)_2\}_2]$. Complexes **(7)** and **(13)** of the type $[M\{C_{10}H_6(1,8\text{-}NHPPh_2)_2\}_2]PF_6$, where M = Cu(I) and Ag(I), respectively, were prepared from ligand **(1)** and $[M(CH_3CN)_4]PF_6$ (M = Cu(I) or Ag(I)), respectively. Reactions of ligands **(14)** and **(15)** with Ag(I) or Cu(I) salts produced complexes of the type $[M\{C_{10}H_6(1,8\text{-}NHPPh_2E)_2\}_2]X$. Ligand **(14)** produced complexes **(19)**-**(22)** and ligand **(15)**

produced complexes **(17)** and **(18)**. The isolation of these complexes was enabled by covalently linking kinetically labile P-N bonds from the bis(amino)phosphine ligands. The percentage yields of the complexes were in the range (20-45 %). Reactions of complexes **(3)** and an iodide analogue of **(6)** produced complexes **(8)** and **(9)** of the type $[Cu_4(\mu_3\text{-}X)_2(\mu_2\text{-}X)_2(O\{PR_2\}_2)_2]$ in 68.6 and 82.5 % yield, respectively. The ^{31}P NMR for Cu(I) complexes showed a singlet peak in the range 23.9-59.2 ppm which indicated that the P-donor atoms of the complexes are chemical equivalent. The ^{31}P NMR for Ag(I) complexes showed two doublets in the ranges of 40.1-39.9 and 37.1-36.9 for **(10)**, 35.4-35.2 and 38.4-38.2 for **(11)** and 34.4-34.2 and 31.7-31.5 for **(12)** ppm. The naturally occurring isotopes of silver (^{107}Ag, 51.82 % and ^{109}Ag, 48.18 %) both have a nuclear spin $I = ½$ and although their magnetogyric ratios are similar in magnitude ($\sim 10^7$ rad $T^{-1}s^{-1}$) $\{\gamma(^{109}Ag)/\gamma(^{107}Ag) = 1.15\}$ the scalar coupling is proportional to the gyromagnetic ratio of the nuclei, and the number for ^{109}Ag and ^{107}Ag is *different*, and this explains the origin of the two doublets. The copper(I) counterparts, complexes **(17)**, **(19-22)** only showed a singlet peak in the ^{31}P NMR spectrum, respectively. The ^{31}P NMR of complexes **(17)** and **(19)** showed singlets at 58.3 and 29.3 ppm, respectively. The ^{31}P NMR spectrum of complex **(18)** showed two peaks of the P-donor atoms which suggested that these were not chemically equivalent in solution. The absorption bands for the following functional groups ν(NH), ν(C=C), ν(P-N), ν(P=S), ν(P=O), ν(Ag-S), ν(Ag-O), ν(Cu-O), ν(Cu-P) and (Ag-P) were in the range 3057-3371, 1645-1413, 817-872, 687-598, 691-690, 514-500, 540-518, 519-410, 515-473 and 543-522 cm^{-1}, respectively. Complexes **(3-6)**, **(8)**, **(9)**, **(10-12)**, **(17)** and **(18)** were isolated and characterized, by single crystal X-ray crystallography. The single crystal X-ray structures of **(3-6)**, **(10-12)** and **(17)** contained a rhombus $\{M_2(\mu\text{-}X)_2\}$ core unit bridged by halogens and chelated by two bis(amino)phosphine ligands which coordinated *via* the P-donor atoms, except for complex **(17)** where the Ag(I) metal centers were bridged by S-donor atoms of the ligands. Complex **(17)** was coordinated to four S-donor atoms forming a Ag(I) complex balanced by a triflate counter ion. The single crystal X-ray structures showed that the bis(amino)phosphine ligands contained P- and N- donor atoms and the metal center where bonded *via* the P-donor atoms.

The UV-Vis spectra of complexes suggested that the π-π* transition arises due to the naphthalene moiety in the complexes. Thermogravimetric analysis showed that the complexes were stable at room temperature and steadily decomposed in a range ~150-350 °C and finally reached their residual peaks in a temperature range ~480 - ~600 °C.

This thesis further reports on the perimidine compounds which were isolated and characterized by single crystal X-ray crystallography and other spectroscopic analysis such as NMR, FTIR and MS. Perimidine compounds of formula $[C_{10}H_6(1,8\text{-}NH)_2(CH_3)\{(CH_2)_2CH_3\}]$ $[C_{10}H_6(1,8\text{-}NH)_2(CH_2CH_3)_2]$, $[C_{10}H_6(1,8\text{-}NH)_2(CH_3)(CH_2CH_3)]$, $[C_{10}H_6(1,8\text{-}NH)_2(CH_3)\{CH(CH_3)_2\}]$, $[C_{10}H_6(1,8\text{-}NH)_2(CH_3)\{(CH_2)_4CH_3\}]$, $[C_{10}H_6(1,8\text{-}NH)_2(CH_3)\{CH_2CH(CH_3)_2\}_2]$, $[C_{10}H_6(1,8\text{-}NH)_2{\cdot}Fe(C_5H_4)_2\{COCH_3\}_2]$, and $[C_{10}H_6(1,8\text{-}NH)_2(CH_3)(C_5H_4N)]$, **(23)-(30)** were prepared by a condensation reaction of *1,8*-diaminonaphthalene and the corresponding alkyl and aryl ketones in satisfactory yield of 85-99 %. The ^{1}H NMR spectra of compounds showed that the proton peaks of the naphthalene were shifted downfield (8.70-6.50 ppm) while the methyl protons of the compounds were shifted further upfield (2.07-0.85 ppm). The IR spectra of compounds showed that the ν(NH) and ν(C=C) absorption bands occurred in the range 3388-3295 and 1702-1406 cm^{-1}, respectively. Compounds **(25)** and **(26)** were characterized by single crystal X-ray crystallography. The UV-Vis spectra showed that the σ-electron rich six membered heterocyclic perimidine ring resulted in π···π* transitions and the molecular spectra also showed that the compounds contained unsaturated naphthalene moieties with shoulders due to ligand centered (LC) π···π*transitions. Thermogravimetric analysis showed that the compounds decomposed at ~310 °C.

Isolated compound **(30)** led to the synthesis of complexes $[Ni(H_2O)_2\{C_{10}H_6(1,8\text{-}NH)_2(CH_3)(C_5H_4N)\}_2]2Cl$, **(31)** which was isolated in 88.6% yield. Complexes $[ZnCl_2\{C_{10}H_6(1,8\text{-}NH)_2(CH_3)(C_5H_4N)\}_2]$ and $[CdI_2\{C_{10}H_6(1,8\text{-}NH)_2(CH_3)(C_5C_4N)\}_2]$, **(32)** and **(33)** were prepared similar to **(31)** from **(30)** using $ZnCl_2$ and CdI_2, respectively, in good yields of 89.95% **(32)** and 71.91 % **(33)**. The ^{1}H NMR for complex **(31)** was paramagnetic whereas, complexes **(32)-(33)** spectra were well resolved. The IR vibration bands were indicated by ν(M-N) at 401-424 cm^{-1}. Compound **(29)** was an attempt to synthesise a ferrocenyl perimidine compound by treating *1,8*-diaminonaphthalene with 1,1′-diacetylferrocene, but instead a co-crystallization of the two starting compounds was produced. To extract information on electron density of the molecular frontier orbitals of the complexes, a DFT study was done. It was found that the HOMO and LUMO are localized around the naphthalene and that there is no electronic communication between the metals and the naphthalenes.

Finally, this study used synthetic compounds as analogues to imitate signal molecules that are potential sources of new drugs that exhibit antimicrobial activity *via* membrane disruption. Compounds **(1)-(33)** were tested against the sensitive and resistant Gram-positive and Gram-negative bacteria, i.e. Gram-positive (sensitive *S .aureus* ATCC 29213 and Methicillin-

resistant S. aureus ATCC 43300) and Gram-negative (sensitive *E. coli* and QC organism ATCC 25922, B-lactam resistant *E. coli* ATCC 35218 and multidrug resistant *P. aeruginosa*). A few of the compounds reduced the microbial activities against Gram negative bacteria and the compounds effectively reduced most of Gram-positive bacteria. The compounds showed promising quorum sensing activities.

Acknowledgements

I would like to acknowledge that this thesis wouldn't have been possible without the will of God. God is everything. Thank You Father. The support that comes from family with love and understand is a pillar and one's strength. I would like to thank both my parents and siblings for everything. Knowledge is power and it can be passed on from generations to generations to empower the world. I would like to thank Professor Werner van Zyl for his guidance and research knowledge through my postgraduate studies, i.e. MSc and PhD. Conducive environment for studying produces better results by simply saying that, I would like to acknowledge the School of Chemistry and Physics at UKZN for providing a good working habitation. A laboratory without colleagues is as dead as not getting results in the lab in due time. I would to thank the friends and colleagues in WvZ's and Bala's groups. We have faced manageable and difficult challenges and yet we still stand. Without funding research is impossible and painful. I would like to give thanks to National Research Foundation (NRF) for their financial support. Collaboration is a form of developing everlasting friendship and relationship with other scientists in the world. For crystal structure elucidations, I acknowledge the help from either Dr Richard J. Staples at the Center of Crystallographic for Research at Michigan State University, or Dr Bernard Owaga and Mr Sizwe Zamisa at UKZN School of Chemistry and Physics I would also like to thank Dr. H. Chania and her students for their insight knowledge of micro-organisms. This sincere gratitude goes out to everyone who have made my time so enjoyable at the University of Kwa-Zulu-Natal and everyone that I probable forgot to mention in the list above. Thank you everybody so much. God bless you all.

Dedications and Quotes

I am dedicating my work to my family at large and everyone who stood by me in my entire life.

"Everything of importance has been said by someone who didn't invert it."

Alfred North Whitehead

“Knowledge is Power”

List of Abbreviations and Symbols

XRD	X-ray diffractometry
ORTEP	Oak Ridge Thermal Ellipsoid Plot Program
Å	Ångström
° (deg)	degrees
°C	degrees Celsius
K	Kelvin
λ (nm)	wavelength in nanometer
α	alpha
β	beta
γ	gamma
σ	sigma
π	Pi
esd's	estimate standard derivations
^{1}H NMR	proton nuclear magnetic resonance
^{13}C NMR	carbon nuclear magnetic resonance
^{31}P NMR	phosphorus nuclear magnetic resonance
$CDCl_3$	deuterated chloroform
DMSO-d_6	dimethyl sulfoxide-d_6
TMS/ $SiMe_4$	tetramethylsilane
δ (ppm)	chemical shift in parts per million
MHz	megahertz
t	triplet
d	doublet
dd	doublet of doublets
q	quartet
s	singlet
m	multiplet
J	coupling constant

br	broad
naph-H	naphthalene protons
phenyl-H	phenyl protons
Cp	cyclopentadienyl
FTIR-ATR	Fourier Transform Infrared- Attenuated Total Reflectance
ν (cm^{-1})	wavenumbers in per centimetre
UV-Vis	ultraviolet-visible spectrophotometer
TGA	thermal gravimetric analysis
$[M(CH_3CN)_4]PF_6$	tetrakis(acetonitrile)metal(I) hexafluorophosphate
M(I)	metal(I)
L	ligand
DMSO	dimethyl sulfoxide
THF	tetrahydrofurane
DCM/ CH_2Cl_2	dichloromethane
Et_2O	diethyl ether
DMF	dimethylformamide
OTF	triflate ion ($CF_3SO_3^-$)
mL	millilitre
r.t.	room temperature
min. or hr(s)	minutes or hour(s)
Ph	Phenyl
Et_3N	triethylamine
^{i}Pr	*iso*-propyl
MW	molecular weight
m.p.	melting point
equiv.	equivalent
E.A.	elemental analysis
calcd. E.A.	calculated elemental analysis
g or mg	gram or milligram
mol or mmol	mole or millimole

(%)	percentage
vs.	versus
MS	mass spectrometry
ESI (m/z)	electrospray ionisation in mass-to-charge ratio
DFT	Density Functional Theory
MO	molecular orbital
HOMO	highest occupied molecular orbital
LUMO	lowest unoccupied molecular orbital
E	Energy

List of Compounds

Scientific nomenclature in the field of chemistry can sometimes be confusing, and the list below is hoped to provide a direct and quick guide to the 33 new compound prepared in this thesis. Ligands, complexes and compounds will be annotated in bold numbers for clarity and simplicity; the same numbering scheme was used throughout the thesis.

1) Bis(amino)phosphines

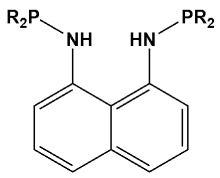

R = Ph (1)
R = $[(CH_3)_2CH]_2$ (2)

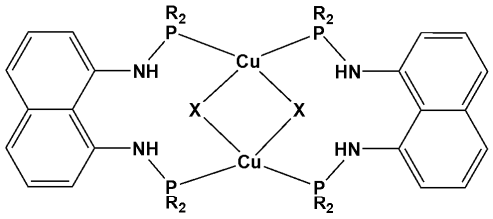

R = Ph, X = Cl (3)
R = Ph, X = Br (4)
R = Ph, X = Br (4*)
R = Ph, X = I (5)
R = $[(CH_3)_2CH]_2$, X = Cl (6)

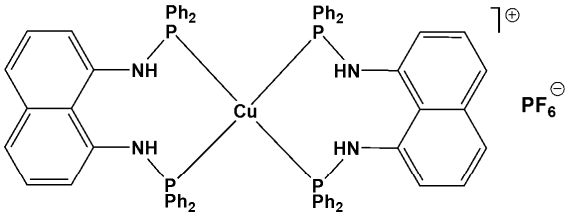

(7)

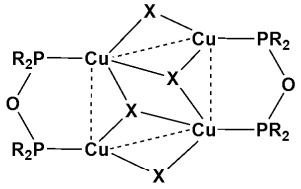

R = Ph, X = Cl (8)
R = $[(CH_3)_2CH]_2$, X = I (9)

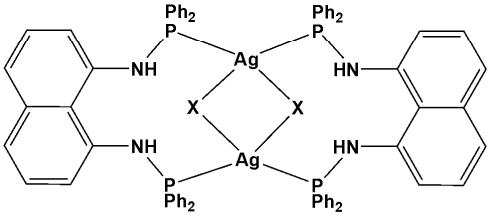

X = Cl (10)
X = Br (11)

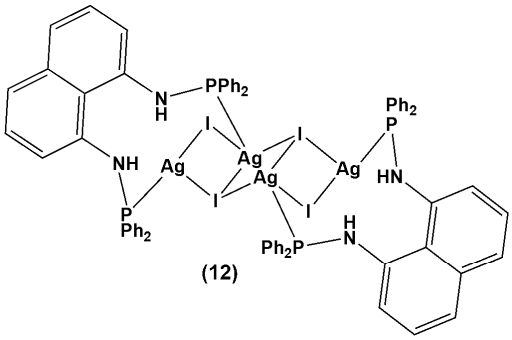

(12)

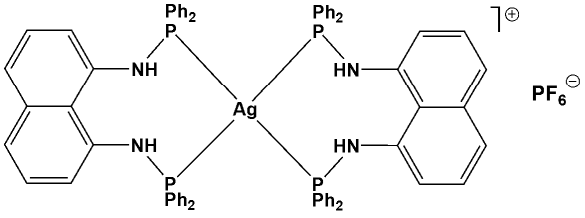

(13)

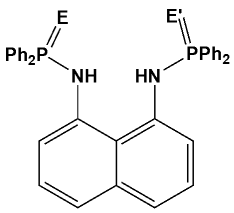

E = E' = O (14)
E = E' = S (15)
E = O, E' = Se (16)

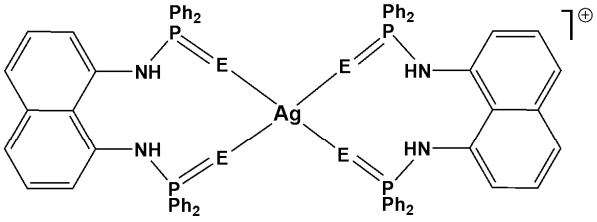

E = S (17)
E = O (19)

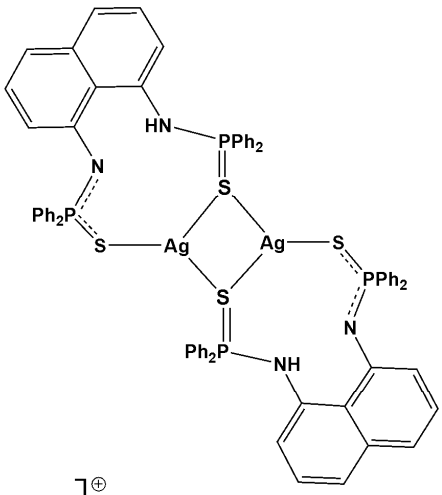

(18)

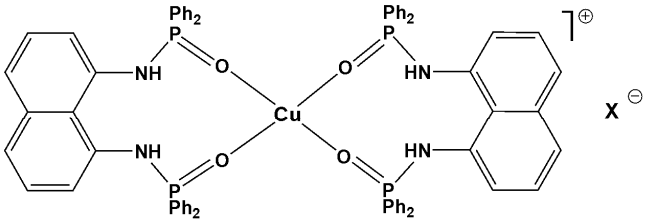

X = Cl (20)
X = Br (21)
X = I (22)

2) Perimidines

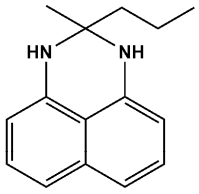

(23)

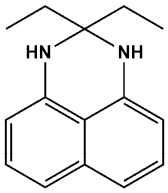

(24)

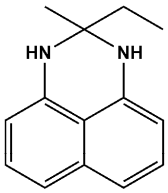

(25)

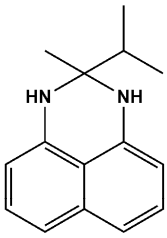

(26)

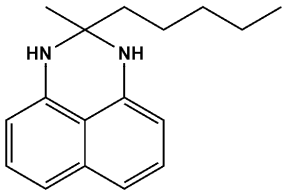

(27)

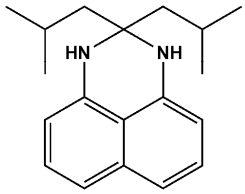

(28)

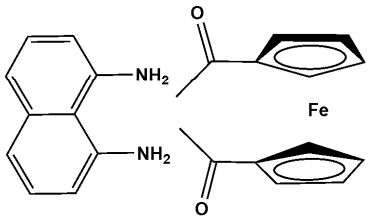

(29)

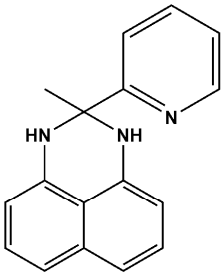

(30) and (30*)

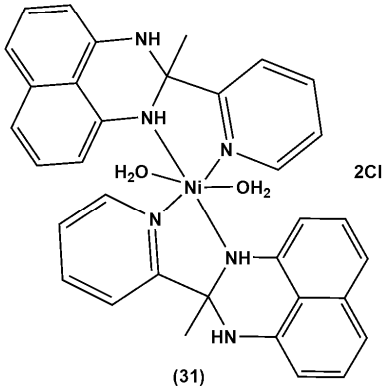

(31)

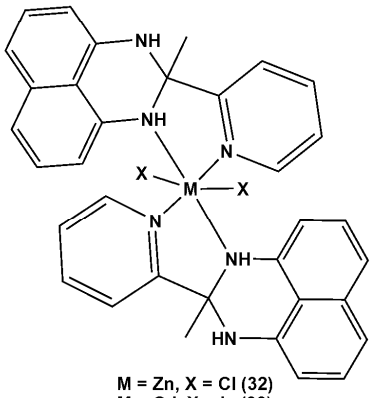

M = Zn, X = Cl (32)
M = Cd, X = I (33)

Table of Contents

Chapter 2 Experimental

List of Figures

List of Schemes

List of Tables

Chapter 1

Introduction

1.1 Chemistry of Naphthalene and Aminophosphines

1.1.1 Nomenclature and Structural Geometry of Naphthalene

Naphthalene and its derivatives are an interesting group of molecules which have been studied extensively due to their structural geometry and the ability to form suitable ligands to study the stability of metal centers.[1] Naphthalene is a polycyclic aromatic hydrocarbon (PAH) compound that was initially isolated from coal tar.[2] The crystal structure shows that it has a backbone structure that is planar and strongly rigid. The structural geometry of the molecule allows for up to eight substituents, i.e. from positions 1 to 8.[3]

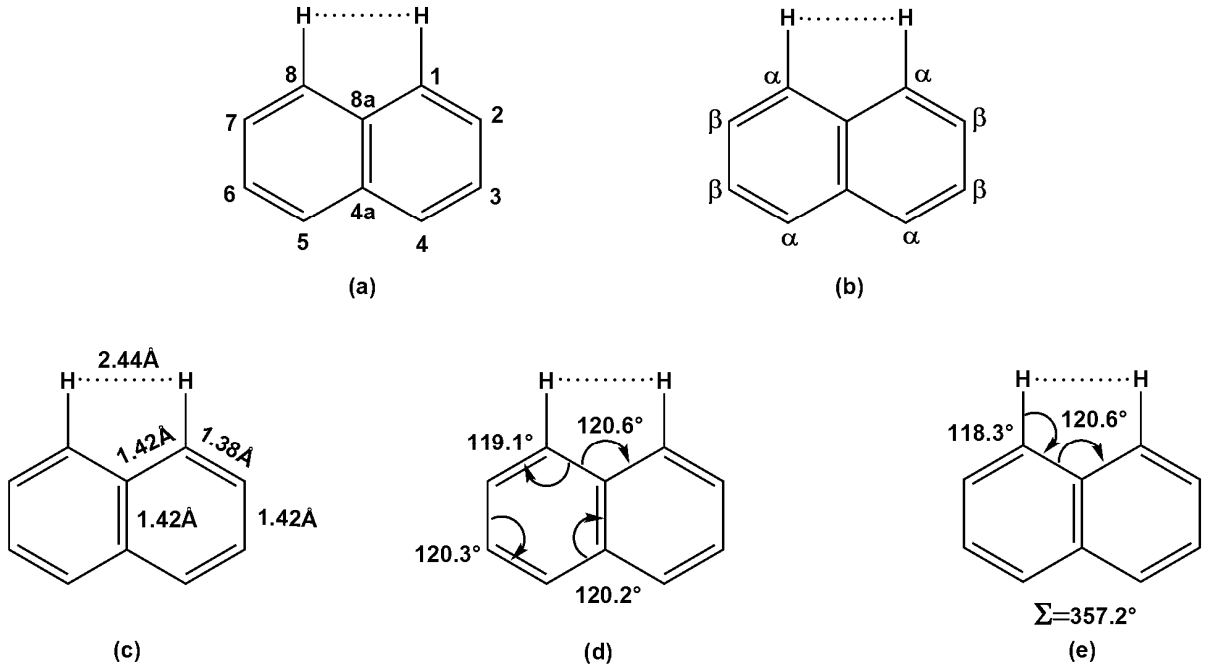

Figure 1.1.1.1. The planar and rigid geometrical structure of naphthalene. Operational numbering system of its nucleus (a). The alpha (α) and beta (β) nomenclature used to distinguish positions 1 and 2 (b). Shows approximate bond lengths and angles (c), (d) and (e).[4]

The alpha (**α**) and beta (**β**) nomenclature that distinguish positions 1 and 2 of molecular naphthalene, is still operational, see Figure 1.1.1.1 **(b)**. Naphthalene seems to resemble two

benzene rings that are fused together, but surprisingly that is not the case because naphthalene has different bond lengths and angles.[4] The structural data of benzene reveals that (**C**$_1$)-(**C**$_6$) have the same bond distance of 1.40 Å and bond angle of 120.0°, whereas naphthalene structural data shows that bond length between (**C**$_1$)-(**C**$_2$) range at 1.36 to 1.38 Å making them shorter than those existing between (**C**$_2$)-(**C**$_3$) which range at 1.41 to 1.42 Å. The structural differences in naphthalene bond lengths are due to the uneven distribution of the π-electron density which appears to be high between (**C**$_1$)-(**C**$_2$). The distance between substituents attached at the positions (**C**$_1$) and (**C**$_8$) or (**C**$_4$) and (**C**$_5$) is shorter with a range of 2.44 to 2.50 Å as opposed to the distance between substituents in positions (**C**$_1$) and (**C**$_2$) which is 3.01 Å apart. The close proximity between (**C**$_1$) and (**C**$_8$) or (**C**$_4$) and (**C**$_5$) is often referred to *peri*-positions which give rise to several unique structural properties of the *peri*-substituted naphthalenes.[3] The name "*peri*" is derived from Greek which means "near".[3, 5] It is reasonable to assume that any molecule or atoms larger than hydrogen in the *peri*-position will give rise to steric hindrance and therefore distortion will arise in the molecular structures of the common backbone and hence this affects the non-bonding atom distances, see Figure 1.1.1.2.

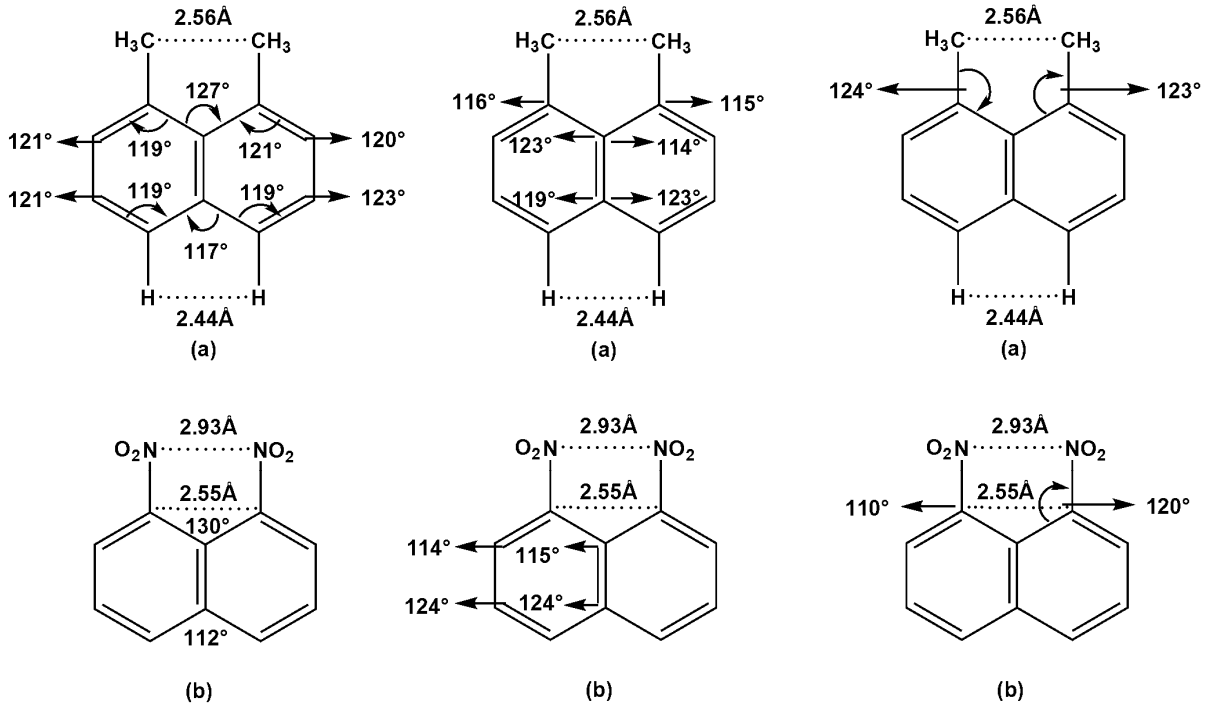

Figure 1.1.1.2. *peri*-Substituted positions show distortion pattern in a planarity of naphthalene backbone. The distorted structure of dimethylnaphthalene (a). The distorted structure of *1,8*-dinitronaphthalene (b).[4]

1.1.2 "*Peri*-Substituted", Distortion and Strain Relief of the Naphthalene Backbone

Over the years chemists have been fascinated by the *peri*-interaction of the position **C**$_{1}$- and **C**$_{8}$-disubstituted naphthalene because of the tunable physical and chemical properties of the compound. The substituted naphthalene on these positions is important in ligand synthesis for metal complexation.[6] Chemists have successfully synthesized the steric hindered *peri*-disubstituted naphthalene derivatives with a "*peri*-substituted proximity effect".[7] This causes distortion in the compounds, see Figure 1.1.1.2, for the non-bonding substituents distances. This is caused by substitution of the hydrogen atoms in the *peri*-position by the atoms which are larger, thus forcing the substituents in the naphthalene molecule to be in closer proximity than any other observed substrate.[4] When the substituents are halides or chalcogens in the *peri*-positions, the distance caused by repulsion tend to be great due to the electronic properties of the atoms.[8] The atoms are in close contact, and in fact gets closer than the sum of their van der Waals radii and therefore cause special interactions such as attractive or repulsive depending on the nature of the atoms of the substituents present in the molecule.[9, 10]. The "Proximity effect" have been observed from the crystallographic data and it has been influenced by the i) intramolecular interaction of the molecular atoms in the *peri*-positions as a result of closeness of the spatial atoms, and ii) repulsive or attraction effect which emerges as a result of steric crowding and weak or strong bonding effect of the substituent.[11-14] The reason the sterically crowded *peri*-substituted compound can be synthesised lies in the intramolecular and transannular interaction which occurs in the compounds.[4] This feature could be observed in 1,4,5,8-tetra(CN) known as (CN-46) where the atoms are placed slightly above and below the plane of the rigid naphthalene.[5] Hence, this results in the distortion of the compound, see Figure 1.1.1.1**(e)**. The transannular intramolecular interaction can be observed when determining the *peri*-length of the substituents which serves as the primary parameter, see Figure 1.1.1.3.

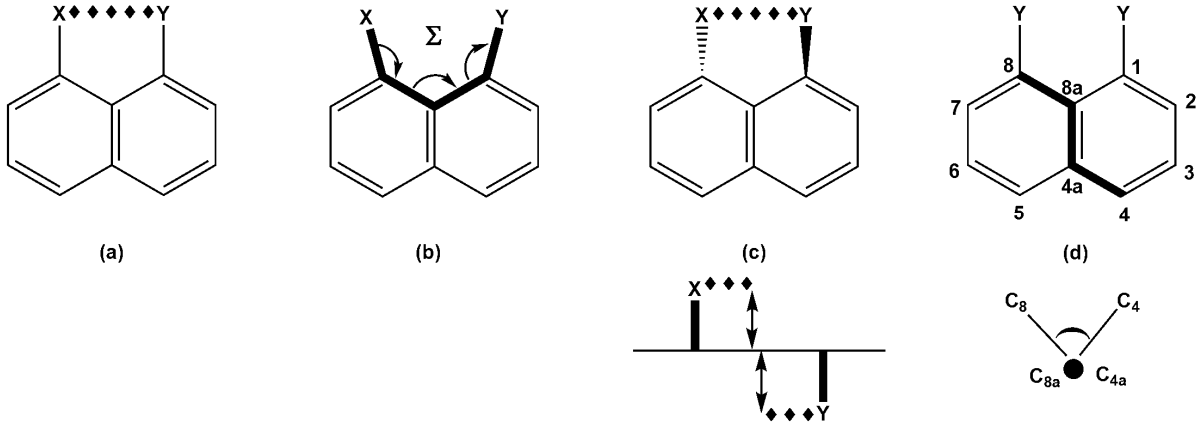

Figure 1.1.1.3. Diagram shows distortion measurements for a steric interaction in an ideal naphthalene molecule. The *peri*-position length interaction in an ideal system (a). The total sum of the bay region angles (i.e. a concave exterior region on some polycyclic aromatic hydrocarbons that have two or three phenyl rings in a non-linear arrangement) in an outward splay (b). The distance of the *peri*-atoms from the rigid plane of naphthalene in an in-plane distortion (c). The torsion angles around bent bonds of C8 to C4 (d).[15]

These parameters are obtained from the evaluation of the quantity of the in-plane, out-of-plane distortions and bulking of the naphthalene backbone that is compared with the authentic naphthalene structural geometry.[8] By determining the splay angle will help to deduce the in-plane distortion values and hence the bulking strain can be determined by calculating the torsion angles of the naphthalene ring system.

The torsion angle of naphthalene is either 0° or 180° which suggest that the molecule lies flat/planar and the splay angle of the normal naphthalene compound is 357.2° in total, see Figure 1.1.1.4 and Figure 1.1.1.1**(e)** for the splay angle.[1, 8, 16, 17]

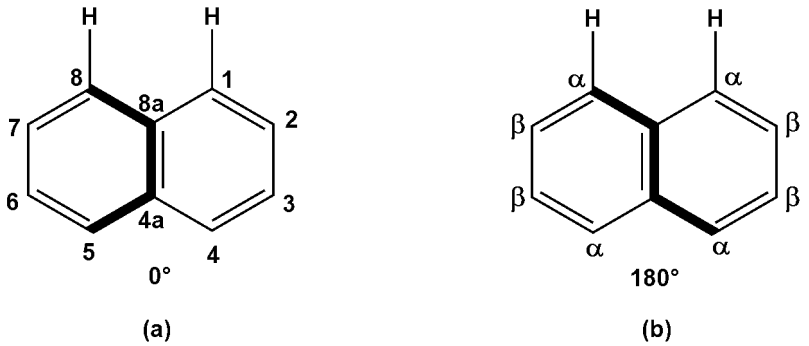

Figure 1.1.1.4. The torsion angles of naphthalene. The torsion angle of 0° passing through bold line of C8 to C5, (a). The torsion angle of 180° passing through bold line of Cα to Cα, (b).[18]

The un-substituted naphthalene backbone certainly prefer to be planar, rigid and undistorted. Substituents in the *peri*-position bring about steric contact 'interaction' which cause steric strains in the molecule. The resonance energy of the compound will be affected as there will be competition between the two rings and this will result in the naphthalene molecule continuing to distort in order to relieve/decrease the strain contacts. There will be an instability in the resonance structure of the naphthalene so that the energy could be lower in order to keep the molecule planar and to lower the distorting effects while the *peri*-disubstituted substituents molecules are being accommodated. The steric strain caused by these bulky substituents can be overcome by (**a**) stretching of the *peri*-substituents bond, (**b**) in-plane and (**c**) out-of-plane deflections of the substituents, and (**d**) distortion or bulking of the naphthalene itself. Amongst the four modes mentioned, the lengthening/stretching of a bond is reasonable due to the fact that even a minimum bond change is affected by enormous energy. The remaining three modes are used to describe the overcrowded organic molecules. The four modes of strain relief are used only to define and give a better understanding of the steric hindrance of naphthalene.
There are cases where more than one mode of strain relief are operational to remove the minimize disorder called "decentralization of the steric strain" or the "distribution of deformation over many coordinates".[4]

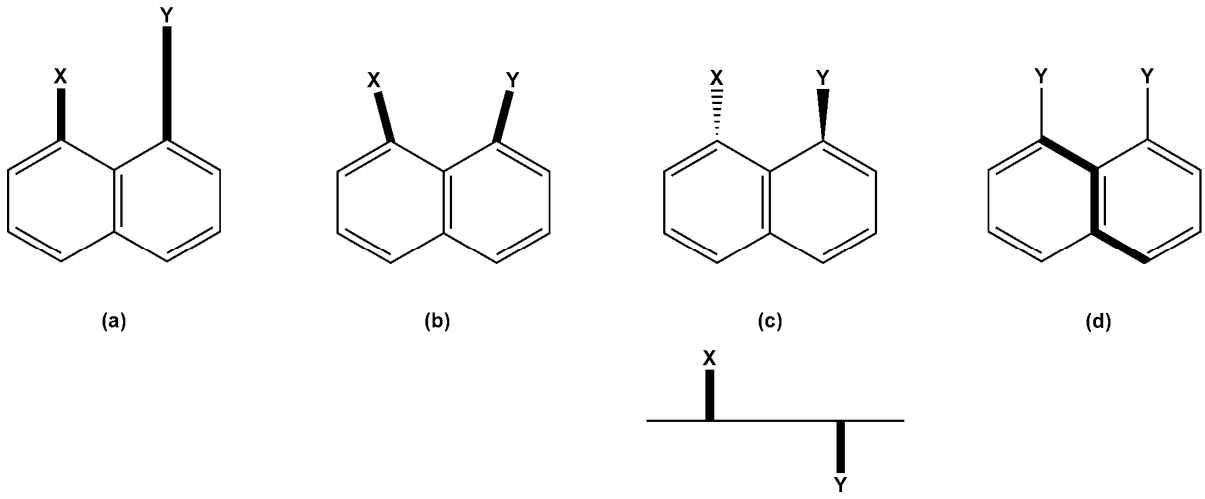

Figure 1.1.1.5. Illustration of bond stretching to relieve the steric strain (a), in-plane distortion (b), and out-of-plane distortion (c) and buckling and bent of the rigid naphthalene plane (d). [4]

Bond stretching in Figure 1.1.1.5**(a)** illustrate the relief of the steric strain as a result of overcoming the energy barrier for the bond to occur. Many compounds have been reported where this behaviour is observable, but those shown by C-Se are interesting as they provide a

means to explain the occurrence.[19] The compound [(Se_2naph)Pt(PPh_3)$_2$] is an example where all four modes of distortion can occur.[18]

The common strain relief in the *peri*-disubstituted naphthalene are those experienced in-plane **5(b)** and out-of-plane **5(c)** when the distortion of the compound causes the exocyclic bonds of naphthalene to deviate from the naphthalene rings to out-of-plane. This occurs due to a lot of energy that is used and then in relatively large strain relief, minimal molecular distortion will occur. During the whole process, there will be a loss in resonance energy due to naphthalene distortion and the deviation of the substituents in the *peri*-position will be affected, resulting in substituents to move out of the plane and therefore decreasing the energy of the steric hindered. The molecule will relieve its strains and the planar aromaticity of the naphthalene will be maintained.

Understanding the meaning of the in-plane and out-of-plane will help to view the structure in a more simplified manner. The measurement determined on the angles around the *peri*-positions **C_1** and **C_8** are used to explain the in-plane defects of the *peri*-substituents of the naphthalene compound. The ideal angle of 120° trigonal planar is taken as a reference point to determine the angle of distortion of the *peri*-disubstituted naphthalene, see Figure 1.1.1.1.[4] The hydrogen placed at the *peri*-position of the normal naphthalene translate to the following angles around **C_1** and **C_8**: (**a**) outer angle 121.0(1)°, (**b**) inner angle is 118.3(1)° and (**c**) 120.6(1)° inside the naphthalene ring system, see Figure 1.1.1.2**(a)** and **(b)**.

Crystallographic evidence has shown on many occasions that the calculated measurement that are used to evaluate the deviation of the substituent around the most suitable naphthalene plane, and that gives a better understanding about the out-of-plane deflection.[20]

The strain relief mentioned herein are in support of the distortion about the naphthalene ring. The evidence stated are in support of the resonance energy taking place in the structure in stabilizing the backbone of the naphthalene. The central bridging carbons get distorted when the *peri*-substituent try to relief strain and affect the naphthalene backbone, which is used to determine and compare the torsion angles of the central bridging carbon with the ideal naphthalene plane of which the angles can either be 0° or 180°.[18, 21, 22]

1.1.3 Physical and Chemical Reactivity: Aromaticity *vs*. Naphthalene

Naphthalene derivatives are electron rich compounds due to the delocalization of electrons within the rings. When derivatised by halogens, especially chlorine, to form polychlorinated products they become a hazard both in a direct and indirect way on the global environmental.[23] The similarities in the electronic structure of naphthalene and benzene help to make a comparative study of the two molecules. Aromaticity of naphthalene and its derivatives should be mentioned because there is a distinct difference between the benzene ring and two or more fused rings joint together by two C-C bonds. This is where the theoretical and experimental aspect to define aromaticity resides, besides giving a definition of aromaticity in cyclic and polycyclic aromatic compounds. Previously, when the term aromaticity was mentioned one would consider only benzene because of its richness in π-electron delocalization. Naphthalene and its derivatives are also electron rich compounds due to the delocalization of electron within the rings, but π-electron system delocalization become more complicated in defining this molecule. Benzene is an example of aromatic molecule because its delocalization of π-electron is complete and for this reason it undergoes electrophilic substitution reactions similar to naphthalene and anthracene. These compounds have resonance structure which stabilizes the molecule so that they undergo nucleophilic substitution reactions to extend their conjugations, rather than addition reaction. Crystallographic data have revealed that benzene has the same bond length around the ring i.e. **C_1-C_6** but that naphthalene bond length is not the same, i.e. **C_1-C_2**, **C_3-C_4**, **C_5-C_6**, **C_7-C_8** bond distance is 1.36 Å (136 pm) and the remaining bonds length of the **C-C** within the structure is 1.42 Å (142 pm).[1, 16, 24] This translate to the fact that naphthalene delocalizes electrons within the two rings in three resonance structures, as shown below. The structures also show that **C_1-C_2**, **C_3-C_4**, **C_5-C_6**, **C_7-C_8** bonds occurs twice in the two of the three resonating structures, see Figure 1.1.1.6.

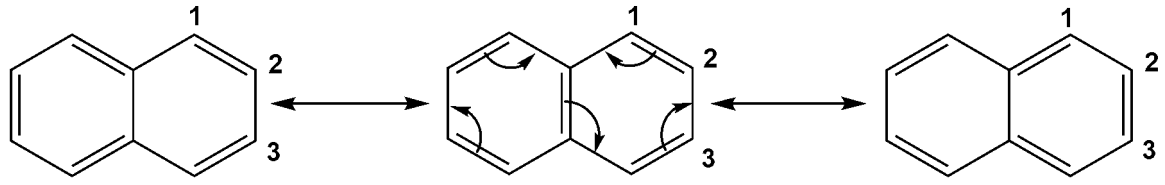

Figure 1.1.1.6. The three resonance structures of naphthalene, 10π-electron annulenes.

The defined resonance energy of naphthalene (255 kJ mol^{-1}) is not twice that of benzene (150 kJ mol^{-1}), but it is lower by 46 kJ mol^{-1}. The energy referred to herein is the energy difference

between hypothetical naphthalene with delocalized π-bonds and real benzene delocalized π-bonds, i.e. (301 kJ mol^{-1}). In the process of the reaction, naphthalene will lose aromaticity in one of its rings during the rate determining step, but will continue having one intact benzenoid ring. Naphthalene has an activation energy of (104 kJ mol^{-1}) as compared to benzene (150 kJ mol^{-1}) for the rate determining step. Naphthalene is more reactive compared to benzene because it undergoes electrophilic aromatic substitution, oxidation and reduction reactions under milder conditions than benzene. The alpha (**α**) positions in the naphthalene molecule are more susceptible to radical attacks and nucleophilic substitutions compared to beta (**β**) positions.[3]

1.1.4 Comparisons between Theoretical and Experimental Aromaticity Studies

Hückel developed a theoretical model to predict the aromatic and non-aromatic annulenes. He stated that if the number of the π-electrons in a cyclic system is equal to (4N+2), where N represent a whole number integer, then the system is aromatic. For anti-aromatic systems to exist the number of π-electrons in a cyclic system is equal to 4N, where N is a whole number integer.[25] His condition strictly stated that if the aromatic molecule is examined, it must meet a criteria that it must have a continuous rings of overlapping p-orbitals which are arranged in a planar or almost planar manner. In the Hückel resonance energy rule, the delocalization energies are equivalent to resonance energies which help stabilize the molecule. The rule has limitations as it accounts for the energy of electrons delocalized, rather than the cyclic electron bonds delocalization of the whole system.[26] To deal with this issue, the aromaticity of benzene, to which all aromatic compounds are related, needs to be revisited. Extension of the Hückel theory to PAH is difficult because rule would lead to the conclusion that fluoranthene and pyrene should be an antiaromatic compounds, which would differ from their known chemical properties. A possible solution for this problem is the evaluation of the PAH as conjugated cyclic polyenes which are internally linked and/or cross-linked to other cyclic polyenes (fluoranthene) or double bond (pyrenes).[27]

Furthermore, the study was succeeded by Dewar and his principle of defining resonance energy (DRE) making a brilliant distinction between aromatic, nonaromatic, and anti-aromatic conjugated molecules where the DRE is positive for an aromatic compound, negative for anti-aromatic compounds, and zero (within 4 and 8 kJ mol^{-1}) for a non-aromatic compound. This different view is achieved by the use of double and single bonds energies in the molecule

appropriate to non-aromatic systems (rather than those for a non-conjugated system) in a reference structural system.

According to Dewar, aromaticity means a cyclic π-electron delocalization which reduces cyclic bond energies resulting in the stability of the molecule. This resonance energy is defined by the ionization enthalpy of a given conjugated system which is observed in the classical Kekulé structure.[28] Kekulé proposed that benzene has a cyclic structure with alternating C=C double and C-C single bonds which was not accurate to state because it would have meant that 1,2-dichlororbenzene existed in two isomers which has never been observed.[29]

In the 1970s, Hess and Schaad made progress in discovering a method for calculating reliable resonance energies within the Hückel molecular orbital (HMO) approximations. Over time, the Hess and Schaad resonance energies found numerous chemical applications detailed in many works. This method is a variant of the DRE which was adjusted to the HMO model. Hess and Schaad calculated the Dewar energy model using HMO which enabled them to distinguish the difference between the energy types of the neighbouring C-C atom bonds.[30] Furthermore, Mayano and Paniagua reported on an improved approach on the energies of the localised molecular π-orbital. Their parameterized methods adjusted the resonance energy leading to a more simplified technique.[31]

Clar demonstrated an easily simplified approach toward understanding the aromaticity around benzene.[32, 33] He stated that for the structure to stabilise the number of π-electrons must increase in the π-electron sextets. The PAH's are known to be pure benzenoid which is stable. In contrast with the HMO-model, aromatic is not a molecular property, but rather localised in the distinct ring. Clar's model predict many of the chemical and physical properties of PAH's. This model also allows the prediction that aromatic compounds undergo electrophilic aromatic substitution reactions, and it can also predict bond length and angles.

Randic *et al.*,[34] and Klein *et al.,*[35] proposed the conjugated-circuit model which simplifies the resonance-theoretic models to study the aromaticity and conjugation in the polycyclic conjugated systems. The model was inspired from an empirical point of view elaborating on the Armit-Robison-Clar's aromatic sextet idea. The conjugated-circuit model can also be explained from a quantum-chemical view combining some of Pauling and Wheland's resonance-theoretic ideas with the Herndon-Simpson model.[36]

The conjugated-circuit model uses Kekulé valence structures. In the individual Kekulé structure, the normal alteration of the C-C single bond and double bond form the so-called conjugated-circuit. PAH's are viewed as a superposition of conjugated circuit instead of a collection of Kekulé valence forms. In all the Kekulé structures conjugated circuit of the six, ten or more (4n+2) bonds are determined and if the number of conjugated circuits is also (4n+2), then the PAH is aromatic.[37] The aromaticity of naphthalene according to the conjugated circuits model is best described by Kekulé.[38]

The individual circuits can be used to calculate the summation of resonance energies. Calculating the resonance energy per π-electrons helps in the comparative study of the aromaticity of PAH's. A classification of PAH's according to their degree of benzene character, i.e. their benzoidicity, can be made using the conjugated circuit model. The results are in accordance with the prediction made by Clar's model. A statistical approach to the C-C model can give a good estimation of the aromaticity for PAH's. This show that a cyclic or polycyclic systems have an aromatic nature if it has (4n+2) π-electrons in its periphery. The (4n) –π-electrons would result in anti-aromatic and the (4n+2) and (4n+3) π-electron system in its periphery would be estimated as non-aromatic. Pyrene is thus an aromatic compound and fluoranthene is non-aromatic.[38]

Further proving the concept of aromaticity in cyclic and polycyclic molecules, the experimental view becomes vitally important. This aspect conceptualises the spectroscopic methods on the frontiers of the subject matter. Techniques such as X-ray diffraction, NMR and DFT (computational chemistry) play an important role in clarifying matters. X-ray diffraction provides accurate bond distances and bond angles and these show that for aromatic character the C-C bonds varies from 1.38-1.40 Å. It is known that the degree of aromaticity is distinguished between alkenes and saturated aromatic compounds based on the type of chemical reaction that each one undergoes e.g. aromatic undergo substitution reaction and alkene undergo addition reaction. The DFT calculation has predicted the stability energies of the molecular compounds based on their HOMO-LUMO, which reveals that aromatic compounds with a high HOMO-LUMO energy gap are likely to have low reactivity towards electrophilic attack. The most basic of all is NMR which shows that the aromatic compounds are naturally diamagnetic diprotic cyclic and polycyclic compounds which exhibit low-field NMR chemical shift profiles relative to the olefinic protons.

1.1.5 Synthesis of *1,8*-Diaminonaphthalene and *1,5*-Diaminonaphthalene

1,8-Diaminonaphthalene **(d)** and **(f)** is an isomer of *1,5*-diaminonaphthalene, see Scheme 1.1.1.1. The scheme below show the steps which lead to production *1,8*-diaminonaphthalene **(d)** and **(f),** step **(1)** is nitration of naphthalene to 1-nitronaphthalene, step **(2)** is nitration of 1-nitronaphthalene to *1,8*-dinitronaphthalene, step **(4)** is the direct dinitration of naphthalene to produce *1,8*-dinitronaphthalene and then step **(3)** and step **(5)** is the metal-acid reduction or catalytic hydrogenation reaction toward the production of *1,8*-diaminonaphthalene. These are the crucial steps in which most of the nitronaphthalenes and nitronaphthalenesulfonic acid undergoes during their production.

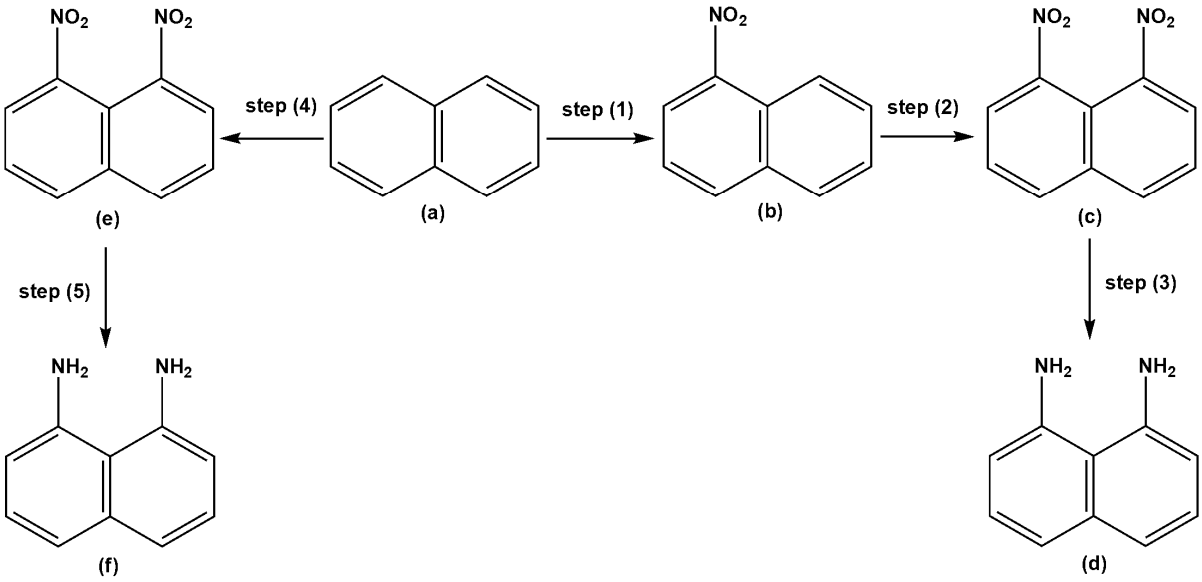

Scheme 1.1.1.1. Simplified scheme toward the synthesis *1,8*-Diaminonaphthalene **(d)** and **(f).**

Both isomers are produced by metal-acid, i.e. iron-acetic acid reduction or by catalytic hydrogenation of *1,8*-dinitronaphthalene and *1,5*-dinitronaphthalene, respectively, during a one-pot reaction. The dinitroamine isomers are produced from the nitration reaction of 1-nitronaphthalene in a ratio of 40:60 % of nitric acid to sulfuric acid. It was observed that similar results could be obtained by a dinitration reaction with mixed acid at the temperature of 40 to 80 °C. The two dinitroamine isomers can be separated from each other by fractional crystallization from ethylene dichloride and solvent extraction processes. The dinitroamines are a product of 1-nitronaphthalene which is produced by nitration of naphthalene with nitric acid and sulfuric at 40 to 50 °C in satisfactory yield. The purification is performed by distillation processes and by recrystallization from alcohol.[39]

1.1.6 Uses of *peri*-disubstituted naphthalenes

Diverse applications of naphthalene and its derivatives have been found in important intermediates in agricultural, construction, pharmaceutical, photographic, rubber, tanning, and textile niche applications, fumigant, and solvents.[40] The *peri*-substituted naphthalenes (including *1,8*-diaminonaphthalene) also plays an important role in a variety of domestic and industrial applications depending on the substituents in the *peri*-positions. Derivatives *o*f *1,8*-dianimonaphthalene are used in the manufacturing process of plastics in automobile turn-signal and warning light lenses as colourant source. If the P(III)-donor atom is chemically bonded to an amino substituent (primary or secondary), an aminophosphine' forms. The substituents enhance the importance of these compounds as they offer the possibility of manipulating them both on the P- and N-donor atoms although, the N-atom is viewed as an additional donor site towards metal substrates. The donor atoms enhance the applications of the aminophosphines.

1.1.7 Nomenclature of Aminophosphines

In 1903, Michaelis isolated the first aminophosphine and thereafter a wide range of phosphorus 3+ compounds became of interest in organophosphorus chemistry.[41] The aminophosphines are compounds composed of a P^{3+} center with either primary or secondary amines. The bis(aminophosphines) and bis(phosphonous diamide) are compounds classified under aminophosphines. Both the P-atom and N-atom are in the 3+ oxidation state, and are tricoordinate to each other to form a multidentate ligand. The two donor atoms lead to a variety of multinuclear complexes yet there are no isolated complexes whereby the metal center coordinate to both the donor atoms.[42] Below in Table 1.1.1.1, same generic phosphorus 3+ containing compounds are summarized.

Table 1.1.1.1. The well-known examples of P^{3+} compounds

Type[a]	Common names	Example, name
PH_3	Phosphine/phosphane	-
PR_3	Phosphine	PPh_3, triphenylphosphine
$P(NRR')_3$	Aminophosphine	$P(NMe_2)_3$, tris(dimethylamino)phosphine
R_2P-PR_2	Bisphosphine	$(Ph)_2$P-P(Ph)2, 1,1,2,2-tetraphenylbiphosphine
$P(OR)_3$	Phosphite	$P(OMe)_3$, trimethylphosphite
$P(SR)_3$	Thiophosphite	$P(SMe)_3$, trimethylthiophosphite
PX_3	Phosphorus trihalide	PCl_3, phosphorus trichloride

[a] **X = halogen; R, R' = alkyl and/or aryl groups.**

Aminophosphanes, phoshinoamines, phosphorus amide, phosphinous amides, amidophosphorus, and phosphinoamides nomenclature is given for P(III)-N compounds. Aminophosphines can either be mono(aminophosphines) or bis(aminophosphines). The bis(aminophosphines) also have other names indiscriminately used in the open literature, e.g. bis(phosphine)amines, amino-bis(phosphines), bis(phosphinoamines) and bis(aminophosphines). With such growth in literature, there is confusion in the nomenclature where the name aminophosphines is used for compounds that does not contain a direct P-N bond, but instead P-C bonds.[43] There are reports available which have rectified the confusion by assigning names such as α- and β- or 2-aminophosphines where a direct P(III)-N bond is lacking and only P-C-N and P-C-C-N linkage are present, respectively.[44] Aminophosphines change nomenclature to 'hybrid electron-rich aminophosphines' if the phosphines contain two amino groups and one alkyl or aryl substituent. The term *hybrid* indicates the presence of both P–C and P–N bonds in a phosphine. The example of hybrid electron-rich aminophosphines is represented by $R'(R_2N)_2P$ where R is the alkyl substituent and R' is the alkyl or aryl substituent.[45] The P-C and P-O type phosphines consisting of one P-N bond also belong to the 'aminophosphine' category, but bear specific names such as acyclic and cyclic P(III)-N systems. There are two types of well-known multidentate ligands encountered, i.e. **(a)** $R'N(PR_2)_2$ and **(b)** $R_2P\text{-}N(R')\text{-}X\text{-}N(R')\text{-}PR_2$. To classify the structure of compounds without ambiguity the following naming is used: bis(phosphino)amine or aminobis(phosphines) for the former [46, 47] and bis(phosphinoamine) or bis(aminophsphine) for the latter.[48]

1.1.8 Physical and Chemical Properties of Aminophosphines Chalcogenides

The common methodological synthesis that are used in the synthesis of aminophosphines involves the condensation,[49] scrambling[50] and transamination reactions[51]. The synthesized aminophosphines are either liquid, off-white to white or light brown solid in colour. They are thermally stable, but quite sensitive to moisture and air because they can undergo oxidation and should be kept under inert atmospheric conditions.[52-54]. They are soluble in the organic solvents like toluene, dichloromethane, chloroform and benzene. Derivatization processes of aminophosphines requires dry solvents,[55, 56] and are malodourous due to the presence of the amine group. The compound is basic in nature due to the presence of the N-atom donor, and are nucleophilic in nature due to the availability of the two lone pairs of electrons present on the phosphorus center alongside the π-electrons on the nitrogen atom.[57, 58] The equation implied

by Brönsted is used to predict the proton basicity of the phosphorus atom in $P(R_2N)_3$ which was found to be more comparative to that of PR_3.[59]

The aminophosphines are highly reactive compounds[60, 61] and are simply treated with chalcogens to form a common oxidative addition reaction. The aminophosphine chalcogenides are more stable compared to a free aminophosphine ligand. The examples of oxidized aminophosphine backbone structure is $(R_2N)_3PE$ where (E = O, S, Se, Te). Elementary chalcogenides (O, S, Se and Te) are typically obtained from commercially available sources, and several organic chalcogen compounds. The sources of oxygen gas can be air, oxygen gas cylinders, hydrogen peroxide, dialkyl peroxides and activated manganese dioxide. Other well-known oxidizing reagents which have been used previously are nitric acid, water, permanganate and dichromates. The chalcogens normally react with P^{3+} atoms of the tricoordinate molecule to form 4-coordinate tetrahedral P^{5+} compounds. The stability of derivatised compounds are as following: -P=O >-P=S > -P=Se > -P=Te.[62-64]

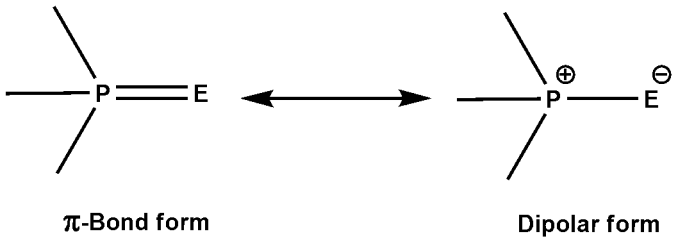

Figure 1.1.1.7. An illustration of a canonical forms of phosphine chalcogenides.

Studies suggest that when phosphorus approaches the *3d*-orbital to interact with the π-bonding substituents, the dipolar moments dominates the P-Se bonding system. This cause the π-bond form to be more significant for E = O containing compounds and the dipole moment to be significant for the E = S and Se containing compounds. This also explains that the polarity increases with an increase in atomic size which then suggests the order of polarity to be P = O < P = S < P = Se.[65]

1.1.9 The Effectiveness of Aminophosphines as Ligands

Aminophosphines are good potential ligands in coordination chemistry because they contain both phosphorus and nitrogen donor atoms.[66] Such donor atoms form strong (dative) covalent bonds during coordination with the weak and strong metal centers. The advantage of having aminophosphines on a naphthalene backbone allows for manipulation of the ligand to suit, for

example, an increase in both homogeneous and heterogeneous catalysis efficiencies.[67] The Tolman cone angles are best used to decide the steric crowding around the metal center and also to determine the coordination number around the centered metal. The Tolman angle is considered an important parameter in understanding the coordination chemistry of metal-phosphine complexes as well as the electronic properties of the ligand, see Figure 1.1.1.8.[68]

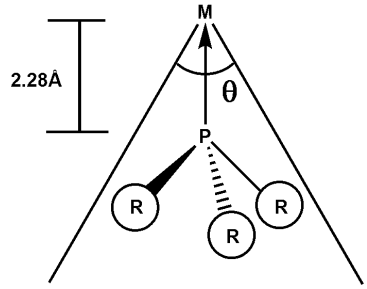

Figure 1.1.1.8. The Tolman representative cone angle for R_3P in "θ".

Mono-, bi- or multidentate ligands all have their own different cone angles. Changing substituents on the nitrogen donor atom thus offers the possibility to manipulate the aminophosphine ligands. Various reports discuss the steric properties of phosphine ligands derived from the ligand exchange studies, molecular mechanics methods, NMR spectral data and theoretical studies[69-71] Importantly, the 'cone angle concept' conveniently describes monodentate phosphine ligands, although for multidentate ligands, but the 'bite angle concept' has to be measured and considered, and indeed helps in calculating the catalyst efficiencies. Changing the steric effects can have significant electronic influence and vice versa. An electronic effect arises if changes to part of molecule result in a different electronic distribution within the molecule [72, 73]

1.1.10 Coordination Chemistry and Behaviour of Aminophosphines

Aminophosphines have the ability to form stable metal complexes because the P-donor atom *3p*-orbitals and the metal center *3d*-orbitals forms a stable bond since they have similar energies in the MO energy diagram. The coordination chemistry of the aminophosphines also has the following features: **(a)** the metal complexes of aminophosphines occurs quite rapid and easy under mild reaction conditions[74, 75], **(b)** the involvement of the aminophosphine hyper-conjugation with the P atom orbitals and cause the metal centers to bind *via* the phosphorous atoms and not the nitrogen atoms[76, 77], **(c)** the low oxidation state soft metal centers , e.g. Cu(I), Ag(I), Au(I), Pt(II), Pd(II), Mo(0), Ru(I), Ru(II) etc., have been extensively used with soft

aminophosphines ligands, **(d)** the complexes have been well investigated by numerous crystallographic studies, **(e)** if the aminophosphines consist of two donor sites, the binding through the metal centers typically occur in a bidentate manner $[M(\mu\text{-}X)_nL_2]$ (L is the aminophosphine ligand)[78], **(f)** it is possible to obtain monodentate coordination depending on the nature of the ligands $[MX_nL]$,[75, 79] **(g)** the metal centers can form dimers under certain reaction conditions due to coordinative unsaturation $[MX_nL]_2$[80], **(h)** in the cases where a more sterically hindered moiety is used, such as an aminophosphine ligand, then the metal center can bind to phosphorous in a bi-and tri-dentate manner[81, 82], **(i)** in cases where the ligand contains two amino groups and one alkyl or aryl substituent, the term hybrid electron rich aminophosphine is used, this is to indicate the presence of P-C and P-N bonds in a phosphine compound[83], **(j)** there are complexes that exhibits either mono-(P) or bidentate behaviour depending on the nature of the metal center and the reaction conditions,[75] **(k)** in some Pt(II) complexes the NMR derived J-coupling constant have been used to predict the structures of the molecules.[75, 84]

1.1.11 Transition Metal complexes: Soft and Hard Metal Centers Coordination

1.1.11.1 The Geometry of Copper(I) and Silver(I) Complexes

Designing ligands with a high affinity for different soft and hard Lewis acid transition metal centers provide coordination flexibility for the formation of stable metal complexes, and potential chelating ligands have a high probability of forming multinuclear complexes. Both Cu(I) and Ag(I) transition metal centers are regarded as low-valent soft metals which display a variety of coordination geometries, display brilliant luminescence, and good catalytic properties.[85, 86] The chemistry of tertiary phosphine complexes of Cu(I) and Ag(I) species as classic d^{10} systems dates back more than 100 years ago. The geometrical aggregates for several Cu(I)X, X= Cl, Br, I and Ag(I)X, X= Cl, Br, I and non-bonding/coordinating counter ions, i.e. NO_3, ClO_4^-, BF_4^-, PF_6^- and pseudo-halides, i.e. CN^-, SCN^-, anions are well known and obtained when the metal salts react with organic ligands in different stoichiometric ratio under different reaction conditions.[87, 88] There are two challenges that are encountered when copper halides are used in the synthesis: **(a)** The inherent instability of copper(I) halides, i.e. CuBr and CuCl, which may oxidize, i.e. Cu(I) to Cu(II) in the presence of dioxygen from the air and/or "wet" solvent. This could form two complexes in solution and the mixture of Cu(I) and Cu(II) complexes could both react making product isolation difficult, **(b)** The solubility of Cu(I)

halides is very poor in many organic solvents and moderately soluble in acetonitrile.[89-91] In contrast, the Ag(I) halides do not oxidize, but the reaction need to be done under reflux for 1-3 hours in a molar ratio of the appropriate phosphine ligand in acetonitrile.[88] Not all silver salts requires harsh reaction conditions. Figure 1.1.1.9 shows the building blocks of copper(I) halide aggregate types and depicts the neutral rhomboid dimer and cubane tetramer.

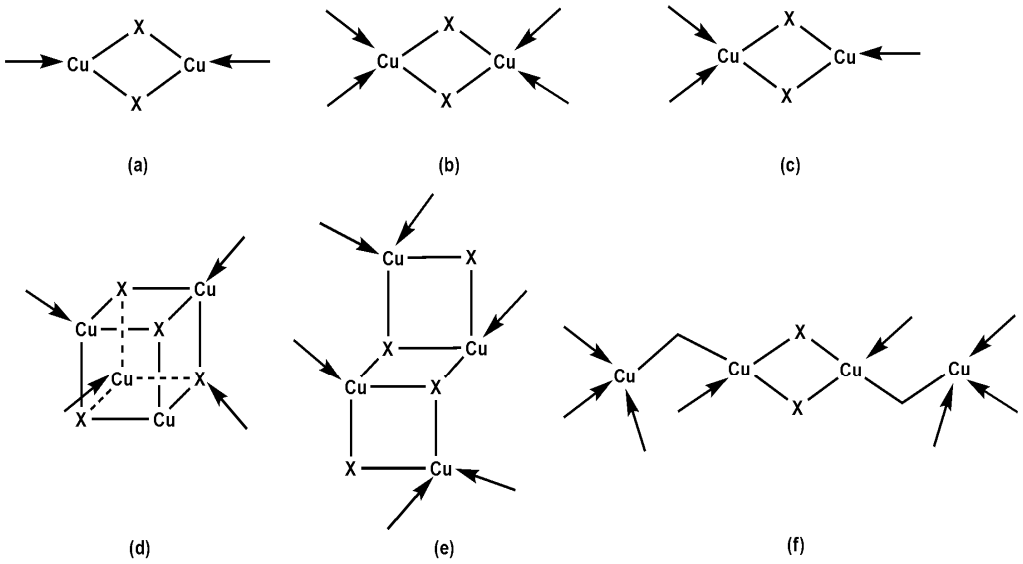

Figure 1.1.1.9. The zero-dimensional aggregate for copper(I) with halides at point (X).

The coordination geometry in **(a)**, **(b)** and **(c)** is rhomboid, the dimers are neutral with Cu_2X_2 manifold. The geometry observed in **(d)** is cubane, **(e)** is stepped cubane and **(f)** is open cubane. The cubane has a chemical formula of Cu_4X_4 and the arrows point towards the possible coordination modes to which ligands can attack and coordinate. There are many other complexes ranging from 1 to 3-dimension, which are not described here. Coordination **(d)** is a secondary building block for Cu(I) types of phosphine molecules; compounds are synthesized according to literature.[87, 92, 93] Copper(I) halide complexes are anionic (Cu_xX_y) and anionic copper(I) halides aggregates are derived from the corner/edge/face-sharing modes of the three simple synthons which are: linear CuX_2^-anion **(a)**, planar triangular CuX_3^{2-} anion **(b)** and tetrahedral CuX_4^{3-}anion, see Figure 1.1.1.10.[94]

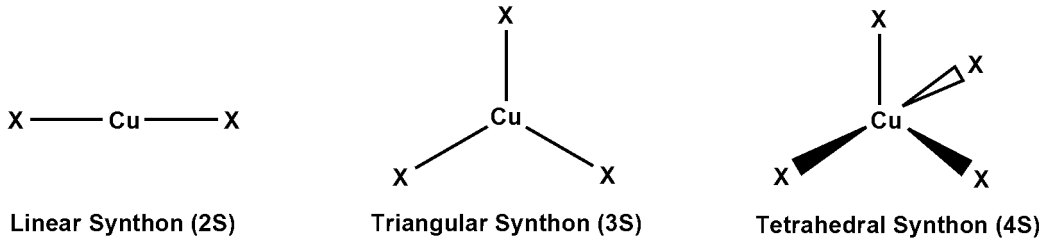

Figure 1.1.1.10. Halocuprate synthons (S) core for complexes.

Silver(I) coordination chemistry have seen a surge in the fields of networks[95], polymers, silver scorpionates and ligands containing nitrogen donor atoms. The Ag(I) complexes can undergo a monodentate coordination with phosphine ligands.[88]

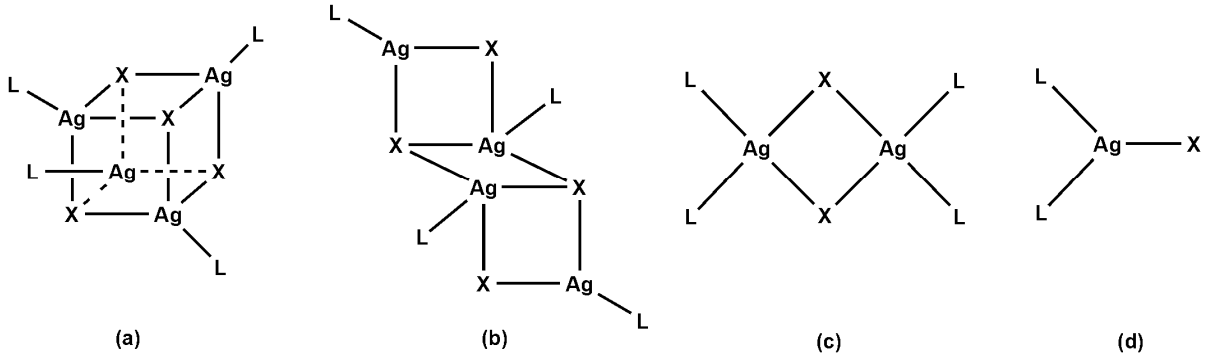

Figure 1.1.1.11. Coordination geometry of Ag(I) monodentate complexes of phosphines (L).

The coordination depends significantly on the M:L stoichiometric ratio. In cases where the Ag(I) is reacted with the ligand in 1:1; 1:2;1:3 and 1:4 ratios, different coordination geometries are observed. Equimolar stoichiometry of Ag(I): L forms the tetranuclear cubane **(a)** and step cubane **(b)**. The more sterically demanding the substituents are, the more the step cubane **(b)** geometry is favoured over tetranuclear cubane **(a)**. Crystallization processes of sterically hindered Ag(I) complexes favours the formation of cubanes while step cubane **(b)** is favoured by the use of pseudo-halides. Another geometry that is commonly known with Ag(I) is linear coordination. This is formed by silver perchlorate and other bulky ligands reacting with Ag(I) halides salts. In general, when Ag(I) reacts with phosphine ligands in (1:2) ratio the dimeric structures are isolated with halides bridging the metal centers, see Figure 1.1.1.11 **(c)**. Another known geometry is trigonal planar, and this forms in mononuclear coordination for Ag(I), see Figure 1.1.1.11 **(d)**. The M: L reaction ratios of (1:3) and (1:4) form the complexes which are counter balanced by X (halides). The M:L reaction ratios of (1:3) favours 3-coordination and balanced by a counter ion. The complexes formed when M:L reaction ratios is (1:4) typically has two to four ligands around the metal center. Most of the Ag(I) complexes formed by the reaction ratio of (1:4) are isolated with non-bonding anions, such reactions related to stoichiometric ratios have been reviewed.[88]

Ag(I) metal salts introduce interesting coordination modes with bidentate phosphorus ligands. Several bis(diphenylphosphino)methane (dppm) Ag(I) complexes have been isolated and they are known to form dinuclear metal complexes. The bis(diphenylphosphino)ethane (dppe)

affords both bridging and chelating silver(I) complexes. Complexes which are prepared from the equimolar Ag:L2 stoichiometry tends to display a range of structural types with the geometry dictated by the bond length of the chain between the two donor atoms.[96, 97]

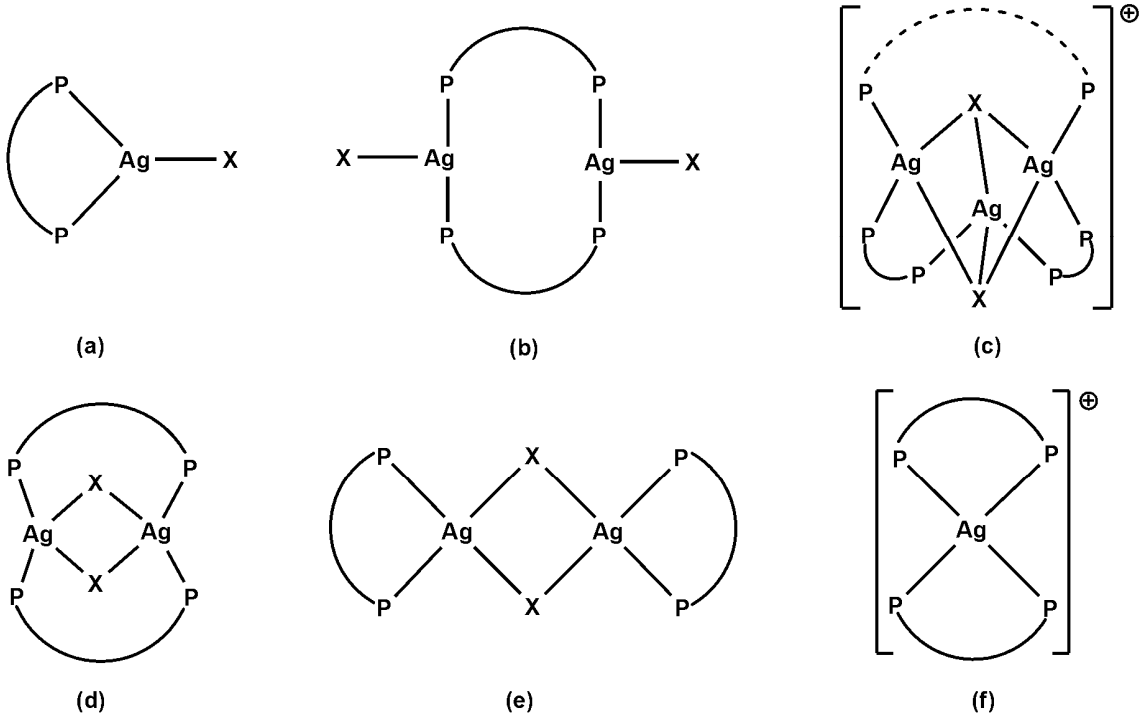

Figure 1.1.1.12: Silver(I) halides representative modes with equimolar Ag:L2 stoichiometry.

1.1.11.2 Biphosphine and Bis(phosphine) Ligands to Metal Centers

The *peri*-disubstituted naphthalene containing bisphosphines behaves like Lewis bases by donating lone pairs of electrons to metal centers during coordination. The *peri*-disubstituted bisphosphine ligands can potentially donate two lone pairs of electrons to metal centers. The ligands form bidentate or multinuclear complexes by the chelation effect which provide additional stability of the metal centers. Aminophosphines are generally *P-N-P*-or *P-N*-type ligands; the *P-N* bond is labile and can readily break. The spacer group in the bis(aminophosphines) is important as it provides a higher degree of flexibility to the compound during formation. Spacers also helps to reduce the strain effects by creating a multidentate site for metal centers coordination. Metal complexes containing different N-atom, i.e ammonia, amino acid ester, piperazine, homopiperazine, urea and hydrazine have been reported.[98, 99] Figure 1.1.1.13 shows a strained biphosphine molecule with a P-P bond which is rigid versus bis(phosphine) molecule with a P-X-P (X = spacer) which provide flexibility for P-donor atoms to chelate to the metal center.

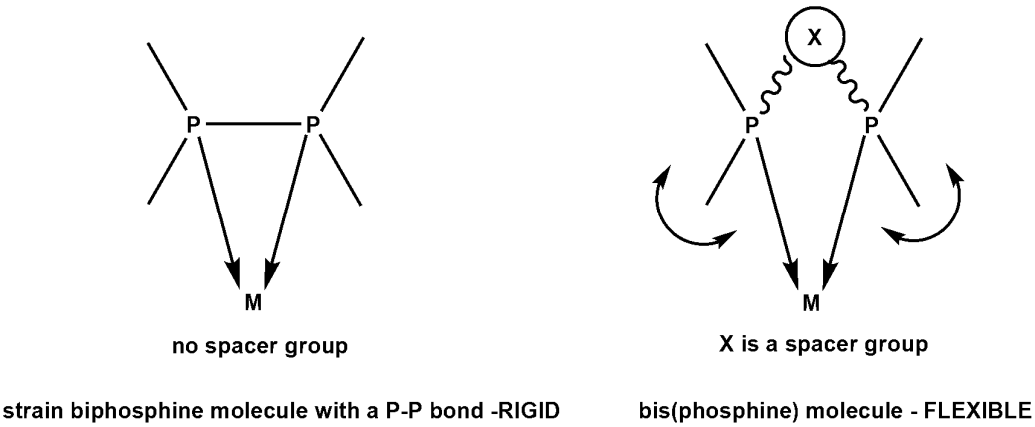

Figure 1.1.1.13. Coordination mode of the biphosphine and bis(phosphine) to metal centers.

1.1.12 Alkyl and Aryl or Benzyl Spacer Behaviour in Aminophosphines

1.1.12.1 Alkyl Spacers in Aminophosphines

Aminophosphines ligands are affected by a large number of different types of organic spacers, e.g. alkyl, aliphatic or aromatic, the unsubstituted hydrocarbon group or any group with chemical functionality. The ligands are synthesized *via* aminolysis type reactions and are characterized by conventional spectroscopic methods. The ^{31}P NMR is commonly employed to monitor the chemical shifts of the ligand peaks(s) relative to their complexes. The ligands bind well with metal centers and are further used in the ternary catalytic mixture, such as Suzuki and Heck coupling reactions. Complexes that contain short and longer alkyl spacer have been synthesized[100-104] and the alkyl spacer allow the ability of the chain length to rotate free, which in turn allows the ligand to bind the metal center in a strain-free environment. The longer the chain length, the higher the degree of rotation which often causes oily compounds.

1.1.12.2 Aryl or Benzyl Spacers in Aminophosphines

The simplest aryl or benzyl spacers are important because they tune the ligand architecture which also influence the electronic properties of the P-donor atom of the aminophosphine. In aminopshophines, a series of bis(DPPA) ligands, where both P,P-donor atoms are attached directly to a phenylene spacer, were reported[105] and extends the work published by Kayan and co-wokers.[106] Complexes were synthesized which show significant ^{31}P NMR chemical

shifts.[107, 108] Other donor atoms such as the Y atom indicated in Figure 1.1.1.14 as can also be included which can also take part in metal coordination, adding stability.

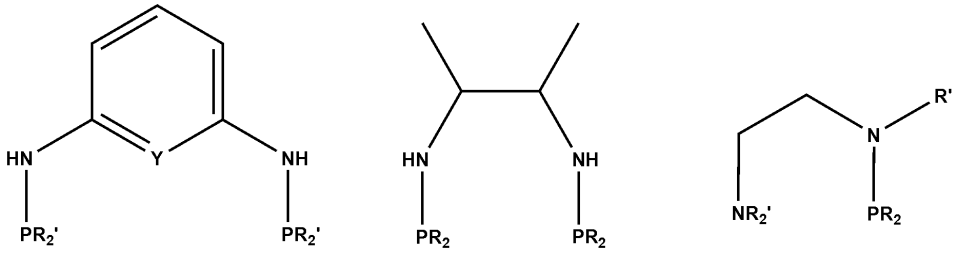

Figure 1.1.1.14. Polydentate aminophosphine ligands.

The pincer spacer ligands show similar characteristics to those of naphthalene and benzene spacers. These ligands are derivatized by the addition of phosphine to the N-atom backbone moiety of the substituted molecule. Below is an illustration of structural bound pincer of *N,N'*-bis(di-iso-propylphosphino)-1,3-benzenediamine which was synthesized mainly to complex classic square planar d^8 systems. The formed complexes potentially improve the stereospecific catalytic activity of aminophosphine. This also helps to tune the cone angle around the phosphorus which play a fundamental role in the catalytic activity, e.g. short or long bite ligands.

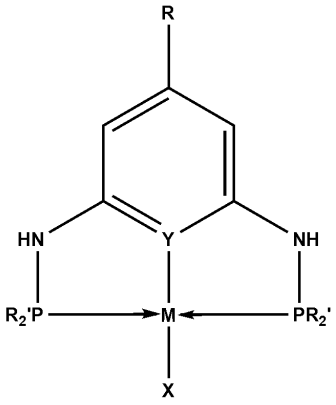

Y = C: PCP Pincer Complex (M-C bond is a covalent bond)
Y = N: PNP Pincer Complex (M-N bond is a dative bond)

Figure 1.1.1.15. The structure of PYP pincer metal complex with P(III)-N bonds.

1.1.13 Synthesis of Metal Complexes of Copper

Reviews by Bhattacharyya[109], Ly[110] and Appleby[111] reports on the synthesis, structure and coordination chemistry of different bidentate aminophosphine ligands of the type (P–N–P). A search on *CCDC* data base found 2840 related structures of ($PPh_2(NR)PPh_2$) including complexes containing different metal centers. Similar compounds were reported by Ganesamoorthy and co-workers where they documented di- and tetranuclear copper(I) complexes of phenylaminobis(phosphonite), $PhN\{P(OC_6H_4OMe\text{-}O)_2\}_2$ ligand.[112] They further studied the complexes reactivity towards bipyridyl ligands and demonstrated the synthesis of $Cu_4(\mu_2\text{-}X)_2(\mu_3\text{-}X)_2(\mu\text{-}PNP)_2$ (X = I, X = Cl; X = Br) dinuclear copper(I) complexes in good yields. The complex containing iodide shows tetranuclear copper(I) geometries when reacted in the present of heat, whereas those of chloride and bromide undergo geometrical changes in the presence of acetonitrile, while $Cu_4(\mu_2\text{-}I)_2(\mu_3\text{-}I)_2(\mu\text{-}PNP)_2$ produces $Cu_2(\mu_2\text{-}I)_2(C_5H_5N)_2(\mu\text{-}PNP)$ in excess pyridine. This suggests that some copper(I) complexes are thermally unstable which can either decompose or structurally change around the metal manifold under different solvent or heating conditions as this behaviour was proven by X-ray analysis.[112]

In 2006, Pan *et al.*,[113] reported on the synthesis and molecular structures of *N,N'*-bis(diphenylphosphino)-2,6- diaminopyridine and their copper(I) and gold(I) complexes. The reaction of CuI with 1 or 2 mole ratio(s) of *N,N*-bis(diphenylphosphino)-2,6-diaminopyridine (BDDP) results in two different complexes, namely $[Cu(I)\mu\text{-}(BDDP\text{-}\kappa P,Npy)]_2$ and $[Cu(BDDP\text{-}\kappa P,Npy)_2]I$, both isolated in very good yields. The geometry around the copper centers are both tetrahedral.

N,N-bis(diphenylphosphino)-2,6-diaminopyridine is an example of a multifunctional ligand in coordination chemistry and has been reacted with different metal salts such as $[M(CO)_3(CH_3CN)_3]$ (M = Cr, Mo, W) and MCl_2 (M = Ni, Pd and Pt) to form complexes. All the metal centers show a planar tridentate chelating ring system. Scheme 1.1.1.2 shows the anticipated multinuclear complex with metal-metal interactions, but instead ionic compounds we formed.

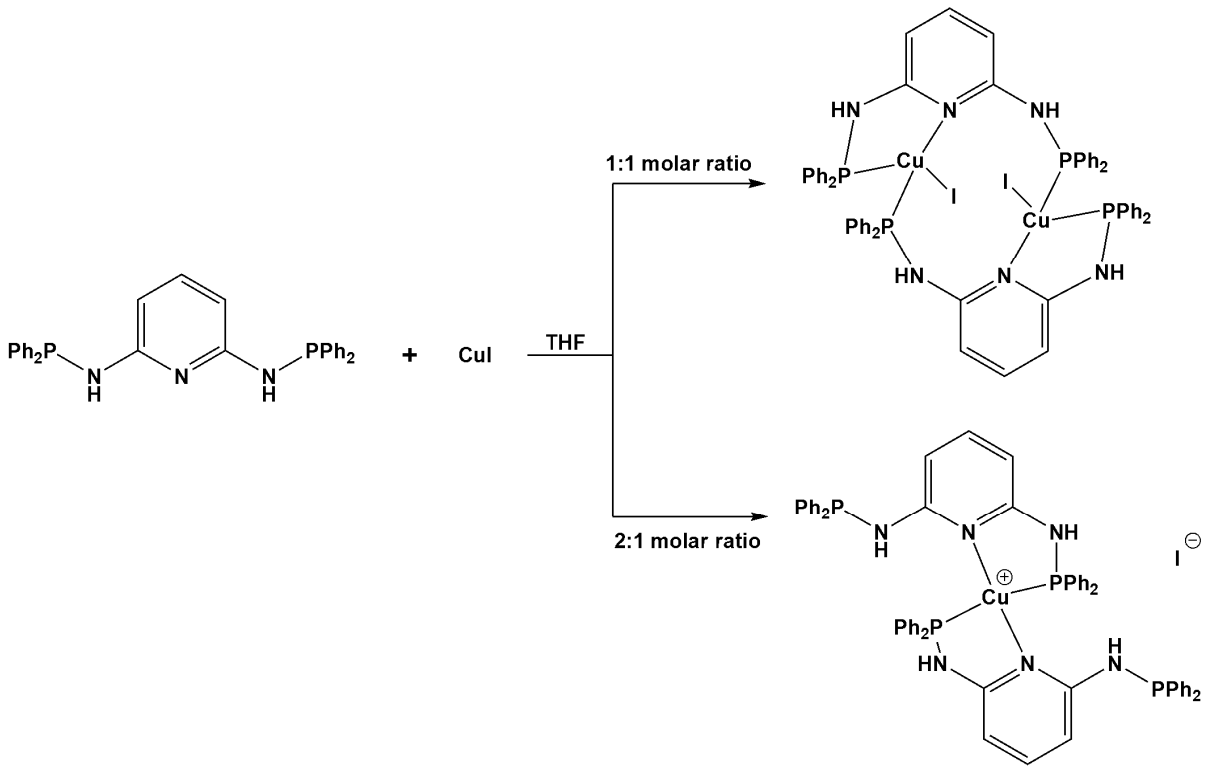

Scheme 1.1.1.2. The influence of stoichiometric ratio on copper(I) centers, leading to different complexes and nuclearities.

The ligand flexibility derived from both N and P atoms allows for docking positions. Steric hindrance and the electronic effects of the donor atoms as well as the inner N-atom allows the molecule to be tuned to suit complexation.[113] The chemistry of the d^{10} system for CuI, AgI and AuI demonstrate variable coordination geometry. The Cu(I) and Ag(I) centers mostly exhibit tetrahedral coordination geometry whereas Au(I) species produces 2-coordinate linear structures. The complexes possess either a trigonal planar or tetrahedral geometry.[114] Complexes of Cu(I) aminophosphines have been reported with or without a spacer unit and are bridged either by halogens or chalcogenide complexes.[115-125]

1.1.14 Synthesis of Metal Complexes of Silver

According to Rosa *et al.*,[126] the silver complexes formed between thioether and diphosphine ligands consists of short-bite angles and this have triggered the formation of trinuclear complexes. Synthesis of two thioether-functionalized bis-(diphenylphosphino)amine ligands, $Ph_2PN(p\text{-}ArSMe)PPh_2$ (L1) and $Ph_2PN(n\text{-}PrSMe)PPh_2$ (L2) allows comparative studies to be

made with the 'unfunctionalized' ligands $Ph_2PN(Ph)PPh_2$ (L3) and $Ph_2PN(n\text{-}Bu)PPh_2$ (L4). The trinuclear complex $[Ag_3(\mu_3\text{-}Cl)_2(\mu_2\text{-}L1\text{-}P,P)_3](BF_4)$ ($1\cdot BF_4$) contains a triangular array of Ag centres sustained by three bridging ligands (L1) and two triply-bridging chlorides. Ligand (L2) produced a coordination polymers of the type $[\{Ag_2(\mu_3\text{-}L2,\text{-}P,P,S)_2(MeCN)_2\}$ and $\{Ag_2(\mu_2\text{-}L2\text{-}P,P)_2(MeCN)_2\}(BF_4)_4]_n$ in which the chained thioether group connects intermolecularly to the Ag_2 entity of the diphosphine bridging the other Ag_2 entity. On the other hand for (L3) and (L4), the same complexes were produced, $[Ag_2(\mu_2\text{-}L3)(BF_4)_2]$ and $[Ag_2\text{-}(\mu_2\text{-}L4)(BF_4)_2]$, respectively, with bridging diphosphine ligands and a BF_4 anion completing the coordination sphere of the metal.

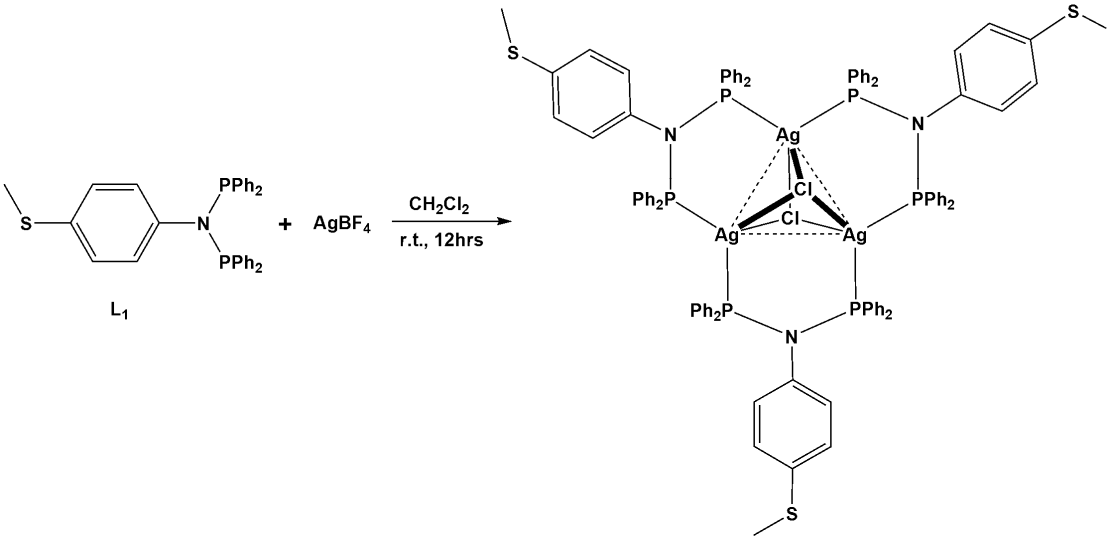

Scheme 1.1.1.3. A tricyclic trinuclear silver(I) complex.

Scheme 1.1.1.3 shows the BF_4 ions on the Ag cation readily replaced by the chlorine atoms from the solvent. The trinuclear geometry of the silver atoms is caused by the weak electron withdrawing group attached to the sulfur atom. A different behaviour is observed when the thiomethyl-group is detached from the phenyl ring, see Scheme 1.1.1.4. Silver complexes could be dinuclear,[126-129] trinuclear,[130, 131] tetranuclear,[119, 132] coordination polymers[133] and could form clusters[134, 135] as well.

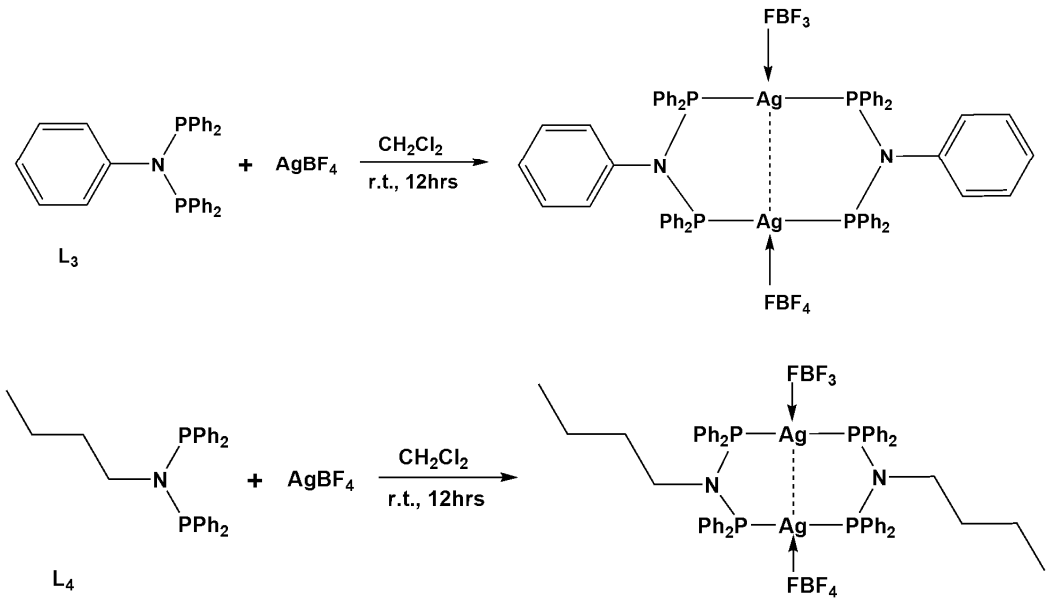

Scheme 1.1.1.4. Formation of a dinuclear silver(I) complex.

The thioether group plays a major role towards influencing the orientation of the molecule. Exchanging L1 with L4 under the same reaction conditions formed a coordination polymer, see Scheme 1.1.1.5.

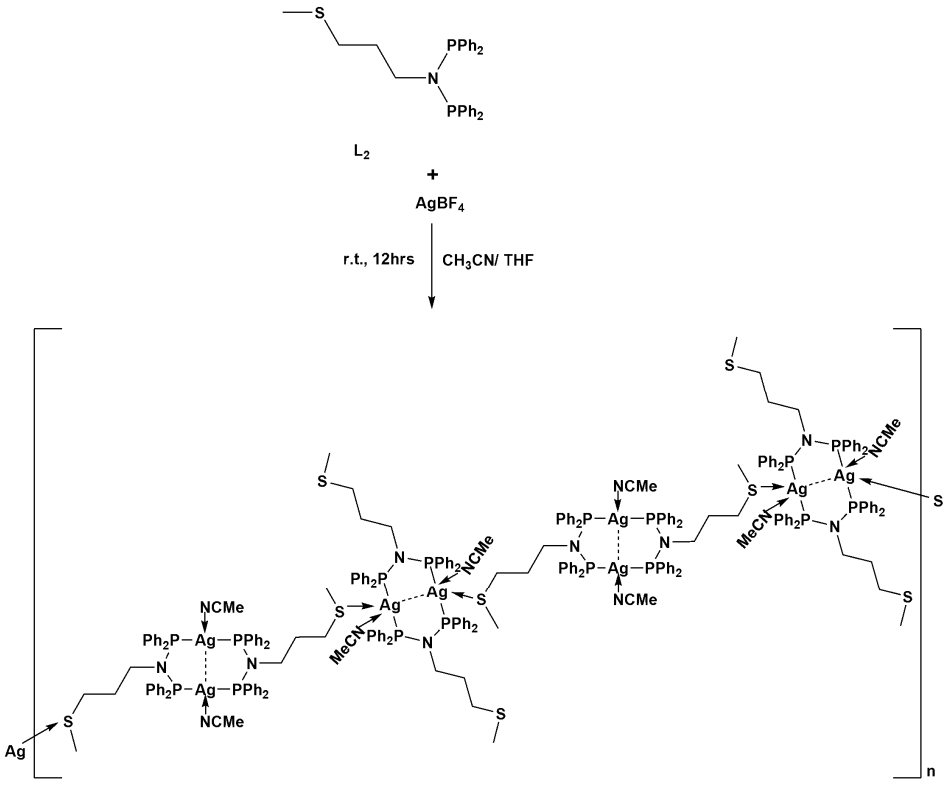

Scheme 1.1.1.5. Neutral coordination polymer of silver(I) complex.

1.1.15 Applications of Aminophosphines

Aminophosphines $(R_2N)_3P$ have relatively weak P-N bonds but have nevertheless found important uses in our daily life as they provide better performance of leaded gasoline (although this does not exist anymore), and used as a catalyst in the preparation for polycondensation of polyhydric alcohols during the production of resins such as polyurethanes. Aminophosphines are used in the production of high-density polypropylene and also as a constituent in the cleaning of metals. The $(RNH)_3P$ group of aminophosphines are used as antiknock additives for gasoline and as an antistatic treatment for plastics. The third group $(R_2N)_2PX$ are helps in curing epoxy resins and are also suitable for the synthesis of peptides.[136] The complexes of Cu, Ag, Pt, Pd, Rh and Ru are all good candidates for different homogeneous catalysis that include the oxidative hydrolysis of olefins, hydrogenation and hydroformylation reactions.

1.2 Chemistry of Perimidines

1.2.1 Perimidines

Pyrimidine is a heterocyclic aromatic organic compound similar to benzene and pyridine. It consists of two nitrogen atoms at positions 1 and 3 of the six-member ring. It is isomeric with two other forms of diazine, see Figure 1.2.1.1.

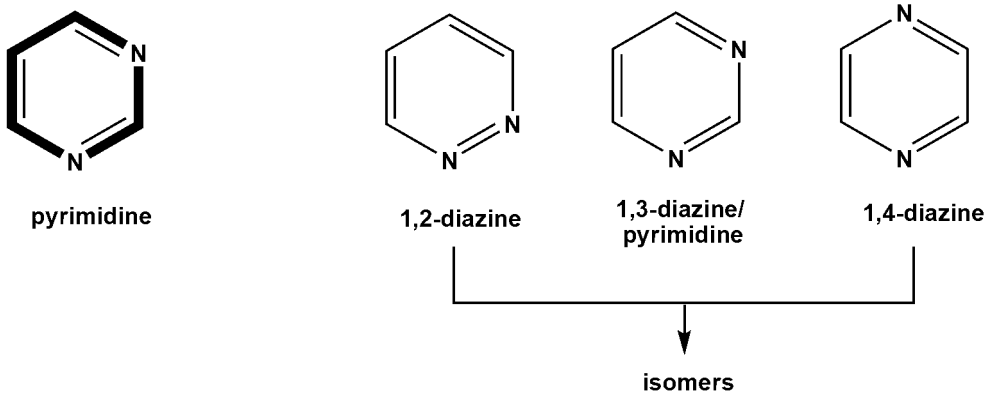

Figure 1.2.1.1. Pyrimidine and its two isomers.

Perimidines are perinaphtho-fused pyrimidines that can be classified under nitrogen-containing heterocyclic organic compounds which exhibit characteristics of both π-deficient (pyridine systems) and π-excessive systems (pyrrole systems).[137, 138] see Figure 1.2.1.2.

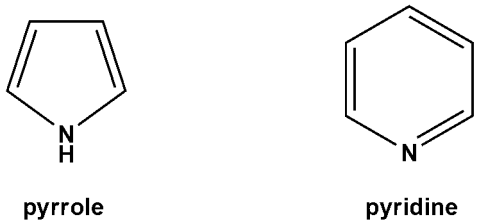

pyrrole pyridine

Figure 1.2.1.2. The molecules pyrrole and pyridine.

Perimidines have attracted attention because of their unusual simulated azines compounds. They contain nitrogen which have electron lone pairs (pyrrole-like nitrogen system) that plays a role in the π-systems of the molecule by transferring electron density from the heterocycle moiety to the naphthalene ring moiety. A perimidine has many properties in common with pyridine, as the number of nitrogen atoms in the ring increases, the ring pi electrons become less energetic and electrophilic aromatic substitution gets more difficult while nucleophilic aromatic substitution becomes more facile.[139]

1.2.2 Applications of Perimidines

Perimidines containing a naphthalene backbone are a class as heterocyclic organic compounds and have attracted attention due to their diverse uses in biological, pharmacological and optoelectronic applications, as well as their potential as organocatalyst compounds. Perimidines have medicinal applications as anti-ulcer, anti-microbial, and anti-fungal agents, and several studies have been performed in the field of biological applications.[140-143] The importance of the perimidines to intercalate into the DNA showed to be effective due to its liphophilicity which enables it to bind to the tumor DNA cell and carcinogenic cell line[144], i.e. breast cancer (MCF-7)[145] and liver cancer (HEPG-2) which showed promising activity and have demonstrated reduction in the growth of cancer cells, but to date none of the perimidines showed good in-vivo activity.[146] Similar to *peri*-disubstituted naphthalenes, they are also used as dye pigments in the manufacturing of plastics, and have been used in synthesis of photovoltaic devices[147] and are efficient intermediates towards the preparations of carbene ligands**.**[148]

Perinaphtho-fused pyrimidines are a heterocyclic aromatic organic compound similar to benzene and pyridine, containing two nitrogen atoms at positions one and three of the six-member ring. The aromaticity of perinaphtho-fused pyrimidines is similar to that of benzene.

1.2.3 Synthesis of Perimidines

1.2.3.1 Schiff Base Reaction

A Schiff base reaction occurs when carbonyl compounds, e.g. aldehyde and ketones, undergo condensation reaction with primary amines. Ketones form Schiff base compounds faster than aldehydes, and the reaction takes place in different solvents and reaction conditions. Most successful condensation reactions are performed in either methanol or ethanol, and a condensation reaction is best favoured by a dehydrating agent like molecular sieves or magnesium sulfate, with the Dean Stark apparatus typically used to remove water. During the preparation of Schiff base, the reaction ratio of primary amine-to-carbonyl is (1:1), whereas diamine requires a (2:1) reaction ratio. The prepared compounds are purified by chromatographic techniques using silica gel, and this process often lead to decomposition of compounds through hydrolysis. A heteroatom amine compounds could be used to prepare ligands as the presence of the donor heteroatom provide binding sites for metal salts.

1.2.3.2 Synthesis of Perimidines: Reactions Involved with Diamines

Perimidines were first synthesized in 1874[149] but only gained better understanding in 1909.[150] Various routes to prepare perimidines have been developed but generally these are organic molecules which are derived from the reaction between *1,8*-dianimonaphhalene and carbonyl containing compounds such as ketones, aldehydes, acyl chloride, aryl anhydrides carboxylic acids and formic acids. They form as a result of electrophilic and oxidation reactions[151] and various 2-substituted 2,3-dihydro-1H-perimidines have been reported.[152]

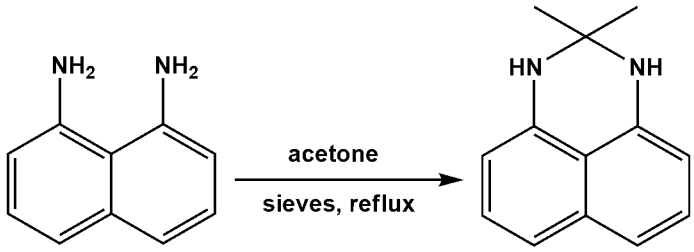

Scheme 1.2.1.1. The condensation reaction of 1,8-diaminonaphthalene and acetone.[153]

Many perimidine compounds are prepared from the reaction of *1,8*-diaminonaphthalene with formic acid, acyl chlorides, aryl anhydrides, aldehydes and ketones. Treatment of aldehyde with *1,8*-diaminonaphthalene in either alcohol or benzene lead to the development of 2,3-dihydroperimidine compounds. The substituents for R = H, CH_3, C_2H_5, C_6H_5, *iso*-C_6H_{13}, halogens, nitrophenyls etc, see Figures 1.2.1.3 and Scheme 1.2.1.2.[154, 155]

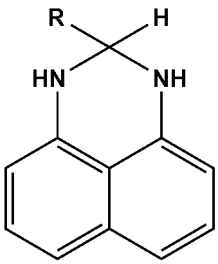

Figure 1.2.1.3. Molecular compound of 2,3-dihydroperimidines.

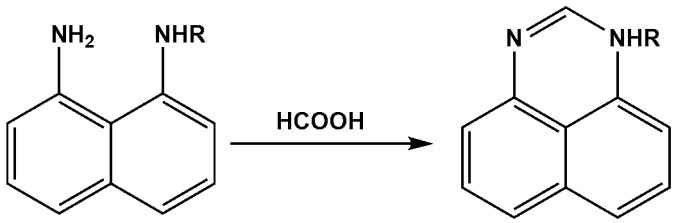

Scheme 1.2.1.2. Reaction of diamine reacting with formic acid, R = H, CH3, C6H6 etc.[156, 157]

The structures of perimidine compounds differ based on the agents used during the reactions. When diamines are treated with acyl halides they form the compounds in Scheme 1.2.1.3. Other examples of acyl halide compounds are 1,2-disubstituted perimidine,[158] 1,4-bis(2-perimidinyl)benzene and 1,5-bis(2-perimidinyl)naphthalene.[159]

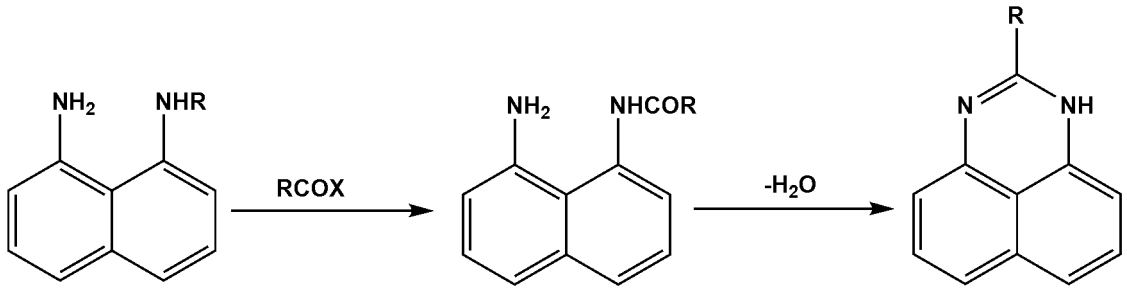

Scheme 1.2.1.3. The formation of perimidine compound from acyl halides.

When 1-amino-8-dimethylaminonaphthalene is refluxed with acetic anhydride 1,2-dimethylperimidine is formed. This reaction forms an intermediate compound at room temperature and at elevated temperature N-methyl is eliminated. Reaction of 1,8-diaminonaphthalene with acetic anhydride or trifluoroacetic anhydride yield either 2-methyl and 2-trifluromethyl-perimidine.[160-163]

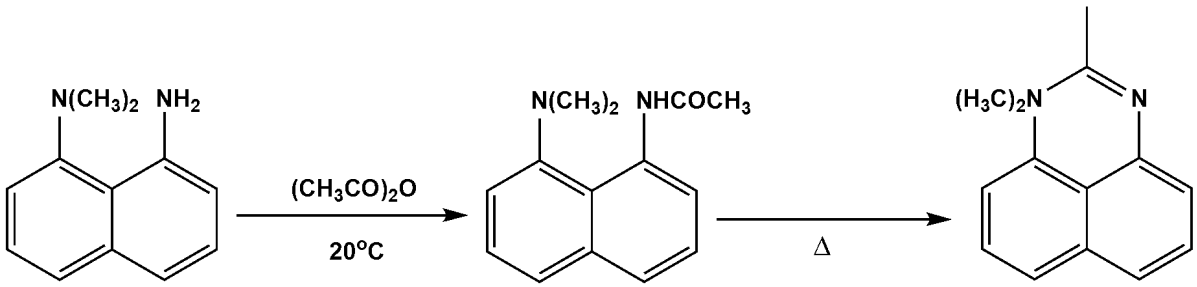

Scheme 1.2.1.4. Synthesis of perimidine from acetic anhydride.

1.2.4 Ring Opening of Perimidines to Asymmetric Amines

The condensation reaction of *1,8*-diaminonaphthalene with ketones such as acetone,[153] lead to the formation of perimidines, Scheme 1.2.1.1and Scheme 1.2.1.5. The naphthalene derived perimidines are 14π-electron compound with some electrons not delocalised, limiting its aromaticity behaviour.

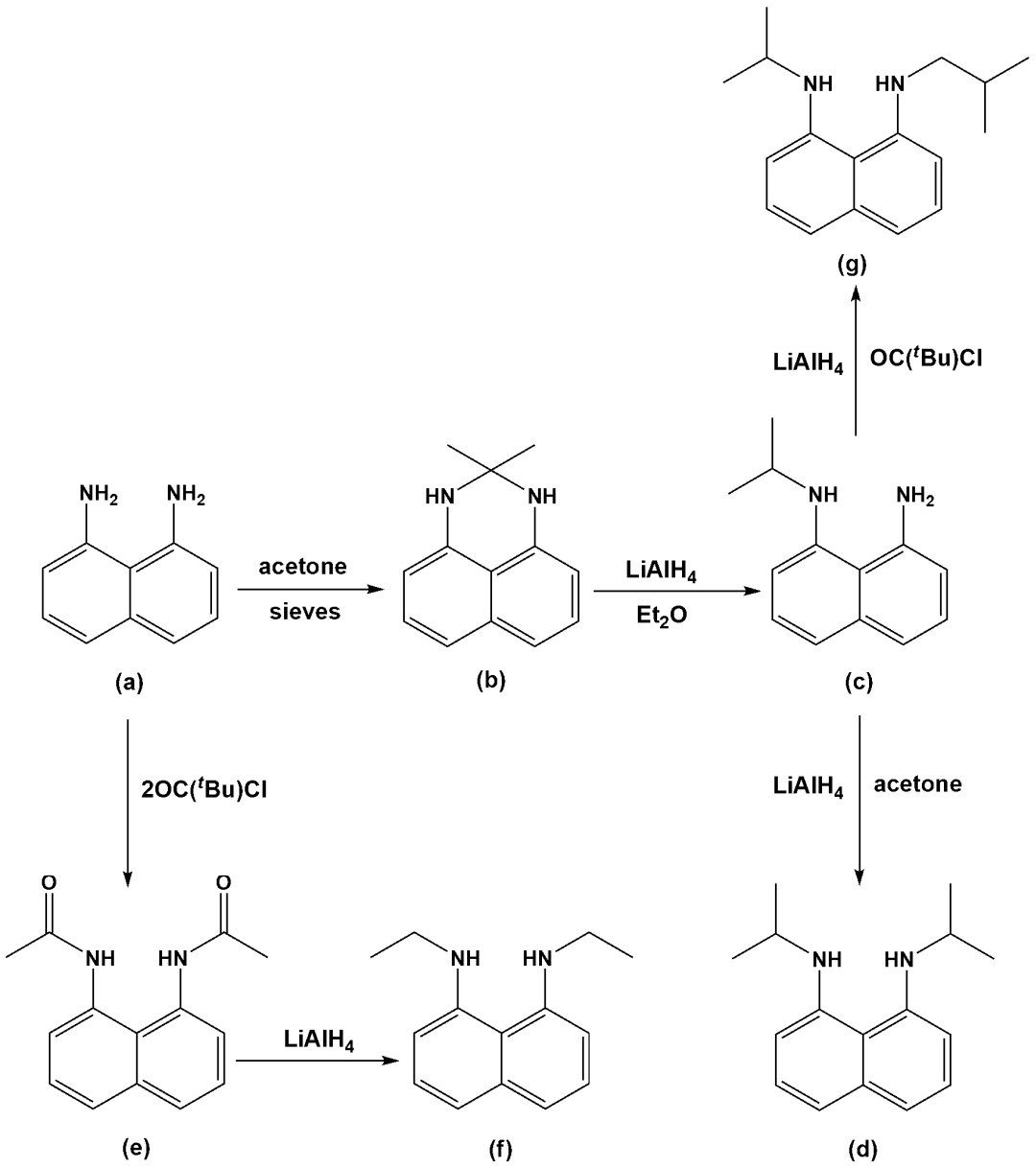

Scheme 1.2.1.5. A typical synthesis methodology leading to a ring opening reaction.

Reduction of perimidines are caused when perimidine **(b)** is treated with strong excess reducing agent such as $LiAlH_4$, which leads to the bond of central *C*-atom to cleave and the perimidine ring opens, leading to the formation of mono-isopropyl-*1,8*-diaminonaphthalene **(c)**. Treatment of the mono-isopropyl-*1,8*-diaminonaphthalene **(c)** with acetone or other ketones containing a long side chain of hydrocarbon give rise to Schiff Base reaction. Further treatment of the compound with excess $LiAlH_4$ reduces the carbonyl group and forms a symmetrical or asymmetric compound. The stability of the molecules depends on the state of the molecules, e.g. solid or liquid oils. Solid compounds are generally more stable for a longer period while

the liquid compounds in non-polar solvents especially chlorinated solvents result in a steady and constant equilibrium between amine and imine which then stabilizes as imines.

1.2.5 Metal Complexes of Perimidine Containing Moieties

The coordination chemistry of perimidine ligands attracts interest because they are heterocyclic systems (cyclic and acyclic) containing nitrogen, oxygen, and sulfur donor atoms which can readily coordinate to metal centers. Perimidines are an interesting group of compounds because they have high π-stacking ability, electron affinity, and reduction potential, and also exhibit a diverse range of biological activities. Metal complexes of perimidine ligands are very rare, especially those containing sold state X-ray structures. In 2013, Azam *et al*., isolated the Pd(II) complex containing 2-(2-thienyl)-2,3-dihydro-1H-perimidine and reported the crystal structure of the ligand but not of the corresponding complex. Below is the proposed coordination mode of the Pd(II) center chelated by the thienyl perimidine.[164] The complexes were prepared according to the Scheme1.2.1.6.

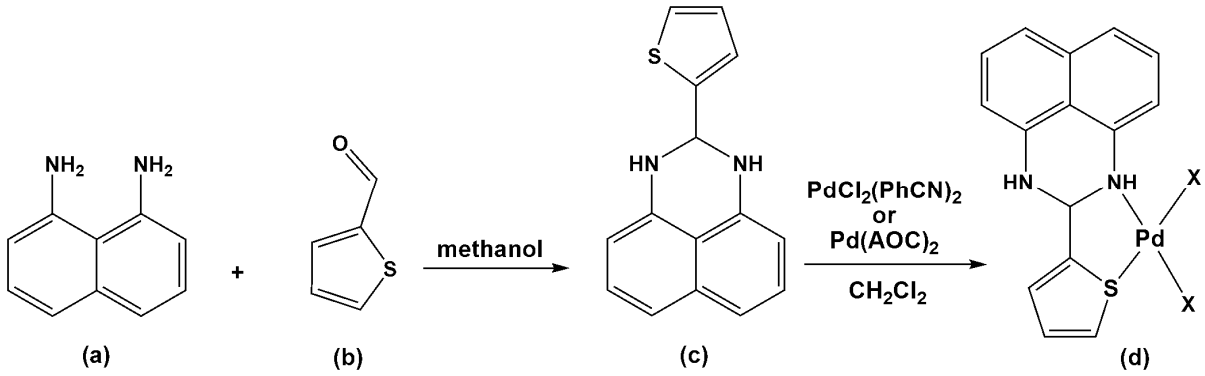

Scheme 1.2.1.6. Synthesis of 2-(2-thienyl)-2,3-dihydro-1H-perimidine and Pd(II) complexes.

Ashwinbhai *et al*., prepared a diversity of perimidine metal complexes and proposed their coordination modes with the aid of a variety characterization techniques, whilst elemental analysis aided to determine the bulk purity. The metal complexes were prepared by treating 2-chloro-1-(2, 3-dihydro-perimidin-1-yl)-ethanone **(a)** with 5-amino-8-hydroxy quinoline **(b)** to afford a 2-(8-hydroxy-quinolin-5-ylamino)-1-(5-methyl-4-methylene-1,4-dihydro-2H-quinazolin-3-yl)-ethanone (PEHQ) **(c)**, Scheme 1.2.1.7. The reaction of (PEHQ) **(c)** with various metal acetates such Cu(II),Co(II) ,Ni(II), Mn(II) and Zn(II) resulted in the expected products, but without supporting molecular structures. The complexes were examined for antimicrobial activity and gave positive results.[165]

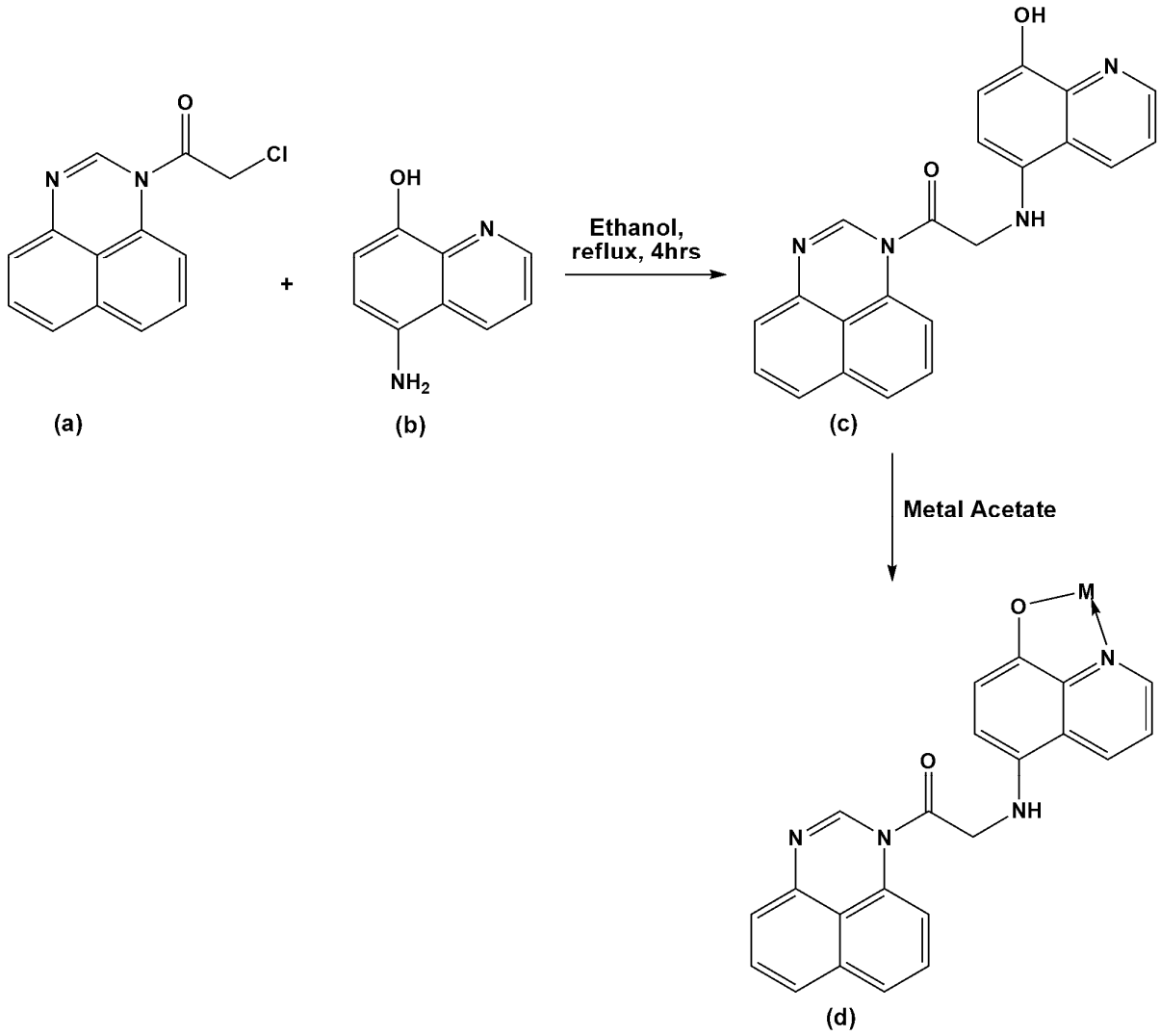

Scheme 1.2.1.7. The synthesis route of (c) and its possible coordination mode to metal salts such as such Cu(II),Co(II) ,Ni(II), Mn(II) and Zn(II) of acetate ion.

Roy *et al*, prepared two interesting NNS tridenate Schiff base ligands of S-methyl-3-((2-S-methyl-6-methyl-4-pyrimidyl)methyl)dithiocarbazate **(a)** and S-benzyl-3-((2-S-methyl-6-methyl-4-pyrimidyl)methyl)dithiocarbazate **(b)**, see Scheme 1.2.1.8.

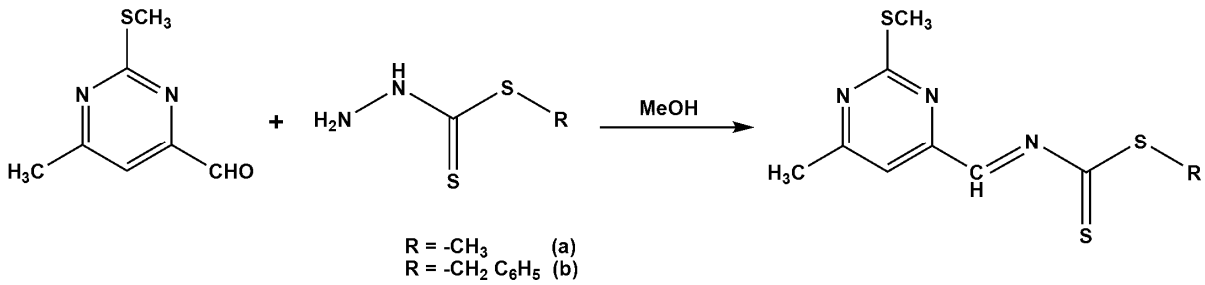

Scheme 1.2.1.8. Synthesis of NNS tridenate *via* Schiff base reaction.

Ni(II) and Co(III) complexes were synthesised in a methanolic solution and afforded quality X-ray crystals. All the bis-chelate complexes have a distorted octahedral arrangement with an N_4S_2 chromophore around the central metal. Each ligand binds the metal using the pyrimidyl and azomethine nitrogen and thiolato sulfur atoms (except in the nickel complex, one ligand molecule uses the thione sulfur instead of thiolato sulfur atom). In the Ni(II) complex, one of the ligands behaves as a neutral tridentate, and the other as a uninegative tridentate ligand, whereas in the Co(III) complex, the ligands are monoanionic tridentate. The complexes were analyzed by single crystal X-ray diffraction and significant differences concerning the distortion from an octahedral geometry of the coordination environment were observed.

1.2.6 Characterization Techniques of Perimidines

The simple perimidines and other perimidines derived from the 1,8-diaminonaphthalene backbone are characterized by well-known spectroscopic techniques. A variety of spectral techniques such as infrared (IR), nuclear magnetic resonance (NMR), mass spectrometer (MS) techniques have been employed for perimidines. Because of the lack of quality single crystals, and challenges encountered to grow crystals, most metal complexes have proposed structures.

For a large number of perimidines and its metal complexes consisting of symmetric and asymmetric substituents, only infrared spectra and elemental analysis have been used for their characterization. For perimidines containing 1,8-diaminonaphthalenes, the vibration bands of ν(NH) are observed around 3300-3500 cm^{-1}.[153] Very sharp and strong vibrational bands of the naphthalene ν(C=C) are at 1600-1400 cm^{-1}. For the simplest perimidines analogue shown in in Scheme 1.2.1.4, the IR values reported by Saha and Mukherjee and others reveals that the bands in the 1590-1410 cm^{-1} region and at 1010 cm^{-1} and 745 cm^{-1} are assigned to the ν(C=C) and ν(C-N) and out-of-plane deformation, respectively, for both 1,2-diazole (pyrazole) and (1, 3)-diazine (pyrimidine) systems,[166] some important vibrational assignments were reported by Mostafa.[167]

Perimidines offer excellent scope for multinuclear NMR spectroscopy, as shown by Chen *et al.*,[168]

1.3 Motivation for Research, and Overview of Chapters

In this thesis, two aspects in the reactivity of *1,8*-diaminonaphthalene are investigated, namely the chemistry of i) aminophosphines and ii) perimidines.

Looking at the background of naphthalene and aminophosphines, one observes that there are many reported primary and secondary aminophosphines compared to diaminophosphines. But known diaminophosphines are prepared from diaminobenzene derivatives and ethane-1,2-diamine and therefore diaminophosphines containing naphthalene are rare. The use of *1,8*-diaminonaphthalene could help bridge the gap between the synthesis of simple (mono)-aminophosphines and diaminophosphines ligands, and provide good templates for synthesis of metal complexes. The applications of aminophosphines leans toward hydrogenation catalysis and more recently cross-coupling, hydroformylation, conjugate addition, cycloaddition and allylic alkylation type reactions with any antimicrobial studies lacking. This study focused on the synthesis of diaminophosphines with *1,8*-diaminonaphthalene using phosphines, and looked into antimicrobial studies for these compounds for the first time.

Perimidines are heteroatomic systems which are divided into excess π-electrons and deficiency π-electron compounds. There is much work done on perimidines, especially on the perimidine compounds that resembles the two isomeric diazines, but perimidines derived from *1,8*-diaminonaphthalene are scarce and still a work in progress. Constructing perimidine complexes derived from *1,8*-diaminonaphthalene is challenging because of the instability of the metal complexes in solution , presumably due to coordination induced by the NH bond, resulting in relatively easy cleavage of the P-N bond. Heterocycles are important class of compounds because more than half of their known organic compounds are used in medicine. Examples of such compounds are quinine, papaverine, emetine, theophylline, atropine, procaine, codeine and morphine as natural drugs. Therefore expanding perimidine ligands to metal complexes may enhance their activity. This study also prepared perimidines derived from *1,8*-diaminonaphthalene and their metal complexes to further study their antimicrobial activities.

1.3.1 Overview

This thesis contains two sections (aminonaphthalene and perimidine chemistry) captured in one chapter, but treated as separate entities. This is due to the fact that the background and the scientific aims and objectives for each section vary. Therefore, the content of the work and the

references are dealt with separately at the end of each chapter, but the molecule numbering is chronological and consistent throughout the thesis and molecules will thus appear in different chapters with same numbering. The two sections in the thesis are however connected by the common backbone of *1,8*-diaminonaphthalene. It is a precursor used to synthesis *peri*-disubstituted naphthalene compounds. The thesis is divided into six chapters and below is a summary of the contents of each chapter.

Chapter 1 presents the background and the motivation to investigate the chemistry of the *peri*-disubstituted naphthalene. The *peri*- disubstituted *1, 8*-diaminonaphthalene is a precursor used to synthesise compounds of the bis(amino)phosphines and perimidines reported in this thesis. The introduction outlines the chemistry of naphthalene and aminophosphines and that of the perimidines. A general introduction to the chemistry of naphthalene and aminophosphines are presented and includes applications. Subsection **1.2** introduces the chemistry of the perimidines and it illustrates the role of the perimidine ligands in the formation of the metal complexes. The chapter also contains the main aims, objectives, and an overview by a chapter of the thesis in the subsection **1.3**.

Chapter 2 states the reaction conditions used to prepare the compounds, followed by outlining the chemicals used in the preparations of the metal salts and other precursors. This chapter list the spectroscopic techniques used to characterize the compounds. The chapter reports the experimental procedures for bis(amino)phosphine ligands and their metal complexes and also the experimental procedures for perimidines compounds and their metal complexes. The experimental procedures for the data collection of single crystal X-ray crystallography is reported in the subsection **2.1.4**.

Chapter 3 discusses the synthesis of bis(amino)phosphine ligands, spectroscopic analysis and crystal structures. The bis(amino)phopshine ligands of the type [($C_{10}H_6$(1,8-$NHPPh_2$)$_2$)] **(1)**, [$C_{10}H_6$(1,8-NH-P{$CH(CH_3)_2$}$_2$)$_2$] **(2)** [$C_{10}H_6$(1,8-$NHPPh_2O$)$_2$] **(14)**, [$C_{10}H_6$(1,8-$NHPPh_2S$)$_2$] **(15)** and [($C_{10}H_6$(1-$NHPPh_2O$)(8-$NHPPh_2Se$] **(16)** are extensively discussed. The chapter also discuss the results for the compounds attained in the study. The use of the MS, IR, NMR and UV-Vis spectroscopic techniques serves as the supporting information. The compounds have been characterized by single crystal X-ray crystallography and TGA. The synthesis of perimidines, spectroscopic analysis and crystal structure are discussed. This section deals with the perimidine compounds of the type [$C_{10}H_6$(1,8-$NH)_2$(C{R}{(R')].

Chapter 4 discusses the synthesis of bis(amino)phosphine complexes, spectroscopic analysis, and crystal structures. The bis(amino)phosphine complexes of the type $[M_2(\mu\text{-}X)_2\{C_{10}H_6(1,8\text{-}NHPR_2)_2\}_2]$, $[Ag_4(\mu_3\text{-}I)_2(\mu_2\text{-}I)_2\{C_{10}H_6(1,8\text{-}NHPPh_2)_2\}_2]$, $[M\{C_{10}H_6(1,8\text{-}NHPPh_2)_2\}_2]PF_6$, $[Cu_4(\mu_3\text{-}X)_2(\mu_2\text{-}X)_2(O\{PR_2\}_2)_2]$ and $[M\{C_{10}H_6(1,8\text{-}NHPPh_2E)_2\}_2]X$ are discussed. This chapter also discusses the results for the complexes synthesized and use the spectroscopic techniques such as MS, IR, NMR and UV-Vis to support the synthesis. The complexes have been characterized by single crystal X-ray crystallography and TGA. Subsection **4.2** discusses the synthesis of perimidine complexes, spectroscopic data and crystal structures. The perimidine complexes of $[Ni(H_2O)_2\{C_{10}H_6(1,8\text{-}NH)_2(CH_3)(C_5H_4N)\}_2]2Cl$, $[ZnCl_2\{C_{10}H_6(1,8\text{-}NH)_2(CH_3)(C_5H_4N)\}_2]$ and $[CdI_2\{C_{10}H_6(1,8\text{-}NH)_2(CH_3)(C_5C_4N)\}_2]$ are discussed.

Chapter 5 discusses the investigation into the electronic properties of the aminophosphines as well as the perimidine compounds *via* theoretical calculations. This chapter also covers the results obtained for the antimicrobial studies for the aminophosphine ligands and their complexes and perimidines compounds and their complexes in the subsection **5.3**.

Chapter 6 gives a summary of the work presented in this thesis, and future prospects.

1.3.2 Research Aims and Objectives

The work presented herein aims to cover the five principles which are as follows:

- Synthesis and characterization of new bis(amino)phosphines to be used as ligands.
- Synthesis and characterization of new perimidines to be used as ligands.
- Synthesis characterization of new Cu(I) and Ag(I) bis(amino)phosphine complexes.
- Synthesis characterization of new Ni(II), Zn(II) and Cd(II) perimidinyl complexes.
- The investigation into the antibacterial applications of the aminophosphines and perimidine compounds.

The research objectives are as follows:

1. Synthesis of new bis(amino)phosphine ligands and their metal complexes.
2. Synthesis and characterization of new bis(amino)phosphine ligands based on chloro-phosphines using trimethylamine, 4-(dimethylamino) pyridine and *1,8*-diaminonaphthalene.
3. Synthesis and characterization of new Cu(I) and Ag(I) complexes derived from bis(amino)phosphine ligands.
4. Design a synthesis method for new perimidine compounds and their metal complexes.
5. Synthesis and characterization of new perimedine compounds based on ketone using alkyl, aryl and 1,8-diaminonaphthalene as precursors.
6. Synthesis and characterization of new Ni(II), Zn(II) and Cd(II) complexes derived from pyridinyl perimidine ligand.
7. Full characterization of all new compounds (bis(mino)phosphine and perimidine) isolated using mass spectrometry, ^{1}H, ^{13}C NMR, FT-IR, UV-Vis spectroscopy and thermogravimetric analysis.
8. Investigate single crystal X-ray crystallographic studies of new bis(mino)phosphine ligands and their complexes as well as new perimidine compounds and their complexes.
9. Perform density functional theory (DFT) studies based on crystallographic structures of bis(amino)phosphine ligands and complexes including perimidine compounds obtained in this work.
10. Carry out antibacterial studies on bis(amino)phosphine ligands and their metal complexes as well as perimidine organic compounds and their metal complexes.

1.4 References

1. J. Oddershede and S. Larsen, *J. Phys. Chem. A*, 2004, 108, 1057-1063.
2. J. Kidd, *Philos. Trans. R. Soc. London, Ser. A*, 1821, 111, 209-221.
3. E. Jakobsson and L. Asplund, *Anthropogenic Compounds Part K*, 2000, 3, 97-126.
4. V. Balasubramaniyan, *Chem. Rev.*, 1966, 66, 567-641.
5. G. Gafner, *Acta Crystallogr.*, 1962, 15, 1081-1092.
6. L. F. Fieser and A. M. Seligman, *J. Am. Chem. Soc.*, 1939, 61, 136-142.
7. R. W. Franck and E. G. Leser, *J. Am. Chem. Soc.*, 1969, 91, 1577-1578.
8. P. Kilian, A. M. Slawin and J. D. Woollins, *Dalton Trans.*, 2003, 3876-3885.
9. P. Kilian, A. M. Slawin and J. D. Woollins, *Phosphorus, Sulfur Silicon Relat. Elem.*, 2004, 179, 999-1002.
10. A. Bondi, *J. Phys. Chem.*, 1964, 68, 441-451.
11. J. Handal, J. G. White, R. W. Franck, Y. H. Yuh and N. L. Allinger, *J. Am. Chem. Soc.*, 1977, 99, 3345-3349.
12. J. F. Blount, F. Cozzi, J. R. Damewood, L. D. Iroff, U. Sjostrand and K. Mislow, *J. Am. Chem. Soc.*, 1980, 102, 99-103.
13. F. R. Knight, R. A. M. Randall, K. S. Athukorala Arachchige, L. Wakefield, J. M. Griffin, S. E. Ashbrook, M. Bühl, A. M. Z. Slawin and J. D. Woollins, *Inorg. Chem.*, 2012, 51, 11087-11097.
14. H. Fujihara and N. Furukawa, *J. Mol. Struct.: THEOCHEM*, 1989, 186, 261-272.
15. F. R. Knight, A. L. Fuller, A. M. Z. Slawin and J. D. Woollins, *Polyhedron*, 2010, 29, 1956-1963.
16. D. Cruickshank, *Acta Crystallogr.*, 1957, 10, 504-508.
17. G. Ferguson and J. M. Robertson, *Adv. Phys. Org. Chem., ed. V. Gold, Academic Press*, 1963, 1, 203-281.
18. S. M. Aucott, H. L. Milton, S. D. Robertson, A. M. Slawin, G. D. Walker and J. D. Woollins, *Chem. Eur. J.*, 2004, 10, 1666-1676.
19. K. Kobayashi, S. Shinhara, M. Moriyama, T. Fujii, E. Horn, A. Yabe and N. Furukawa, *Tetrahedron Lett.*, 1999, 40, 5211-5214.
20. I. Majerz and T. Dziembowska, *J. Phys. Chem. A*, 2014, 118, 7118-7129.
21. W. Nakanishi, S. Hayashi and S. Toyota, *J. Org. Chem.*, 1998, 63, 8790-8800.
22. W. Nakanishi, S. Hayashi and T. Uehara, *J. Phys. Chem. A*, 1999, 103, 9906-9912.
23. T. Wiedmann and K. Ballschmiter, *Fresenius J Anal Chem*, 346, 800-804.
24. D. W. J. Cruickshank and R. A. Sparks, *Proc. Math. Phys. Eng. Sci.*, 1960, 258, 270-285.
25. E. Hückel, *Z. Phys. A-Hadron Nucl.*, 1931, 70, 204-286.
26. V. I. Minkin, M. N. Glukhovtsev and B. Simkin, *Aromaticity and antiaromaticity*, J. Wiley & Sons, 1994.
27. A. Streitwieser, *Molecular orbital theory for organic chemists, Wiley, New York*, 1961.
28. M. J. S. Dewar and C. d. Llano, *J. Am. Chem. Soc*, 1969, 91, 709-795.
29. A. Kekuié, *Justus Liebigs Ann. Chem.*, 1866, 137, 129-196.
30. J. Đurđević, B. Furtula, I. Gutman and S. Radenković, *Kragujevac Journal of Science*, 2006, 28, 57-64.
31. A. Moyano and J. C. Paniagua, *J. Org. Chem.*, 1986, 51, 2250-2257.
32. E. Clar, *Polycyclic Hydrocarbons, Academic Press Inc., London*, 1964.
33. M. Zander, *Angew. Chem*, 1960, 72, 513.
34. M. Randic, *J. Am. Chem. Soc.*, 1977, 99, 444-450.
35. D. Klein and N. Trinajstic, *Pure Appl. Chem.*, 1989, 61, 2107-2115.
36. L. Pauling and G. W. Wheland, *J. Chem. Phys.*, 1933, 1, 362-374.
37. S. Nikolić, M. Randić, D. J. Klein, D. Plavšić and N. Trinajstić, *J. Mol. Struct.*, 1989, 198, 223-237.

38. M. Randić, D. Plavšić and N. Trinajstić, *J. Mol. Struct.: THEOCHEM*, 1989, 185, 249-274.
39. G. Booth, in *Ullmann's Encyclopedia of Industrial Chemistry*, Wiley-VCH Verlag GmbH & Co. KGaA, 2000, DOI: 10.1002/14356007.a17_009.
40. G. Collin, H. Höke and H. Greim, *Ullmann's encyclopedia of industrial chemistry*, 2003.
41. A. Michaelis, *Justus Liebigs Annalen der Chemie*, 1903, 326, 129-258.
42. M. Becke-Goehring and J. Schulze, *Chem. Ber.*, 1958, 91, 1188-1195.
43. M. Oliana, F. King, P. N. Horton, M. Hursthouse and K. K. Hii, *J. Org. Chem.*, 2006, 71, 2472-2479.
44. K. Abdur-Rashid, R. Guo, A. J. Lough, R. H. Morris and D. Song, *Adv. Synth. Catal.*, 2005, 347, 571-579.
45. C. Romming and J. Songstad, *Acta Chem. Scand. Ser. A*, 1978, 32, 689-699.
46. S. Priya, M. S. Balakrishna, J. T. Mague and S. M. Mobin, *Inorg. Chem.*, 2003, 42, 1272-1281.
47. S. Priya, M. S. Balakrishna and S. M. Mobin, *Polyhedron*, 2005, 24, 1641-1650.
48. M. C. B. Dolinsky, W. O. Lin and M. L. Dias, *J. Mol. Catal. A: Chem.*, 2006, 258, 267-274.
49. G. Ewart, A. P. Lane, J. McKechnie and D. S. Payne, *J.Chem.Soc.A*, 1964, 1543-1547.
50. J. R. VanWazer and L. Maier, *J. Am. Chem. Soc.*, 1964, 86, 811-814.
51. A. Tarassoli, R. C. Haltiwanger and A. D. Norman, *Inorg. Chem.*, 1982, 21, 2684-2690.
52. J. Gopalakrishnan, *Studies on tricoordinate P(III)-N systems: synthesis, structure and reactivity, Ph.D. Thesis, Department of Chemistry, Indian Institute of Technology Madras, Chennai, India*, 1998, pp. 245.
53. D. F. Shriver and M. A. Drezdzon, *The Manipulation of Air-sensitive Compounds, 2nd edn. John Wiley and Sons Inc.: New York*, 1986.
54. R. J. Errington, *Advanced Practical Inorganic and Metalorganic Chemistry. Blackie Academic and Professional: London*, 1997.
55. D. D. Perrin, *Purification of laboratory chemicals / D. D. Perrin and W. L. F. Armarego and D. R. Perrin*, Pergamon Press, Oxford ; New York, 1980.
56. D. D. Perrin, W. L. F. Armarego and D. R. Perrin, *Purification of Laboratory Chemicals. Pergamon Press: Oxford*, 1980.
57. K. Maartmann-Moe, C. Romming and J. Songstad, *Acta Chem. Scand. A*, 1982, 36, 9.
58. C. Romming, *Acta Chem. Scand. A*, 1980, 34.
59. R. F. Hudson, *Structure and mechanism in organophosphorus chemistry / R.F. Hudson*, Academic Press, London ; New York, 1965.
60. K. Issleib, *Kristall und Technik*, 1981, 16, 456-456.
61. R. B. King and P. Sundaram, *J. Org. Chem.*, 1984, 49, 1784-1789.
62. C. Romming, K. Maartmann-Moe and J. Songstad, *Acta Chem. Scand. A*, 1984, 38, 349-357.
63. J. G. Verkade and L. D. Quin, *Phosphorus-31 NMR Spectroscopy in Stereochemical Analysis. VCH: Florida*, 1987.
64. J. A. Nuretdinov, E. I. Loginova and L. V. Nurmukhamedova, *Bull. Acad.Sci. USSR*, 1973, 22, 2765.
65. S. O. Grim and E. D. Walton, *Inorg. Chem.*, 1980, 19, 1982-1987.
66. R. R. Carlson and D. W. Meek, *Inorg. Chem.*, 1974, 13, 1741-1747.
67. S. Priya, M. S. Balakrishna, J. T. Mague and S. M. Mobin, *Inorg. Chem.*, 2003, 42, 1272-1281.
68. C. A. Tolman, *Chem. Rev.*, 1977, 77, 313-348.
69. C. A. Tolman, *J. Am. Chem. Soc.*, 1970, 92, 2956-2965.
70. C. A. Tolman, *J. Am. Chem. Soc.*, 1970, 92, 2953-2956.
71. T. L. Brown and K. J. Lee, *Coord. Chem. Rev.*, 1993, 128, 89-116.
72. Z. Freixa and P. W. N. M. VanLeeuwen, *Dalton Trans.*, 2003, 1890-1901.
73. P. Dierkes and P. W. N. M. VanLeeuwen, *J. Chem. Soc., Dalton Trans.*, 1999, 1519-1530.

74. M. S. Balakrishna, S. Priya and R. Panda, *Phosphorus, Sulfur Silicon Relat. Elem*, 2004, 179, 911-914.
75. M. L. Clarke, D. J. Cole-Hamilton, A. M. Slawin and J. D. Woollins, *Chem. Commun.*, 2000, 2065-2066.
76. S. A. Katz, V. S. Allured and A. D. Norman, *Inorg. Chem.*, 1994, 33, 1762-1769.
77. Q. Zhang, G. Hua, P. Bhattacharyya, A. M. Slawin and J. D. Woollins, *Dalton Trans.*, 2003, 3250-3257.
78. M. S. Balakrishna, T. K. Prakasha, S. S. Krishnamurthy, U. Siriwardane and N. S. Hosmane, *J. Organomet. Chem.*, 1990, 390, 203-216.
79. I. M. Dixon, E. Lebon, G. Loustau, P. Sutra, L. Vendier, A. Igau and A. Juris, *Dalton Trans.*, 2008, 5627-5635.
80. M. S. Balakrishna, D. Suresh, P. P. George and J. T. Mague, *Polyhedron*, 2006, 25, 3215-3221.
81. S. M. Aucott, A. M. Slawin and J. D. Woollins, *J. Chem. Soc., Dalton Trans.*, 2001, 2279-2287.
82. S. M. Aucott, M. L. Clarke, A. M. Slawin and J. D. Woollins, *J. Chem. Soc., Dalton Trans.*, 2001, 972-976.
83. F. Majoumo-Mbe, P. Lönnecke and E. Hey-Hawkins, *Z. Anorg. Allg. Chem.*, 2008, 634, 2385-2390.
84. K. G. Moloy and J. L. Petersen, *J. Am. Chem. Soc.*, 1995, 117, 7696-7710.
85. P. C. Ford, E. Cariati and J. Bourassa, *Chem. Rev.*, 1999, 99, 3625-3648.
86. F. G. Mann, A. F. Wells and D. Purdue, *J. Chem. Soc.*, 1937, 1828.
87. R. Peng, M. Li and D. Li, *Coord. Chem. Rev.*, 2010, 254, 1-18.
88. R. Meijboom, R. J. Bowen and S. J. Berners-Price, *Coord. Chem. Rev.*, 2009, 253, 325-342.
89. H. Feng, X.-P. Zhou, T. Wu, D. Li, Y.-G. Yin and S. W. Ng, *Inorg. Chim. Acta*, 2006, 359, 4027-4035.
90. M. Scherer, D. Stein, F. Breher, J. Geier, H. Schönberg and H. Grützmacher, *Z. Anorg. Allg. Chem.*, 2005, 631, 2770-2774.
91. A. J. Blake, N. R. Brooks, N. R. Champness, M. Crew, A. Deveson, D. Fenske, D. H. Gregory, L. R. Hanton, P. Hubberstey and M. Schröder, *Chem. Commun.*, 2001, 1432-1433.
92. R. Peng, S.-R. Deng, M. Li, D. Li and Z.-Y. Li, *CrystEngComm*, 2008, 10, 590-597.
93. Z.-G. Zhao, J. Zhang, X.-Y. Wu, Q.-G. Zhai, L.-J. Chen, S.-M. Chen, Y.-M. Xie and C.-Z. Lu, *CrystEngComm*, 2008, 10, 273-275.
94. C. H. Arnby, S. Jagner and I. Dance, *CrystEngComm*, 2004, 6, 257-275.
95. C. E. Housecroft, *Coord. Chem. Rev.*, 1996, 152, 87-105.
96. P. Bhattacharyya and J. D. Woollins, *Polyhedron*, 1995, 14, 3367-3388.
97. G. Hu and E. M. Holt, *Acta Crystallogr., Sect. C*, 1994, 50, 1890-1892.
98. S. Miyano, M. Nawa, A. Mori and H. Hashimoto, *Bull. Chem. Soc. Jpn.*, 1984, 57, 2171-2176.
99. B. D. Vineyard, W. S. Knowles, M. J. Sabacky, G. L. Bachman and D. J. Weinkauff, *J. Am. Chem. Soc.*, 1977, 99, 5946-5952.
100. B. Gümgüm, O. Akba, F. Durap, L. T. Yıldırım, D. Ülkü and S. Özkar, *Polyhedron*, 2006, 25, 3133-3137.
101. O. Akba, F. Durap, M. Aydemir, A. Baysal, B. Gümgüm and S. Özkar, *J. Organomet. Chem.*, 2009, 694, 731-736.
102. T. Jiang, H. Chen, Y. Ning and W. Chen, *Chin. Sci. Bull.*, 2006, 51, 521-523.
103. B. Zhang, Y. Wang, T. Jiang and L. Xing, *Chin. J. Catal.*, 2006, 27, 416-420.
104. K. Blann, A. Bollmann, H. de Bod, J. T. Dixon, E. Killian, P. Nongodlwana, M. C. Maumela, H. Maumela, A. E. McConnell and D. H. Morgan, *J. Catal.*, 2007, 249, 244-249.
105. K. G. Gaw, M. B. Smith and J. W. Steed, *J. Organomet. Chem.*, 2002, 664, 294-297.

106. C. Kayan, N. Biricik, M. Aydemir and R. Scopelliti, *Inorg. Chim. Acta*, 2012, 385, 164-169.
107. N. Biricik, Z. Fei, R. Scopelliti and P. J. Dyson, *Helv. Chim. Acta*, 2003, 86, 3281-3287.
108. F. Majoumo, P. Lönnecke, O. Kühl and E. Hey-Hawkins, *Z. Anorg. Allg. Chem.*, 2004, 630, 305-308.
109. P. Bhattacharyya and J. D. Woollins, *Polyhedron*, 1995, 14, 3367-3388.
110. T. Q. Ly and J. D. Woollins, *Coord. Chem. Rev.*, 1998, 176, 451-481.
111. T. Appleby and J. D. Woollins, *Coord. Chem. Rev.*, 2002, 235, 121-140.
112. C. Ganesamoorthy, M. S. Balakrishna, P. P. George and J. T. Mague, *Inorg. Chem.*, 2007, 46, 848-858.
113. Z. Pan, M. T. Gamer and P. W. Roesky, *Z. Anorg. Allg. Chem.*, 2006, 632, 744-748.
114. M. A. Carvajal, J. J. Novoa and S. Alvarez, *J. Am. Chem. Soc.*, 2004, 126, 1465-1477.
115. R. Ahuja, M. Nethaji and A. G. Samuelson, *J. Organomet. Chem.*, 2009, 694, 1144-1152.
116. Z. Yu, Q.-F. Zhang, Y. Song, W.-Y. Wong, A. Rothenberger and W.-H. Leung, *Eur. J. Inorg. Chem.*, 2007, 2007, 2189-2197.
117. L. Han, L.-X. Shi, L.-Y. Zhang, Z.-N. Chen and M.-C. Hong, *Inorg. Chem. Commun.*, 2003, 6, 281-283.
118. R. Ahuja, M. Nethaji and A. G. Samuelson, *Inorg. Chim. Acta*, 2011, 372, 220-226.
119. Q.-F. Zhang, Z. Yu, A. Rothenberger, D. Fenske and W.-H. Leung, *Inorg. Chim. Acta*, 2007, 360, 1568-1574.
120. T. Tsukuda, A. Nakamura, T. Arai and T. Tsubomura, *Bull. Chem. Soc. Jpn.*, 2006, 79, 288-290.
121. R. Ahuja, M. Nethaji and A. G. Samuelson, *Polyhedron*, 2007, 26, 142-148.
122. S. Daly, M. F. Haddow, A. G. Orpen, G. T. A. Rolls, D. F. Wass and R. L. Wingad, *Organometallics*, 2008, 27, 3196-3202.
123. B. J. Johnson, S. V. Lindeman and N. P. Mankad, *Inorg. Chem.*, 2014, 53, 10611-10619.
124. W.-N. Zhao, L. Han and C.-C. Luo, *Acta Crystallogr. Sect. C*, 2008, 64, m280-m282.
125. J. Mo, H.-Y. Qian, X.-D. Du and W. Chen, *Acta Crystallogr. Sect. E*, 2007, 63, m2449.
126. V. Rosa, C. Fliedel, A. Ghisolfi, R. Pattacini, T. Aviles and P. Braunstein, *Dalton Trans.*, 2013, 42, 12109-12119.
127. H. Krishna, S. S. Krishnamurthy and M. Nethaji, *Inorg. Chim. Acta*, 2009, 362, 38-42.
128. J. Ellermann, J. Utz, F. A. Knoch and M. Moll, *Z. Anorg. Allg. Chem.*, 1996, 622, 1871-1878.
129. H. Liu, M. J. Calhorda, M. G. B. Drew, V. Felix, J. Novosad, L. F. Veiros, F. F. d. Biani and P. Zanello, *J. Chem. Soc., Dalton Trans.*, 2002, 4365-4374.
130. Q.-F. Zhang, J. Ding, Z. Yu, Y. Song, A. Rothenberger, D. Fenske and W.-H. Leung, *Inorg. Chem.*, 2006, 45, 8638-8647.
131. H. Krishna, S. S. Krishnamurthy and M. Nethaji, *Polyhedron*, 2006, 25, 3189-3200.
132. U. Schubert, D. Neugebauer and A. A. M. Aly, *Z. Anorg. Allg. Chem.*, 1980, 464, 217-232.
133. H. Krishna and S. S. Krishnamurthy, *Inorg. Chim. Acta*, 2007, 360, 3462-3466.
134. Q.-H. Wei, G.-Q. Yin, L.-Y. Zhang, L.-X. Shi, Z.-W. Mao and Z.-N. Chen, *Inorg. Chem.*, 2004, 43, 3484-3491.
135. H.-W. Xu, L.-X. Zhang and Y.-H. Li, *Synthesis and Reactivity in Inorganic, Metal-Organic, and Nano-Metal Chemistry*, 2013, 43, 6-9.
136. J. Gopalakrishnan, *Appl. Organomet. Chem.*, 2009, 23, 291-318.
137. P. Bazinet, T.-G. Ong, J. S. O'Brien, N. Lavoie, E. Bell, G. P. A. Yap, I. Korobkov and D. S. Richeson, *Organometallics*, 2007, 26, 2885-2895.
138. S. Anga, S. Biswas, R. K. Kottalanka, B. S. Mallik and T. K. Panda, *Can Chem Trans.*, 2014, 2, 72-82.
139. T. P. Selvam, C. R. James, P. V. Dniandev and S. K. Valzita, *Research in Pharmacy*, 2015, 2.
140. T. A. Farghaly and M. M. Abdalla, *Bioorg. Med. Chem.*, 2009, 17, 8012–8019.

141. V. Alagarsamy, V. R. Soloma and K. Dhanabal, *Bioorg. Med. Chem.*, 2007, 15, 235–241.
142. A. K. Ganguly, A. K. Doll and V. M. Girijavallabhan, *Curr. Med. Chem.*, 2001, 8, 1419–1436.
143. B. M. Banachiewicz and T. Kaminska, *Eur. J. Med. Chem.*, 2001, 1, 93–99.
144. J. M. Herbert, P. D. Woodgate and W. A. Denny, *J. Med. Chem.*, 1987, 30, 2081–2086.
145. T. Farghaly, E. Abbas, K. Dawood and T. El-Naggar, *Molecules*, 2014, 19, 740.
146. T. A. Farghaly and H. K. Mahmoud, *Arch. Pharm. Chem. Life Sci.*, 2013, 346, 392-402.
147. X. Wan, X. Lv, G. He, A. Yu and Y. Chen, *Eur. Polym. J.*, 2011, 47, 1018–1030.
148. P. Bazinet, G. P. A. Yap and D. S. Richeson, *J. Am. Chem. Soc.*, 2003, 125, 13314–13315.
149. *de Aguiar, A. Ber. Dtsch. Chem. Ges.*, 1874, 7, 309-319.
150. F. Sachs, *Ann. Chem.*, 1909, 53, 365.
151. V. Paragamian, M. B. Baker, B. M. Puma and J. Reale, *J. Heterocycl. Chem.*, 1968, 5, 591-597.
152. A. Mobinikhaledi, N. Forughifar and N. Bassaki, *Turk. J. Chem.*, 2009, 33, 555-560.
153. S. Maloney, A. M. Z. Slawin and J. D. Woollins, *Acta Crystallogr. E*, 2013, 69, o246-o246.
154. I. A. Smellie, A. Fromm, S. A. Moggach and R. M. Paton, *Carbohydr. Res.*, 2011, 346, 43-49.
155. F. D. Popp and A. Catala, *J. Heterocycl. Chem.*, 1964, 1, 108-109.
156. A. F. Pozharskii and V. Dal'Nikovskaya, *Russ. Chem. Rev.*, 1981, 50, 816-835.
157. F. Sachs and R. Forster, *Eur. J. Inorg. Chem.*, 1911, 44, 1738-1748.
158. E. A. Filatova, I. V. Borovlev, A. F. Pozharskii, Z. A. Starikova and N. V. Vistorobskii, *Mendeleev Commun.*, 2000, 10, 178-180.
159. Z. Yoshida, Y. Shimada and R. Oda, *J. Chem. Soc. Japan*, 1952, 55, 523-524.
160. V. G. Pesin, V. A. Sergeev and E. V. Barkalaya, *Chem. Heterocycl. Compd.*, 1971, 4, 587-588.
161. V. G. Pesin, V. A. Sergeev and E. V. Barkalaya, *Chem. Heterocycl. Compd.*, 1968, 4, 587-589.
162. V. Paragamian, M. Baker, B. Puma and J. Reale, *J. Heterocycl. Chem.*, 1968, 5, 591-597.
163. M. H. Elnagdi, S. M. Fahmy, E. A. A. Hafez, M. R. H. Elmoghayar and S. A. R. Amer, *J. Heterocycl. Chem.*, 1979, 16, 1109-1111.
164. M. Azam, I. Warad, S. I. Al-Resayes, N. Alzaqri, M. R. Khan, R. Pallepogu, S. Dwivedi, J. Musarrat and M. Shakir, *J. Mol. Struct.*, 2013, 1047, 48-54.
165. P. S. Ashwinbhai, F. Bux and A. Singh, *J.Chem.*, 2010, 3, 240-245.
166. N. Saha and D. Mukherjee, *Transition Met. Chem.*, 1987, 12, 156-159.
167. S. I. Mostafa, C. Papatriantafyllopoulou, S. P. Perlepes and N. Hadjiliadis, *Bioinorg Chem Appl.*, 2009, 2008.
168. W.-Z. Chen, H.-Y. Wei and D.-Y. Yang, *Tetrahedron*, 2013, 69, 2775-2781.

Chapter 2

Experimental

2.1 Experimental Section

2.1.1 General Procedures and Chemicals used for Bis(amino)phosphines and Perimidines

2.1.1.1 Materials and Measurements

Unless otherwise specified, all reactions were carried out using standard Schlenk or vacuum-line techniques under either nitrogen or an argon atmosphere. The reagents copper(I)halides, silver(I)halides, *1,8*-diaminonaphthalene, triethylamine, chlorodiphenylphosphine, chlorodiisopropylphosphine and 4-dimethylaminopyridine were purchased from Aldrich Chemical Company and used without further purification. Perimidines were prepared according to procedure methods reported on 2,3-dihydro-1H-perimidine.[1] All reaction solvents were dried before use and were saturated with nitrogen. The precursor $[M(CH_3CN)_4]PF_6$ (M = Ag and Cu) was synthesized according to the literature method.[2] The ligand $[C_{10}H_6(1,8\text{-}NHPPh_2S)_2]$ **(15)** was prepared according to the literature methods.[3] Ligand $[C_{10}H_6(1,8\text{-}NHPPh_2O)_2]$ (**14**) was prepared in our laboratory. The ligand $[C_{10}H_6(1,8\text{-}NHPPh_2)_2]$ **(1)** have not previously been isolated and herein we characterize the compound. We have also isolated ligand $[C_{10}H_6(8\text{-}NHPPh_2Se)(1\text{-}NHPPh_2O)]$ **(16)** in our laboratory. Silver complexes were prepared in the absence of light where the reaction vessel was covered with foil.

2.1.1.2 Anhydrous Solvent Drying

Tetrahydrofuran (THF), diethyl ether (Et_2O) and hexane were freshly distilled from sodium benzophenone ketyl. Dichloromethane (DCM) was distilled from calcium hydride (CaH_2) and toluene was distilled from calcium chloride ($CaCl_2$) or sodium benzophenone ketyl. Dimethyl sulfoxide (DMSO) and dimethylformamide (DMF) were dried *via* molecular sieves before usage. Despite being dry under distillation, the solvents were degassed prior to use and where necessary 4Å molecular sieves were used to dry the solvent before and during the reaction. The

pre-drying methods for the above solvents were discussed in the literature contained within the referenced literature by Williams and Lawton[4] and others.[5]

2.1.1.3 Schlenk Line Technique

The reactions performed in this work were mostly air and moisture sensitive and hence moisture and air free environment was created. This was achieved *via* a Schlenk line technique which consisted of a dual-manifold line glass. Prior to each experiment the solvent and/or chemicals underwent three cycles of a vacuum treatment, followed by a N_2 inlet cycle, in order to keep the reaction inert during synthesis. The vacuum outlet was also used to remove volatile solvent under high pressure which was trapped in a liquid N_2 trap.

2.1.1.4 NMR Spectroscopy

^{1}H, ^{13}C and ^{31}P NMR spectra were recorded on Bruker Ultra-Shield™ Avance^{III} operating at 400 MHz. Deuterated solvents were purchased from Merck. The chemical shift (δ) are reported with reference to $SiMe_4$ at 0.00 in parts per million. The NMR spectra were recorded at ambient temperature unless noted otherwise.

2.1.1.5 Melting Point

Melting points were determined on an Electrothermal Digital melting point 9100 apparatus. This confirms the bulk purity together with other micro-analysis spectroscopies. Melting points are uncorrected.

2.1.1.6 FTIR Spectroscopy

FTIR spectra were recorded on a universal diamond crystal ATR spectrophotometer in the range of 380-4000 cm^{-1} using Perkin-Elmer® Precisely, Universal ATR Sampling Accessory. The samples were analysed as solid powders and pastes free from solvents.

2.1.1.7 UV-Vis Spectroscopy

UV-Vis spectrophotometry was performed in degassed chloroform and were recorded on a PerkinElmer® Precisely, Lambda 35, UV/VIS spectrometer in the range of 200-800 nm for all compounds. For clarity, some spectra have been represented in the range of 200-500 nm.

2.1.1.8 Mass Spectroscopy

Electron spray ionization (ESI) and fast atom bombardment (FAB) mass spectra were recorded on a Kratos Concept 1H mass spectrometer. Mass spectra were obtained in positive-ion mode with 3-nitrobenzyl alcohol used as the matrix for the FAB spectra.

2.1.1.9 Elemental Analysis

The CHN elemental analyses were carried out using Thermo Scientific Flash 2000 Elemental Analyser at the Mass Spectrometry laboratory, School of Chemistry and Physics, UKZN. In a case where the compound was sensitive to the moisture elemental analysis was an exempted and other analysis like mass spectroscopy was used.

2.1.1.10 Thermogravimetric analysis

Thermal analysis curves (TG, DTA and DTG) were obtained using TA instruments SDT Q600, second generation simultaneous TGA/ DSC thermal analyzer in a dynamic nitrogen atmosphere with the flow rate of 80 cm^3 min^{-1}. A sample size of 5-10 mg and a heating rate of 10 °C min^{-1} were used. The TGA temperature range starts from 25-1000°C.

2.1.1.11 Theoretical Calculations

Density functional theory (DFT) was determined using a 2CPU workstation UNIV-D2G/ Silent. The geometry optimization was achieved *via* the Becke3LYP functional and LANL2DZ with ECP basis set for all the complexes studied in the presented work with a restricted Hartree-Fock formalism. All DFT calculation were determined using the Gaussian 03 program[6] (Revision XBPA-400, and XBPA-500).

2.1.2 Syntheses of Bis(amino)phosphine Ligands and Complexes

2.1.2.1 Synthesis of [($C_{10}H_6$(1,8-$NHPPh_2$)$_2$)] (1)

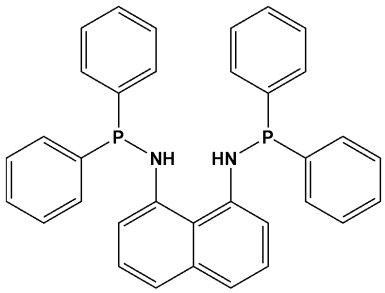

A dried and degassed 250 mL Schlenk tube equipped with a magnetic stirrer bar was charged with *1,8*-diaminonaphthalene (2000 mg, 12.6 mmol), trimethylamine (3.53 mL, 25.3 mmol), 4-(dimethylamino) pyridine (160 mg, 1.31 mmol) in THF (75 mL). Dropwise a solution of chlorodiphenylphosphine (4.54 mL, 25.3 mmol) was added into the flask. The reaction was stirred for 3 hours then the solution was filtered through a sintered glass funnel to remove $[Et_3NH]\cdot Cl$ salt. The filtrate solvent was removed under high vacuum. Upon further drying of the solid material under high vacuum for a week, a free flowing powder was isolated.

Yield 4993 mg (75.0 %). Mp: 47 ºC. Elemental analysis calcd (%) for $C_{34}H_{28}N_2P_2$ (526.17 g mol^{-1}): C, 77.56; H, 5.36; N, 5.32; found: C, 77.50; H, 5.32; N, 5.30; ^{1}H NMR (400 MHz, $CDCl_3$, δ, ppm): δ = 7.45-7.41 (m, 2H), 7.30-7.28 (m, 5H, phenyl-H), 7.21-7.17 (m, 5H, phenyl-H), 7.14 (m, 2H), 7.12-7.11 (m, 10H, phenyl-H), 7.08-7.07 (m, 2H), 6.04-6.02 (d, *J* = 8.36Hz, 2H, naph-H); $^{13}C\{^1H\}$ NMR (100 MHz, $CDCl_3$, δ, ppm): δ = 131.5, 131.3, 129.0, 1286, 128.5, 125.6, 122.2, 119.5, 115.2, $^{31}P\{^1H\}$ NMR (121.49M Hz, $CDCl_3$, δ, ppm): δ = 33.5. FT-IR (selected bands): ν = 3049 (NH), 1576, 1433, 1026, 691 cm^{-1}. ESI-MS (positive): (m/z) = 527 (100 %) $[M+H]^+$.

2.1.2.2 Synthesis of [$C_{10}H_6$(1,8-NH-P{$CH(CH_3)_2$}$_2$)$_2$] (2)

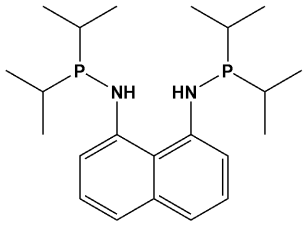

Ligand **(2)** was synthesised *via* aminolysis: A dried and degassed 250 mL Schlenk tube equipped with a magnetic stirrer bar was charged with *1,8*-diaminonaphthalene (497 mg, 3.14 mmol), trimethylamine (0.88 mL, 6.28 mmol), 4-(dimethylamino) pyridine (50.0 mg, 0.409 mmol) in a THF (75 mL) solution. A solution of chlorodiisopropylphosphine (1.00 mL, 6.28 mmol) in THF (20 mL) was added dropwise into the flask. The reaction was stirred for 3 hours and then the solution was filtered through a sintered glass funnel to remove

[Et_3NH]·Cl salt. The filtrate solvent was removed under high vacuum. The red to pink paste was treated with ethanol to yield an off-white to light red powder.

Yield 822 mg (67.1 %). Mp: 35 ºC. Elemental analysis calcd (%) for $C_{22}H_{36}N_2P_2$ (390.48 g mol^{-1}): C, 67.67; H, 9.29; N, 7.17; found: C, 68.98; H, 9.26; N, 7.14; ^{1}H NMR (400 MHz, $CDCl_3$, δ, ppm): δ = 7.38-7.36 (d, *J* = 8.00Hz, 2H), 7.26 (br, 2H, NH), 7.20-7.17 (t, *J* = 5.18Hz, 2H), 6.93-6.91 (d, *J* = 7.40, 2H), 2.51-2.45 (m, 4H), 1.25-1.19 (q, *J* = 7.31Hz, 12H), 1.12-1.06 (q, *J* = 8.08Hz, 12H); ^{13}C{^{1}H} NMR (100 MHz, $CDCl_3$, δ, ppm): δ = 140.9, 140.8, 140.8, 137.0, 125.2, 123.6, 119.3, 26.5, 19.3, ^{31}P{^{1}H} NMR (121.49M Hz, $CDCl_3$, δ, ppm): δ = 55.7. FT-IR (selected bands): ν = 2948, 2602, (NH), 2921, 2497, 1641, 1579, 1474, 1444, 1397, 1292, 1172, 1035, 807, 758, 470 cm^{-1}. ESI-MS (positive): (m/z) = 266 (45 %) $[M+C_{10}H_8]^+$, 159 (100 %) $[M+C_{12}H_{28}P_2]^{+\cdot}$.

2.1.2.3 Synthesis of $[Cu_2(\mu\text{-}Cl)_2\{C_{10}H_6(1,8\text{-}NHPPh_2)_2\}_2\cdot 2CH_2Cl_2]$, (3)

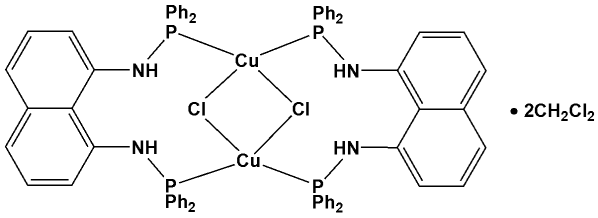

Into an oven dried 150 mL Schlenk tube equipped with a magnetic stirrer bar, [$C_{10}H_6$(1,8-$NHPPh_2$)$_2$] (819 mg, 0.155 mmol, 1 mol equiv.) was added and dissolved in dried degassed DMSO or 1,4-dioxine or acetronitrile (30 mL) and stirred at room temperature. Into this clear solution, CuCl (154 mg, 0.155 mmol, 1 mol equiv.) was added as a solid. After 10 minutes an off-white precipitate in a pink solution was observed and the reaction was further stirred for 90 minutes. An off-white complex was isolated *via* suction filtration and stored as a powder. Crystals were grown by slow diffusion of dichloromethane: diethyl ether (50:50) or dichloromethane: hexane (50:50).

Yield 697 mg (35.9 %). Mp: 209 ºC. Elemental analysis calcd (%) for $C_{68}H_{56}Cl_2Cu_2N_4P_4$ (1248.14 g mol^{-1}): C, 65.28; H, 4.51;N, 4.48; found: C, 65.10; H, 4.53; N, 4.44; ^{1}H NMR (400 MHz, $CDCl_3$, δ, ppm): δ = 7.49-7.48 (m, 16H, phenyl-H), 7.22 (m, 4H, phenyl-H), 7.21 (m, 4H, naph-H), 7.19 (m, 4H, phenyl-H), 7.12-7.08 (m, 20H, phenyl-H), 6.81-6.77 (t, *J* = 7.74Hz, 4H, naph-H), 6.58-6.56 (d, *J* = 6.56Hz, 4H, naph-H); ^{13}C{^{1}H} NMR (100 MHz, $CDCl_3$, δ, ppm): δ = 132.8, 132.4, 132.3, 129.0, 128.8, 125.0, 122.4, 116.7, ^{31}P{^{1}H} NMR (121.49M Hz,

$CDCl_3$, δ, ppm) : δ = 30.2. FT-IR (selected bands): ν = 3337 (NH), 2852, 1580, 1420, 1283, 1119, 1047, 872, 819, 743, 693, 515, 473 cm^{-1}. TOF MS ESI (positive): (m/z) = 1215 (35 %) $[M+Cl]^+$, 581 (100 %) $[M+C_{43}H_{36}N_4P_2]^+$.

2.1.2.4 Synthesis of $[Cu_2(\mu\text{-}Br)_2\{C_{10}H_6(1,8\text{-}NHPPh_2)_2\}_2]$, (4) and (4*)

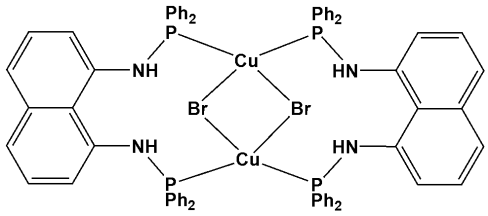

Complexes **(4)** and **(4*)** are polymorphs synthesized from DMSO and THF as reaction medium, respectively. The same compounds were successfully synthesized from 1,4-dioxine or DMSO or acetonitrile as the reaction medium. Into an oven dried 150 mL Schlenk tube equipped with a magnetic stirrer bar, $[C_{10}H_6(1,8\text{-}NHPPh_2)_2]$ (405 mg, 0.769 mmol, 1 mol equiv.) was added and dissolved in a dry degassed THF (30 mL) solution and stirred at room temperature. Into this clear solution, CuBr (110 mg, 0.769 mmol, 1 mol equiv.) was added as a solid. After 10 minutes an off-white to grey precipitate with pink solution was observed and the reaction was stirred for an additional 90 minutes. An off-white complex was isolated *via* suction filtration and stored as a powder. In a case where the solvent used in the reaction was THF, the volatiles were removed under high vacuum and an off-white solid was isolated. Crystals were grown by slow diffusion of dichloromethane: diethyl ether (50:50) or dichloromethane: hexane (50:50).

Yield 545 mg (53.0 %). Mp: 219 ºC. Elemental analysis calcd (%) for $C_{68}H_{56}Br_2Cu_2N_4P_4$ (1336.04 g mol^{-1}): C, 60.95; H, 4.21; N, 4.18; found: C, 60.84; H, 4.18; N, 4.16; ^1H NMR (400 MHz, $CDCl_3$, δ, ppm): δ = 7.66-7.60 (m, 4H, phenyl-H), 7.53-7.52 (m, 16H, phenyl-H), 7.23-7.22 (m, 4H), 7.20 (m, 4H, naph-H), 7.13-7.09 (m, 20H, phenyl-H), 6.81-6.77 (t, *J* = 7.86Hz, 4H, naph-H), 6.63-6.61 (d, *J* = 7.44Hz, 4H, naph-H); $^{13}C\{^1H\}$ NMR (100 MHz, $CDCl_3$, δ, ppm): δ = 139.0, 133.0, 132.4, 132.3, 129.4, 128.1, 124.9, 122.6, 117.3, $^{31}P\{^1H\}$ NMR (121.49M Hz, $CDCl_3$, δ, ppm): δ = 28.1. FT-IR (selected bands): ν = 3265 (NH), 3051, 28853, 1971, 1578, 1508, 1480, 1458, 1433, 1413, 1276, 1182, 1120, 1098, 1042, 998, 873, 819, 743, 692, 524, 510, 460 cm^{-1}. ESI-MS (positive): (m/z) = 1259 (3%) $[M\text{-}Br]^+$, 341 (70 %) $[M+C_{46}H_{38}Br_2Cu_2N_2P_3]^+$, 203 (100 %) $[M+C_{56}H_{50}Br_2Cu_2N_2P_3]^+$.

2.1.2.5 Synthesis of $[Cu_2(\mu\text{-}I)_2\{C_{10}H_6(1,8\text{-}NHPPh_2)_2\}_2 \cdot 2CH_2Cl_2]$, (5)

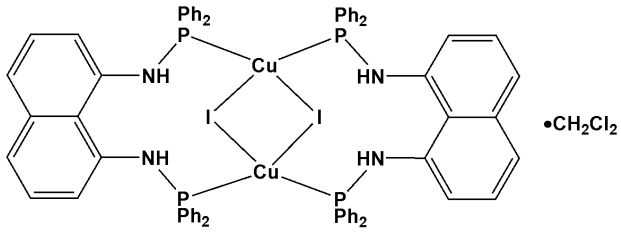

Complex **(5)** was synthesized similarly to complex **(3)**. CuBr was replaced by CuI: $[C_{10}H_6(1,8\text{-}NHPPh_2)_2]$ (448 mg, 0.851 mmol, 1 mol equiv.), CuCl (162 mg, 0.851 mmol, 1 mol equiv.) in DMSO solvent.

Yield 371 mg (30.4 %). Mp: 223 ºC. Elemental analysis calcd (%) for $C_{68}H_{56}I_2Cu_2N_4P_4$ (1432.01 g mol^{-1}): C, 56.95; H, 3.94; N, 3.91; found: C, 56.91; H, 3.92; N, 3.88; ^1H NMR (400 MHz, $CDCl_3$, δ, ppm): δ = 7.55-7.50 (m, 17H), 7.46-7.43 (m, 3H, phenyl-H), 7.25-2.23 (m, 4H), 7.22-7.19 (m, 4H, phenyl-H), 7.14-7.10 (m, 20H, phenyl-H), 6.82-6.78 (t, *J* = 7.88Hz, 4H, naph-H), 6.64-6.62 (d, *J* = 7.60Hz, 4H, naph-H); $^{13}C\{^1H\}$ NMR (100 MHz, $CDCl_3$, δ, ppm): δ = 139.3, 132.8, 132.6, 132.4, 129.4, 128.1, 125.0, 122.4, 116.7, $^{31}P\{^1H\}$ NMR (121.49M Hz, $CDCl_3$, δ, ppm): δ = 23.9. FT-IR (selected bands): ν = 3324 (NH), 3051, 2850, 1600, 1578, 1433, 1413, 1276, 1118, 1096, 1044, 872, 817, 742, 692, 612, 523, 505, 459 cm^{-1}. ESI-MS (positive): (m/z) = 808 (10 %) $[M+Na+C_{42}H_{38}N_5P]^+$, 341 (100 %) $[M+C_{46}H_{38}Cu_2I_2N_2P_3]^+$.

2.1.2.6 Synthesis of $[Cu_2(\mu\text{-}Cl)_2(C_{10}H_6\{1,8\text{-}NH\text{-}P\{CH(CH_3)_2\}_2\}_2)_2]$, (6)

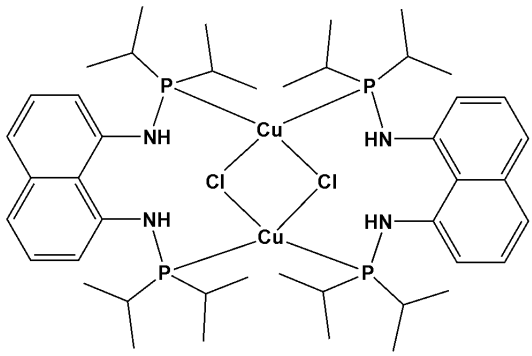

Into an oven dried 50 mL Schlenk tube equipped with a magnetic stirrer bar, $[C_{10}H_6(1,8\text{-}NH\text{-}P\{CH(CH_3)_2\}_2)_2]$ (50.0 mg, 0.128 mmol, 1 mol equiv.) was added and dissolved in dried degassed THF (15 mL) solvent and stirred at room temperature. Into this clear solution, CuCl (12.7 mg, 0.128 mmol, 1 mol equiv.) was added in one portion. The reaction was stirred for 12 hours. The solvent was removed by a high vacuum to yield **(6)**. Crystals were grown from the $CDCl_3$ solvent in a NMR tube.

Yield 822 mg (67.1 %). Mp: 235 ºC. Elemental analysis calcd (%) for $C_{44}H_{72}Cl_2Cu_2N_4P_4$ (978.96 g mol^{-1}): C, 53.98; H, 7.41; N, 5.72; found: C, 54.01; H, 7.44; N, 5.73; ^{1}H NMR (400 MHz, $CDCl_3$, δ, ppm): δ = 7.38-7.36 (d, *J* = 8.00Hz, 2H), 7.26 (br, 2H, NH), 7.20-7.17 (t, *J* = 5.18Hz, 2H), 6.93-6.91 (d, *J* = 7.40, 2H), 2.51-2.45 (m, 4H), 1.25-1.19 (q, *J* = 7.31Hz, 12H), 1.12-1.06 (q, *J* = 8.08Hz, 12H); ^{13}C{^{1}H} NMR (100 MHz, $CDCl_3$, δ, ppm): δ = 140.9, 140.8, 140.8, 137.0, 125.2, 123.6, 119.3, 26.5, 19.3, ^{31}P{^{1}H} NMR (121.49M Hz, $CDCl_3$, δ, ppm): δ = 59.2. FT-IR (selected bands): ν = 3320, 3228 (NH), 2921, 2958, 2866 CH_3, 1575, 1456, 1411, 1366, 1276, 1040, 1030, 878, 829, 748, 667, 507 cm^{-1}. ESI-MS (positive): (m/z) = 713 (12 %) $[M\text{-}C_{12}H_{32}N_2P_2]^+$, 399 (84 %) $[M+C_{36}H_{58}N_4P_2Cl]^+$, 145 (100 %) $[M+C_{34}H_{66}Cl_2Cu_2N_3P_4]^+$.

2.1.2.7 Synthesis of $[Cu\{C_{10}H_6(1,8\text{-}NHPPh_2)_2\}_2]PF_6$, (7)

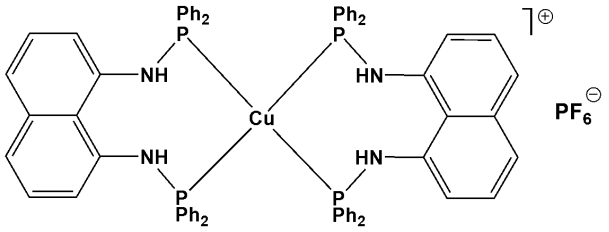

Into an oven dried 150 mL Schlenk tube equipped with a magnetic stirrer bar, $[C_{10}H_6(1,8\text{-}NHPPh_2)_2]$ (604 mg, 1.15 mmol, 1 mol equiv.) was added and dissolved in a dried degassed acetonitrile (30 mL) and stirred at room temperature. Into this clear solution, $[Cu(CH_3CN)_4]PF_6$ (427 mg, 1.15 mmol, 1 mol equiv.) in acetonitrile (10 mL) was added dropwise. The reaction was stirred for an hour. The solvent was removed by a high vacuum and the solid was stirred for an hour again in diethyl ether to extract oxidised phosphines. The solid was filtered of as microcrystalline powder of compound **(7)**.

Yield 675 mg (46.7 %). Mp: 113 ºC. Elemental analysis calcd (%) for $C_{68}H_{56}I_2Cu_2N_4P_4$ (1261.60 g mol^{-1}): C, 64.74; H, 4.47; N, 4.44; found: C, 65.05; H, 4.49; N, 4.48; ^{1}H NMR (400 MHz, $CDCl_3$, δ, ppm): δ = 8.60-8.58 (br, 4H, NH), 7.74-7.69 (m, 16H), 7.49-7.47 (m, 4H), 7.45-7.43 (m, 4H, naph-H), 7.43-7.41 (m, 4H, phenyl-H), 7.32-7.28 (m, 16H, phenyl-H), 7.04-7.00 (t, *J* = 7.86Hz, 4H, naph-H), 6.57-6.55 (d, *J* = 7.52Hz, 4H, naph-H); ^{13}C{^{1}H} NMR (100 MHz, $CDCl_3$, δ, ppm): δ = 131.6, 130.8, 129.1, 127.2, 127.1, 123.6, 120.0, 114.4, ^{31}P{^{1}H} NMR (121.49M Hz, $CDCl_3$, δ, ppm): δ = 55.1, 130.9, 135.3, 139.7, 144.1, 148.5, 152.6. FT-IR (selected bands): ν = 3055 (NH), 1651, 1578, 1512, 1483, 1437, 1408, 1310, 1121, 1039,

833, 745, 692, 555, 519 cm^{-1}. ESI-MS (positive): (m/z) = 931 (30 %) $[M+C_{22}H_{18}NP]^+$, 342 (85 %) $[M+ C_{46}H_{38}CuN_2P_3+PF_6]^+$, 791 (100 %) $[M+ C_{22}H_{18}NP+PF_6]^+$.

2.1.2.8 Synthesis of $[Cu_4(\mu_3\text{-}Cl)_2(\mu_2\text{-}Cl)_2(O\{PPh_2\}_2)_2]$ (8)

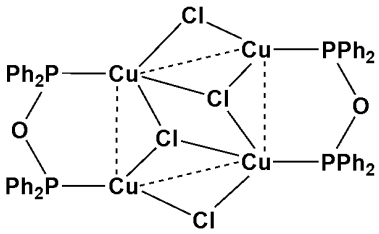

Complex **(8)** was obtained accidentally in an attempted to perform an oxidative addition on complex **(3)** with iodobenzene dichloride: Iodobenzene dichloride (110 mg, 0.401 mmol) was added to a solution of complex **(3)** (500 mg. 0.401 mmol) in THF (30 mL). The solution precipice out in few minutes to a white powder and the solution was stirred for 3 hours. Upon removal of the solvent under high vacuum pump, an off-white to green coloured compound was obtained. Complexes **(8)** was reproduced by treating complex **(3)** with 1.5 mole excess of deionized water in THF (30 mL). The solvent was removed under high vacuum. The product was extracted with dichloromethane to yield complex **(8)**. X-ray single crystals were obtained by slow diffusion of dichloromethane: hexane (50:50).

Yield 321 mg (68.6 %). Mp: 179 ºC. Elemental analysis calcd (%) for $C_{48}H_{40}C_{l4}Cu_4O_2P_4$ (1168.68 g mol^{-1}): C, 49.33; H, 3.45; found: C, 48.93; H, 3.33; ^1H NMR (400 MHz, C_6D_6, δ, ppm): δ = 7.52-7.14 (m, 40H, phenyl-H); $^{13}C\{^1H\}$ NMR (100 MHz, DMSO-d_6, δ, ppm): δ = 132.6, 131.3, 128.6, $^{31}P\{^1H\}$ NMR (121.49M Hz, C_6D_6, δ, ppm): δ = 34.7. FT-IR (selected bands): ν = 3048, 1477, 1434 cm^{-1}.

2.1.2.9 Synthesis of $[Cu_4(\mu_3\text{-}I)_2(\mu_2\text{-}I)_2(O\{P[CH(CH_3)_2]_2\}_2)_2]$ (9)

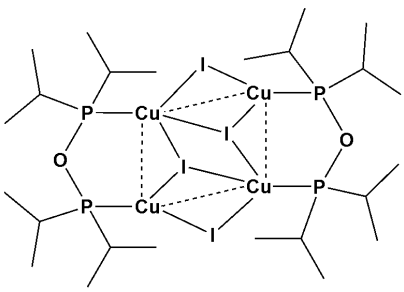

Complex **(9)** was obtained by treating complex **(6.1)** an analogue of **(6)** with equivalent molar of H_2O in THF (20 mL). The solvent was concentrated to dryness and the product was extracted into dichloromethane. The removal of solvent gives **(9)** as a solid. X-ray single crystals were obtained by slow diffusion of dichloromethane: hexane (50:50).

Yield 447 mg (82.5 %). decom. > 200 ºC. Elemental analysis calcd (%) for $C_{24}H_{56}Cu_4I_4O_2P_4$ (1262.37 g mol^{-1}): C, 22.83; H, 4.47; found: C, 23.12; H, 4.42; ^{1}H NMR (400 MHz, DMSO-d_6, δ, ppm): δ = 2.87-2.82 (m, 8H), 0.99-0.74 (m, 48H); $^{13}C\{^1H\}$ NMR (100 MHz, C_6D_6, δ, ppm): δ = 45.7, 15.2, $^{31}P\{^1H\}$ NMR (121.49M Hz, C_6D_6, δ, ppm): δ = 62.5. FT-IR (selected bands): ν = 3279, 2957, 1646, 1587, 1457, 1386, 1362, 1156, 1018, 888, 868, 706, 677, 633 cm^{-1}.

2.1.2.10 Synthesis of $[Ag_2(\mu\text{-}Cl)_2\{C_{10}H_6(1,8\text{-}NHPPh_2)_2\}_2\cdot DMF]$, (10)

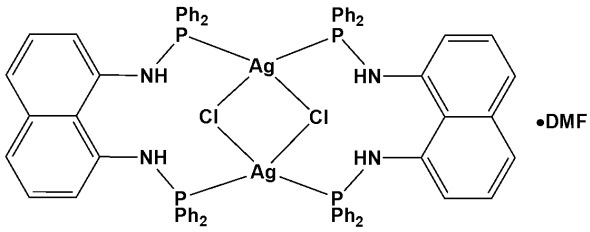

Complexes **(10)** to **(13)** were synthesised by the same procedure methods. Into an oven dried 150 mL Schlenk tube equipped with a magnetic stirrer bar, $[C_{10}H_6(1,8\text{-}NHPPh_2)_2]$ (688 mg, 1.31 mmol, 1 mol equiv.) was added and dissolved in 1,4-dioxine (30 mL) and stirred at room temperature. Into this clear solution, AgCl (187 mg, 1.31 mmol, 1 mol equiv.) was added as a solid. After 3 minutes an off-white to grey precipitate (ppt) was observed and the reaction was stir further for a 90 minutes. An off-white complex was isolated *via* gravity filtration and stored as a powder. Crystals were grown by slow evaporation in DMF.

Yield 368 mg (21.0 %). Mp: 214 ºC. Elemental analysis calcd (%) for $C_{68}H_{56}Cl_2Ag_2N_4P_4$ (1339.74 g mol^{-1}): C, 60.96; H, 4.21; N, 4.18; found: C, 58.98; H, 4.88; N, 4.12; ^{1}H NMR (400 MHz, $CDCl_3$, δ, ppm): δ = 8.21-8.14 (br, 4H, NH), 7.55 (m, 17H, phenyl-H), 7.24-7.23 (m, 3H, phenyl-H), 7.21 (m, 4H, naph-H), 7.16-7.12 (m, 20H, phenyl-H), 6.80-6.76 (d, *J* = 7.86Hz, 4H, naph-H), 6.58-6.57 (d, *J* = 7.44Hz, 4H, naph-H); $^{13}C\{^1H\}$ NMR (100 MHz, $CDCl_3$, δ, ppm): δ = 138.4, 136.5, 133.6, 130.6, 129.5, 128.3, 124.7, 123.5, 119.1, $^{31}P\{^1H\}$ NMR (121.49M Hz, $CDCl_3$, δ, ppm): δ = 40.1-39.9 and 37.1-36.9 (dd, $J(^{109}AgP)$ 453.9 and $J(^{107}AgP)$ 524.0Hz). FT-IR (selected bands): ν = 3371 (NH), 3209, 3055, 2852, 1579, 1461, 1433, 1415, 1276, 1254, 1118, 1033, 872, 820, 746, 696, 613, 524, 510, 457 cm^{-1}. ESI-MS (positive): (m/z) = 1303 (15 %) $[M\text{-}Cl]^+$, 341 (64 %) $[M+ C_{46}H_{38}Ag_2Cl_2N_2P_3]^+$, 539 (100 %) $[M\text{-}Cl+C_{46}H_{39}N_3P_3]^+$.

2.1.2.11 Synthesis of $[Ag_2(\mu\text{-}Br)_2\{C_{10}H_6(1,8\text{-}NHPPh_2)_2\}_2)\cdot DMF]$, (11)

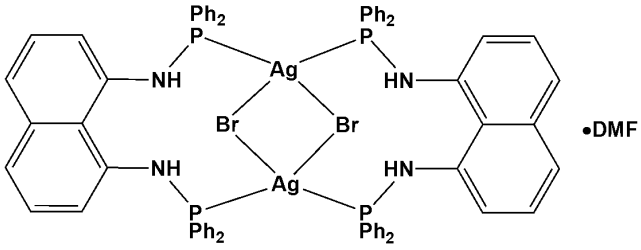

Complex **(11)** was synthesized similarly to complex **(10)**. AgCl was replaced by AgBr: $[C_{10}H_6(1,8\text{-}NHPPh_2)_2]$ (420 mg, 0.798 mmol, 1 mol equiv.), AgBr (150 mg, 0.798 mmol, 1 mol equiv.) in 1,4-dioxine solvent. The crystals were grown by slow evaporation in DMF.

Yield 276 mg (25.8 %). Mp: 218 ºC. Elemental analysis calcd (%) for $C_{68}H_{56}Br_2Ag_2N_4P_4$ (1428.64 g mol^{-1}): C, 57.17; H, 3.95;N, 3.92; found: C, 56.87; H, 3.93;N, 3.89; ^1H NMR (400 MHz, $CDCl_3$, δ, ppm): δ = 8.03-7.96 (br, 4H, NH), 7.60-7.57 (m, 15H, phenyl-H), 7.25-7.24 (m, 5H, phenyl-H), 7.22 (m, 4H, naph-H), 7.17-7.15 (m, 20H, phenyl-H), 6.79-6.75 (t, *J* = 7.80Hz, 4H, naph-H), 6.59-6.58 (d, *J* = 6.80Hz, 4H, naph-H); $^{13}C\{^1H\}$ NMR (100 MHz, $CDCl_3$, δ, ppm): δ = 132.5, 130.7, 130.6, 129.6, 128.9, 128.3, 124.7, 123.4, 118.9, $^{31}P\{^1H\}$ NMR (121.49M Hz, $CDCl_3$, δ, ppm): δ = 38.4-38.2 and 35.4-35.2 (dd, $J(^{109}AgP)$ 441.7 and $J(^{107}AgP)$ 509.9Hz 464.1). FT-IR (selected bands): ν = 3368 (NH), 3213, 2851, 1977, 1601, 1579, 1508, 1461, 1433, 1413, 1275, 1118, 1033, 872, 820, 745, 695, 613, 523, 503, 458 cm^{-1}. TOF-ESI-MS (positive): (m/z) = 1379 (15 %) $[M+Br]^+$, 341 (33 %) $[M+C_{46}H_{38}Ag_2Br_2N_2P_3]^+$, 1139 (100 %) $[M+Na+C_{68}H_{56}AgN_4P_4]^+$.

2.1.2.12 Synthesis of $[Ag_4(\mu_3\text{-}I)_2(\mu_2\text{-}I)_2\{C_{10}H_6(1,8\text{-}NHPPh_2)_2\}_2\cdot 2DMF]$, (12)

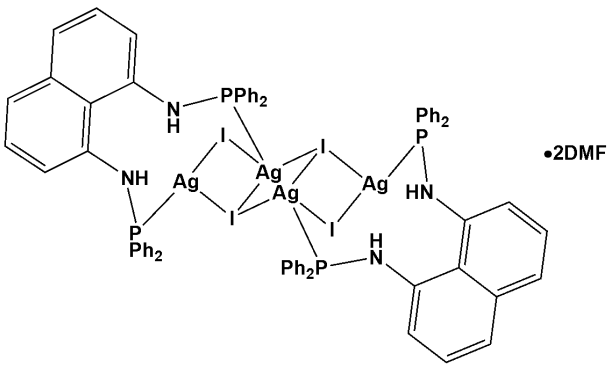

Complex **(12)** was synthesized similarly to complex **(10)**. AgCl was replaced by AgI: $[C_{10}H_6(1,8\text{-}NHPPh_2)_2]$ (548 mg, 1.04 mmol, 1 mol equiv.), AgI (254 mg, 1.041 mmol, 1 mol equiv.) in 1,4-dioxine solvent. Crystals were grown by slow evaporation in DMF.

Yield 547 mg (26.2 %). Mp: 218 ºC. Elemental analysis calcd (%) for $C_{68}H_{56}I_4Ag_4N_4P_4$ (1992.18 g.mol^{-1}): C, 41.00; H, 2.83; N, 2.81; found: C, 40.92; H, 2.80; N, 2.79; ^{1}H NMR (400 MHz, $CDCl_3$, δ, ppm): δ = 7.70-7.58 (m, 20H), 7.25 (m, 4H), 7.23 (m, 4H), 7.15 (m, 20H), 6.79-6.75 (t, *J* = 7.86Hz, 4H), 6.63-6.61 (d, *J* = 7.56Hz, 4H); ^{13}C{^{1}H} NMR (100 MHz, $CDCl_3$, δ, ppm): δ = 132.8, 132.4, 132.2, 129.4, 128.4, 128.1, 128.0, 122.6, 117.3, ^{31}P{^{1}H} NMR (121.49M Hz, $CDCl_3$, δ, ppm): δ = 34.4-34.2 and 31.7-31,5 (dd, *J*(^{109}AgP) 407.3 and *J*(^{107}AgP) 469.9Hz). FT-IR (selected bands): ν = 3358(NH), 3048, 2851, 1645, 1579, 1517, 1434, 1413, 1275, 1180, 1119, 1040, 872, 818, 744, 693, 522, 509cm^{-1}. ESI-MS (positive): (m/z) = 1630 (15 %) [M-AgI_3]$^+$, 341 (25 %) [M+$C_{46}H_{38}Ag_4I_4N_2P_3$]$^+$, 581 (100 %) [M+$C_{46}H_{39}Ag_3I_3N_2P_3$]$^+$.

2.1.2.13 Synthesis of [Ag{$C_{10}H_6$(1,8-NHPPh_2)$_2$}$_2$]PF_6, (13)

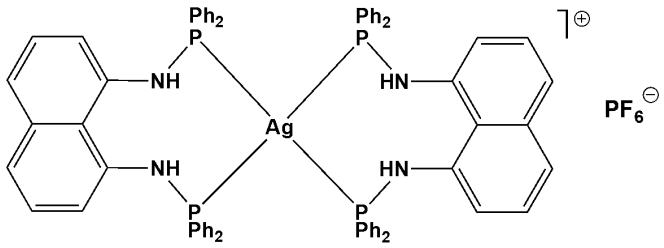

Into an oven dried 150 mL Schlenk tube equipped with a magnetic stirrer bar, [$C_{10}H_6$(1,8-NHPPh_2)$_2$] (437 mg, 0.831 mmol, 1 mol equiv.) was added and dissolved in a dried degassed acetonitrile (30 mL) and stirred at room temperature. Into this clear solution, [Ag(CH_3CN)$_4$]PF_6 (374 mg, 0.831 mmol, 1 mol equiv.) in acetonitrile (10 mL) was added dropwise. The reaction was stirred for an hour. The solvent was removed by a high vacuum and the solid was stirred for an hour again in diethyl ether to extract oxidised phosphines. The solid was filtered of as microcrystalline powder. Crystals were grown by slow diffusion of dichloromethane: diethyl ether (50:50) or dichloromethane: hexane (50:50).

Yield 620 mg (40.5 %). Mp: 118 ºC. Elemental analysis calcd (%) for $C_{68}H_{56}AgF_6N_4P_5$ (1305.93 g mol^{-1}): C, 62.54; H, 4.32; N, 4.29; found: C, 63.01; H, 4.82; N, 4.43; ^{1}H NMR (400 MHz, $CDCl_3$, δ, ppm): δ = 7.66-7.63 (m, 20H, phenyl-H), 7.57 (m, 4H), 7.55 (br, 4H, NH), 7.50-7.46 (m, 20H, phenyl-H), 7.44-7.42 (m, 4H,), 7.37-7.31 (m, 2H); ^{13}C{^{1}H} NMR (100 MHz, $CDCl_3$, δ, ppm): δ = 130.9, 129.6, 129.2, 128.8, 128.2, 127.7, 127.0, 129.6, 126.4. ^{31}P{^{1}H} NMR (121.49M Hz, $CDCl_3$, δ, ppm): δ = 22.7 and 135.1, 139.5, 143.9, 148.3, 152.7. FT-IR (selected bands): ν = 3057 (NH), 1580, 1515, 1414, 1437, 1415, 1277, 1246, 1156, 1124, 1027, 893, 727, 691, 635, 543, 515 cm^{-1}. ESI-MS (positive): (m/z) = 991 (3 %) [M+2($C_{10}H_{10}N_2$)]$^+$, 837 (100 %) [M+ $C_{22}H_{18}NP$]$^+$.

2.1.2.14 Synthesis of [$C_{10}H_6$(1,8-$NHPPh_2O)_2$] (14)

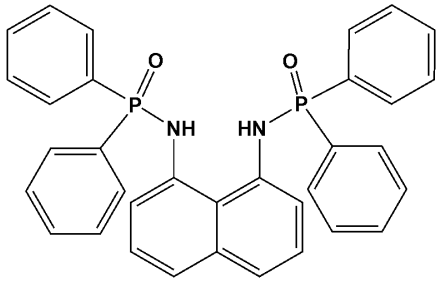

A purple solid of *1,8*-diaminonaphthalene (2000 mg, 13.0 mmol) was charged into a 250 mL Schlenk tube purged with the argon gas and THF (50 mL) was added to dissolve the solid forming a light peach colour. Triethylamine (3.80 mL, 28.6 mmol) and a catalyst 4-(dimethylamino)pyridine (160 mg, 12.0 mmol) were added into the reaction vessel. The solution was stirred at room temperature for 15 minutes until all the solid had dissolved. To this solution chlorodiphylphosphine (4.60 mL, 28.6 mmol) dissolved in THF (50 mL) was added dropwise and an immediate white precipitate of $[Et_3NH]\cdot Cl$ was observed. The reaction was continuously stirred for 3 hours. After which the solution was filtered through a sintered funnel packed with a pad of Celite into an oven dried Schlenk tube. The organic solvent was removed under a high vacuum to give a light brown oily substance, intermediate [$C_{10}H_6$(1,8-$NHPPh_2)_2$]. An oily substance was dissolved in THF (20 mL) and it was stirred under a continuous purging of oxygen for 30 minutes. Thereafter H_2O_2 (0.75 mL, 32.0 mmol) dissolved in THF (10 mL) was added dropwise and the reaction was allowed to stir in air until white precipitated was observed ~3 hours. The volatile were removed under high vacuum pump and Et_2O was added to crush the product and the reaction was stirred for 30 minutes and immediately when the Et_2O was remove in *vacuo*, hexane (50 mL) was added and the reaction was stirred overnight. The powdered compound was filtered under Suction and 3670 mg was obtained. The crystals grown by diffusion of either dichloromethane or chloroform into either diethyl ether or hexane were twined. This was confirmed by XRD.

Yield 3671 mg (50.6 %). Mp: 168 ºC. Elemental analysis calcd (%) for $C_{34}H_{28}N_2P_2O_2$ (558.55 g mol^{-1}): C, 73.11; H, 5.05; N, 5.02; found: C, 72.91; H, 4.98; N, 5.00; ^{1}H NMR (400 MHz, $CDCl_3$, δ, ppm): δ = 8.37-8.36 (br, 2H, NH), 7.7.3-7.68 (m, 10H, phenyl), 7.51-7.49 (d, *J* = 7.84Hz, 2H, naph-H), 7.41-7.37 (m, 4H, phenyl), 7.28-7.24 (m, 6H), 7.06-7.02 (t, *J* = 7.72Hz, 2H, naph-H), 6.99-6.97 (d, *J* = 7.44Hz, 2H, naph-H); $^{13}C\{^1H\}$ NMR (100 MHz, $CDCl_3$, δ, ppm): δ = 134.0, 132.1, 132.0, 131.7, 130.6, 128.9, 128.4, 128.3, 126.7, 125.2, $^{31}P\{^1H\}$ NMR (121.49M Hz, $CDCl_3$, δ, ppm): δ = 23.5. FT-IR (selected bands): ν = 3052(NH), 1581, 1460, 1437, 1421, 1315, 1282, 1177, 1107, 1037, 894, 825, 745, 720, 690, 538, 516 cm^{-1}. ESI-MS (positive): (m/z) = 560 (100 %) $[M+H]^+$.

2.1.2.15 Synthesis of [$C_{10}H_6$(1,8-$NHPPh_2S)_2$] (15)

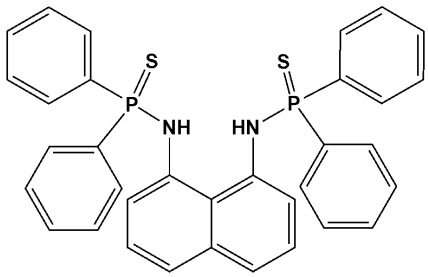

A purple solid of *1,8*-diaminonaphthalene (500 mg, 3.25 mmol) was charged into a 250 mL Schlenk tube purged with the argon gas and THF (50 mL) was added to dissolve the solid forming a light peach colour. Triethylamine (0.95 mL, 7.15 mmol) and a catalyst 4-(dimethylamino)pyridine (40.0 mg, 0.300 mmol) were added into the reaction vessel. The solution was stirred at room temperature for 15 minutes until all the solid had dissolved. To this solution chlorodiphenylphosphine (1.15 mL, 6.40 mmol) dissolved in THF (50 mL) was added dropwise and an immediate white precipitate of $[Et_3NH]\cdot Cl$ was observed. The reaction was continuously stirred for 3 hours. The organic solvent was removed under a high vacuum to give a light brown oily compound **(1)**. After which the solution containing **(1)** was filtered through a sintered funnel packed with a pad of Celite into an oven dried Schlenk tube. Ligand **(1)** was dissolved in THF (50 mL) and sulphur (6.40 mmol) was added. The yellow sulphur powder gradually disappeared and the flask felt warm as all the sulphur dissolved. The solvent was removed from the reaction mixture in *vacuo* and the material was washed with carbon disulphide (2 x 15 mL) and diethyl ether (2 x 15 mL) to yield ligand **(15)**.

Yield 1375 mg (73.0 %). Mp: 238 ºC. Elemental analysis calcd (%) for $C_{34}H_{28}N_2P_2S_2$ (590.68 g mol^{-1}): C, 69.13; H, 4.78; N, 4.74; found: C, 68.45; H, 4.69; N, 4.72; ^{1}H NMR (400 MHz, $CDCl_3$, δ, ppm): δ = 7.79-7.44 (m, 10H, phenyl), 7.44-7.41 (d, *J* = 8.16Hz, 2H, naph-H), 7.33-7.30 (m, 3H, phenyl), 7.23-7.18 (m, 7H), 6.98-6.94 (t, *J* = 7.86Hz, 2H, naph-H), 6.77-6.75 (d, *J* = 7.44Hz, 2H, naph-H); ^{13}C{^{1}H} NMR (100 MHz, $CDCl_3$, δ, ppm): δ = 132.9, 132.4, 131.4, 130.8, 130.6, 127.7, 127.2, 125.4, 124.0, 123.9, ^{31}P{^{1}H} NMR (121.49M Hz, $CDCl_3$, δ, ppm): δ = 57.7. FT-IR (selected bands): ν = 3138, 3053(NH), 1640, 1559, 1436, 1392, 1309, 1264, 1094, 1034, 891, 835, 696, 687, 627, 518, 501 cm^{-1}. ESI-MS (positive): (m/z) = 591 (100 %) $[M+H]^+$.

2.1.2.16 Synthesis of [($C_{10}H_6$(1-$NHPPh_2O$)(8-$NHPPh_2Se$] (16)

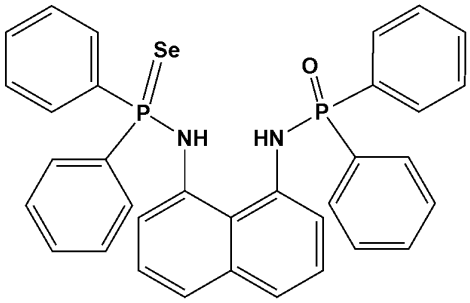

Into a 150 mL Schlenk tube purged with the argon gas the intermediate [$C_{10}H_6$(1,8-$NHPPh_2$)$_2$] (1000 mg, 1.90 mmol) in THF (50 mL) was slowly treated with H_2O_2 (65.0 mg, 1.90 mmol) for 30 minutes under a constant stir of the reaction. The solvent was removed in *vacuo* and the product washed with ether (2 × 30 mL) to give a yield of 985 mg (98.4%) of [$C_{10}H_6$($NHPPh_2$)(1-$NHPPh_2O$)]. The [$C_{10}H_6$($NHPPh_2$)(1-$NHPPh_2O$)] (802 mg, 1.52 mmol) compound was dried under *vacuo* for a day and was charged into a (100 mL) Schlenk tube purged with argon gas in a THF (30 mL) solution. Excess Se (300 g, 3.81 mmol) was added in one portion and the reaction was stirred continuously at 80°C for 2 hours. The reaction was filtered and the filtrate solvent was concentration to dryness and washed with methanol to yield an off-white compound **(16)**.

Yield 701 mg (74.1 %). Mp: 222-226 ºC. Elemental analysis calcd (%) for $C_{34}H_{28}N_2OP_2Se$ (621.51 g mol^{-1}): C, 65.71; H, 4.54; N, 4.51; found: C, 67.72; H, 4.52; N, 4.98; ^{1}H NMR (400 MHz, $CDCl_3$, δ, ppm): δ = 7.68-7.60 (m, 10H, phenyl), 7.46-7.44 (m, 2H, naph-H), 7.43-7.19 (m, 10H, phenyl), 7.01-6.97 (t, *J* = 7.94Hz, 2H, naph-H), 6.94-6.92 (d, *J* = 7.60Hz, 2H, naph-H); ^{13}C{^{1}H} NMR (100 MHz, $CDCl_3$, δ, ppm): δ = 134.0, 132.1, 132.0, 131.7, 130.6, 128.9, 128.4, 128.3, 126.7, 125.2, ^{31}P{^{1}H} NMR (121.49M Hz, $CDCl_3$, δ, ppm): δ = 55.3 {Se}[^{1}J(PSe) 766] and 24.4 {O}. FT-IR (selected bands): ν = 3052(NH), 11576, 1435, 1391, 1309, 1265, 1186, 1097, 1034, 891, 755, 725, 687, 542, 514 cm^{-1}. ESI-MS (positive): (m/z) = 557 (90 %) $[M\text{-}Se]^+$, 341 (100 %) $[M+ C_{12}H_{10}PSeO]^+$.

2.1.2.17 Synthesis of [Ag{$C_{10}H_6$(1,8-$NHPPh_2S$)$_2$}$_2$·$2CH_2Cl_2$]CF_3SO_3 (17)

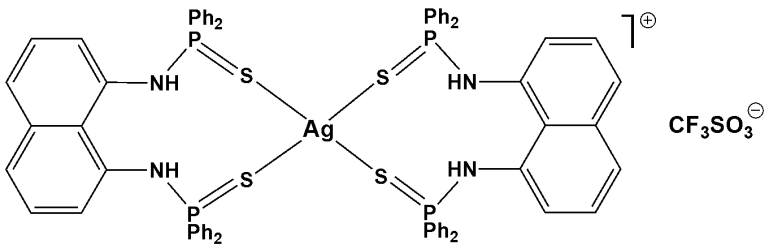

Into an argon flushed 100 mL Schlenk tube, THF solution (30 mL) of [$C_{10}H_6$(1,8-$NHPPh_2S$)$_2$] (500 mg, 0.847 mmol) and THF (30 mL) of $AgCF_3O_3S$ (218 mg,

0.847 mmol) at room temperature were added, respectively and stirred for an hour. Upon the additon the colour of the reaction changed to a light brown-off-white colour ppt. The volitile solvents were removed under high vacuum and the coumplex was extracted with DCM to yield a crystalline brown solid, complex **(17)**. Crystals were grown by slow diffusion of dichloromethane: hexane (50:50).

Yield: 120 mg (41.3 %). Mp: 177-179 ºC. Elemental analysis calcd (%) for $C_{69}H_{56}AgF_3N_4O_3P_4S_5$ (1438.29 g mol^{-1}): C, 57.62; H, 3.92; N, 3.90; found: C, 57.01; H, 3.82; N, 3.93; ^{1}H NMR (400MHz, $CDCl_3$, δ, ppm): δ = 9.42-9.40 (br, 4H, NH), 7.82-7.77 (q, *J*= 7.20Hz, 16H, phenyl-H), 7.49 (s, 2H). 7.47 (m, 4H), 7.44 (m, 4H), 7.42 (s, 2H), 7.34-7.29 (m, 16H, phenyl-H), 7.07-7.03 (t, *J* = 7.86, 4H, naph-H), 6.67-6.65 (d, *J* = 7.56, 4H, naph-H), 4.0 (br, 4H, NH); ^{13}C{^{1}H} NMR (100 MHz, $CDCl_3$, δ, ppm): δ = 132.3, 130.1, 130.0, 129.4, 128.5, 128.4, 125.3, 124.6, 121.1, 24.5(DCM), ^{31}P{^{1}H} NMR (121.49M Hz, $CDCl_3$, δ, ppm): δ = 58.3. FT-IR (selected bands): ν = 3051 (NH), 1577, 1435, 1026, 690, 513 cm^{-1}. ESI-MS (positive): (m/z) = 699 (10 %) $[M+C_{45}H_{37}N_3P_2O_3SF_3]^+$, 259 (100 %) $[M+Na+C_{69}H_{56}N_4P_4O_3SF_3]^+$.

2.1.2.18 Synthesis of $[Ag_2(\mu\text{-}S)_2\{C_{10}H_6(1,8\text{-}NHPPh_2S)\}_2]$ (18)

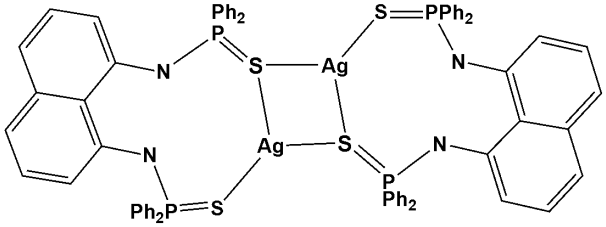

Into an oven dried 150 mL Schlenk tube equipped with a magnetic stirrer bar, a solid $AgClO_4$ (85.6 mg, 0.413 mmol) sample was added to a THF (30 mL) solution of $[C_{10}H_6(1,8\text{-}NHPPh_2S)_2]$ (244 mg, 0.413 mmol) and the grey colour to off-white (ppt) was stirred for 12 hours. The product was collected under suction filtration as a solid. Crystals were grown by slow evaporation DMF.

Yield: 304 mg (52.8 %). Mp: 197 ºC. Elemental analysis calcd (%) for $C_{68}H_{52}Ag_2N_4P_4S_4$ (1393.06 g mol^{-1}): C, 58.63; H, 3.76; N, 4.02; found: C, 58.46; H, 3.74; N, 3.98; ^{1}H NMR (400MHz, $CDCl_3$, δ, ppm): δ = 9.05 (br, 4H, NH), 7.83-7.77 (q, *J* = 7.19Hz, 16H, phenyl-H), 7.48 (m, 4H, naph-H), 7.47-7.44 (m, 4H), 7.42 (m, 4H, phenyl-H), 7.34-7.29 (m, 16H, phenyl-H), 7.06-7.02 (t, *J* = 7.80Hz, 4H, naph-H), 6.69-6.64 (d, *J* = 6.00Hz, 4H, naph-H); ^{13}C{^{1}H} NMR (100 MHz, $CDCl_3$, δ, ppm): δ = 132.3, 130.1, 130.0, 129.4, 128.5, 128.4, 125.3, 124.6,

121.1, $^{31}P\{^{1}H\}$ NMR (121.49M Hz, $CDCl_3$, δ, ppm): δ = 69.4 and 58.5. FT-IR (selected bands): ν = 3200 (NH), 1650, 1574, 1508, 1481, 1437, 1414, 1310, 1273, 1191, 1098, 1044, 996, 860, 706, 687, 619, 598, 580, 516, 500 cm^{-1}. ESI-MS (positive): (m/z) = 882 (20 %) $[M+C_{22}H_{19}N_2PS_2Ag]^+$, 359 (100 %) $[M+C_{46}H_{38}Ag_2N_3P_3S_3]^+$.

2.1.2.19 Synthesis of $[Ag\{C_{10}H_6(1,8\text{-}NHPPh_2O)_2\}_2]CF_3SO_3$ (19)

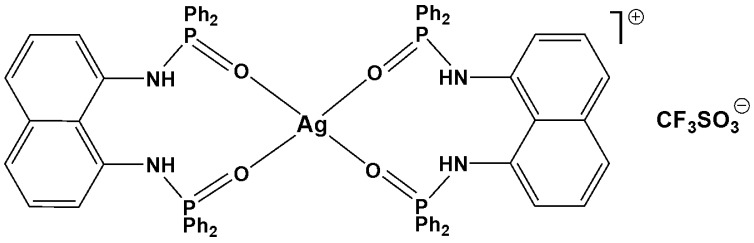

Into an argon flushed 100 mL Schlenk tube, THF solution (30 mL) of $[C_{10}H_6(1,8\text{-}NHPPh_2O)_2]$ (500 mg, 0.847 mmol) and THF (30 mL) of $AgCF_3O_3S$ (218 mg, 0.847 mmol) at room temperature were added, respectively and stirred for an hour. Upon the additon the colour of the reaction changed to a light brown-off-white colour ppt. The volitile solvents were removed under high vacuum and the coumplex was extracted with DCM to yield a crystalline brown solid, complex **(19)**.

Yield: 461 mg (39.6 %). Mp: 178 ºC. Elemental analysis calcd (%) for $C_{69}H_{56}AgF_3N_4O_7P_4S^-$ (1374.03 g mol^{-1}): C, 60.31; H, 4.11; N, 4.08; found: C, 58.98; H, 4.03; N, 4.10; ^{1}H NMR (400MHz, $CDCl_3$, δ, ppm): δ = 7.83-7.75 (m, 4H), 7.70-7.65 (m, 18H, phenyl-H), 7.50-7.49 (m, 2H, phenyl-H), 7.47 (m, 4H, naph-H), 7.43-7.41 (m, 4H, naph-H), 7.40-7.38 (m, 2H-phenyl-H), 7.36-7.31 (m, 18H, phenyl-H), 7.20-7.12 (m, 4H, naph-H); $^{13}C\{^{1}H\}$ NMR (100 MHz, $CDCl_3$, δ, ppm): δ = 133.1, 131.9, 131.7, 130.5, 129.2, 128.8, 128.4, 125.8, 125.4, 124.2, $^{31}P\{^{1}H\}$ NMR (121.49M Hz, $CDCl_3$, δ, ppm): δ = 29.3. FT-IR (selected bands): ν = 3077 (NH), 1587, 1437, 1225, 1174, 1153, 1120, 1069, 1026, 953, 754, 726, 690, 635, 546, 520, 432 cm^{-1}. ESI-MS (positive): (m/z) = 559 (9 %) $[M+C_{35}H_{28}AgN_2O_5P_2F_3S]^+$, 359 (100 %) $[M+C_{46}H_{38}AgN_2O_3P_3]^+$.

2.1.2.20 Synthesis of [Cu{$C_{10}H_6$(1,8-NHPPh_2O)}$_2$]Cl (20)

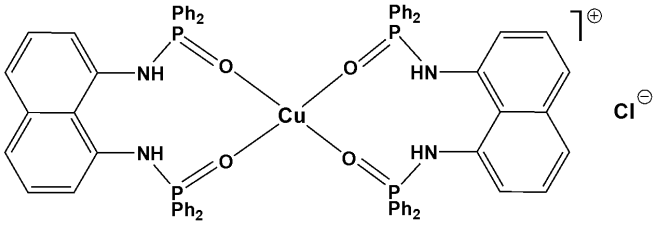

To a solution of [$C_{10}H_6$(1,8-NHPPh_2S)$_2$] (500 mg, 0.847 mmol) in CH_3Cl (30mL) was added CuCl (83.9 mg, 0.847 mmol) in one portion and the reaction was stirred un reflux for 90 minutes. The reaction was filtered throught Celite and the concentrated filtrate yielded **(20)**. Complexes **(21)**-**(22)** were synthesized similarly to **(20)**.

Yield: 565 mg (54.9 %). Mp: 107 ºC. Elemental analysis calcd (%) for $C_{68}H_{56}ClCuN_4O4P_4^-$ (1216.09 g mol^{-1}): C, 67.16; H, 4.64; N, 4.61; found: C, 68.87; H, 4.58; N, 4.68; ^{1}H NMR (400MHz, $CDCl_3$, δ, ppm): δ = 7.89 (m, 4H, naph-H), 7.74 (m, 10H, phenyl-H), 7.58-7.51 (m, 4H, naph-H), 7.38-7.36 (m, 10H, phenyl-H), 7.27 (m, 20H, phenyl-H), 6.92 (m, 4H, naph-H); ^{13}C{^{1}H} NMR (100 MHz, $CDCl_3$, δ, ppm): δ = 132.0, 131.9, 131.0. 130.7, 128.8, 128.4, 126.4, 126.0, 125.2, ^{31}P{^{1}H} NMR (121.49M Hz, $CDCl_3$, δ, ppm): δ = 25.9 (*broad*). FT-IR (selected bands): ν = 3053 (NH), 1623, 1588, 1473, 1436, 1292, 1256, 1167, 1123, 1105, 1039, 822, 749, 725, 691, 519 cm^{-1}. ESI-MS (positive): (m/z) = 195 (100 %) $[M+C_{58}H_{48}ClCuN_2O_4P_3]^+$.

2.1.2.21 Synthesis of [Cu{$C_{10}H_6$(1,8-NHPPh_2O)$_2$}$_2$]Br (21)

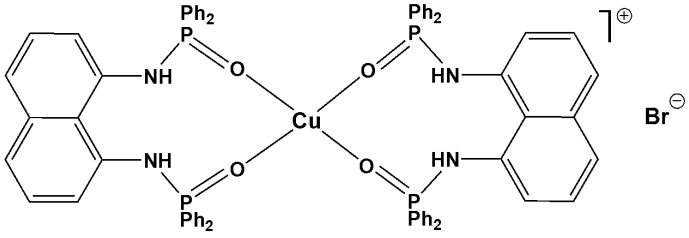

Yield: 677 mg (63.4 %). Mp: 145 ºC. Elemental analysis calcd (%) for $C_{68}H_{56}BrCuN_4O_4P_4^-$ (1260.54 g mol^{-1}): C, 64.79; H, 4.48; N, 4.44; found: C, 63.82; H, 4.44; N, 4.40; ^{1}H NMR (400MHz, $CDCl_3$, δ, ppm): δ = 7.90-7.89 (m, 4H, naph-H), 7.75 (m, 10H, phenyl-H), 7.64-7.59 (m, 2H, phenyl-H), 7.50-7.48 (m, 4H, naph-H), 7.42-7.38 (m, 10H, phenyl-H), 7.27-7.26 (m, 18H, phenyl-H), 7.06 (m, 4H, naph-H); ^{13}C{^{1}H} NMR (100 MHz, $CDCl_3$, δ, ppm): δ = 132.0, 131.7, 131.3, 128.9, 128.4, 126.4, 125.2, ^{31}P{^{1}H} NMR (121.49M Hz, $CDCl_3$, δ, ppm) : δ = 25.9-23.6 (*broad*). FT-IR (selected bands): ν = 3053 (NH), 1581, 1462, 1436, 1282, 1178, 1122, 1106, 1037, 895, 822, 746, 722, 691, 540, 518 cm^{-1}. ESI-MS (positive): (m/z) = 1139 (100 %) $[M+H_4O_2Br]^+$.

2.1.2.22 Synthesis of [Cu{$C_{10}H_6$(1,8-$NHPPh_2O)_2$}$_2$]I (22)

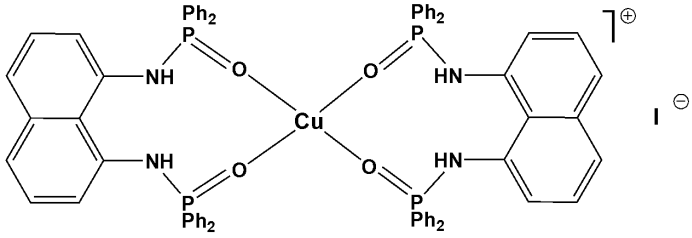

Yield: 810 mg (73.1 %). Mp: 157 ºC. Elemental analysis calcd (%) for $C_{68}H_{56}CuIN_4O_4P_4^-$ (1307.54 g mol^{-1}): C, 62.46; H, 4.32; N, 4.28; found: C, 60.98; H, 4.28; N, 3.84; ^{1}H NMR (400MHz, $CDCl_3$, δ, ppm): δ = 7.94-7.89 (m, 4H, naph-H), 7.77-7.73 (m, 10H, phenyl-H), 7.51-7.49 (m, 4H, naph-H), 7.46-7.38 (m, 10H, phenyl-H), 7.29-7.26 (m, 20H, phenyl-H), 7.06-7.05 (m, 4H, naph-H); ^{13}C{^{1}H} NMR (100 MHz, $CDCl_3$, δ, ppm): δ = 132.0, 131.9, 131.0. 130.7, 128.8, 128.4, 126.4, 126.0, 125.2, ^{31}P{^{1}H} NMR (121.49M Hz, $CDCl_3$, δ, ppm) : δ = 31.3-18.6 (*broad*). FT-IR (selected bands): ν = 3054 (NH), 1646, 1582, 1463, 1437, 1419, 1325, 1284, 1177, 1122, 1037, 959, 895, 812, 746, 722, 690, 539, 517 cm^{-1}. ESI-MS (positive): (m/z) = 1139 (15 %) $[M+Na+C_{10}H_9N]^+$, 359 (100 %) $[M+C_{46}H_{38}CuN_2O_3P_3I]^+$.

2.1.3 Synthesis of Perimidines Compounds and Complexes

2.1.3.1 Synthesis of [$C_{10}H_6$(1,8-$NH)_2$(C{CH_3}{$(CH_2)_2CH_3$})], (23)

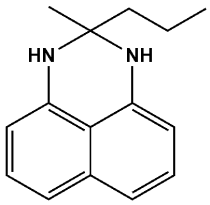

To a 150 mL three necked round bottom Schenk flask was added 1,8-diaminonaphthalene (5000 mg, 31.6 mmol), activated molecular sieves (5000 mg) and 2-pentanone (26270 mg, 319 mmol). The reaction was heated to 80°C overnight. The reaction mixture was filtered and the solids were washed with diethyl ether. The ether solutions were combined and all volatiles were removed under vacuum to give a red/purple solid that was identified as compound **(23)**. Systems **(24-28)** were prepared similar to compounds **(23)**.

Purple solid; Yield 6604 mg (94.5 %). Mp: 91-92 ºC. Elemental analysis calcd (%) for $C_{15}H_{18}N_2$ (226.32 g mol^{-1}): C, 79.61; H, 8.02; N, 12.38; found: C, 79.51; H, 8.04; N, 12.79; ^{1}H NMR (400 MHz, $CDCl_3$, δ, ppm): δ = 7.15-7.02 (m, 4H), 6.39-6.37 (d, *J* = 7.32Hz, 2H), 4.07 (br, 2H, NH), 1.60-1.56 (m, 2H), 1.37-1.36 (m, 2H), 1.32 (s, 3H), 0.82 (t, *J* = 7.28Hz,3H); ^{13}C{^{1}H} NMR (100 MHz, $CDCl_3$, δ, ppm): δ = 140.2, 134.6, 127.0, 117.1, 113.0, 105.8, 66.6,

43.1, 27.7, 17.3, 14.3. FT-IR (selected bands): ν = 3365 (NH), 1595 (aromatic C-H), 1407 (C=C), 1034, 755, 641, 459 cm^{-1}. ESI-MS (positive): (m/z) = 227 (100%) $[M+H]^+$.

2.1.3.2 Synthesis of $[C_{10}H_6(1,8\text{-}NH)_2(C\{CH_2CH_3\}_2)]$, (24)

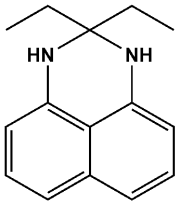

Purple solid; Yield 5965 mg (85.4 %). Mp: 97-98 ºC. Elemental analysis calcd (%) for $C_{15}H_{18}N_2$ (226.32 g mol^{-1}): C, 79.61; H, 8.02; N, 12.38; found: C, 79.59; H, 7.98; N, 12.48; ^1H NMR (400 MHz, $CDCl_3$, δ, ppm): δ = 7.17-7.11 (t, *J* = 7.78Hz, 2H), 7.03-7.01 (d, *J* = 8.48Hz, 2H),6.37-6.35 (d, *J* = 7.04Hz, 2H), 4.11 (br, 2H, NH), 1.67-1.61 (q, *J* = 7.48, 4H), 0.88-0.85 (t, *J* = 7.48, 6H); $^{13}C\{^1H\}$ NMR (100 MHz, $CDCl_3$, δ, ppm): δ = 139.3, 133.6, 126.0, 115.5, 111.8, 104.4, 67.8, 29.4, 6.70. FT-IR (selected bands): ν = 3373 (NH), 1596 (aromatic C-H), 1426 (C=C), 1035, 756, 639, 454 cm^{-1}. ESI-MS (positive): (m/z) = 227 (100 %) $[M+H]^+$.

2.1.3.3 Synthesis of $[C_{10}H_6(1,8\text{-}NH)_2(C\{CH_3\}\{CH_2CH_3\})]$, (25)

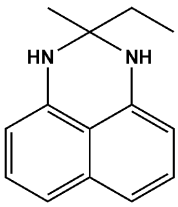

Purple solid; Yield 5915 mg (88.2 %). Mp: 57 ºC. Elemental analysis calcd (%) for $C_{14}H_{16}N_2$ (212.29 g mol^{-1}): C, 79.21; H, 7.60; N, 13.20; found: C, 79.18; H, 7.58; N, 13.22; ^1H NMR (400 MHz, $CDCl_3$, δ, ppm): δ = 7.15-7.02 (m, 4H), 6.37-6.35 (d, *J* = 7.56 Hz, 2H), 3.89-3.87 (br, 2H, NH), 2.07 (s, 3H), 1.67-1.61 (q, *J* = 7.47 Hz, 2H), 0.89-0.85 (t, *J* = 7.46Hz, 3H); $^{13}C\{^1H\}$ NMR (100 MHz, $CDCl_3$, δ, ppm): δ = 139.2, 133.6, 126.0, 115.8, 112.0, 104.7, 65.7, 29.8, 7.10. FT-IR (selected bands): ν = 3360 (NH), 1596 (aromatic C-H), 1406 (C=C), 1033, 758, 642, 531 cm^{-1}. ESI-MS (positive): (m/z) = 213 (100 %) $[M+H]^+$.

2.1.3.4 Synthesis of [$C_{10}H_6$(1,8-NH)$_2$(C{CH_3}{$CH(CH_3)_2$})], (26)

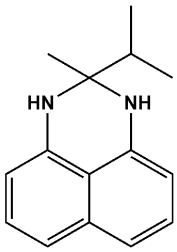

Purple solid; Yield 7111 mg (99.5 %). Mp: 73-75 ºC. Elemental analysis calcd (%) for $C_{15}H_{18}N_2$ (226.32 g mol^{-1}): C, 79.61; H, 8.02; N, 12.38; found: C, 79.59; H, 7.98; N, 12.35; ^{1}H NMR (400 MHz, $CDCl_3$, δ, ppm): δ = 7.18-7.02 (m, 4H), 6.37-6.36 (d, *J* = 7.24Hz, 2H), 4.27-4.22 (br, 2H, NH), 2.09-1.97 (m, 1H), 1.28 (s, 2H), 0.94-0.92 (d, *J*= 6.92Hz, 3H), ^{13}C{^{1}H} NMR (100 MHz, $CDCl_3$, δ, ppm): δ = 139.0, 133.5, 126.0, 115.6, 112.0, 104.4, 67.8, 34.0, 21.2, 15.6. FT-IR (selected bands): ν = 3370 (NH), 1596 (aromatic C-H), 1407 (C=C), 1033, 755, 637, 496 cm^{-1}. ESI-MS (positive): (m/z) = 227 (100 %) $[M+H]^+$.

2.1.3.5 Synthesis of [$C_{10}H_6$(1,8-NH)$_2$(C{CH_3}{$(CH_2)_4CH_3$})], (27)

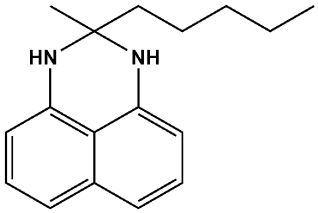

Purple solid; Yield 7987 mg (99.4 %). Mp: x ºC (liquid sample). Elemental analysis calcd (%) for $C_{17}H_{22}N_2$ (254.18 g mol^{-1}): C, 80.27; H, 8.72; N, 11.01; found: C, 80.24; H, 8.69; N, 11.15; ^{1}H NMR (400 MHz, $CDCl_3$, δ, ppm): δ = 7.11-6.99 (m, 4H), 6.28-6.27 (d, *J* = 7.20Hz, 2H), 4.02 (br, 2H, NH), 1.49-1.45 (d, *J* = 8.80Hz, 2H), 1.26-1.20 (m, 2H), 1.21 (s, 3H), 1.17-1.106 (m, 6H), 0.75-0.72 (t, *J* = 7.06Hz, 3H), ^{13}C{^{1}H}140.3, 134.6, 127.1, ^{13}C NMR (100 MHz, $CDCl_3$, δ, ppm): δ = 139.0, 133.5, 126.0, 115.6, 111.8, 104.5, 65.4, 39.7, 25.5, 22.4, 21.5, 14.2. FT-IR (selected bands): ν = 3365 (NH), 1598 (aromatic C-H), 1406 (C=C), 1033, 757, 642, 420 cm^{-1}. ESI-MS (positive): (m/z) = 255 (100 %) $[M+H]^+$.

2.1.3.6 Synthesis of [$C_{10}H_6$(1,8-NH)$_2$(C{CH_3}{$CH_2CH(CH_3)_2$}$_2$)], (28)

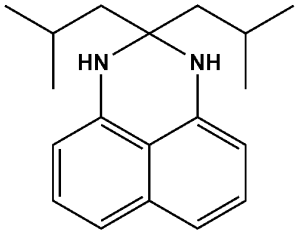

Purple solid; Yield 7861 mg (88.1 %). Mp: x ºC (liquid sample). Elemental analysis calcd (%) for $C_{19}H_{26}N_2$ (282.42 g mol^{-1}): C, 80.80; H, 9.28; N, 9.92; found: C, 79.88; H, 9.26; N, 9.82; ^{1}H NMR (400 MHz, $CDCl_3$, δ, ppm): δ = 7.23-7.15 (m, 4H,), 6.45 (s, 2H), 4.22 (br, 2H, NH), 2.27 (s, 4H, CH_2), 1.48 (m, 2H), 0.94-0.88 (s, 12H,$(CH_3)_4$), ^{13}C{ NMR (100 MHz, $CDCl_3$, δ, ppm): δ = 140.3, 134.6, 127.1, 116.7, 112.8, 105.6, 67.0, 52.3, 24.5, 22.2. FT-IR

(selected bands): ν = 3362, 2954 (NH), 1702 (aromatic C-H), 1599 (C=C), 1366, 1164, 1034, 810, 756, 643, 541 cm^{-1}. ESI-MS (positive): (m/z) = 283 (100 %) $[M+H]^+$.

2.1.3.7 Synthesis of $[C_{10}H_6(1,8\text{-}NH)_2{\cdot}Fe(C_5H_4)_2\{COCH_3\}_2]$, (29)

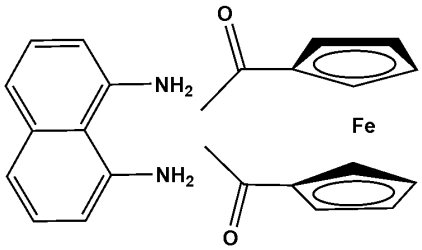

To a 150 mL three necked round bottom Schenk flask was added 1,8-diaminonaphthalene (613 mg, 3.87 mmol), activated molecular sieves (5000 mg) and dissolved in ethanol (40 mL) and 1,1'-diacetylferrocene (523 mg, 1.94 mmol). The reaction was heated to 80°C overnight. The reaction mixture was filtered *via* Celite. The volatiles were removed under vacuum to give a black/brown coloured compound. The product was extracted with methanol (3 x 25 mL) and concentrated to yield an orange co-crystal **(29)**.

Orange; Yield 512 mg (61.8 %). Mp: 54.7 ºC. Elemental analysis calcd (%) for $[C_{10}H_6N_2][Fc\{CO(CH_3)\}_2]$(428.3 g mol^{-1}): C, 59.28; H, 4.56; N, 11.52; found: C, 58.88; H, 4.52; N, 11.68; ^1H NMR (400 MHz, $CDCl_3$, δ, ppm) : δ = 7.15-7.22 (m, 4H), 658-6.61 (dd, *J* = 8.16Hz, 2H), 4.77-7.78 (t, *J* = 3.76Hz, 4H, *Cp*), 4.51-4.52 (t, *J* = 3.81Hz, 4H, *Cp*), 4.02 (br, 4H, NH $_{\text{overlaps with CpH}}$), 2.36 (s, 6H, CH_3), $^{13}C\{^1H\}$ NMR (100 MHz, $CDCl_3$, δ, ppm): δ = 144.4, 137.01, 126.2, 119.7, 117.1, 111.5, 105.9, 80.7, 73.58, 70.9, 28.9. FT-IR (selected bands): ν = 3339 (NH), 3100, 3042, 1651 (aromatic C-H), 1580 (C=C), 1452, 1401, 1373, 1273, 1115, 812, 756, 474 cm^{-1}.

2.1.3.8 Synthesis of $[C_{10}H_6(1,8\text{-}NH)_2(C\{CH_3\}\{C_5H_4N\})]$, (30) and (30*)

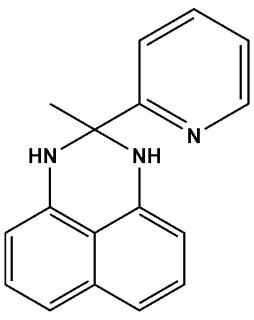

To a 150 mL three necked round bottom Schenk flask was added 1,8-diaminonaphthalene (2000 mg, 12.6 mmol), activated molecular sieves (2000 mg) and 1-(pyridin-2-yl)ethanone (15310 mg, 126 mmol). The reaction was heated to 80°C overnight. The reaction mixture was filtered and the solid was washed with diethyl ether. The ether solutions were

combined and left open in air to form crystals of compound **(30)**. Crystal of **(30*)** were grown in acetonitrile.

Light brown; Yield 2950 mg (89.4 %). Mp: 139-140 ºC. Elemental analysis calcd (%) for $C_{27}H_{44}N_2P_2$ (261.32 g mol^{-1}): C, 78.13; H, 5.79; N, 16.08; found C, 78.10; H, 5.78; N, 16.07; ^{1}H NMR (400 MHz, $CDCl_3$, δ, ppm): δ = 8.70-8.51 (d,d, *J* = 4.68Hz, 1H), 8.07-8.55 (d, *J* = 7.24Hz, 1H), 7.45-7.44 (m, 2H), 7.24-7.20 (t, *J* = 7.76Hz, 2H), 7.12-7.10 (d, *J* = 8.04Hz, 2H), 7.05-7.01 (m, 1H), 6.62-6.60 (d, *J* = 7.28Hz, 2H), 5.33 (br, 2H), 1.80 (s, 3H); ^{13}C{^{1}H} NMR (100 MHz, $CDCl_3$, δ, ppm): δ = 164.5, 149.3, 140.1, 136.8, 134.5, 127.1, 122.1, 121.6, 119.4, 113.9, 106.3, 68.9, 30.1. FT-IR (selected bands): ν = 3372, 3243 (NH), 1598, 1588 (aromatic C-H), 1510 (C=C), 1423, 1144, 812, 780, 763, 674, 470 cm^{-1}. ESI-MS (positive): (m/z) = 262 (100 %) $[M+H]^+$.

2.1.3.9 Synthesis of $[Ni(H_2O)_2\{C_{10}H_6(1,8\text{-}NH)_2(C\{CH_3\}\{C_5H_4N\})\}_2]2Cl$, (31)

To a solution of **(30)** (213 mg, 0.817 mmol) in ethanol (40 mL) was added $NiCl_2$:$CH_3OCH_2CH_2OCH_3$ (179 mg, 0.817 mmol). The resulting solution was then allowed to stir up at room temperature for 12 hours. This solvent was removed under high vacuum pump to yield the complex **(31)**. The crystals were grown in ethanol: acetone by slow evaporation.

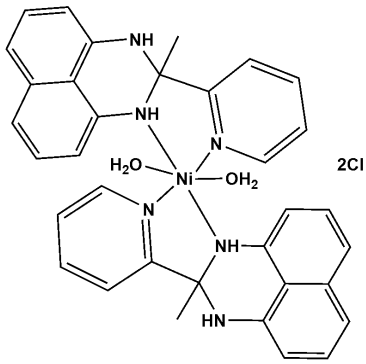

Very light green; Yield 282 mg (88.6 %). Mp: 245 ºC. Elemental analysis calcd (%) for $C_{34}H_{30}Cl_2N_6Ni$ (652.24 g mol^{-1}): C, 62.61; H, 4.64; N, 12.88; found: C, 63.11; H, 4.62; N, 12.98; FT-IR (selected bands): ν = 3196(NH) and (OH), 1655, 1629, 1599 (aromatic C-H), 1400, 1378 (C=C), 1311, 1257, 1161, 1096, 827, 765, 591 cm^{-1}. The complex is paramagnetic, No NMR. ESI-MS (positive): (m/z) = 574 (4 %) $[M+H+2Cl]^+$, 635 (6 %) $[M+H\text{-}O]^+$, 262 (100 %) $[M+C_{19}H_{21}N_3NiO_2]^+$.

2.1.3.10 Synthesis of [$ZnCl_2${$C_{10}H_6$(1,8-NH)$_2$(C{CH_3}{C_5H_4N})}$_2$], (32)

To a solution of **(30)** (399 mg, 0.676 mmol) in ethanol (40 mL) was added $ZnCl_2$ (92.2 mg, 0.676 mmol). The resulting solution was then allowed to stir up at room temperature for 12 hours. This solvent was removed under high vacuum pump to yield complex **(32)**.

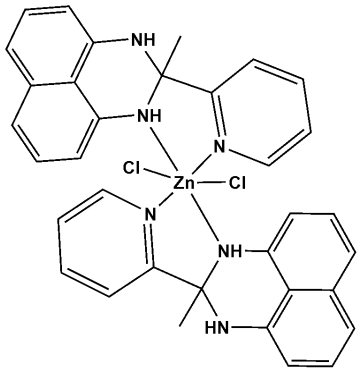

Brown; Yield 401 mg (90.0 %). Mp: 85 ºC. Elemental analysis calcd (%) for $C_{34}H_{30}Cl_2N_6Zn$ (658.96 g mol^{-1}): C, 61.97; H, 4.59; N, 12.75; found: C, 61.78; H, 4.60; N, 12.19; ^{1}H NMR (400 MHz, C_6D_6, δ, ppm): δ = 8.73-8.47 (m, 2H, phenyl-H), 7.99-7.96 (m, 2H, phenyl-H), 7.61-7.58 (m, 2H, phenyl-H), 7.51-7.49 (m, 2H, phenyl-H), 7.14 (br, 4H, NH), 7.09-7.05 (t, *J*= 7.78Hz, 4H, naph-H), 6.84-6.82 (d, *J* = 8.08Hz, 4H, naph-H), 6.52-6.50 (d, *J* = 7.36Hz, 4H, naph-H), 1.64 (s, 6H); ^{13}C{^{1}H} NMR (100 MHz, C_6D_6, δ, ppm): δ = 165.6, 149.1, 141.6, 137.4, 136.3, 134.4, 127.6, 126.9, 121.9, 119.8, 114.7, 104.1, 68.3, 29.3. FT-IR (selected bands): ν = 3296(NH), 1675, 1598 (aromatic C-H), 1468, 1404 (C=C), 1309, 1251, 1163, 1089, 1045, 877, 816, 762, 668, 617, 589 cm^{-1}. ESI-MS (positive): (m/z) = 183 (15 %) $[M+C_{17}H_{15}C_{12}N_3Zn]^+$, 262 (30 %) $[M+C_{17}H_{15}Cl_2N_3Zn]^+$, 449 (100 %) $[M+Na+C_{12}H_{12}N_2]^+$.

2.1.3.11 Synthesis of [CdI_2{$C_{10}H_6$(1,8-NH)$_2$(C{CH_3}{C_5C_4N})}$_2$], (33)

To a solution of **(30)** (372 mg, 1.42 mmol) in ethanol (40 mL) was added CdI_2 (521 mg, 0.1.42 mmol). The resulting solution was then allowed to stir up at room temperature for 12 hours. This solvent was removed under high vacuum pump to yield the complex **(33)**.

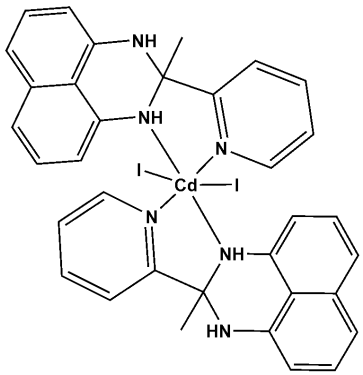

Light orange; Yield 910 mg (71.9 %). Mp: 115 ºC. Elemental analysis calcd (%) for $C_{34}H_{30}CdI_2N_6$ (888.86 g mol^{-1}): C, 45.94; H, 3.40; N, 9.45; found: C, 46.94; H, 3.48; N, 9.49; ^{1}H NMR (400 MHz, C_6D_6, δ, ppm): δ = 8.72-8.47 (m, 2H, phenyl-H), 7.99-7.94 (m, 2H,

phenyl-H), 7.60-7.58 (m, 2H, phenyl-H), 7.51-7.49 (m, 2H, phenyl-H), 7.14 (br, 4H, NH), 7.09-7.06 (t, *J* = 7.78Hz, 4H, naph-H), 6.84-6.82 (d, *J* = 8.12Hz, 4H, naph-H), 6.53-6.51 (d, *J* = 7.34Hz, 4H, naph-H), 1.64 (s, 6H); $^{13}C\{^{1}H\}$ NMR (100 MHz, C_6D_6, δ, ppm): δ = 165.6, 149.1, 141.6, 137.4, 136.3, 134.0, 127.6, 126.9, 121.9, 119.8, 114.7, 104.1, 68.3, 29.3. FT-IR (selected bands): ν = 3372, 3247(NH), 1675, 1597 (aromatic C-H), 1468, 1423, 1376 (C=C), 1308, 1247, 1161, 1145, 1050, 1013, 970, 815, 763, 748, 668, 612, 586 cm^{-1}. ESI-MS (positive): (m/z) = 761 (1 %) $[M+H+I]^+$, 135 (75 %) $[M+C_{27}H_{23}CdI_2N_3]^+$, 102 (100 %) $[M+C_{29}H_{28}CdI_2N_4]^+$.

2.1.4 X-Ray Crystallography Procedures

Crystal structure elucidations for compounds **(3)**, **(4)**, **(4*)**, **(5)** and **(17)** were performed at Michigan State University, USA. X-Ray crystallographic data was collected on Bruker CCD (charge coupled device) diffractometer using a Mo *K*α radiation source (λ = 0.71073 Å) equipped with an Oxford Cryostream low-temperature apparatus operating at 173(2) K. The crystallographic data and numerical results for the structural determinations reported in this thesis are given in the appendix section. The crystals were mounted on a Nylon loop using very small amount of paratone oil. The total number of images was based on results from the program COSMO[7] where redundancy was expected to be 4.0 and completeness of a d-spacing resolution of 100% out to 0.83 Å. Cell parameters were obtained using APEX II software[8] and refined using SAINT on all observed reflections. The data reduction was performed using the SAINT software[9] which corrects for Lp (Lorentz–polarization). Scaling and absorption corrections were applied using SADABS[10] multi-scan technique, supplied by George Sheldrick. The structures are solved by the direct method using the SHELXS-97 program and refined by least squares method on F^2, using SHELXL- 97[11], which are incorporated in OLEX2[12]. The crystals used for the diffraction study showed no decomposition during data collection.

Crystal structure elucidations for compounds **(6)**, **(8)**, **(9)**, **(10)**, **(11)**, **(12)**, **(15)**, **(16)**, **(25)**, **(26)**, **(29)**, **(30)**, **(30*)** and **(31)** were performed at UKZN, School of Chemistry and Physics. Crystal structure of **(23)** and **(24)** were unresolved and they were not discussed in this thesis.

The above crystals were selected, attached onto the tip of glass fibers using epoxy glue, and centered in the X-ray beam by the aid of a video camera. Crystal evaluation and data collection

were done on a Bruker Smart APEX2 diffractometer with Mo *K*α radiation (λ = 0.71073 Å) equipped with an Oxford Cryostream low-temperature apparatus operating at 100(1) K. The initial cell matrix was determined from three series of scans consisting of twelve frames collected at intervals of 0.5° in a 6° range with the exposure time of ten seconds per frame. Each of the three series of scans was collected at different starting angles and the *APEXII*[13] program suite used to index the reflections. The data collection involved using omega scans of 0.5° width with an exposure time of 20 s per frame. The total number of images was based on results from the program *COSMO*[14] whereby the expected redundancy was to be 4.0 and completeness of 100% out to 0.75 Å. Cell parameters were retrieved using *APEXII*[13] and refined using *SAINT*[15] on all observed reflections. Data reduction was performed using *SAINT* software, and the scaling and absorption corrections were applied using *SADABS*[16] multi-scan technique. The structures were solved by the direct method using the *SHELXS*[11] program and refined.

The visual crystal structures were presented using *ORTEP*-3[17], *MERCURY*[18], and *DIAMOND*[19] system software. Non-hydrogen atoms were first refined isotropically and then by anisotropic refinement with full-matrix least squares based on F^2 using *SHELXL*[11]. All hydrogens were positioned geometrically, allowed to ride on their parent atoms, and refined isotropically.

All the refinement data was subjected to the online check CIF routines of the IUCr. What is important to note from these online reports is that you should NOT have any series alerts pertaining to quality of the model you propose (i.e. the model you propose should be chemically sound and fit experimental data). If these criteria are satisfied then all the discussion you make on the geometrical aspect are trustworthy.

Chapter 3 and 4, all the non-hydrogen atoms for crystal structures were refined anisotropically, whereas structure **(31)** all refined isotropically.

All drawings are done at 50% ellipsoids. Reliability factors are defined as $R1 = \Sigma \mid\mid F_o \mid - \mid F_c \mid\mid / \Sigma \mid F_o \mid$. [b] $wR2 = \{\Sigma [w(F_o^2 - F_c^2)^2] / \Sigma [w(F_o^2)^2]\}^{1/2}$ and the crystallographic data, selected bond lengths and angles are summarized in Chapters.

2.2 References

1. P. Bazinet, T.-G. Ong, J. S. O'Brien, N. Lavoie, E. Bell, G. P. A. Yap, I. Korobkov and D. S. Richeson, *Organometallics*, 2007, 26, 2885-2895.
2. G. Kubas, B. Monzyk and A. Crumbliss, *Inorg. Synth.*, 2007, 19, 90-92.
3. T. Q. Ly, A. M. Z. Slawin and J. D. Woollins, *J. Chem. Soc., Dalton Trans.*, 1997, 1611-1616.
4. D. B. G. Williams and M. Lawton, *J. Org. Chem.*, 2010, 75, 8351-8354.
5. A. B. Pangborn, M. A. Giardello, R. H. Grubbs, R. K. Rosen and F. J. Timmers, *Organometallics*, 1996, 15, 1518-1520.
6. M. J. Frisch and A. B. Nielsen, *Gaussian 03 Programmer's Reference*, Gaussian, 2003.
7. C. V1.61, *Software for the CCD Detector Systems for Determining Data Collection Parameters. Bruker Analytical X-ray Systems*, Madison, WI (2009).
8. A. V2010.11-3, *Software for the CCD Detector System; Bruker Analytical X-ray Systems*, Madison, WI (2010).
9. S. V. 7.68A, *Software for the Integration of CCD Detector System Bruker Analytical X-ray Systems*, Madison, WI (2010).
10. R. Blessing, *Acta Crystallogr. A*, 1995, 51, 33-38.
11. G. M. Sheldrick, *Acta Crystallogr. Sect. A: Found. Crystallogr.*, 2008, 64, 112-122.
12. O. V. Dolomanov, L. J. Bourhis, R. J. Gildea, J. A. Howard and H. Puschmann, *J. Appl. Crystallogr.*, 2009, 42, 339-341.
13. *Bruker. In APEXII, Bruker AXS, Madison, WI* 2009.
14. *Bruker. In COSMO, Bruker AXS, Madison, WI* 2009.
15. S.-N. Bruker, *Bruker AXS Inc., Madison, Wisconsin, USA*, 2009.
16. *Bruker. In SADABS, Bruker AXS, Madison, WI* 2009.
17. L. J. Farrugia, *J. Appl. Crystallogr.*, 2012, 45, 849-854.
18. C. F. Macrae, I. J. Bruno, J. A. Chisholm, P. R. Edgington, P. McCabe, E. Pidcock, L. Rodriguez-Monge, R. Taylor, J. v. Streek and P. A. Wood, *J. Appl. Crystallogr.*, 2008, 41, 466-470.
19. K. Brandenburg, *In DIAMOND. Crystal Impact GbR, Bonn, Germany*, 2005.

Chapter 3

Bis(amino)phosphine and Perimidine Ligands

3.1 Synthesis of Bis(amino)phosphine Ligands, Spectroscopic Analysis and Crystal Structures

3.1.1 Background

The class of compounds described herein represents the ligands bis(amino)phosphines (BAMP). These compounds contain two P-N bonds around the trivalent phosphorus centre.[1] The P-N bonds are stable toward lithium and Grignard[2] reagents and they can undergo a series of nucleophilic substitution reactions in both cyclic and acyclic systems.[3] The first type of BAMP ligand was discovered by Michaelis in 1903.[4] Moreover, P-N bonds are easily cleaved by hydrolysis in the presence of trace amounts of acid/ base impurities and during the formation of transition metals complexes.[5] The importance of having both P and N donor atoms on the same ligand, is to provide different chemical and physical properties of the organic BAMP ligand.[6] This will assist the ligand in chelating to the metal centers. A number of these BAMP have been reported and their synthesis methods is well established.[7] It was discovered that an electron-donating group often lead to the formation of P(III) aminophosphines [P-N-P], whereas an electron-withdrawing group like nitrile and trifluoromethyl at the *ortho*-position of aryl ligands often forms iminophosphines [P(III)-P(V)=N].[8] There are two other related ligands to BAMP and those are diphosphinites and aminophosphane-phosphinites (AMPP). These should not be confused with BAMP.

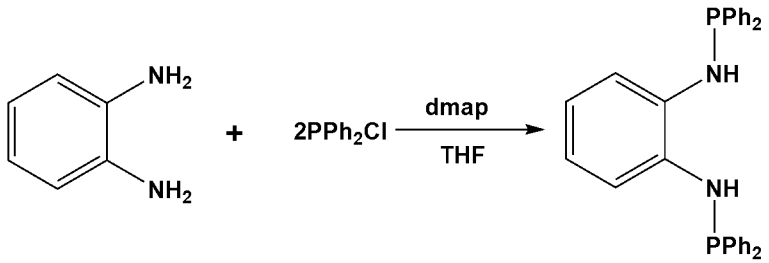

Scheme 3.1.2.1. Synthesis of free BAMP/ bis(amino)phosphine ligand, where (dmap) is 4-dimethylaminopyridine.

The present study report the synthesis of BAMP which is used as a co-catalyst in many catalytic processes. Furthermore, the oxidation of P(III)-N(III) BAMP ligands with chalcogenide donor atoms (O, S or Se) to [P(V)-N(III)] provided a wide spectrum of coordination studies. The BAMP ligand could be considered to have similar reactivity and coordination modes when compared to the well-studied bis(diphenylphosphino)amine ligand,[9] dppa, as shown in Figure 3.1.1.1

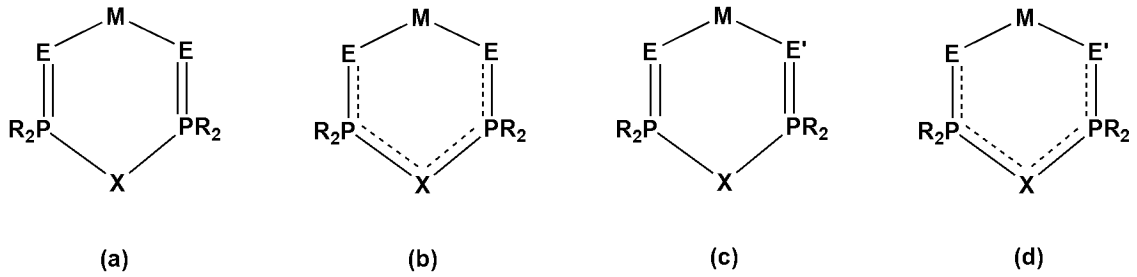

Figure 3.1.1.1. Coordination modes of dppa x = CH_2, NH or CH or N, E = O, S, Se.

Moreover, the BAMP ligands could be used for selective extraction of certain metal centers.[10] The addition of donor atoms provide a better variety of coordination modes to the transition metal centers, as well as variation in electronic properties. Free bis(amino)phosphine ligands can be further derivatized into their own respective chalcogenide [S, Se and Te] and oxides [O] oxidation products. The chalcogenide-oxidized BAMP type ligands are also highly reactive toward metal complexation. In most cases the sterically hindered substituents tend to be slow towards oxygenation and a much stronger oxidising agent such as hydrogen peroxide [H_2O_2] is needed. The oxygenation process can also be achieved *via* the treatment of the free aminophosphine ligand with water, nitric acid, permanganate and dichromate.[11-14]

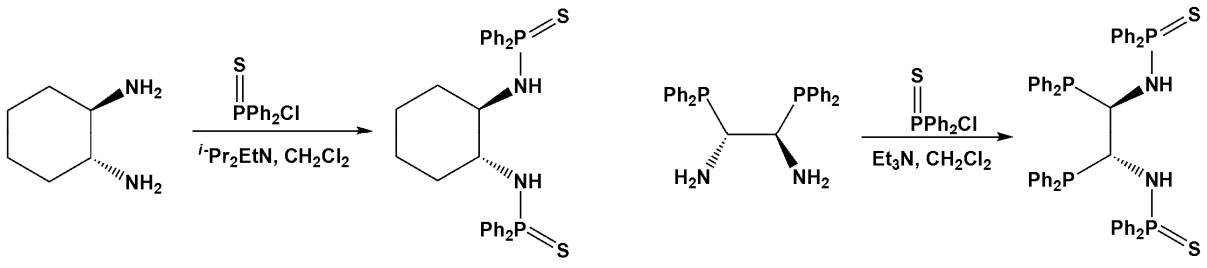

Scheme 3.1.2.2. Indirect synthesis of bis(amino)phosphine ligands by an oxidized phosphine.

Bis(amino)phosphine chalcogenide ligands can also be prepared by oxidising the corresponding chlorophenylphosphine prior to the aminolysis reaction. The treatment of the amine with the oxidised chlorophosphine, using diisopropylethylamine or Et_3N as a base, could attach the two reagents and form a P-N product in dichloromethane.[15] Importantly, the solvent plays a vital role in the preparation of aminophosphino-chalcogenide ligands and the use of toluene and THF in the oxidation process was extensively employed.[16, 17]

3.1.2 Results and Discussion

3.1.2.1 Synthesis of Bis(amino)phosphine Ligands

Two neutral P(III) and three neutral P(V) BAMP ligands described herein were synthesised *via* commercially available starting materials from Sigma-Aldrich, see Experimental Section 2.1.2. The reactions were performed either as a one or two steps procedure under inert atmosphere, Scheme 3.1.2.3. The ligands $[C_{10}H_6(1,8\text{-}NHPPh_2O)_2]$ **(14)** and $[C_{10}H_6(1,8\text{-}NHPPh_2S)_2]$ **(15)** were obtained by oxidizing $[(C_{10}H_6(1,8\text{-}NHPPh_2)_2)]$ **(1)** with respective chalcogenide donor atoms (O and S), respectively. Ligand $[(C_{10}H_6(1\text{-}NHPPh_2O)(8\text{-}NHPPh_2Se]$ **(16)** was synthesized in a two-steps reaction from **(1)**. Ligand $[C_{10}H_6(1,8\text{-}NH\text{-}P\{CH(CH_3)_2\}_2)_2]$ **(2)** was prepared similar to **(1)**.

Ligands **(1)** and **(2)** were prepared by an aminolysis reaction. The reaction of PR_2Cl (R = Ph **(1)** and $[(CH_3)_2(CH)]_2$ **(2)**), respectively, with *1,8*-diaminonaphthalene (amino spacer) in the presence of 4-dimethylaminopyridine (a catalyst) in tetrahydrofuran produced the ligands. Tetrahydrofuran appears to be a suitable solvent in the preparation of bis(amino)phosphine ligands. During the formation of the P-N bond, a white precipitate salt of $[Et_3NH]\cdot Cl$ formed in tetrahydrofuran. The salt $[Et_3NH]\cdot Cl$ have high solubility in most polar solvent which prevents proper isolation of pure bis(amino)phosphine compounds. In THF, the salt precipitated and was easily filtered to isolate the product. Ligand **(1)** was first isolated as a paste which slowly decomposes with time as monitored by ^{31}P NMR. Allowing the compound to dry in high pressure vacuum resulted into a more stable brown solid which gradually decomposes on exposure to moisture. Ligand **(1)** was obtained in good yield (75 %). Ligand **(2)** was prepared similarly to ligand **(1)** in a moderate yield of 70 %. The microanalysis and spectroscopic techniques of the molecule are in agreement with the proposed structures, see Experimental section. After successfully synthesising ligand **(1)**, a series of ligands **(14)**, **(15)**

and **(16)** were then prepared. Treatment of **(1)** with two molar equivalents of elemental sulphur in either toluene or tetrahydrofuran formed **(15)**. Ligand **(14)** was produced by reacting **(1)** with two molar equivalents of hydrogen peroxide in air. Ligand **(16)** was synthesized in two steps from **(1)**. Although compound (**16**) was discovered by accident, we managed to reproduce the result. Ligand **(1)** was treated with one molar equivalent of 30% H_2O_2 in THF and the compound was isolated with one O donor atom attached to the P atom. The isolated product was further reacted with excess Se at 80 °C that oxidized the second P atom, and purified with methanol to give a 74 % yield of **(16)**. Long exposure to air eventually replaces the Se atom with another O donor atom, as expected. The three oxidized compounds **(14)**-**(16)** forms with exothermic reaction. The flask slightly warms upon adding the chalcogenide donor atoms. The temperature was controlled by an ice-bath during the addition process of the chalcogenide. The physical appearance of the sulphur containing ligand was off-white after washing with carbon disulfide (CS_2) and diethyl ether, while the oxygen-containing ligand after recrystallization with chloroform and hexane was white. The oxidized products, i.e. **(14)**-**(16)** are more stable than ligand **(1)**. The percentage yield of ligands ranged from poor to satisfactory. The percentage yield of the oxidized ligands are as follows {E = E = O (50.6 %) **(14)** and S (73 %) **(15)}**.The bulk purity of the ligands were determined by mass spectral analysis, i.e. ESI-MS (positive): (m/z) = 527 (100 %) $[M+H]^+$ **(1)**, ESI-MS (positive): (m/z) = 266 (45 %) $[M+C_{10}H_8]^+$, 159 (100 %) $[M+C_{12}H_{28}P_2]^+$ **(2)**, ESI-MS (positive): (m/z) = 560 (100 %) $[M+H]^+$ **(14)**, (m/z) = 591 (100 %) $[M+H]^+$ **(15)** and ESI-MS (positive): (m/z) = 557 (90 %) $[M-Se]^+$, 341 (100 %) $[M+ C_{12}H_{10}PSeO]^+$ **(16)**. The microanalysis data were found to be in agreement with the theoretical values.

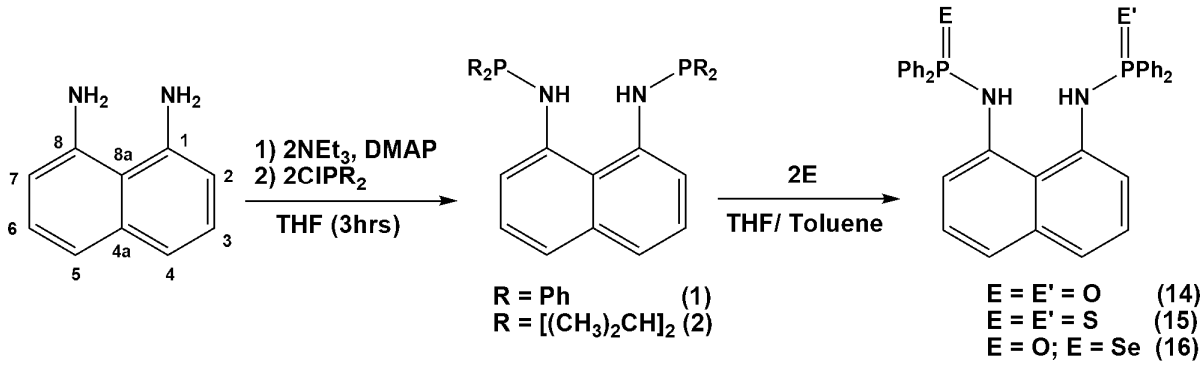

Scheme 3.1.2.3. Synthesis of bis(amino)phosphine ligands.

3.1.2.2 Characterisation: Spectroscopic Analysis ^{1}H, ^{13}C and ^{31}P NMR

The five ligands were further characterised by ^{1}H, ^{13}C and ^{31}P NMR, see Experimental section and spectrums in the Appendix. The ^{1}H NMR of ligand **(1)** was challenging to achieve due to the stability of the compound compared to the oxidised ligands. Therefore, ligands **(1)** and **(2)** had to be dried under high vacuum before they were subjected into the 400MHz NMR for analysis.

The ^{1}H NMR of ligand **(1)** is diamagnetic in deuterated chloroform ($CDCl_3$) showing all the molecular peaks shifted downfield. The resonance of the phenyl-H proton are appearing in the expected region from 7.07-7.45 ppm. The naphthalene protons in position two and seven relative to the *peri*-position, appears in the region 6.02-6.04 ppm as doublets with a coupling constant of J = 8.36 Hz also shifted downfield (see Scheme 3.1.2.3) . In the ^{31}P NMR spectra, one signal resonate in the upfield region at 33.4 ppm. This indicates that both the phosphorus atoms in the molecule are magnetically equivalent in solution. The ^{1}H NMR of **(2)** integrated well to its respective peaks, see Figure 3.1.2.1. The alkyl peaks are overlapping and the spectra shows some trace impurity from the THF solvents. The region of the overlapping peaks is expanded in the Appendix section and the integration fits the expected compound.

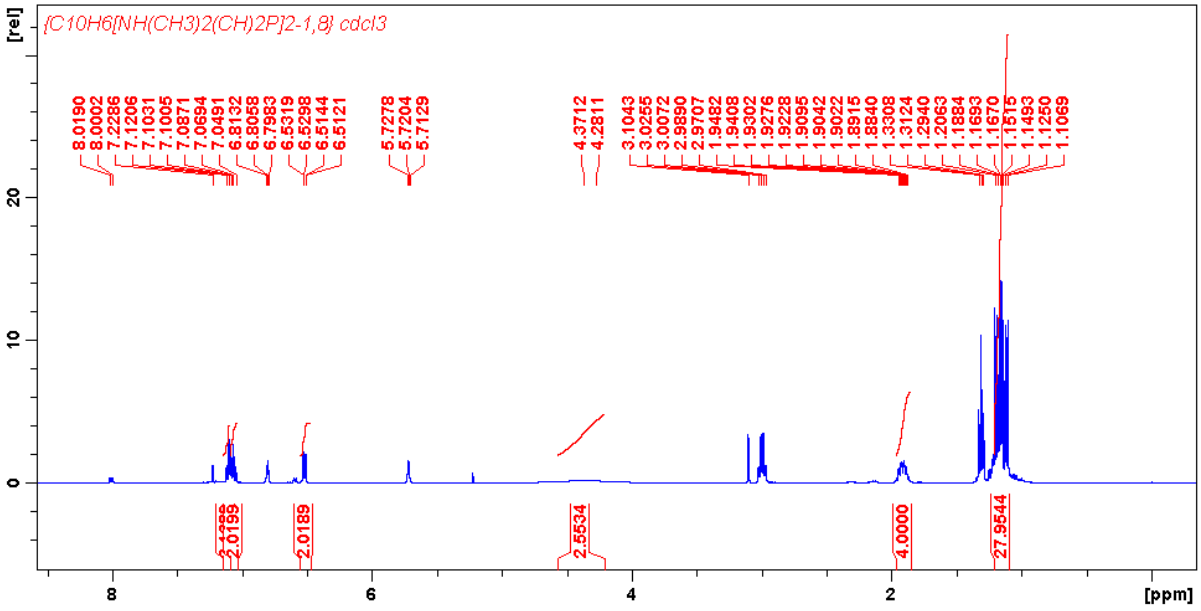

Figure 3.1.2.1. The ^{1}H NMR spectrum of compound **(2)**.

The ^{1}H NMR spectra of **(14)** and **(15)** are well resolved. There is not much difference in the proton resonance signal of oxidized ligands compared to **(1)**. The information given by the ^{1}H NMR of the oxidised bis(amino)phosphines does not provide full evidence that the chalcogenide have been inserted in the ligands. The peaks in the spectra integrate according to their structures. The five ligands were distinguished from each other by ^{31}P NMR. The ^{31}P NMR signal of ligands **(1)** and **(2)** show a prominent singlet peak which resonates at 33.4 and 55.7 ppm, respectively. The ^{31}P NMR of signal ligand **(15)** shows a protruding singlet resonance peak at 57.7 ppm and ligand **(14)** signal peaks resonated at 23.5 ppm. The four ligands, i.e. **(1)**-**(2)** and **(14)** and **(15)**, are symmetrical in nature and the resonance of a single peak in each compound spectrum indicates that the two P-atoms adjacent to each other are equivalent and hence they are in the same chemical environment. The ^{1}H NMR of **(16)** show the chemical shift at 8.39-6.69 ppm for both naphthalene and phosphine groups. The ^{31}P NMR spectrum showed two peaks at 55.3 and 24.4 ppm which indicated that the two P atoms are not chemically equivalent due to different chalcogenides attached to each of them. The ^{31}P NMR signal peaks of **(15)** are shifted downfield by ca. 24 ppm relative to the ligand **(1)**. The ^{31}P NMR of ligand **(14)** appeared to be shifted up-field by ca. 11 ppm to the ligand **(1)**. The results showed the electronic influence of the chalcogenide to the P-N groups of the ligands. For comparative data, refer to the appendices for a better view of the spectra. Figure 3.1.2.2 shows the ^{31}P NMR spectra of **(2)** and **(14)**.

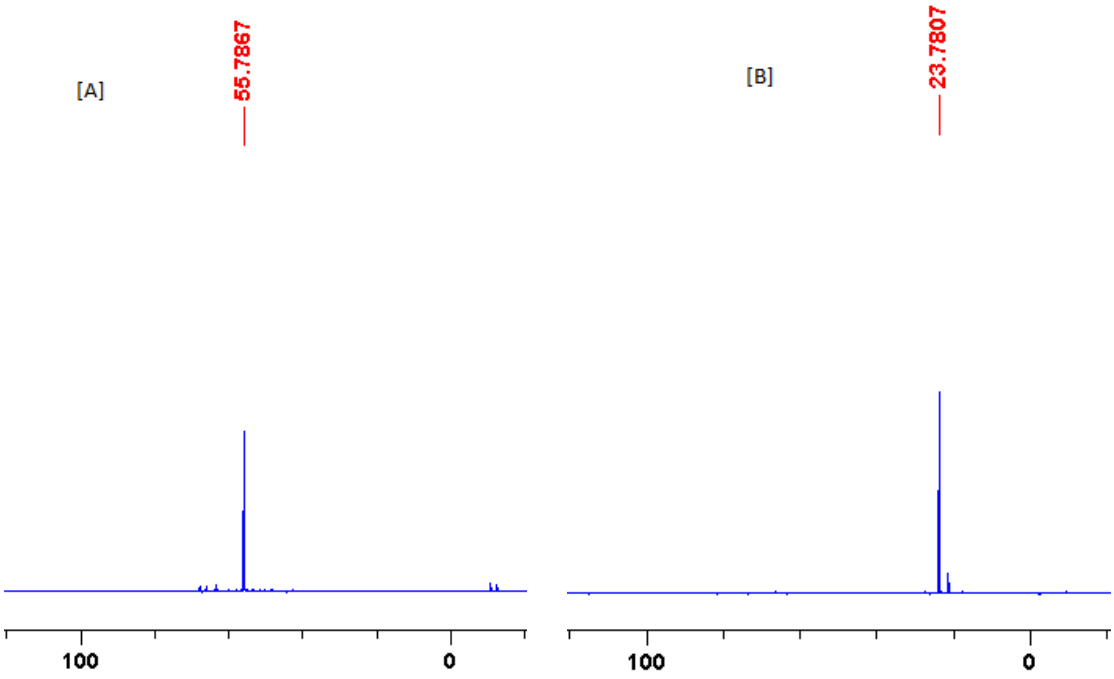

Figure 3.1.2.2. The ^{31}P NMR spectra of compounds **(2)** in **[A]** and **(14)** in **[B]**.

Literature shows that the ^{31}P NMR signal of oxide-aminophosphines appears in a range of 0 to 30 ppm,[18] those of sulfide and selenide appears at more downfield ranges of 50 to 80 ppm.[19-22] The spectral data of selenides in particular are more scarce compared to those of sulphides, yet the latter are more stable. The ^{13}C NMR signals of all five ligands are in agreement with the chemical shifts of the ^{1}H NMR signals of the ligands.

3.1.2.3 Characterisation: FTIR Spectroscopic Analysis

The IR spectra of the five ligands **(1)**, **(2)**, **(14)**, **(15)** and **(16)** were observed as outlined in the experimental section. Ligand **(1)** showed stretching bands of ν(P-Ph) at 1433-1412 and ν(P-N) at 849-812 cm^{-1}. The sharp strong vibrational band of ν(C=C naphthalene) were observed at 1576 and the broad band of ν(NH) at 3050 cm^{-1}. The FTIR bands of compound **(2)** showed strong vibration frequencies of the CH_3 group in *iso*-propyl at 2602 and 2497 cm^{-1}. The vibrational bands of ν(C=C naphthalene) were observed at 1641-1474 and the broad band of ν(NH) at 2948 cm^{-1}. The IR frequencies of the bis(amino)phosphine ligands **(15)** and **(14)** were also studied and compared with those of ligand **(1)**. Ligand **(15)** showed bands of ν(P-Ph) occurring at 1436-1392 and a band of ν(P-N) at 891-835 cm^{-1}. The sharp strong vibrational bands of ν(C=C naphthalene) were observed at 1640-1559 and the broad band of ν(NH) at 3138-3052 cm^{-1}. The FTIR strong absorption of ν(P=S) were observed to stretch around 627 and 629 cm^{-1}. Ligand **(14)** bands of ν(P-Ph) occurred at 1460-1421 and ν(P-N) at 894-825 cm^{-1}. The ν(C=C naphthalene) vibration band was noted at 1581 and ν(NH) observed at 3052 cm^{-1}. The ν(P=O) vibrational frequency occurred 1177 cm^{-1}. In compound **(16)**, the ν(NH, P=O and P=Se) band stretches at 3052, 1265 and 542 cm^{-1}, respectively. Comparing the vibrational frequencies of ν(P-N), ν(NH) and ν(P-Ph) of ligand **(1)** to those of oxidized ligands, the vibrational frequencies were shifted to lower energy frequencies due to the less π-bond contribution of the chalcogenide heavier atoms. We have noted that the groups attached to the P-atoms of the bis(amino)phosphines slightly influences the vibrational frequencies of the ν(P=E). Previous studies have shown that the ν(P=E) vibrations of the oxides occurred in the range of 1090-1415, sulfides 515-870 and selenides 420-600 cm^{-1}.[23-26] Results from previous studies suggest that the influence of π-bond contribution was more important for oxides and the dipolar form was more important for P=E, S and Se because the polarity of these molecule increases with the increase in atomic size, i.e. O<S<Se.[27]

3.1.2.4 Molecular Structures of Bis(amino)phosphine Ligands

Crystals, suitable for single X-ray analysis of ligands **(1)** and **(2)** could not be grown. Growth of quality single crystals for the ligands **(15)** and **(16)** were successful by slow diffusion of neat hexane into a dichloromethane solution of the ligands. Single crystals for compound **(14)** were obtained *via* the slow diffusion of hexane into a dichloromethane/ chloroform solution. The molecular structure of **(14)** could not be solved due to poor diffraction of the crystal. Crystals of the oxidized ligands can also be obtained by the slow evaporation of the ligand dissolved in chloroform. For the ligands, there were no solvates included in the crystal lattice. Crystal structures of ligands **(15)** and **(16)** were determined at different temperatures, see Table 3.1.2.1. Ligand **(16)** was discovered accidentally in the process of preparing complex [Ag($C_{10}H_6$(1,8-$NHPPh_2Se)_2\}_2$] CF_3SO_3, an isomorph of **(17)**. The ligand [($C_{10}H_6$(1,8-$NHPPh_2Se)_2\}_2$] substituted one Se for an O atom on the oxophilic P atom to form ligand **(16)**. This compound was successfully reproduced. Selected bond lengths and angles of compound **(15)** and **(16)** are shown in Table 3.1.2.2. Ligand **(15)** is a polymorph of the compound reported by Ly *et al*., in 1997.[20] The crystallographic data shows that the amino N-donor atoms in the *peri*-positions of ligand **(15)** are approximately coplanar. In ligand **(15)**, the PPh_2S moiety shift off the plane by 10.10° relative to the distorted naphthalene molecule. The P-donor atoms of the PPh_2O and PPh_2Se moieties of ligand **(16)** are positioned slightly off the plane of the naphthalene backbone. The P-donor atoms in ligand **(16)** are orientated on same plane of axis, hence the chalcogenides point in the opposite directions to each other. Ligand **(15)** shows the P-donor atoms are oriented on a different plane of axis relative to the rigid naphthalene moiety, see Figure 3.1.2.3. The distance of the non-bonding N···N *peri*-atoms for compound **(16)** is 2.754 Å. Ligand **(15)** and **(16)** are isomorphous and closely related compounds have been reported by Ly *et al*. [20] Comparative selected bond lengths (Å) for compounds **(15)** and (1**6)** are reported in Table 3.1.2.2. Compound **(15)** contains two P=S moieties relatively having the same bond distances of 1.96Å. The bond distances of P=O and P=Se are contained within the same molecule of **(16)** and they show that the P=O is 1.49Å and P=Se is 2.09Å. These values reveal that the P=O < P=S < P=Se. This is due to atomic radius size of oxygen being smaller than that of sulphur and sulphur being smaller than the atomic size of selenium. In passing down the group from oxygen to polonium there is a gradual change towards metallic character due to the increased shielding effect of the inner electron on the outer *ns* and *np* electrons as the quantum number *n* varies from 2 to 6. The atomic radius increase down the group as a result of the outermost electrons which are further from the nucleus as the *n* increases. Therefore, the

electron shielding prevents these outer electrons from being attracted by the nucleus, thus they are loosely held and the atomic radius get larger.

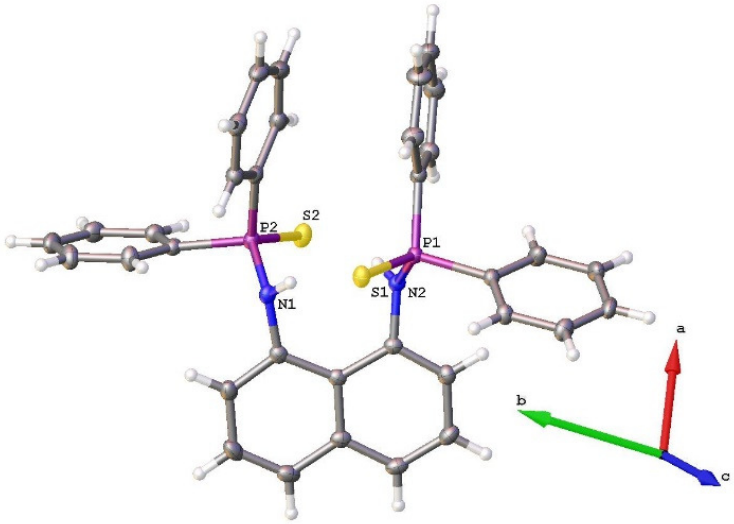

(15)

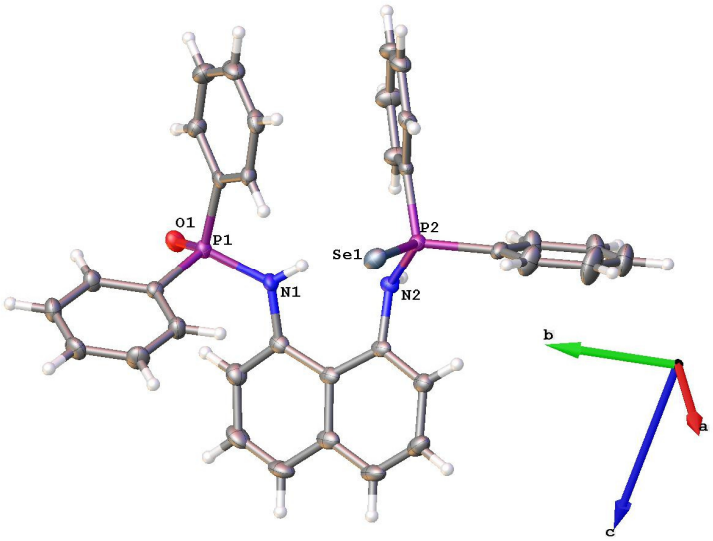

(16)

Figure 3.1.2.3. The molecular structures of **(15)** and (**16)**, drawn at 50% probability using OLEX 2.

Noteworthy is that the N atoms in **(15)** and **(16)** possesses a pyramidalization phenomenon. The nitrogen atoms undergo a deformation of a trigonal planar molecule into a tetrahedral arrangement which make the whole ligand structure chiral. The compounds have a (*R, R*)

conformation around the N-atoms. The molecular structures **(15)** is non-centrosymmetric (Flack value of 0.008(13)) and **(16)** is centrosymmetric with a mirror plane crystallographic center of symmetry characterized by weak intermolecular hydrogen bond between NH···O moieties of the adjacent molecules. Ligands **(15)** and **(16)** occupies two and four molecules in the unit cell, respectively. The spectroscopic data is consistent with the proposed structures. Proposed structures in Scheme 3.1.2.3 superimpose the molecular structures in Figure 3.1.2.3. The molecular structures are isostructural with minimal structural differences due to the nature of the chalcogenide attached to the P-atoms. The molecular structures reveal that the ligands could act in a bidentate or multidentate fashion because of multiple donor atoms. The compounds **(15)** and **(16)** crystallises in the monoclinic system with a space group of $P2_1$ and $P2_1/c$, respectively. The naphthalene moiety are expected to be planar, but due to the atoms in the *peri*-position are larger than H-atoms, there is a slight distortion observed in the structure. The molecules were distorted with a dihedral angle of > 5° compared to the flat un-substituted naphthalene molecule.[28]

Table 3.1.2.1. Crystallographic information for **(15)** and **(16)**.

	15	**16**
Formula	$C_{34}H_{28}N_2P_2S_2$	$C_{34}H_{28}N_2OP_2Se$
M_r	590.64	621.48
Space group	P 2_1	$P2_1/c$
a, Å	9.6605(10)	12.3451(2)
b, Å	15.8279(16)	11.3582(2)
c, Å	10.2767(10)	21.7588(4)
α, deg	90	90
β, deg	115.745(4)	104.3540(10)
γ, deg	90	90
V, *Å*^{3}	1415.4(3)	2955.73(9)
Z	2	4
ρcalcd, g cm^{-3}	1.386	1.397
M, mm^{-1}	0.329	1.409
T, K	293(2)	100(2)
Reflections collected	30294	33094
Independent reflections	6963	5480
R_{int}	0.0205	0.0631
Final *R* indices [I > 2σ(*I*)][a]	R1 = 0.0252, wR2 = 0.0640	R1 = 0.0356, wR2 = 0.0719
R indices (all data)	R1 = 0.0267, wR2 = 0.0649	R1 = 0.0551, wR2 = 0.0779
Absolute structure parameter	0.008(13)	none
Largest diff. peak and hole, e / Å	0.402 and -0.153	0.370 and -0.374

[a] $R1 = \Sigma \mid\mid F_o \mid - \mid F_c \mid\mid / \Sigma \mid F_o \mid$. [b] $wR2 = \{\Sigma [w(F_o^2 - F_c^2)^2] / \Sigma [w(F_o^2)^2]\}^{1/2}$

The P(1)-S(1) and P(2)-S(2) are marginally different because:1) they are really different despite symmetric nature of molecules, 2) solid state packing environment, 3) ellipsoid sizes differ, perhaps loose packing at the P-S center and also large vibrations cause shorter distances, and 4) they could be some artefacts in data collection.

Table 3.1.2.2. Selected bond distances (Å) and angles (deg) for **(15)** and **(16)** with esd's in parentheses.

Compound **15**			
P(1)-S(1)	1.9603(7)	P(2)-S(2)	1.9561(7)
N(1)-P(2)	1.6704(16)	N(2)-P(1)	1.6596(17)
N(2)-P(1)-S(1)	115.67(7)	N(1)-P(2)-S(2)	116.15(7)
C(18)-N(1)-P(2)	120.40(13)	C(6)-N(2)-P(1)	123.19(14)
Compound **16**			
O(1)–P(1)	1.4932(18)	P(1)–N(1)	1.659(2)
N(2)–P(2)	1.673(2)	P(2)–Se(1)	2.0989(7)
O(1)–P(1)–N(1)	115.22(11)	O(1)–P(1)–C(18)	112.19(11)
N(1)–P(1)–C(18)	103.42(11)	O(1)–P(1)–C(17)	111.29(11)
C(18)–P(1)–C(17)	107.07(11)	N(2)–P(2)–C(30)	102.64(12)
N(2)–P(2)–C(24)	107.52(11)	C(30)–P(2)–C(24)	103.78(11)
N(2)–P(2)–Se(1)	112.31(9)	C(30)–P(2)–Se(1)	114.58(8)
C(24)–P(2)–Se(1)	113.19(9)	C(10)–N(1)–P(1)	124.73(17)

The average bond distances of P-N for ligands **(15)** and **(16)** are comparable to those previous reported in literature.[15] The average bond distance for **(15**) and **(16)** of P-N range from 1.673(2)-1.659(2) Å. The bond angles of N-P-S for **(15)** range from 116.15(7)-115.67 (7)°.The bond angles of N-P-Se and N-P-O for **(16)** are 112.31(9) and 115.22(11)°, respectively. The bond length for **(15)** of P-S 1.9503(7)-(1.9561(7) Å, **(16)** of P-Se is 2.0989(7) Å and P-O is 1.4932(18) Å. Compounds prepared from chlorophosphanes with diols and amino-ols are related to chloro-amines **(15)** and **(16)**. The bis(amino)phosphine chalcogenide compounds have a lone pairs on each N-atom. These donor atoms were found to be "antiperiplanar" to the P=E bond while others were found to be orthogonal to the P=E bond. This have an impact on the orientation of the chalcogenide on the P-atoms of the ligands. Comparison studies of the ligands reported herein and those reported previously found that the P-N bond length, hybridisation of the N-atoms, the lone pair repulsions, bond angles around the P-atom and the steric effect of the molecules are responsible factors for the geometry around the P-atoms.

3.1.2.5 UV-Vis Spectroscopic Analysis of Compounds

The electronic UV-Vis spectra of compounds **(14)-(16)** and their molar absorptivity coefficient are shown in Figure 3.1.2.4 and Table 3.1.2.3.

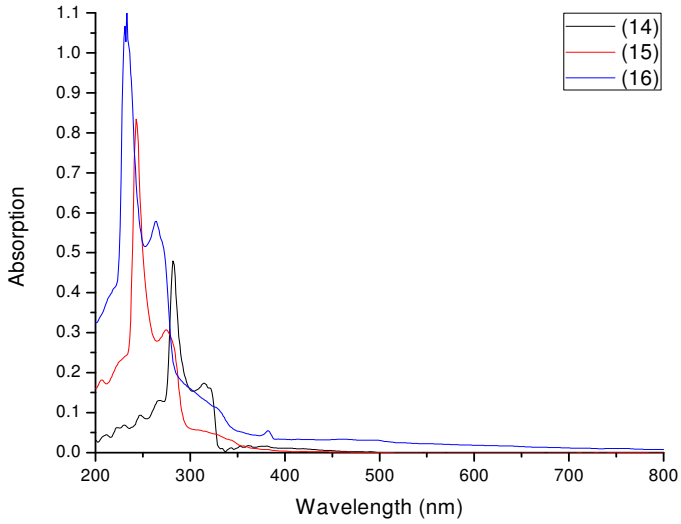

Figure 3.1.2.4. The UV-Vis spectra of **(14)**-(**16)**.

The solution behaviour of the compounds was recorded in dry chloroform. Ligands **(14)**-**(16)** consist of two absorption bands in range ~230-318 nm which are slightly red-shifted compared with *1,8*-diaminonaphthalene. The two prominent absorption bands in the spectra are assigned to the intraligand L→L* transitions.

Table 3.1.2.3. Molar extinction coefficient of compounds (**14**)-(**16**).

Compounds	λ_{max} [a](nm)	ε [b]($M^{-1}cm^{-1}$)
14	280, 318	5302, 1888
15	244, 276	9334, 3481
16	230, 263	9001, 4287

[a] wavelength, [b] Molar extinction coefficient

From the molar extinction coefficient of the ligands (**14)-(16)**, it is evident that the bis(amino)phosphine ligands in general absorb stronger in the UV-Vis region. The numbers are lower than those of naphthalene L→L* transitions which is 221 nm/133000 ($M^{-1}cm^{-1}$) for

peak 1, 286 nm/ 9300 ($M^{-1}cm^{-1}$) for peak 2 and 121 nm/ 289 ($M^{-1}cm^{-1}$) for peak 3.[29] The difference is due to phenyl rings in the 14-16 ligands, which are not present in the naphthalene portion of the compound. The UV-Vis of ligands **(1)** and **(2)** are not reported because they were found not to be stable in solution.

3.1.2.6 Thermogravimetric Analysis Data of Ligands

The thermal behaviour of ligands **(1)** and **(14)**-**(16)** were studied by thermogravimetric analysis in the temperature range of 25-1000°C, see Figure 3.1.2.5. The black curve indicates that the intermediate ligand **(1)** is not stable at room temperature. The ligands start to steadily melt at ~27-200°C. At ~210-350°C the same ligand decomposes until the residual weigh is reach at ~420°C. The red, blue and green line curves shows the thermal behaviour of ligands **(14)**-**(16)**. They follow a similar decomposition profile pattern of **(1)**. The stability of the ligands is varied by the type of chalcogenide attached to the P-donor atoms. Ligand **(14)** appears to lose less weight due to its strong O-P bond which is followed by ligand **(15)** which consist of sulfur and then ligand **(16)** which contains a mixed O/Se chalcogenide system. The compounds show that they are stable at room temperature followed by a spontaneous melt phase at ~240-258°C. The decomposition starts immediately after the first temperature interval until it reaches ~400°C and 550°C, and at ~555°C the residual weight is reached. Ligand **(2)** was not evaluated because it was found to be very unstable which means it can be oxidized easily by oxygen.

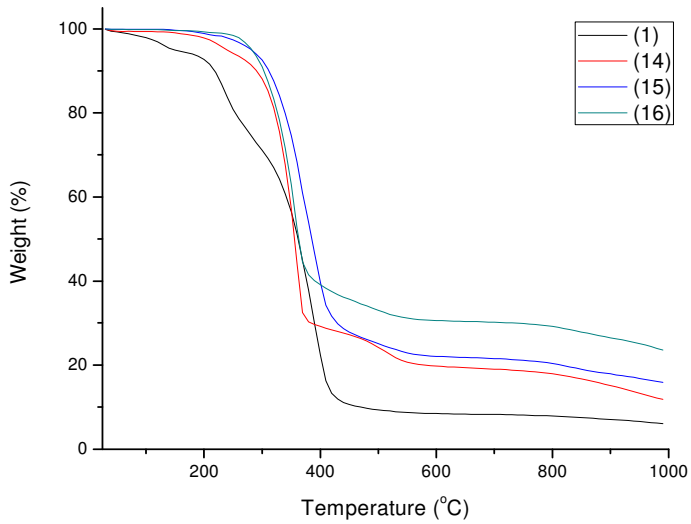

Figure 3.1.2.5. TGA curves of compounds **(1)**, **(14)**-**(16)**.

3.2 Synthesis of Perimidines, Spectroscopic Analysis and Crystal Structure

3.2.1 Background

The genesis of perimidine chemistry dates back to 1874.[30] Perimidines exhibits one carbon-nitrogen ring and two nitrogen atoms in their structures e.g. cytosine, thymine and uracil. Perimidines are similar to purine in that they are involved in the production of RNA and DNA, likewise proteins and starches, which regulates the enzymes and serve as energy source for cells. Hence, this class of compounds display various and vital biological activities.[31-33]

Perimidines are a well-known class of compounds that exhibits anti-tumor, anti-ulcers, anti-malarial and anti-fungal agents.[34] The crucial development of new and affordable drugs at low cost is always in demand, especially due to the expensive cost of antibiotics and chemotherapeutics available for medical use. Over the years, reports show that multi-resistant pathogens, i.e. fungi and bacteria, remain a challenge to overcome and therefore infectious diseases have continued to escalate and the development of resistant antimicrobial drugs to supersede the mechanism of action for these organism has to be developed.[34, 35]

Perimidine ligands are isoelectronically equivalent to the N-heterocyclic carbenes (NHCs) and hence the heteroatoms stabilizes the molecules. The scaffold of the carbenes possess strong σ-donor properties with less π-accepting ability which probe nucleophic abilities of the ligand and therefore give rise to a strong catalytic activities in their coordination mode to transition metal complexes.[36] Studies have shown that perimidines have characteristics of both π-deficient and π-excessive classifications due to the transfer of electron density from the heterocycle to the naphthalene ring.[37, 38] Various methods to prepare perimidine derivatives have been implemented.[39-44] Amongst the many methods reported, including the well-known condensation reaction of *1,8*-diaminonaphthalene with different carbonyl groups, Mobinikhaledi *et al*.,[45] have a simple method for the synthesis of perimidine compounds. They have investigated the use of solid inorganic acid zeolites catalysts as an alternative method toward the preparative methods of perimidines because of their suitable acidity, insolubility in organic solvents, thermal stability, and low cost. More recently Chen *et al*.,[46] and Ghosh[47] and co-workers have shown that derivatives of perimidine could be achieved *via* the irradiation of visible light through the photochemistry of organic molecules. The process is accomplished in the absence of any photocatalysts *via* the introduction of an electron donor and an electron

acceptor (photo-electron induced transfer) into the reaction mixture. The reaction generates temporary radical species which proceed to products *via* chemical transformations. The omission of photocatalysts reduces possible side reaction.

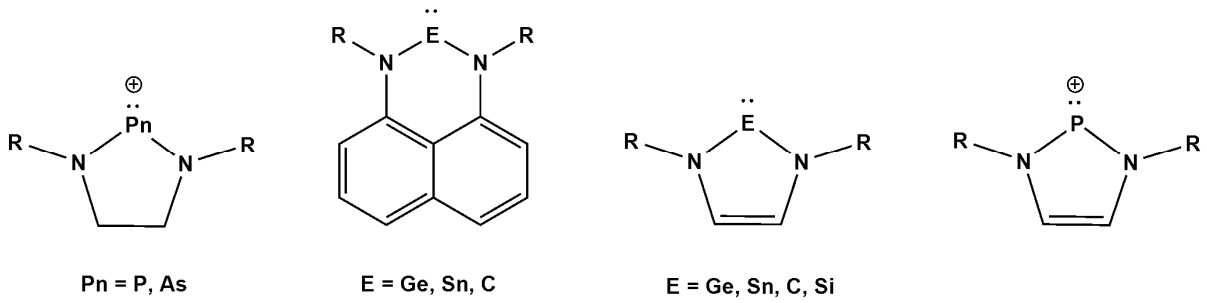

Figure 3.2.1.1. Electron-rich framework pnictogenium cations scaffold.[48, 49]

Molecules in Figure 3.2.1.1 possess a novel topology and electronic framework in which the dicoordinate pnictogen center resides in a σ-electron-rich, six-membered heterocyclic ring.[50] Cucciolito *et al*., suggested that fewer case studies which deal with carbenes where the metal center is shared between to one N-atom and any donor atoms from a different compound have been conducted. In the case of the perimidines derived from *1,8*-diaminonaphthalene there are no coordination complexes reported with a direct M-N bond.[51]

The advantage of well-developed readily available starting materials, synthetic methods, vast biological properties and the interest in developments of the chemistry of perimidine create curiosity for further developments in this field of chemistry

3.2.2 Results and Discussion

3.2.2.1 Synthesis of Perimidines as Organic Compounds and Ligands

The perimidine compounds of the formulas $[C_{10}H_6(1,8\text{-}NH)_2(C\{CH_3\}\{(CH_2)_2CH_3\})]$ **(23)**, $[C_{10}H_6(1,8\text{-}NH)_2(C\{CH_2CH_3\}_2)]$ **(24)** $[C_{10}H_6(1,8\text{-}NH)_2(C\{CH_3\{CH_2CH_3\})]$ **(25)**, $[C_{10}H_6(1,8\text{-}NH)_2(C\{CH_3\}\{CH(CH_3)_2\})]$, **(26)**, $[C_{10}H_6(1,8\text{-}NH)_2(C\{CH_3\}\{(CH_2)_4CH_3\})]$ **(27)**, $[C_{10}H_6(1,8\text{-}NH)_2(C\{CH_3\}\{CH_2CH(CH_3)_2\}_2)]$ **(28)**, $[C_{10}H_6(1,8\text{-}NH)_2{\cdot}Fe(C_5H_4)_2\{COCH_3\}_2]$ **(29)**, $[C_{10}H_6(1,8\text{-}NH)_2(C\{CH_3\}\{C_5H_4N\})]$, **(30)** and **(30*)**, respectively, were prepared according to the proposed Scheme 3.2.2.1 by condensation reaction of simple alkyl and aryl ketones with

1,8-diaminonaphthalene at 80°C for 12 hours. An advantage of this reaction is that it requires no catalyst and/or solvents, although the presence of molecular sieves are useful in absorbing water as by-product. The reaction proceeds smoothly in the presence of molecular sieves that prohibit any hydrolysis from cleaving the P-N bonds during the formation of desired products. The ketones used herein, are liquids and therefore no solvent was required. The ketones were reacted with the diamine in a ratio (10:1). The excess ketone allows all of the diamine to be consumed without forming any side products.

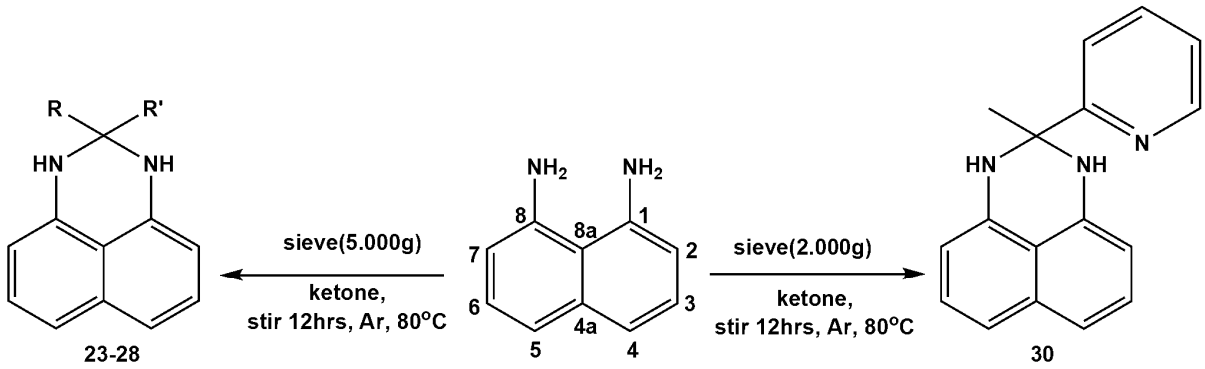

R = CH_3, R' = $CH_3CH_2CH_2$ (propanyl) (23)
R = CH_3CH_2, R' = CH_3CH_2 (ethyl) (24)
R = CH_3, R' = CH_3CH_2 (ethyl) (25)
R = CH_3, R' = CH_3CHCH_3(iso-propyl) (26)
R = CH_3, R' = $CH_3CH_2CH_2CH_2CH_2$ (pentanyl) (27)
R = $(CH_3)_2CHCH_2$, R' = $(CH_3)_2CHCH_2$ (isobutane) (28)

Scheme 3.2.2.1. Synthesis of Perimidines.

Compound **(29)** was prepared by treating *1,8*-diaminonaphthalene with 1,1'-diacetylferrocene in ethanol solution. This compound is covered in Chapter 4, under section 4.2.2.1. Compounds **(23)**-**(26)** and **(30)** are isolated as solids and **(25)** and **(28)** are pastes. All the compounds were isolated in satisfactory yields of 85-99%. The aim was to prepare compounds **(22)**-**(28)** at first and deprotonate the NH group with a mild reagent and thereafter incorporate metal salts. However, the products in the presence of metal salts decomposed either in solution or when isolated. The bulk purity of the compounds were confirmed by MS, i.e. ESI-MS (positive): (m/z) = 227 (100%) $[M+H]^+$ **(23)**, ESI-MS (positive): (m/z) = 227 (100%) $[M+H]^+$ **(24)**, ESI-MS (positive): (m/z) = 213 (100%) $[M+H]^+$ **(25)**, ESI-MS (positive): (m/z) = 227 (100%) $[M+H]^+$ **(26)**, ESI-MS (positive): (m/z) = 255 (100%) $[M+H]^+$ **(27)**, ESI-MS (positive): (m/z) = 283 (100%) $[M+H]^+$ **(28)** and ESI-MS (positive): (m/z) = 262 (100%) $[M+H]^+$ **(30)**. The microanalysis and spectroscopic data for all compounds agree with the proposed structures. Reaction of PPh_2Cl with simple perimidines **(23)**-**(28)** appeared unsuccessful due to unresolved

^{1}H NMR spectra due to by-products. Derivatives of perimidine containing a donor atom in the adjacent substituent, i.e. N-atoms or P-atom, was then prepared. This introduced the synthesis of a perimidine complex containing a diamine backbone, which are not known not known from literature. For perimidine containing N-atom, *1,8*-diaminonaphthalene was treated with 1-(pyridin-2-yl)ethanone to afford **(30)** which was subsequently prepared in high purity and formed a potential ligand for further investigations of diamine perimidine coordination chemistry. The molecular structures of **(25)**, **(26)** and **(30)** were established by single X-ray diffraction analysis.

3.2.2.2 Characterisation: Spectroscopic Analysis ^{1}H and ^{13}C NMR

For ^{1}H NMR discussion that follows, see Scheme 3.2.2.1 for the key to assigning proton positions. In the ^{1}H NMR spectra of compounds **(23)**-**(28)** and **(30)** the protons of the naphthalene backbones resonates downfield in the range of 6.45-6.27 ppm for proton positions {4 and 5}, 7.15-6.99 ppm for proton positions {3 and 6} and 7.23-7.07 ppm for proton positions {2 and 7}. The resonance signals are doublets and triplets and the coupling constant values are listed under the experimental section. The terminal CH_3 attached to the bridging secondary carbon resonate in the range 1.28-1.57 ppm for compounds **(23)** and **(25)**-**(27)** with a prominent singlet peak upfield. The terminal CH_3 of compounds **(23)** and **(25)**-**(27)** attached to the CH_2 of the alkyl chain resonate in the range 0.94-0.72 ppm. Compound **(24)** and **(28)** are symmetric and their terminal CH_3 are situated further upfield compared to those of compounds **(23)** and **(25)**-**(27)**. Compound **(24)** have CH_3 as triplets resonating in the range of 0.88-0.85 ppm and compound **(28)** four CH_3 resonate at 0.94-0.88 ppm as multiplets. The CH_2 of compounds **(24)** and **(28)** are appearing in a range of 2.27-1.61 ppm as doublets. The broad amine peak of NH for compounds **(23)**-**(28)** resonate in the range of 4.22-3.89 ppm. The remaining protons in the molecules correspond to the predicted molecular structures. Compound **(30)** NMR data correspond with the proposed structure, see experimental and Figure 3.2.2.1.

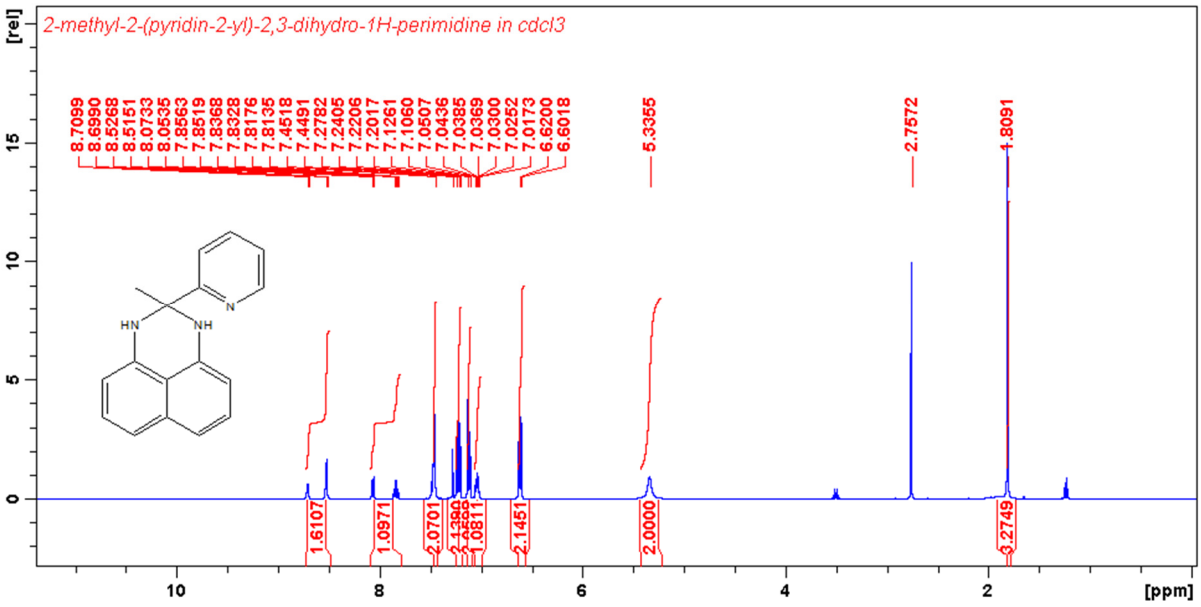

Figure 3.2.2.1. The ^{1}H NMR spectrum of **30**.

The spectrum in Figure 3.2.2.1 shows the resonance of different substituents of compound **(30)**. Similar to compound **(23)**-**(28)**, the spectrum of **(30)** shows that the CH_3 is shifted upfield as a prominent singlet which integrates to three protons. The amine protons show a broad peak around 5.33 ppm. The naphthalene protons at positions {4 and 5} are resonating at 6.62-6.60 ppm. The pyridinyl protons are further downfield and they appear to integrate to one proton although the splits as multiplets. The ^{13}C NMR spectra correspond to the ^{1}H NMR, see appendix and experimental section.

3.2.2.3 Characterisation: FTIR Spectroscopic Analysis

The FT-IR of compounds **(23)**-**(28)** and **(30)** shows the characteristic absorption band of ν(NH) in the range 3360-3373 cm^{-1} and absorption peaks of aromatic ν(C=C) in the range 1406-1702 cm^{-1}. There is a small difference in frequency between the commercial available *1,8*-diaminonaphthalene and compounds **(23)**-**(28)** and **(30)**. The vibrations frequencies of *1,8*-diaminonaphthalene for ν(NH) and aromatic regions appear at 3385-3295 and 1598-1402 cm^{-1}, respectively. The presence of these functional groups and their frequency shifts confirms the formation of the compounds. The FT-IR of compound **(30)** is different from that of compounds **(23)**-**(28)**. Compound **(30)** show bands at 3372 and 3243 cm^{-1} for ν(NH), 2982 and 1922 cm^{-1} for ν(N=C) of the pyridinyl moiety of the ligand. The frequencies of the functional groups

ν(C=C, C-C) of the naphthalene are shifted to 1697, 1623, 1588, 1598, 1510, 1467, 1423 cm^{-1}. The spectrum is presented below.

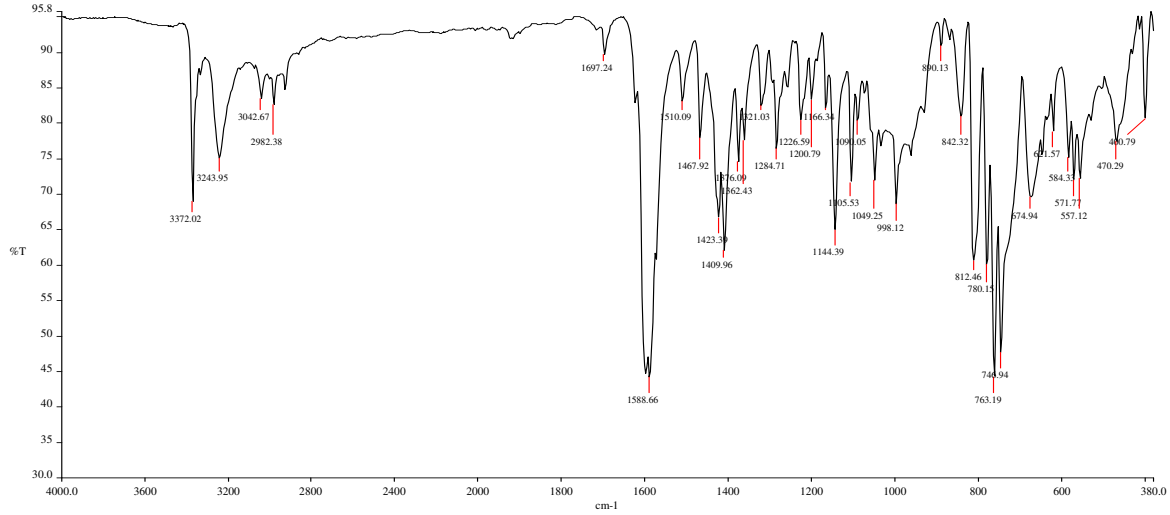

Figure 3.2.2.2. The FT-IR spectrum of (**30**).

3.2.2.4 Molecular Structures of Perimidine Organic Compounds

The solid-state molecular structure of compounds **(25)**-**(26)** and **(30)** were determined by single-crystal X-ray diffraction analysis and the crystallographic data is presented in Table 3.2.2.1. The molecular structures are shown in Figure 3.2.2.3. The selected bond lengths and angles are shown in Table 3.2.2.2. Compound **(25)** crystals were grown in mixture of methanol: dichloromethane solvents by slow evaporation. Compound **(26)** was obtained by slow evaporation of hexane during recrystallization process and **(30)** was grown in diethyl ether by slow evaporation.

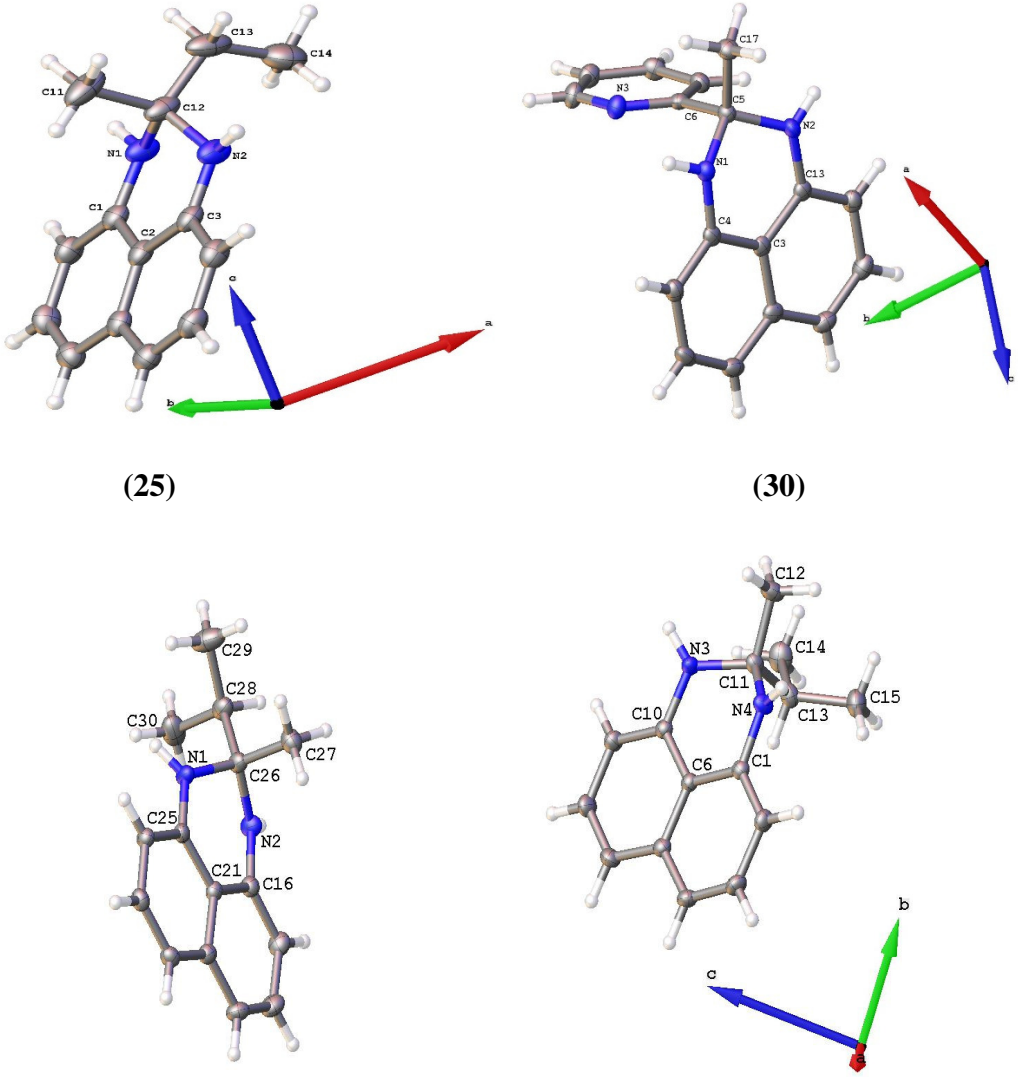

(25) **(30)**

(26)

Figure 3.2.2.3. Molecular structures of (**25**), (**26**) and (**30**), respectively. The molecules are drawn at 50% probability.

Compound **(25)** and **(26)** crystallizes in space groups tetragonal (P-42$_1$c) and monoclinic (Pn), respectively. Compounds **(25)** and **(26)** are non-centrosymmetric with a Flack parameter value of -3(5) and 0.1(3), respectively. Compound **(25)** has eight molecules in a unit cell whereas compound **(26)** have four, see appendix. A brief summary containing structural parameter data for compound **(25)** and **(26)** is shown in Table 3.2.2.1. The amine N-atoms showed a pyramidal geometry. Compound **(30)** crystalize in a space group P2$_1$/c. Compound **(30)** contain four molecule within the asymmetric unit. Compound **(30)** has a centrosymmetric center of inversion. Figure 3.2.2.3, shows that compound **(30)** can either act as a monodentate or a

bidentate ligands. Compound **(30*)** is a polymorph of **(30)** and was also obtained co-crystallizing with acetonitrile molecule. This polymorph is attached in the appendix.

Table 3.2.2.1. Crystallographic data for compounds **(25)**, **(26), (30), (30*)**.

	25	**26**	**30**	**30***
Formula	$C_{14}H_{16}N_2$	$C_{15}H_{18}N_2$	$C_{17}H_{15}N_3$	$C_{36}H_{33}N_7$
M_r	212.29	226.31	261.32	563.69
Space group	P-42$_1$c	Pn	P2$_1$/c	P2$_1$/c
a, Å	16.6273(4)	9.13870(10)	12.2805(3)	9.1950(3)
b, Å	16.6273(4)	9.7964(2)	10.1807(3)	13.2366(3)
c, Å	8.3726(2)	14.2817(2)	10.5281(3)	25.0263(3)
α, deg	90	90	90	90
β, deg	90	94.3840(10)	98.4840(10)	100.2580(10)
γ, deg	90	90	90	90
V, Å^3	2314.75(12)	1274.85(3)	1340.22(6)	2997.28(15)
Z	8	4	4	4
ρcalcd, g cm^{-3}	1.218	1.179	1.295	1.249
M, mm^{-1}	0.073	0.070	0.079	0.076
T, K	100(2)	173(2)	296(2)	100(2)
Reflections collected	59716	26773	10440	40316
Independent reflections	2884	6290	2911	7429
R_{int}	0.0539	0.0223	0.0.249	0.0266
Final *R* indices [I > 2σ(*I*)][a]	*R*1 = 0.0488 w*R*2 = 0.1058	*R*1 = 0.0363 w*R*2 = 0.100	*R*1 = 0.0412 w*R*2 = 0.1093	*R*1 = 0.0424 w*R*2 = 0.1030
R indices (all data)	*R*1 = 0.0850 w*R*2 = 0.1222	*R*1 = 0.0381 w*R*2 = 0.1020	*R*1 = 0.0464 w*R*2 = 0.1145	*R*1 = 0.0592 w*R*2 = 0.1120
Absolute structure parameter	-3(5)	0.1(3)	none	none
Largest diff. peak and hole, e / Å	0.287 and -0.183	0.298 and -0.237	0.270 and -0.323	0.357 and -0.235

[a] $R1 = \Sigma \mid\mid F_o \mid - \mid F_c \mid\mid / \Sigma \mid F_o \mid$. [b] $wR2 = \{\Sigma [w(F_o^2 - F_c^2)^2] / \Sigma [w(F_o^2)^2]\}^{1/2}$

The distance between the non-bonding N···N atoms in the *peri*-position of compounds **(25)**, **(26)** and **(30)** is, 2.348, 2.354 and 2.348 Å, respectively. The distance between the non-bonding N···N of the *1,8*-diaminonaphthalene is 1.495Å. The difference between the non-bonding N···N atoms distance of the compounds **(25)**, **(26)** and **(30)** and the distances of the non-bonding N···N atoms of *1,8*-diaminonaphthalene is 0.853 Å. The difference in the calculated values could be influenced by the experimental conditions, i.e. 100-173-296 K and difference 100 and 296 K is 196 K. The angles of the *peri*-N atoms relative to the naphthalene, i.e. N-C_8-N, N-C_1-N and C_8-C_{8a}-C_1 for compounds **(25)** and **(26)** is 0° which makes them coplanar. The molecular structures of compounds **(25)** and **(26)** bends out of the plane at N-$C_{12\text{ or }5}$-N atoms position of the molecular cycle due to the steric effect caused by the axial positions of the aryl ring and hydrogen intermolecular interactions.[51]

Table 3.2.2.2. Selected bond distances (Å) and angles (deg) for **(25), (26)** and **(30)** with esd's in parentheses.

Compound **25**			
C(12)–N(1)	1.464(3)	C(12)–N(2)	1.476(3)
C(12)–C(13)	1.518(4)	C(13)–C(14)	1.503(4)
N(1)–C(12)–N(2)	106.03(18)	N(1)–C(12)–C(13)	110.0(2)
N(2)–C(12)–C(13)	109.0(2)	N(1)–C(12)–C(11)	110.6(2)
N(2)–C(12)–C(11)	110.04(2)	C(13)–C(12)–C(11)	110.7(2)
C(14)–C(12)–C(11)	110.7(2)		
Compound **26**			
C(25)–N(1)	1.382(2)	C(26)–N(2)	1.464(2)
C(26)–N(1)	1.468(2)	C(16)–N(2)	1.379(2)
C(26)–C(28)	1.542(2)	C(26)–C(27)	1.540(3)
N(2)–C(26)–N(1)	106.58(14)	N(2)–C(26)–C(27)	110.19(15)
Compound **30**			
N(1)–C(5)	1.4625(13)	N(1)–C(4)	1.3897(14)
N(2)–C(13)	1.3874(14)	N(3)–C(16)	1.3383(15)
N(3)–C(6)	1.3419(14)	N(2)–C(5)	1.4550(14)
C(4)–N(1)–C(5)	116.91(9)	C(13)–N(2)–C(5)	117.97(9)
N(2)–C(5)–CN(1)	107.20(9)	N(2)–C(5)–C(6)	112.04(9)
N(3)–C(6)–C(5)	115.03(9)	N(1)–C(5)–N(2)	107.20(19)

The bond angles of N(1)-C(12)-N(2), N(1)-C(26)-N(2) and N(1)-C(5)-N(2) in a σ-electron-rich six-membered heterocyclic ring of compounds **(25)**, **(26)** and **(30)** are 106.03(18), 106.58(14) and 107.20(19)°, respectively. In compound **(26)**, the C-N bond lengths of the *1,8*-diaminonaphthalene are in the ranges of 1.464(2)-1.468(2) and 1.382(2)-1.379(2), respectively. The bond distances of compound **(25)** and **(26)** are in Table 3.2.2.2. The bond distances are within the range of the typical known C-N bonds.[51, 52] Table 3.2.2.2 shows bond distances and

bond lengths of compound **(30)** which are similar to those reported by Cucciolito *et al*.[51] All the compounds are held together by an intermolecular hydrogen bond of the NH interacting with the π electrons of the adjacent naphthalene rings. There are no observed π-π stacking centroid-centroid distances which usually stabilizes the packing of naphthalene molecules in the crystal lattice. The symmetry transformations used to generate equivalent atoms for all crystal structures reported here in Chapter 3 will be provided in the appendix of this work.

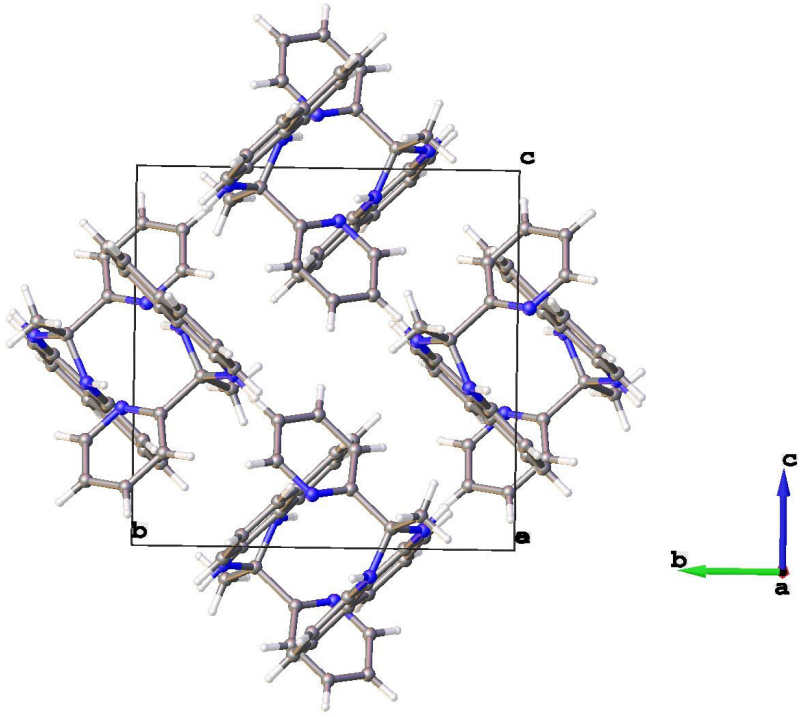

Figure 3.2.2.4. OLEX 2 drawing of molecular packing of **(30)** drawn at 50% probability.

3.2.2.5 UV-Vis Spectroscopic Analysis and Photophysical Properties

Figure 3.2.2.5 shows the UV-Vis spectra of compounds **(23)**-**(28)** and **(30)** as illustrated in **[A]** and emission profile of compounds **(23)**-**(28)** and **(30)** in **[B]**, respectively. Compounds **(23)**-**(28)** shows three sets of λ_{max} peaks at (a) longest λ at~280 nm, (b) peak shoulder at λ at ~315 nm and (c) ~379 nm. As expected, the molecular spectra show that the compounds contain unsaturated naphthalene moieties with shoulders due to ligand centered (LC) π···π*transitions, see peak bands at (a) and (b). The extra peak at (c) is due to the σ-electron rich six membered heterocyclic perimidine ring assigned to n···π*transitions. Compound **(30)** is blue shifted compared to other six perimidines due to the pyridinyl ring π···π*transitions.

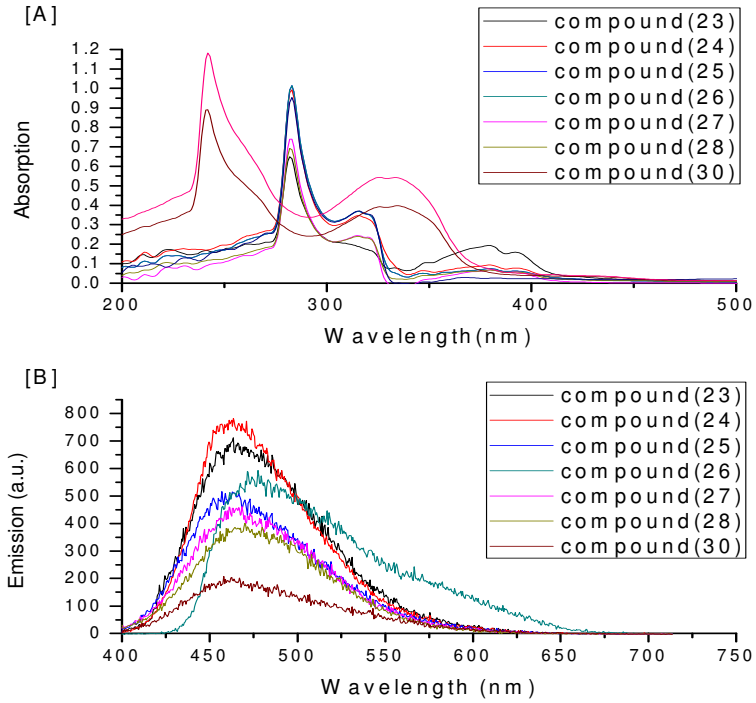

Figure 3.2.2.5. Display UV-Vis and Luminescence spectra of compounds **(23)**-**(28)** and **(30)** in **[A]** and **[B]**, respectively, in chloroform.

Table 3.2.2.3. Photophysical data of compounds **(23)**-**(28)** and **(30)**.

Compounds	λ_{abs}[a] (nm)	λ_{em}[b] (nm)	Δ_v[c] (cm^1)	ε_{max}[d] ($M^{-1}cm^{-1}$)
23	280, 315, 379	462	14069	2585
24	281, 315, 379	462	13942	4121
25	280, 315, 379	476	14706	4255
26	280, 315, 379	461	14023	5856
27	280, 315, 379	467	14301	3006
28	281, 315, 379	462	14071	5056
30	241, 335, 700	460	19754	6018

[a] Longest wavelength absorption maximum recorded in dichloromethane, [b] Fluorescence maximum, [c] Stokes shifts in cm^{-1} as calculated from the λ_{abs} and λ_{em} data, [d] Molar extinction coefficient at the longest wavelength absorption maximum.

Table 3.2.2.3 also shows comparable Stokes shifts of compounds **(23)**-**(28)** which were calculated on the basis of the maxima of the comparative broad and structured absorption and emission bands. The values were around 13942-20660 cm^{-1}. The values are quite large which probe interest in photophysical properties of the compounds in terms of their applications in the dye industries. This is an advantage, because large Stokes shift suppress the reabsorption of the fluorescent in the condensed phase as this could lead to emission quenching.

3.2.2.6 Thermogravimetric Analysis Data of Perimidines

Figure 3.2.2.6, shows the thermal decomposition graphs for compounds (**23**)-(**28**), (**30***) and (**31**). Their differential scanning calorimetry (DSC) curves are given in the appendix. Compounds (**23**)-(**28**) have similar weight loss percentage profile, although they differ in their morphology, e.g. solids and liquids.

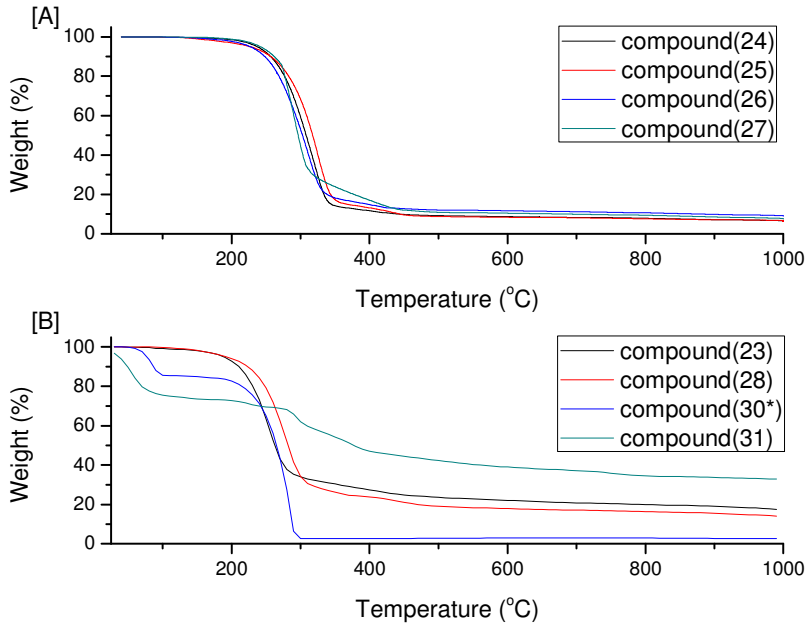

Figure 3.2.2.6. Thermal stability curves of compounds **(24)**-**(27)** in **[A]** and **(23)**, **(28)**, **(30*)** and **(31)** in **[B]**.

All compounds are stable at room temperature, but start to rapidly decompose at ~250 °C until they reach their residual material temperature at ~310 °C. The DSC profile curves indicates that the melt process occurs before the decomposition temperature, as an endothermic process. At ~ 84 and 98 °C compound **(30*)** experience weight loss of acetonitrile. Compound **(30*)**

starts to rapidly decompose at ~220 °C until it reaches its residual material at ~300°C. At ~50-~91 °C complexes **(31)** experience weight loss due to water molecules attached to the Ni(II) metal center. This was followed by a rapid decomposition at ~228 °C until the residual material was obtained at ~401 °C.

3.3 References

1. J. Gopalakrishnan, *Studies on tricoordinate P(III)-N systems: synthesis, structure and reactivity, Ph.D. Thesis, Department of Chemistry, Indian Institute of Technology Madras, Chennai, India*, 1998, pp. 245.
2. M. T. Ashby and Z. Li, *Inorg. Chem.*, 1992, 31, 1321-1322.
3. M. S. Balakrishna, V. S. Reddy, S. S. Krishnamurthy, J. F. Nixon and J. C. T. R. B. S. Laurent, *Coord. Chem. Rev.*, 1994, 129, 1-90.
4. A. Michaelis, *Ann. Chim.*, 1903, 129-258.
5. M. S. Balakrishna, B. D. Santarsiero and R. G. Cavell, *Inorg. Chem.*, 1994, 33, 3079-3084.
6. F. Majoumo-Mbe, P. Lönnecke and E. Hey-Hawkins, *Organometallics*, 2005, 24, 5287-5293.
7. P. Bergamini, V. Bertolasi and F. Milani, *Eur. J. Inorg. Chem.*, 2004, 2004, 1277-1284.
8. F. Durap, N. Biricik, B. Gümgüm, S. Özkar, W. H. Ang, Z. Fei and R. Scopelliti, *Polyhedron*, 2008, 27, 196-202.
9. T. Q. Ly and J. D. Woollins, *Coord. Chem. Rev.*, 1998, 176, 451-481.
10. P. Bhattacharyya, A. M. Slawin and M. B. Smith, *J. Chem. Soc., Dalton Trans.*, 1998, 2467-2476.
11. K. D. Berlin and G. B. Butler, *Chem. Rev.*, 1960, 60, 243-260.
12. L. P. Kuhn, J. O. Doali and C. Wellman, *J. Am. Chem. Soc.*, 1960, 82, 4792-4794.
13. R. D. Kroshefsky and J. G. Verkade, *Phosphorus, Sulfur Silicon Relat. Elem.*, 1979, 6, 391-395.
14. R. D. Kroshefsky, R. Weiss and J. G. Verkade, *Inorg. Chem.*, 1979, 18, 469-472.
15. M. Shi and W.-S. Sui, *Tetrahedron: Asymmetry*, 2000, 11, 773-779.
16. A. M. Z. Slawin, J. Wheatley and J. D. Woollins, *Polyhedron*, 2004, 23, 2569-2574.
17. T. Q. Ly, A. M. Z. Slawin and J. Derek Woollins, *J. Chem. Soc., Dalton Trans.*, 1997, 1611-1616.
18. M. M. Crutchfield, C. H. Dungan, J. H. Letcher and J. R. VanWazer, *31 P Nuclear Magnetic Resonance. Interscience: New York*, 1967.
19. J. G. Verkade and L. D. Quin, *Phosphorus-31 NMR Spectroscopy in Stereochemical Analysis. VCH: Florida*, 1987.
20. T. Q. Ly, A. M. Z. Slawin and J. D. Woollins, *J. Chem. Soc., Dalton Trans.*, 1997, 1611-1616.
21. W. M. McFurlane and D. S. Rycroft, *J. Chem. Soc., Dalton Trans.* , 1973, 2162-2166.
22. W. M. McFurlane and D. S. Rycroft, *J.Chem.Soc.,Chem.Commun.* , 1972, 902-903.
23. J. Emsley and D. Hall, *The Chemistry of Phosphorus. Harper and Row: New York*, 1976.
24. T. Thorstenson and J. Songstad, *Acta Chem. Scand.*, 1976, A30, 781-786.
25. R. F. Hudson, *Structure and Mechanism in Organophosphorus Chemistry. Academic Press: London*, 1965.
26. D. J. Williams, *Ph.D. thesis, University of Georgia, Athens, USA*, 1974.
27. R. R. Carlson and D. W. Meek, *Inorg. Chem.*, 1974, 13, 1741-1747.
28. J. Oddershede and S. Larsen, *J. Phys. Chem. A*, 2004, 108, 1057-1063.
29. H. Kunkely and A. Vogler, *Inorg. Chem.Commun.* , 2001, 4, 692-694.
30. de Aguiar*, A. Ber. Dtsch. Chem. Ges.*, 1874, 7, 309-319.
31. J. M. Herbert, P. D. Woodgate and W. A. Denny, *J. Med. Chem.*, 1987, 30, 2081-2086.
32. X. Bu, L. W. Deady, G. J. Finlay, B. C. Baguley and W. A. Denny, *J. Med. Chem.*, 2001, 44, 2004-2014.
33. A. E. A. Porter, *"Comprehensive Heterocyclic Chemistry" ed. By A. R. Katritsky, C. W. Ress., Pergamon Press, Oxford*, 1984.
34. M. Azam, I. Warad, S. I. Al-Resayes, N. Alzaqri, M. R. Khan, R. Pallepogu, S. Dwivedi, J. Musarrat and M. Shakir, *J. Mol. Struct.*, 2013, 1047, 48-54.

35. P. S. Ashwinbhai, F. Bux and A. Singh, *J.Chem.*, 2010, 3, 240-245.
36. W. A. Herrmann, *Angew. Chem., Int. Ed.*, 2002, 41, 1290-1309.
37. A. F. Pozharskii and V. V. Dalnikovskaya, *Russ. Chem. Rev.*, 1981, 50, 816-835.
38. K. C. Liu, *Zhonghua Yaoxue Zazhi*, 1988, 40, 203-216.
39. I. Yavari, M. Adib, F. Jahani-Moghaddam and H. R. Bijanzadeh, *Tetrahedron*, 2002, 58, 6901-6906.
40. J. J. V. Eynde, F. Delfosse, P. Lor and Y. Van Haverbeke, *Tetrahedron*, 1995, 51, 5813-5818.
41. J. B. Hendrickson and M. S. Hussoin, *J. Org. Chem.*, 1987, 52, 4137-4139.
42. L. W. Deady and T. Rodemann, *J. Heterocycl. Chem.*, 1998, 35, 1417-1419.
43. U. T. Mueller-Westerhoff, B. Vance and D. I. Yoon, *Tetrahedron*, 1991, 47, 909-932.
44. N. Starshikov and F. Pozharskii, *Chem. Heterocycl. Compd.*, 1973, 9, 922-924.
45. A. Mobinikhaledi, N. Forughifar and N. Bassaki, *Turk. J. Chem.*, 2009, 33, 555-560.
46. W.-Z. Chen, H.-Y. Wei and D.-Y. Yang, *Tetrahedron*, 2013, 69, 2775-2781.
47. S. Ghosh, F. Saikh, J. Das and A. K. Pramanik, *Tetrahedron Lett.*, 2013, 54, 58-62.
48. H. A. Spinney, G. P. A. Yap, I. Korobkov, G. DiLabio and D. S. Richeson, *Organometallics*, 2006, 25, 3541-3543.
49. P. Bazinet, T.-G. Ong, J. S. O'Brien, N. Lavoie, E. Bell, G. P. A. Yap, I. Korobkov and D. S. Richeson, *Organometallics*, 2007, 26, 2885-2895.
50. H. A. Spinney, I. Korobkov, G. A. DiLabio, G. P. A. Yap and D. S. Richeson, *Organometallics*, 2007, 26, 4972-4982.
51. M. E. Cucciolito, B. Panunzi, F. Ruffo and A. Tuzi, *Tetrahedron Lett.*, 2013, 54, 1503-1506.
52. S. Maloney, A. M. Z. Slawin and J. D. Woollins, *Acta Crystallogr. E*, 2013, 69, o246-o246.

Chapter 4

Bis(amino)phosphine and Perimidine Complexes

4.1 Synthesis of Bis(amino)phosphine Complexes, Spectroscopic Analysis, and Crystal Structures

4.1.1 Background to Structural and Reactivity Properties

Bis(diphosphines) are good candidates to enforce the coordination of d^{10} coinage-metal complexes due to a number of factors such as the P-donor atoms lone pairs of electrons and unfilled/unoccupied *3d* orbitals.[1] The use of Cu(I) halides in the presence of L = diphosphines or N, S based organic ligand, show a remarkable number of structural motifs, i.e. dinuclear **(a)**, cubane **(b)** and staircase **(c)**, see Figure 4.1.1.1.[2, 3]

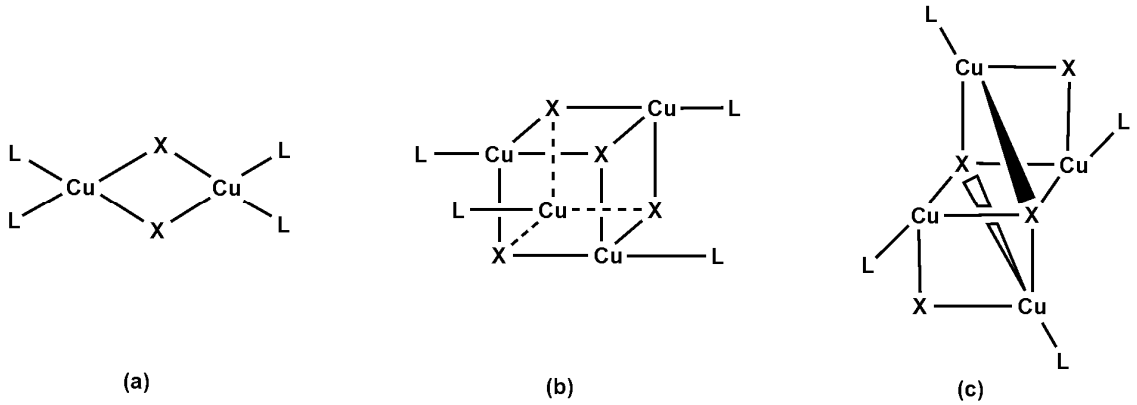

Figure 4.1.1.1. Selected coordination modes of Cu(I) halides with diphosphines.

Similarly, if the Ag-salts are coordinated to bulky phosphines and the counterion have a low coordination ability such as NO_3^-, ClO_3^- and CN^-,[4] the resulting complex will be of the type $[Ag(P(R)_2)_2]^+$ (R = mesityl, or related). If the phosphine is bulky and the counterion have high coordination ability such as halides, then complexes of the type $AgXP(R)_2$ (R = mesityl, or related) are obsvered.[5] The coordination number is also influenced by the type of the phosphine substituent used; the smaller phosphines increase the coordination number around the metal center to favour a tetrahedral geometry. The use of bidentate phosphine ligands can alter the geometry around the complex due to an increase in the chain length attaching the donor atoms to the metal.[6, 7]. The occurrence of the coordination mode tetranuclear "cubane" **(d)** and step

cubane **(e)** is subject to the type of ligand and solvent used during the reaction and the relative stereochemical parameters of the metal and halides,[8, 9] dimeric bridge **(c)**[10, 11] and trigonal planar[12] occurs as a result of simple coordinating monodentate phosphine ligands due to variation in stoichiometry.

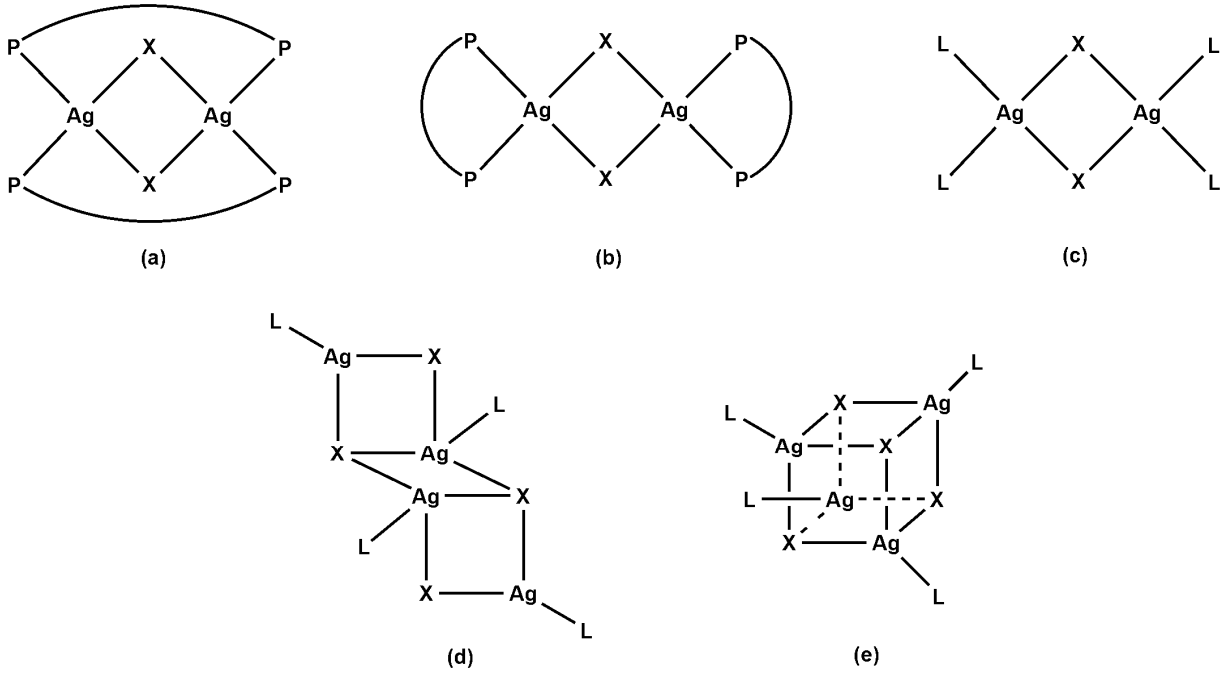

Figure 4.1.1.2. Some selected coordination modes of Ag(I) with diphosphines.

The bidentate ligand reported by Camalli *et al*.,**[13]** showed the coordination geometry presented in **(a)**[14, 15] and **(b)**[16, 17] and this depends on the length of the chain between the donor atoms of the ligand. The longer chain length between the donor atoms give **(a)** and the shorted chain length between donor atoms forms **(b)**.[18]

Transition-metal centers such as Cu(I) display very important biological processes including oxidation, dioxygen transport and electron transfer.[19] Copper exhibits rich coordination chemistry with complexes known in oxidation states ranging from 0 to +4, although the Cu(II) (cupric) and the Cu(I) (cuprous) oxidation states are by far the most common. Compounds of copper have found extensive practical use, including as catalysts in both homogeneous and heterogeneous reactions, as fungicides, pesticides, and wood preservatives, as pigments for paints and glasses, and in the so-called high-temperature superconductors, etc.[20] The coordination numbers and geometries of copper complexes vary with oxidation state. For the

spherically symmetric d^{10} Cu(I) metal, the common geometries are 2-coordinate linear, 3-coordinate trigonal planar, and 4-coordinate tetrahedral. Cu(I) compounds are diamagnetic and colourless, except where colour results from charge-transfer bands, or a counterion. These complexes are readily oxidized to Cu(II) compounds. The d^9 Cu(II) metal is usually found in a octahedral coordination environment, with four short equatorial bonds and another one or two longer axial bonds although complexes with other structures are known, including tetrahedral, square planar, and trigonal bipyramidal geometries. Most of the Cu(II) compounds are blue or green because of *d-d* absorptions in the 600 to 900 nm region; exceptions generally also have charge-transfer bands tailing into the visible, causing a red or brown appearance.

Silver(I) compounds, on the other hand, are used as potent antibacterial agents.[21] Amongst the coinage metals, silver compounds are the most potent compounds to destroy bacteria and other microorganisms. This is exploited by the use of silver(I) compounds for medicinal purposes; silver nitrate has been used to combat infantile blindness[22] and silver sulfadiazine is commonly found in creams used to treat severe burns and infectious skin diseases.[23]

Halides of Ag(I) metal shows the dominant oxidation state of silver complexes, and the Ag(I) metal with spherically symmetric configuration d^{10} exhibits a range of coordination numbers from 2 to 6. Silver halides can be prepared directly by addition of halide to Ag^+ solutions, although AgF is usually prepared from silver oxide and hydrofluoric acid. The colour and insolubility of silver halides in water increase in the order Cl < Br < I. The ultrahigh light-sensitivity of these halides (AgF only to the ultraviolet), particularly AgBr, is the basis for their use in photography. In the preparation of metal complexes, it is important that the reactions are prepared in the absence of ultraviolet light to avoid decomposition. The rare silver(II) complexes form stable complexes with a variety of nitrogen donor ligands such as pyridine, substituted bipyridine, phenanthroline, or citrazinic acid. They are usually obtained by oxidation reaction of a Ag(I) salt with peroxodisulfate in the presence of the ligand.[24]

The coordination modes of metal centers greatly influence their binding energies and to some degree their site of attachment to a ligand. Group 11 metals generally have a strong preference for a specific coordination mode, and this could play an important role in the biological functions of metal-containing biological agents. The metal-specific binding sites of some proteins and enzymes achieve their selectivity by providing a coordination environment preferred by only one metal center naturally found in living systems. Significantly, some metals

that are not naturally found in living systems owe their toxicity to their ability to coordinate strongly and compete selectively for the binding sites of biologically important metal ions.

4.1.2 Results and Discussion

4.1.2.1 Synthesis of Bis(amino)phosphine Complexes from Ligand Type [$C_{10}H_6$(1,8-$NHPR_2)_2$] (R = Phenyl, *iso*-Propyl)

Reactions presented in this section are summarized in Scheme 4.1.2.1. The previous work performed by Hill *et al*,[25] and Sarıöz and co-workers[26] have demonstrated that primary and secondary amines reacts readily with chloro-phosphines in the presences of a base to form bis(amino)phosphines. Thus, the reaction of regioselective *1,8*-diaminonaphthalene with chloro-phosphines in the present of trimethylamine in THF afforded [($C_{10}H_6$(1,8-$NHPPh_2)_2$)] (**1**) and [$C_{10}H_6$(1,8-NH-P{$CH(CH_3)_2$}$_2$)$_2$] **(2)**, (Chapter 3.1).

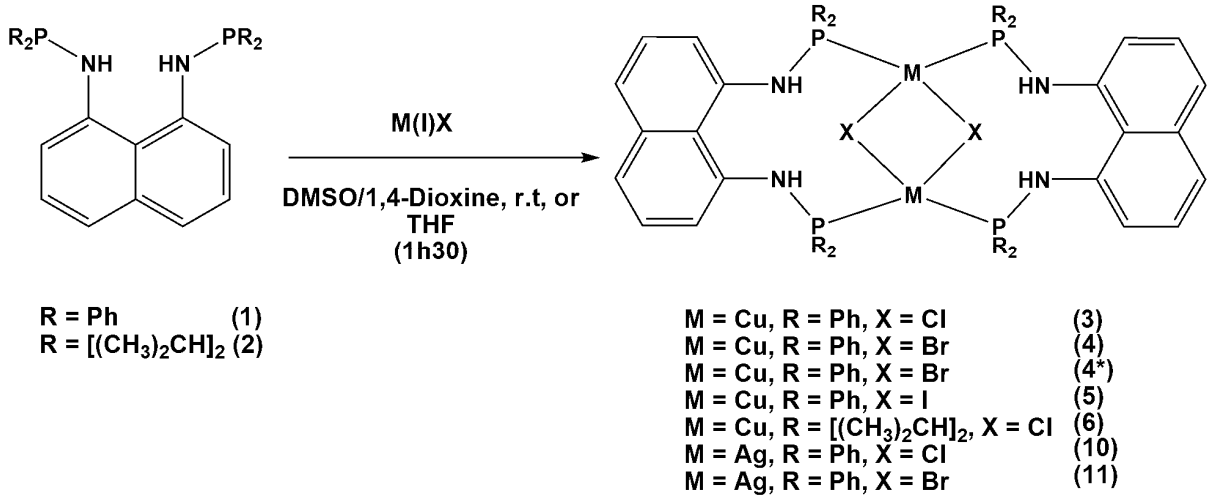

Scheme 4.1.2.1. Synthesis of dinuclear copper and silver complexes.

Scheme 4.1.2.1 shows the preparation of complexes **(3)-(6)** and **(10)-(11)** of the type [M_2(μ-$X)_2${$C_{10}H_6$(1,8-$NHPR_2)_2$}$_2$], where M = Cu(I) and Ag(I), respectively, in relatively low to moderate yields of 30-68%. Complexes **(3)-(6)** are bridged by X = Cl, Br, and I, respectively. Complexes **(3)**-**(5)** of the type [Cu_2(μ-$X)_2${$C_{10}H_6$(1,8-$NHPPh_2)_2$}$_2$], were obtained by mixing the appropriate copper(I) halide with ligand **(1)** in either dimethyl sulfoxide (DMSO) or 1,4-dioxine. Complex **(6)** of the type [Cu_2(μ-$Cl)_2${$C_{10}H_6$(1,8-$NHPR_2)_2$}$_2$], R = [$(CH_3)_2CH$] was synthesized in THF similarly to **(3)**-**(5)**. The reactions were performed by adding the copper halide to a solution of **(1)** in (1:1) ratio that resulted in an isolable precipitate. With silver

complexes, ligand **(1)** was treated with corresponding silver halide in 1,4-dioxane to give complexes **(10)** and **(11)** of the type $[Ag_2(\mu\text{-}X)_2\{C_{10}H_6(1,8\text{-}NHPPh_2)_2\}_2]$ as white precipitate and with relatively poor yield of 21-26%. Complexes **(10)** and **(11)** were bridged by X = Cl and Br, respectively. The precipitate contains a dimeric $\{Cu_2(\mu\text{-}X)_2\}$ core unit, where the halides bridge the two copper ions. The complexes are insoluble in most organic solvents, but moderately soluble in dichloromethane and chloroform, and completely soluble in DMF. The slight solubility was sufficient to allow the complexes to be characterized by spectroscopic analysis and X-ray diffraction. The obtained solid-state molecular structures reveal that the dimeric structures are heavily solvated to stabilize the structures. Solvent molecules filled the voids within the crystal structure of the copper complexes as observed in the molecular packing. Complex **(12)** of the type $[Ag_4(\mu_3\text{-}I)_2(\mu_2\text{-}I)_2\{C_{10}H_6(1,8\text{-}NHPPh_2)_2\}_2]$ was synthesized similarly to all the complexes in Scheme 4.1.2.1. Surprisingly, a different coordination complex was obtained with a low yield, falling within the range described of **(10)** and **(11)**, see Scheme 4.1.2.2.

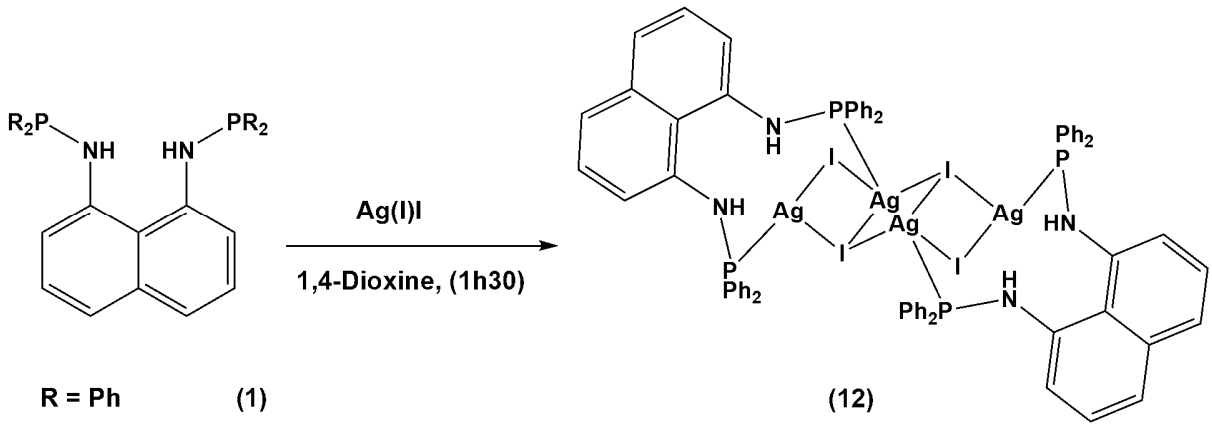

Scheme 4.1.2.2. Synthesis of multinuclear silver(I) complex.

Complexes **(7)** and **(13)** of the type $[M\{C_{10}H_6(1,8\text{-}NHPPh_2)_2\}_2]PF_6$, where M = Cu(I) and Ag(I), respectively, were obtained by treating **(1)** with $[M(CH_3CN)_4]PF_6$ (M = Cu(I) or Ag(I)), respectively, in acetonitrile and the spectroscopic analysis confirmed the product of a blue-purple complex **(7)** whereas, **(13)** was obtained as an off-white complex which was hygroscopic on exposure to air (40%).

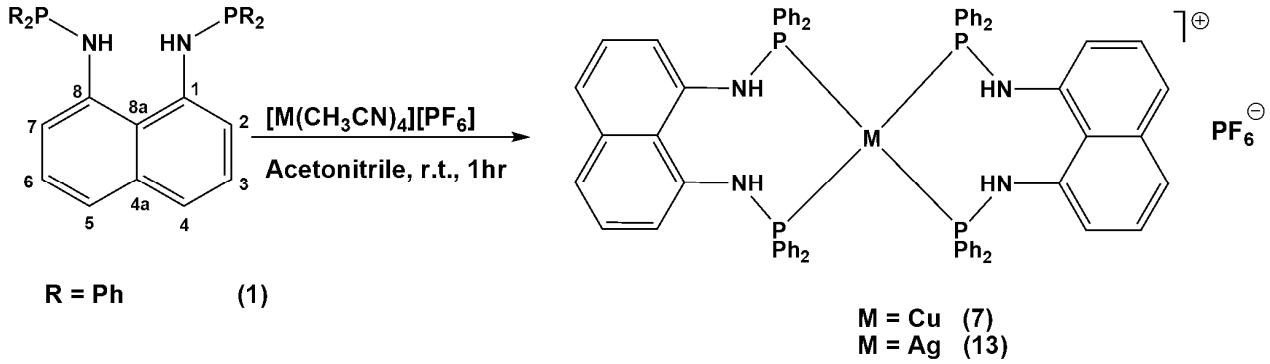

Scheme 4.1.2.3: Synthesis of mononuclear copper(I) and silver(I) complexes.

Reports indicated that conditions for the complexes to form, such as temperature, solvent, reaction stoichiometry, the nature of the ligand involved (stereogeometry and electron density), influence the outcome of the molecular structures. This was observed in **(12)** because the reaction was expected to yield a structure similar to those in Scheme 4.1.2.1.

4.1.2.2 Spectroscopic Characterisation: ^{1}H, ^{13}C and ^{31}P NMR

In ^{1}H NMR, the protons of complexes **(3)-(5)** and **(10)-(11)** were shifted downfield in the spectra. The protons of the naphthalene and phenyl-H are distinct from one another. Complex **(6)** consisted of *iso*-propyl-H and the CH_3 was shifted upfield as doublets. The ^{31}P NMR showed that all the P atoms were in the same environment and thus chemically equivalent in solution and resonated as a single peak. Complexes **(3)-(6)** showed singlets in the range 28.1 - 59.2 ppm. The peaks of the P atoms in the complexes appeared in the same region of the P atoms for aminophosphine complexes.[27]

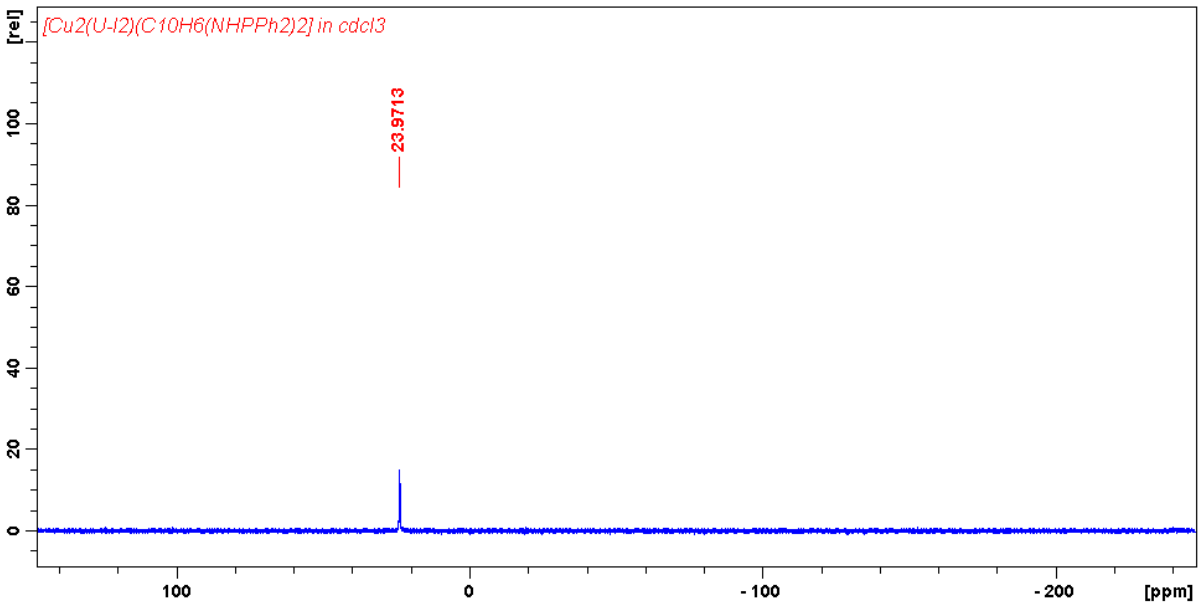

Figure 4.1.2.1. The ^{31}P NMR spectrum of **(5)**.

For the ^{1}H NMR discussion that follows, see Scheme 4.1.2.3 for the key to assigning proton positions. In the ^{1}H NMR spectra of complexes **(10)**-**(12)**, similar behaviour to Cu(I) complexes was observed. The ^{1}H NMR spectrum showed that the naphthalene protons {7 and 2} was doublets and resonated in the range of 6.63-6.57 ppm, for {6 and 3} there was an observed triplet in the range of 6.80-6.75 ppm and the resonance assignments for {5 and 3} was observed in the range of 7.27-7.17 ppm. The resonance assignments to the phenyl-H appeared in the range 7.16-7.13 ppm and 7.70-7.57 ppm.

The ^{31}P NMR spectra of complexes **(10)**-**(12)** were vastly different from the Cu(I) analogs **(3)**-**(6)** and warrant further discussion. The ^{31}P NMR spectra of Ag(I) complexes **(10)**-**(12)** showed two doublets and they appeared in approximately (1:1) ratio in the range of 40.1-34.2 ppm and 37.1-31.5ppm. The two doublets occurred due to the coupling of the P atom with two Ag nuclei, ^{107}Ag and ^{109}Ag. The corresponding $^{1}J(^{107,109}$ Ag-^{31}P) coupling constants are within the expected values reported by Caruso and co-workers.[28] The *J*-coupling constants are stated in the experimental section. The ^{1}H NMR and ^{31}P NMR spectra of complex **(7)** and **(13)** were comparable. The ^{31}P NMR spectrum showed the PF_6 anion consisted of five resonant peaks in the range -130.9 to -152.9 ppm. For the P atoms in complex **(7)**, the ^{31}P NMR spectrum showed a singlet at 55.1 ppm and for complex **(13)**, the spectrum shows a singlet peak at 22.7 ppm. The naturally occurring isotopes of silver (^{107}Ag, 51.82% and ^{109}Ag, 48.18%) both have a nuclear spin I = ½ and although their magnetogyric ratios are similar in magnitude (~10^{7} rad

$T^{-1}s^{-1}$) {$\gamma(^{109}Ag)/\gamma(^{107}Ag) = 1.15$} the scalar coupling is proportional to the gyromagnetic ratio of the nuclei, and the number for ^{109}Ag and ^{107}Ag is different. When the molecules are sufficiently rigid in solution (as appears to be the case for complexes **(10)-(12)**), two doublet pairs can normally be observed at ambient temperature, otherwise only at low temperature. Therefore, the ^{31}P NMR spectra of Ag(I) complexes with P-donor ligands show splitting due to ^{1}J(Ag-P) coupling, and this splitting is due to the gyromagnetic ratio of the nuclei for ^{109}Ag and ^{107}Ag that is different; and confirms solution rigidity of the cubane-type structure, as also observed in related studies.[11]

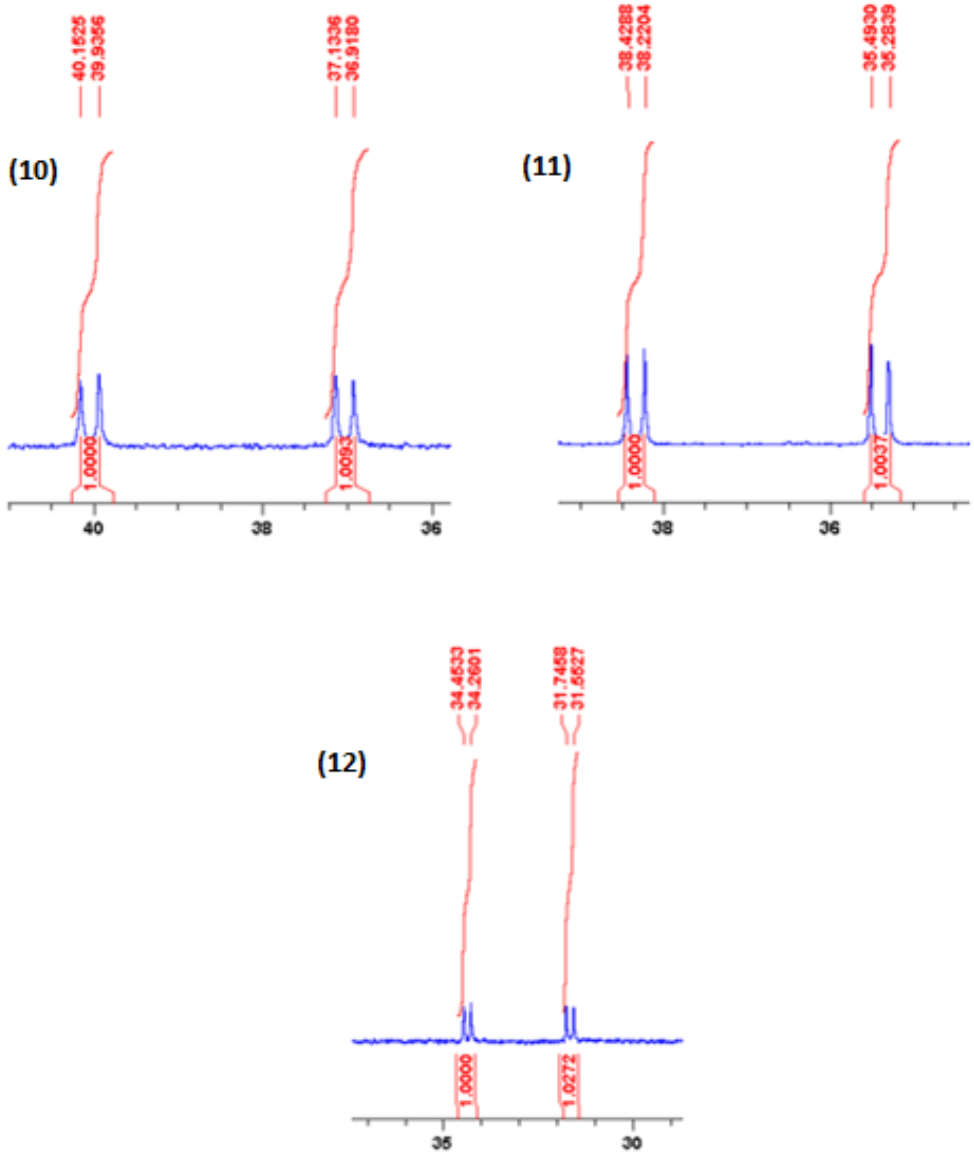

Figure 4.1.2.2. ^{31}P NMR spectra of complexes **(10)**-**(12)**, respectively. It is suggested that the two doublets derive from the coupling of the P atom with two Ag nuclei, ^{107}Ag and ^{109}Ag.

4.1.2.3 Characterisation: FTIR Spectroscopic Analysis

The FT-IR of complexes **(3)-(7)** showed that four important functional groups are present and showed band stretches at different wavelength to that of free *1,8*-diaminonaphthalene. There was a very small difference between the vibrational band of the ligands and their complexes. The important information is obtained in the stretches of the Cu-P band which showed complex formation. The complexes showed characteristic broad peaks at ~3000 cm^{-1} for ν(NH), ~800 cm^{-1} for ν(PN) and ~1600-1400 cm^{-1} for ν(C=C). Figure 4.1.2.3 shows the FT-IR spectrum of complex **(3)**. The IR absorption bands for complex **(3)** appeared at 3337cm^{-1} for ν(NH), 872 cm^{-1} for ν(PN), 515-473 cm^{-1} for ν(Cu-P) and 1580-1420 cm^{-1} for ν(C=C). The peaks were generally sharp.

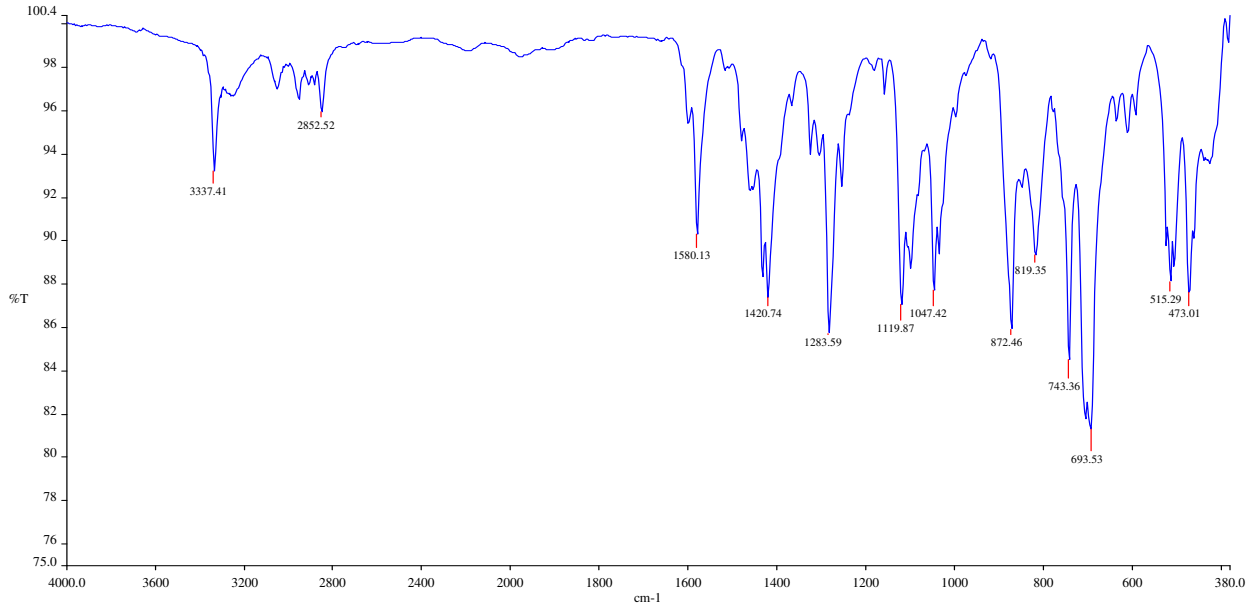

Figure 4.1.2.3. The FT-IR spectrum of **(3)**.

The FT-IR of complexes **(10)**-**(13)** showed characteristic broad peaks due to NH, PN, C=C and P-Ag and the bands are reported in the range that include complexes **(3)**-**(7)**. The characteristic bands appeared in the range of 3371-3358 cm^{-1} for ν(NH), 872-818 cm^{-1} for ν(PN), 524-522 cm^{-1} for ν(Ag-P) and 1645-1413 cm^{-1} for ν(C=C) and those of complex **(13)** were observed at 3057 cm^{-1} for ν(NH), 893 cm^{-1} for ν(PN), 543 cm^{-1} for ν(Ag-P) and 1580-1414 cm^{-1} for ν(C=C) which confirmed the formation of the products.

4.1.2.4 Molecular Structures of Complexes (3)-(6) of the Type $[Cu_2(\mu\text{-}X)_2\{C_{10}H_6(1,8\text{-}NHPR_2)_2\}_2]$ (R = Phenyl or *iso*-Propyl)

Single crystal X-ray structural analysis was used to determine the molecular structures of complexes **(3)**, **(4)** and **(4*)**, **(5)** and **(6)**. Figure 4.1.2.4-9 shows molecular structures of complexes **(3)**, **(4)** and **(6)**. Relevant crystallographic data of **(3)**, **(4)** and **(4*)**, **(5)** and **(6)** are shown in Table 4.1.2.1. The single crystal X-ray structure for **(3)**-**(6)** and $[Cu_4(\mu_3\text{-}Cl)_2(\mu_2\text{-}Cl)_2(O\{PPh_2\}_2)_2]$ and $[Cu_4(\mu_3\text{-}I)_2(\mu_2\text{-}I)_2(O\{P[CH(CH_3)_2]_2\}_2)_2]$, **(8)**-**(9)** respectively, were obtained by slow diffusion of hexane solvent into a dichloromethane solution (50:50). In some cases, hexane was substituted with diethyl ether.

Table 4.1.2.1. Crystallographic data for **(3)**, **(4)** and **(4*)**, **(5)** and **(6)**.

	3	**4**	**4***	**5**	**6**
Formula	$C_{70}H_{56}Cl_4Cu_2N_2P_4$	$C_{68}H_{56}Br_2Cu_2N_2P_4$	$C_{68}H_{56}Br_2Cu_2N_2P_4$	$C_{69}H_{58}Cl_2Cu_2I_2N_2P_4$	$C_{44}H_{74}Cl_2Cu_2N_2P_4$
M_r	1416.87	1339.94	1339.95	1518.85	978.98
Space group	*P*-1	$P2_1/c$	*P*-1	*P*-1	*P*-1
a, Å	10.4088(4)	23.070(7)	10.3233(13)	14.3504(8)	13.258(6)
b, Å	12.4512(5)	15.137(5)	14.5420(18)	15.1585(9)	14.0576(6)
c, Å	14.1436(6)	18.381(6)	21.121(3)	16.4336(10)	14.2669(7)
α, deg	68.5590(10)	90	93.993(2)	87.9970(10)	84.642(2)
β, deg	69.9710(10)	112.777(3)	95.288(2)	82.3790(10)	65.655(2)
γ, deg	81.0360(10)	90	106.1060(10)	64.7090(10)	77.862(2)
V, *Å*^{3}	1602.01(11)	5919(3)	3018(7)	3202(3)	2368.45(19)
Z	1	4	2	2	2
ρcalcd, g cm^{-3}	1.469	1.504	1.474	1.575	1.373
M, mm^{-1}	1.060	2.223	2.180	1.856	1.181
T, K	100(2)	173(2)	173.0	173.0	100.0(2)
Reflections collected	14758	96094	50543	53443	20400
Independent reflections	5843	10812	11073	11747	8620
R_{int}	0.0283	0.0524	0.0460	0.0355	0.0322
Final *R* indices [I > 2σ(*I*)][a]	*R*1 = 0.0290, w*R*2 = 0.1231	*R*1 = 0.0345, w*R*2 = 0.0699	*R*1 = 0.0326 w*R*2 = 0.0751	*R*1 = 0.0285 w*R*2 = 0.0753	*R*1 = 0.0599 w*R*2 = 0.1451
R indices (all data)	*R*1 = 0.0305 wR2 = 0.1265	*R*1 = 0.0487 wR2 = 0.0779	*R*1 = 0.0477 w*R*2 = 0.0819	*R*1 = 0.0336 w*R*2 = 0.0753	*R*1 = 0.0794 w*R*2 = 0.1598
Largest diff. peak and hole, e / Å	0.961 and -0.848	0.48 and -0.34	0.59 and -0.30	1.32 and -1.14	1.717 and -0.838

[a] $R1 = \Sigma \mid\mid F_o \mid - \mid F_c \mid\mid / \Sigma \mid F_o \mid$. [b] $wR2 = \{\Sigma [w(F_o^2 - F_c^2)^2] / \Sigma [w(F_o^2)^2]\}^{1/2}$

The highest difference electron density peaks of complexes **(3)** and **(5)** are due to disordered dichloromethane molecule(s) in **(3)**, **(5)** and in complex **(6)**, the two *peri*-naphthalene moieties are twisted to relief the strain stress of the complex.

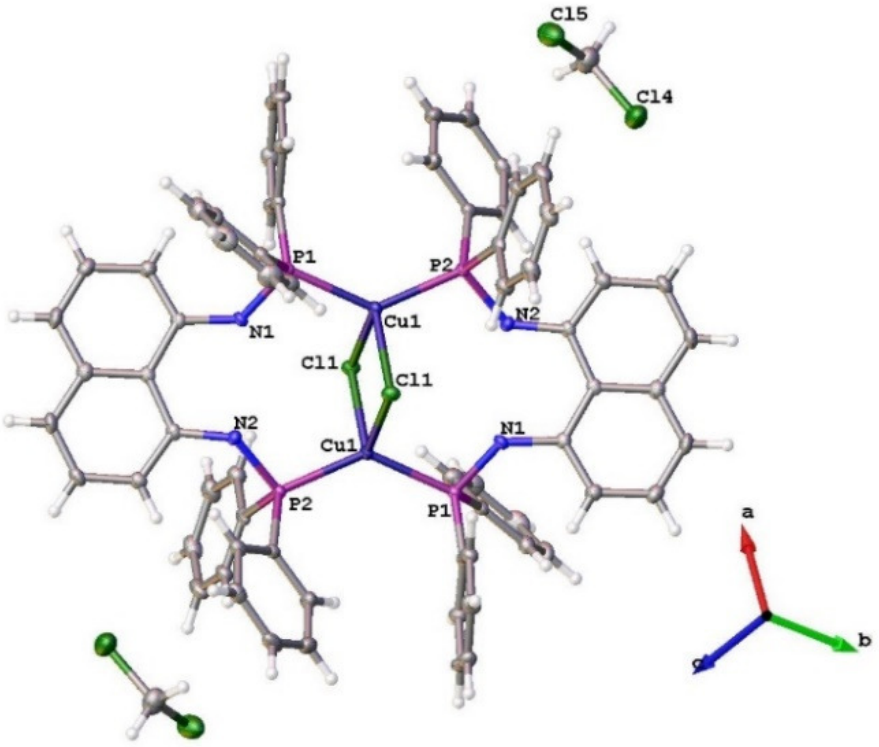

Figure 4.1.2.4. Molecular structure of **(3)** drawn at 50% probability with OLEX2.

Table 4.1.2.2. Selected bond distances (Å) and angles (deg) for **3** with esd's in parentheses.

Compound **3**			
Cl(1)–Cu(1)	2.3953(4)	Cl(1)–Cu(1ii)	2.4549(4)
Cu(1)–P(2)	2.2270(5)	Cu(1)–P(1)	2.2315(5)
Cu(1)–P(1ii)	2.2270(5)	N(1)–P(1)	1.6987(14)
N(2)–P(2)	1.6983(15)		
Cu(1)–Cl(1)–Cu(1ii)	88.210(14)	P(2)–Cl(1)–P(1)	132.711(17)
P(2)–Cu(1)–Cl(1)	105.835(17)	P(1)–Cu(1)–Cl(1)	112.024(17)
P(2)–Cu(1)–Cl(1ii)	107.340(17)	P(1)–Cu(1)–Cl(1ii)	98.884(16)
Cl(1)–Cu(1)–Cl(1ii)	91.790(14)	N(1)–P(1)–Cu(1)	103.70(5)

Symmetry transformations used to generate equivalent atoms: [1]1-X,1-Y,-Z; [2]-X,2-Y,1-Z.

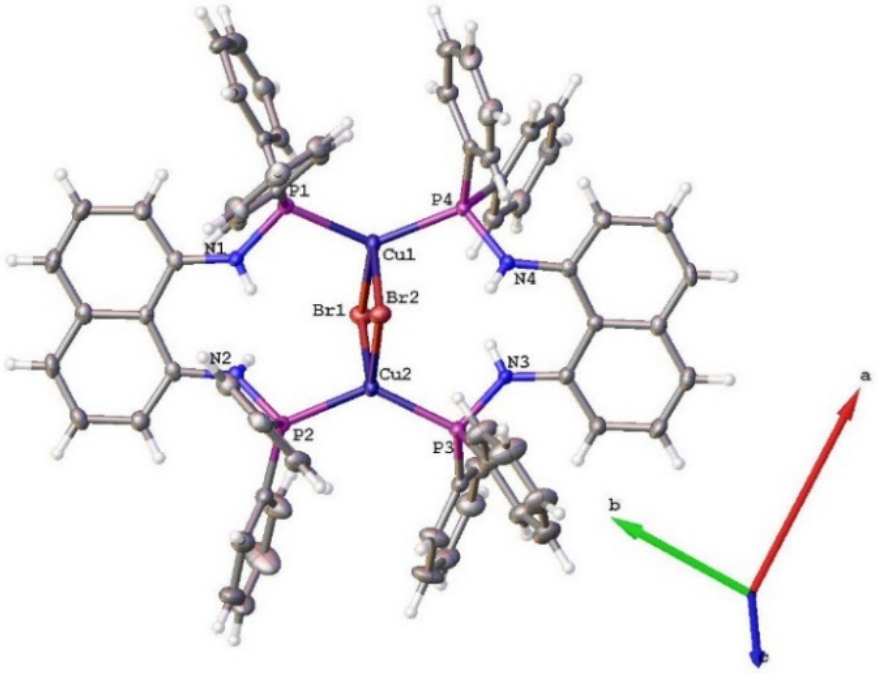

Figure 4.1.2.5. Molecular structure of **(4)** drawn at 50% probability with OLEX2.

Table 4.1.2.3. Selected bond distances (Å) and angles (deg) for **4** with esd's in parentheses.

Compound **4**			
P(1)–Cu(1)	2.2445(11)	Cu(1)–Br(1)	2.5540(7)
P(2)–Cu(2)	2.2232(10)	Cu(1)–Br(2)	2.5152(8)
P(3)–Cu(2)	2.2174(11)	Cu(2)–Br(1)	2.5578(8)
P(4)–Cu(1)	2.2319(10)	Cu(2)–Br(2)	2.5300(7)
N(1)–P(1)–Cu(1)	106.53(10)	N(2)–P(2)–Cu(2)	106.80(10)
N(3)–P(3)–Cu(2)	106.42(10)	N(4)–P(4)–Cu(1)	106.71(10)
P(1)–Cu(1)–Br(1)	109.16(3)	P(1)–Cu(1)–Br(2)	97.48(3)
P(4)–Cu(1)–P(1)	133.34(3)	P(4)–Cu(1)–Br(1)	110.50(3)
P(4)–Cu(1)–Br(2)	99.56(3)	Br(2)–Cu(1)–Br(1)	99.07(3)
P(2)–Cu(2)–Br(1)	104.29(3)	P(2)–Cu(2)–Br(2)	104.40(3)
P(3)–Cu(2)–P(2)	131.20(3)	P(3)–Cu(2)–Br(1)	109.77(3)
P(3)–Cu(2)–Br(2)	103.88(3)	Br(2)–Cu(2)–Br(1)	98.58(3)
Cu(1)–Br(2)–Cu(2)	81.80(3)		

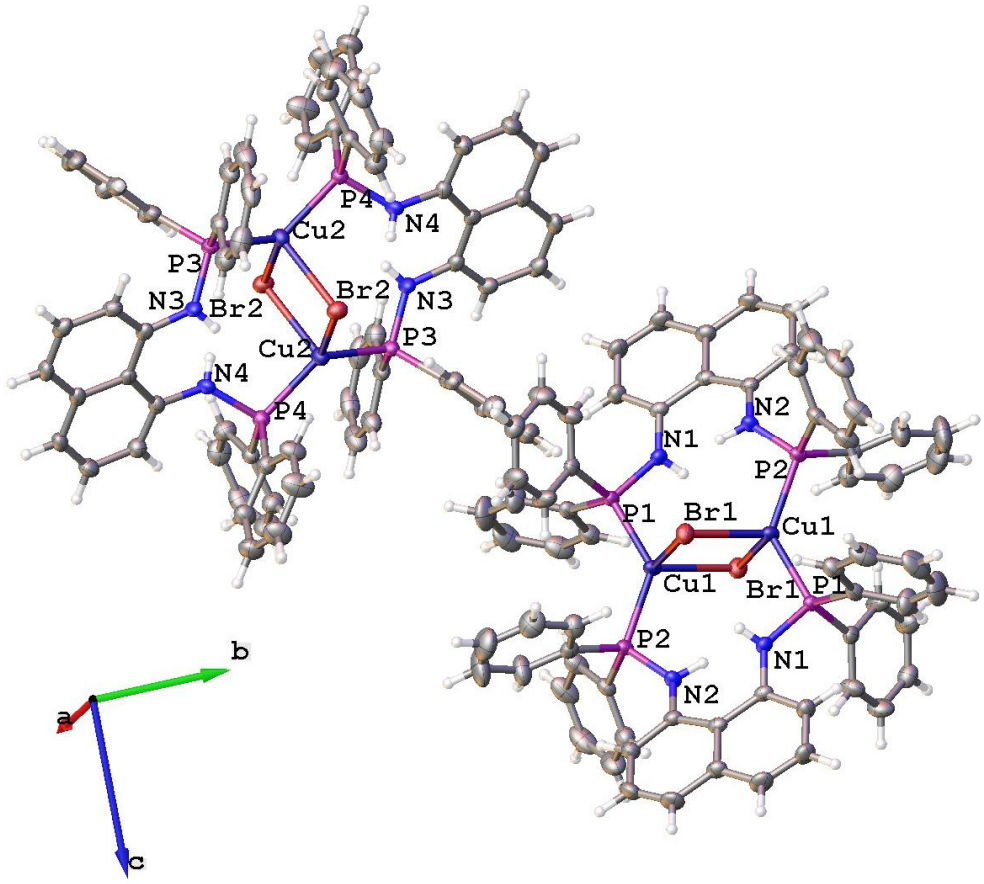

Figure 4.1.2.6. Molecular structures of **(4*)** drawn at 50% probability with OLEX2.

Table 4.1.2.4. Selected bond distances (Å) and angles (deg) for **4***with esd's in parentheses.

Compound **4***			
N(3)–P(3)	1.681(2)	N(4)–P(4)	1.683(2)
N(1)–P(1)	1.695(2)	N(2)–P(2)	1.688(2)
P(3)–Cu(2)	2.2255(8)	P(4)–Cu(2i)	2.2277(8)
P(1)–Cu(1)	2.2300(8)	Cu(2)–P(4i)	2.2276(8)
P(2)–Cu(1)	2.2166(8)	Cu(2)–Br(2)	2.5822(5)
Cu(1)–Br(1i)	2.4863(5)	Cu(2)–Br(2i)	2.5190(5)
Cu(1)–Br(1)	2.5966(5)	Br(2)–Cu(2i)	2.5190(5)
Br(1)–Cu(1ii)	2.4863(5)	N(3)–P(3)–Cu(2)	108.94(9)
N(1)–P(1)–Cu(1)	105.37(9)	N(4)–P(4)–Cu(2i)	104.00(9)

N(2)–P(2)–Cu(1)	107.95(9)	P(3)–Cu(2)–P(4i)	133.86(3)
P(1)–Cu(1)–Br(1ii)	104.90(2)	P(3)–Cu(2)–Br(2)	100.37(2)
P(1)–Cu(1)–Br(1)	101.43(2)	P(3)–Cu (2)–Br(2i)	107.17(2)
P(2)–Cu(1)–P(1)	131.54(3)	P(4i)–Cu(2)–Br(2)	100.41(2)
P(2)–Cu(1)–P(1ii)	112.22(2)	P(4i)–Cu(2)–Br(2i)	111.48(2)
P(2)–Cu(1)–Br(1)	103.93(2)	Br(2i)–Cu(2)–Br(2)	94.969(14)
Br(1ii)–Cu(1)–Br(1)	96.678(14)	Cu(2i)–Br(2)–Cu(2)	85.029(14)
Cu(1ii)–Br(1)–Cu(1)	183.322(14)		

Symmetry transformations used to generate equivalent atoms: [1]1-X,1-Y,-Z; [2]-X,2-Y,1-Z.

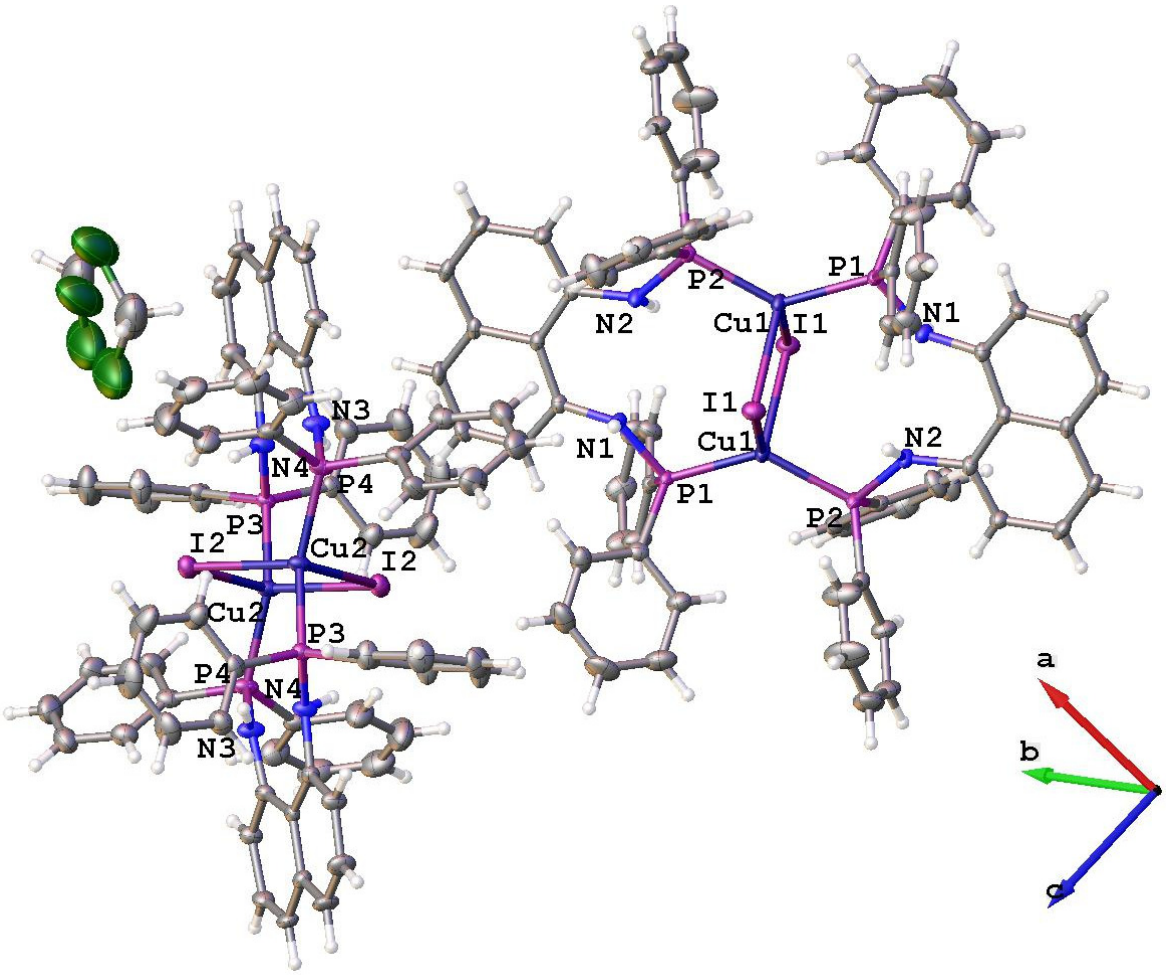

Figure 4.1.2.7. Molecular structures of **(5)** drawn at 50% probability with OLEX2.

Table 4.1.2.5. Selected bond distances (Å) and angles (deg) for **5** with esd's in parentheses.

Compound **5**			
N(1)–P(1)	1.690(2)	N(2)–P(2i)	1.695(5)
P(1)–Cu(1)	2.2313(8)	P(2)–N(2i)	1.695(2)
N(3)–P(4)	1.689(2)	N(4)–P(3ii)	1.694(2)
N(3)–P(4ii)	1.694(2)	P(3)–Cu(2)	2.2346(8)
P(4)–Cu(2)	2.2314(8)	Cu(2)–I(2)	2.7252(4)
Cu(2)–I(2ii)	2.6865(4)	I(2)–Cu(2ii)	2.6866(4)
Cu(1)–I(1i)	2.7463(4)	Cu(1)–I(1)	2.6657(4)
P(2)–Cu(1)	2.2430(8)	P(2)–N(2i)	1.695(2)
C(29)–P(2)	1.819(3)	N(3)–P(4)–Cu(2)	107.27(9)
N(2i)–P(2)–Cu(1)	105.73(8)	P(1)–Cu(1)–P(2)	131.96(3)
P(1)–Cu(1)–I(1)	105.73(2)	P(1)–Cu(1)–I(1i)	105.09(2)
P(2)–Cu(1)–I(1i)	100.24(2)	P(3)–Cu(2)–I(2)	104.18(2)
P(3)–Cu(2)–I(2ii)	103.37(2)	P(4)–Cu(2)–P(3)	131.41(3)
P(4)–Cu(2)–I(2ii)	102.46(3)	P(4)–Cu(2)–I(2)	109.33(2)
I(2ii)–Cu(2)–I(2)	102.629(13)	Cu(2ii)–I(2)–I(2)	77.372(13)
Cu(1)–I(1)–Cu(1i)	78.382(13)	I(1)–Cu(1)–I(1i)	101.619(13)
P(2)–Cu(1)–I(1i)	108.22(2)	N(1)–P(1)–Cu(1)	108.46(9)
N(4ii)–P(3)–Cu(2)	104.78(9)		

Symmetry transformations used to generate equivalent atoms: [1]1-X,-Y,1-Z; [2]1-X,1-Y,2-Z where [1]1 = i and [2]1 = ii.

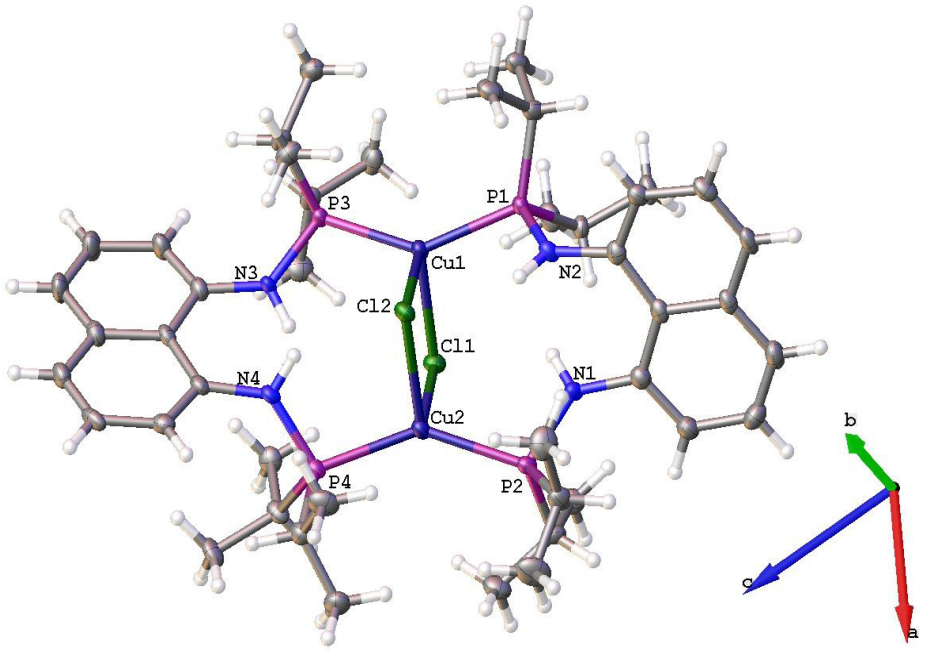

Figure 4.1.2.8. Molecular structure of **(6)** drawn at 50% probability with OLEX2.

Table 4.1.2.6. Selected bond distances (Å) and angles (deg) for **6** with esd's in parentheses.

Compound **6**			
C1(1)–Cu(1)	2.3857(13)	C1(1)–Cu(2)	2.4337(13)
Cu(2)–P(2)	2.2557(14)	Cu(2)–P(4)	2.2574(14)
Cu(2)–Cl(2)	2.5493(13)	Cu(1)–P(3)	2.2314(13)
Cu(1)–P(1)	2.2329(13)	Cu(1)–Cl(2)	2.5864(13)
Cu(1)–Cl(1)–Cu(2)	93.97(4)	P(2)–Cu(2)–P(4)	141.56(5)
P(2)–Cu(2)–Cl(1)	97.66(5)	P(4)–Cu(2)–Cl(1)	110.87(5)
P(2)–Cu(2)–Cl(2)	109.32(5)	P(4)–Cu(2)–Cl(2)	96.79(5)
Cl(1)–Cu(2)–Cl(2)	89.60(4)	P(3)–Cu(1)–P(1)	141.12(5)
P(3)–Cu(1)–Cl(1)	102.67(5)	P(1)–Cu(1)–Cl(1)	107.13(5)
Cl(1)–Cu(1)–Cl(2)	89.79(4)		

The molecular structures of **(3)** and **(5)** co-crystallize with two solvated dichloromethane molecules. The dichloromethane solvate derives from the same solvent used to grow the crystals. Complexes **(3)**, **(4*)**, **(5)** and **(6)** are isomorphous and crystallizes in the centrosymmetric triclinic space group P-1. Complexes **(4)** and **(4*)** are polymorphs which crystallized in the space groups monoclinic $P2_1/c$ and triclinic P-1, respectively, see Table 4.1.2.1. Complex **(4)** was obtained in DMSO and **(4*)** in THF solvents, respectively. Complex **(4)** has one molecule in the unit cell whereas **(4*)** consist of two molecules in the unit cell. The molecules are non-superimposable on each other but instead each molecular structure lies on its own axis of rotation. Complexes **(4*)** and **(5)** consist of two molecular structures within a unit cell. Ligand **(1)**, in the complexes **(3)**, **(4)**, **(4*)** and **(5)** binds the two Cu-atoms through the P donor atoms in a bridging manner to form dinuclear complexes. Ligand **(2)** coordinated to the Cu(I) center in a manner similar to the geometry of **(3)**-**(5)**. The two Cu(I) centers were bridged by halogens {X = Cl **(3)** and **(6)**, Br **(4)** and **(4*)** and I **(5)**} forming a tetrahedral geometry around the metal center. The halides linked the Cu atoms to form a rhomboid core where the Cu···Cu and X···X aligned diagonally to each other. The $\{Cu_2(\mu\text{-}X)_2\}$ units of the complexes **(3)**, **(4)**, **(4*)**, **(5)** and **(6)** are planar with centrosymmetric inversion center coinciding with the midpoint of the Cu···Cu vectors. Complex **(6)** in Figure 4.1.2.9 shows weak intramolecular Cl···H hydrogen bonding which stabilizes the crystal packing.

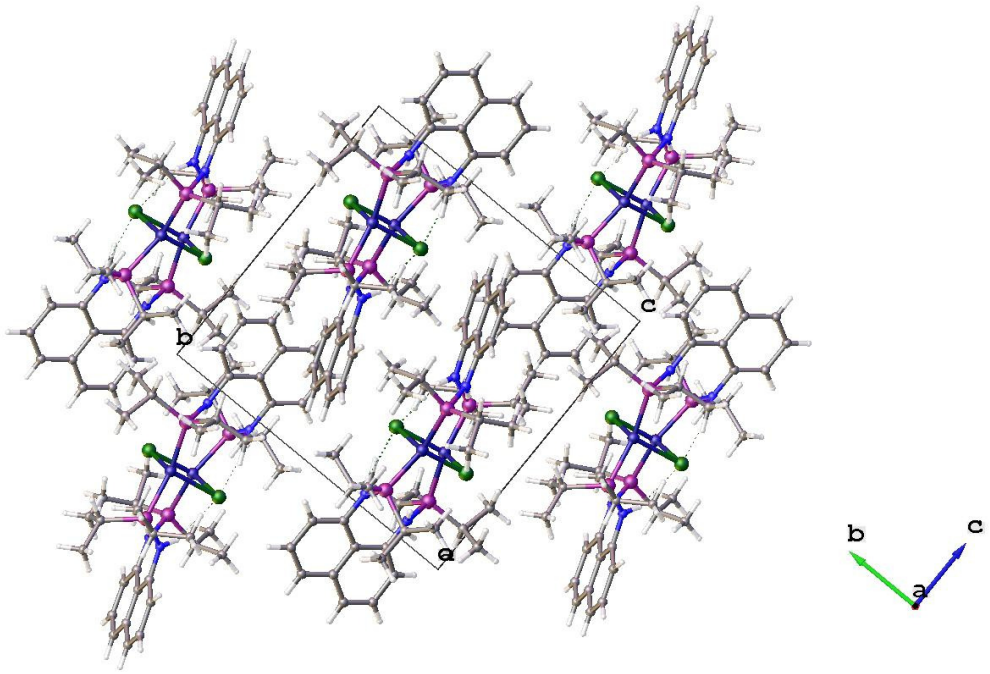

Figure 4.1.2.9. Crystal structure of **(6)**.

Complexes **(3)**, **(4)**, **(4*)**, **(5)** and **(6)** exhibited strong π-π* interaction from the adjacent naphthalene rings held together hydrogen bonding of NH. Complexes that contain the solvates such as CH_2Cl_2 were stabilized by inter- and intramolecular interactions caused by the solvent in the complexes.

Table 4.1.2.2-6 represents selected bond lengths (Å) and angles (°) of the complexes **(3)**-**(6)**, respectively. Figure 4.1.2.4-9 shows the solid state molecular structure of complexes **(3)**-**(6)**, where coordination geometries around the Cu centers are defined by the two P-atoms of **(1)** and the two halide atoms bridging the Cu(I) species.

Table 4.1.2.7. Selected bond distances (Å) and angles (deg) of complexes **3**-**6** for discussion.

Distances (Å) and Angles (°)	**3 (X = Cl)**	**4 (X = Br)**	**4* (X = Br)**	**5 (X= I)**	**6 (X = Cl)**
Distances (Å)					
Cu···Cu	3.38	3.30	3.30	3.42	3.52
Cu-P	2.23	2.23	2.24	2.24	2.26
Cu-X	2.45	2.56	2.58	2.75	2.55
Angles (°)					
Cu-X-Cu	88.21	85.03	81.80	78.38	93.97
X-Cu-X	91.79	96.68	99.07	101.62	89.60
P-Cu-P	132.71	131.54	133.34	131.96	141.56
X-Cu-P	107.34	112.2	110.50	105.73	110.57

For bond lengths and bond angles discussion that follows, see Table 4.1.2.7. In complex **(3)**, the Cu-P and Cu-Cl bond lengths are in the range 2.2270(5)-2.2315(5) and 2.3953(4)-2.4529(4) Å, respectively. The corresponding bond angles of complex **(3)** are in the range 88.210(14)-132.711(17)°, see Table 4.1.2.4. Complex **(3)** have a Cu···Cu distances of 3.376Å. The Cu-P and Cu-X bond lengths for complexes **(4), (4*)** and **(5)** are in the ranges {[2.2174(11)-2.2445(11) Å] Cu-P and [2.5152(8)-2.5578(8) Å] Cu-Br for **(4)}** and {[2.2166(8)-2.2277(8) Å] Cu-P and [2.4863(5)-2.5966(5) Å] Cu-Br for **(4*)**} and {[2.2313(8)-2.2430(8) Å] and [2.6657(4)-2.7463(4) Å] Cu-I for **(5)**}, respectively. The Cu···Cu distances of complexes **(4), (4*)** and **(5)** are 3.303, 3.303 and 3.421Å, respectively. The bond angles of P-Cu-P, X-Cu-X and X-Cu-P defines the type of the geometries the complexes **(4)**, **(4*)** and **(5)** will form. The

values of the bond angles are {(P-Cu-P: 132.71(17) for **(3)**, 131.20(3) for **(4*)** and 131.97(3) for **(5)** }°, respectively, and {X-Cu-X: 91.79(14) for **(4)**, 80.51-81.80(3) for **(4*)** and 101.62(13) for **(5)}**°, respectively and {Cl-Cu-P: 107.34(17) for **(4)**, 97.48-109.77(3) for **(4*)** and 100.24(2)-108.21(2) for **(5)**}°, respectively. The bond lengths and the Cu···Cu distances are related to those reported by Trivedi *et al.*,[29] for copper(I) complexes containing 1,1-bis(dipenylphosphino)ferrocene (dppf) in doubly bridged mode which are {Cu-P: (2.253-2.277Å), Cu-Cl: (2.396-2.400Å) and Cu···Cu: (3.216-3.218Å)} for the chlorine containing complex, {Cu-P (2.270Å), Cu-Br (2.515Å) and Cu···Cu (3.331Å)} for the bromine containing complex and {Cu-P (2.271-2.283Å), Cu-I (2.692-2.6766Å) and Cu···Cu (3.323-3.527Å)} for the iodine containing complex. These are slightly longer than those reported by Knight *et al.*,[30] and shorter than those reported by Tsuboyama and co-workers.[1] Literature[31, 32] reported Cu···Cu distances of less than 2.7Å for the unit of the cubane clusters of the type $\{Cu_4(\mu_3\text{-}X)_4\}$. Kobayashi and colleagues[33] reported $\{Cu_2(\mu\text{-}X)_2\}$ rhombus complexes of the type Cu_2I_2-[O,O] and Cu_2Br_2-[O,O] with a Cu···Cu distance of 2.998 and 3.111Å, respectively. The [O,O] in the complexes Cu_2X_2-[O,O] represent the DMSO ligands which are coordinated to the metal centers in a monodentate manner. The Cu···Cu distance for complexes **(3), (4), (4*)** and **(5)** are longer than the Cu···Cu distances of the complexes Cu_2I_2-[O,O] and Cu_2Br_2-[O,O], but shorter than twice the van der Waals radius of Cu···Cu, which is 2.80Å. The difference is due to a larger ionic radius of iodine compared to that of bromine. The bond distances and angles of complex **(6)** are presented in Table 4.1.2.5 and Table 4.1.2.7 and are similar to **(3)**. The difference between the complexes **(3)** and **(6)** is the substituents attached to the P donor atoms and also the naphthalene rings are twisted in complex **(6)** whilst in **(3)** are planar.

Figure 4.1.2.10-12 shows the molecular structures of **(10)**, **(11)** and **(12)**, respectively, see Table 4.1.2.8 for crystallographic data. The selected bond lengths and angles are shown in Table 4.1.2.9-11. Single crystals were grown by the slow evaporation of dimethylformamide in the dark. Complexes **(10)** and **(11)** are isomorphous and they crystallized in space group triclinic P-1 and monoclinic $P2_1/c$, respectively. Complex **(12)** crystallized in a triclinic space group P-1. Complexes **(10)** and **(11)** are characterized by the structural units $\{Ag_2(\mu\text{-}Cl)_2\}$ **(10)** and $\{Ag_2(\mu\text{-}Br)_2\}$ **(11)**, with P atoms of the ligand **(1)** bridging the two Ag(I) metals. The N atoms of the complexes are not coordinating to the metal centers. The core structural unit $\{Ag_2(\mu\text{-}X)_2\}$ of the complexes are planar with the crystallographic center of inversion (complexes are centrocemmetric) coinciding with the midpoint of the of the Ag···Ag vectors. The two Ag(I)

metal centers in the complexes **(10)** and **(11)** have a tetrahedral geometry. Each P-donor atom in the ligand of the complexes is coordinated to a Ag(I) metal center which is bridged by two halides.

Table 4.1.2.8. Crystallographic data for **(10)**, **(11)**, and **(12)**.

	10	**11**	**12**
Formula	$C_{75}H_{70}Cl_2Ag_2N_6O_2P_4$	$C_{74}H_{70}Br_2Ag_2N_6O_2P_4$	$C_{80.5}H_{84.5}Ag_4I_4N_4P_4$,2($C_3H_7NO$),2 ($C_{3.25}H_{7.25}NO$)
M_r	1485.88	1574.78	2290.92
Space group	*P*-1	$P2_1/c$	*P*-1
a, Å	10.5333(6)	13.4547(6)	12.2846(4)
b, Å	12.5042(7)	14.7771(6)	12.7984(4)
c, Å	14.5322(8)	18.0401(8)	14.2709(5)
α, deg	102.6690(10)	90	67.832(2)
β, deg	109.6690(10)	99.3440(10)	80.095(2)
γ, deg	102.9960(10)	90	81.374(2)
V, Å^3	1664.32(16)	3539.2(3)	2037.97(12)
Z	1	2	1
ρcalcd, g cm^{-3}	1.482	1.478	1.867
M, mm^{-1}	0.817	1.822	2.594
T, K	173.15	100(2)	103(2)
Reflections collected	20247	76464	44500
Independent reflections	6123	8804	9750
R_{int}	0.0328	0.0339	0.0680
Final *R* indices [I > 2σ(*I*)][a]	*R*1 = 0.0342, w*R*2 = 0.0839	*R*1 = 0.0268 w*R*2 = 0.0936	*R*1 = 0.0503 w*R*2 = 0.1246
R indices (all data)	*R*1 = 0.0409 wR2 = 0.0900	*R*1 = 0.0345 w*R*2 = 0.1033	*R*1 = 0.0880 w*R*2 = 0.1571
Largest diff. peak and hole, e / Å	0.69 and -0.85	1.495 and -1.233	1.58 and -1.98

[a] $R1 = \Sigma \mid\mid F_o \mid - \mid F_c \mid\mid / \Sigma \mid F_o \mid$. [b] $wR2 = \{\Sigma [w(F_o^2 - F_c^2)^2] / \Sigma [w(F_o^2)^2]\}^{1/2}$

The highest difference electron density peaks of complexes **(10)**-**(12)** are due to disordered DMF molecule(s) in the compounds.

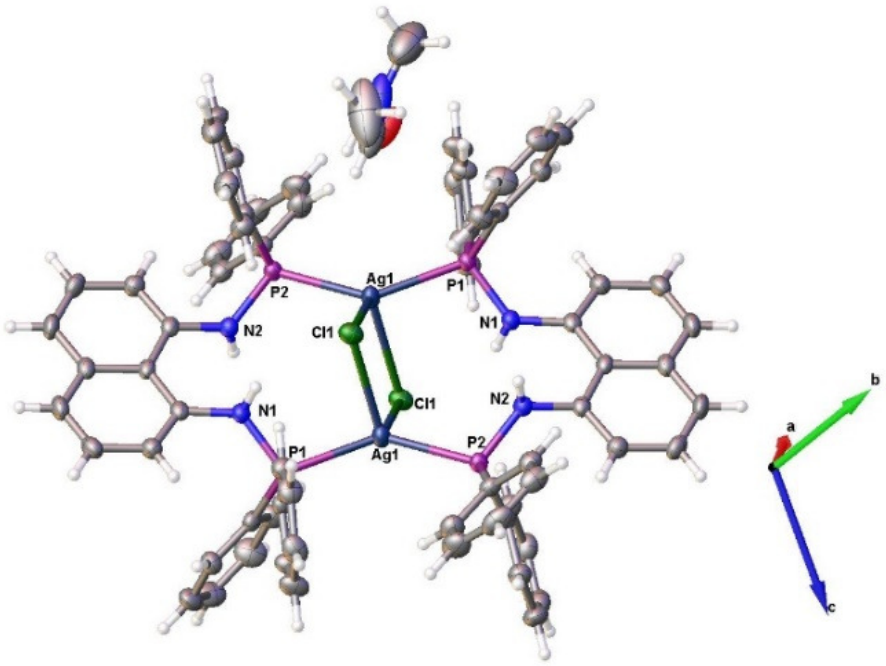

Figure 4.1.2.10. Molecular structure of **(10)** drawn at 50% probability with OLEX2.

Table 4.1.2.9. Selected bond distances (Å) and angles (deg) for **10** with esd's in parentheses.

Compound **10**			
Ag(1)–P(1)	2.4184(7)	Ag(1)–P(2)	2.4158(7)
Ag(1)–Cl(1)	2.6318(7)	Ag(1)–Cl(1ii)	2.7182(7)
P(1)–N(1)	1.695(2)	P(2)–N2(2)	1.690(2)
Cl(1)–Ag(1)–Cl(1ii)	97.86(2)	N(2)–P(2)–Ag(1)	109.37(8)
P(1)–Ag(1)–Cl(1)	112.74(2)	N(1)–P(1)–Ag(1)	105.94(8)
P(1)–Ag(1)–Cl(1ii)	90.22(2)	P(2)–Ag(1)–Cl(1ii)	111.67(2)
P(2)–Ag(1)–P(1)	138.83(2)	Ag(1)–Cl(1)–Ag(1ii)	82.14(2)

Symmetry transformations used to generate equivalent atoms: [1]-X,2-Y,1-Z.

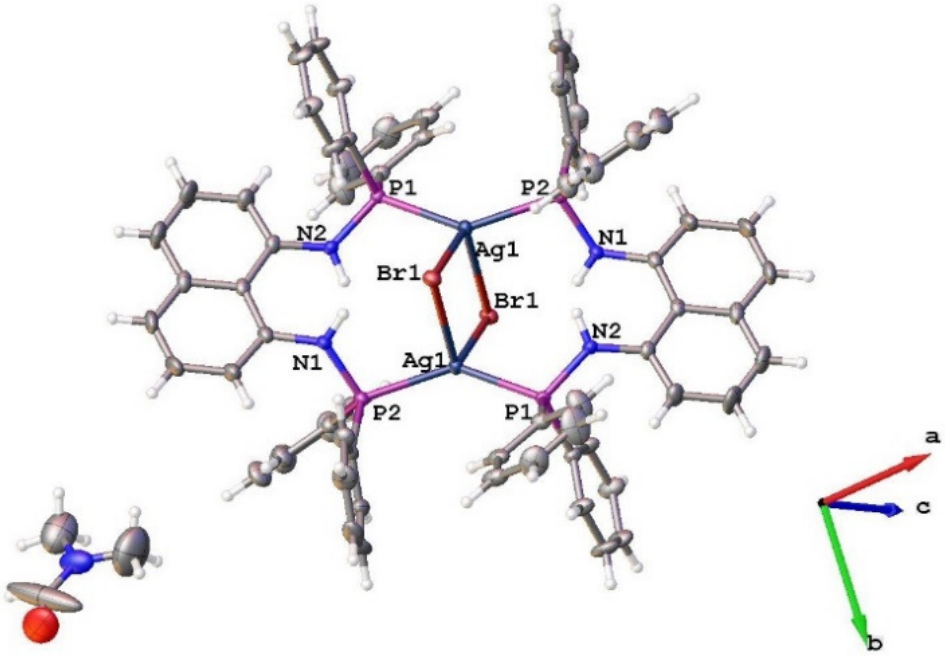

Figure 4.1.2.11. Molecular structure of **(11)** drawn at 50% probability with OLEX2.

Table 4.1.2.10. Selected bond distances (Å) and angles (deg) for **11** with esd's in parentheses.

Compound **11**			
Ag1(1)–P(2)	2.4175(5)	Ag1(1)–P(1)	2.4249(5)
Ag1(1)–Br(1ii)	2.7223(3)	Ag1(1)–Br(1)	2.9143(3)
N(1)–P(2)	1.68566(18)	N(2)–P(1)	1.6887(18)
P(2)–Ag(1)–P(1)	136.474(18)	P(2)–Ag(1)–Br(1ii)	115.459(14)
P(1)–Ag(1)–Br(1ii)	101.069(13)	P(2)–Ag(1)–Br(1)	92.597(14)
P(1)–Ag(1)–Br(1)	99.471(13)	Br(1ii)–Ag(1)–Br(1)	106.114(7)
Ag(1ii)–Br(1)–Ag(1)	73.888(7)		

Symmetry transformations used to generate equivalent atoms: #1 -x+1,-y,-z+2 where (#1 = ii)

Structure **(11)** consist of one disordered DMF molecule, while the structure **(12)** consist of two disordered DMF molecules. DMF molecules in **(12)** were much distorted compared to structure **(11)** and hence the distorted molecules had to be refined to improve the quality of the molecules.

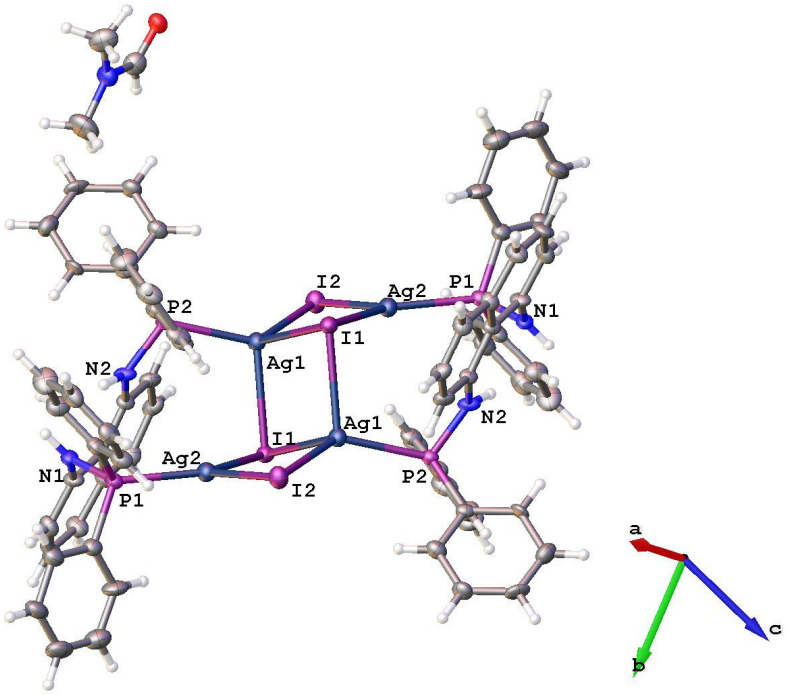

Figure 4.1.2.12. Molecular structure of **(12)** drawn at 50% probability with OLEX2.

Table 4.1.2.11. Selected bond distances (Å) and angles (deg) for **12** with esd's in parentheses.

Compound **12**			
Ag(1)–I(1i)	2.9573(7)	Ag(1)–I(1)	2.9317(7)
Ag(1)–I(2i)	2.8035(7)	Ag(1)–P(2)	2.4505(18)
Ag(2)–I(1)	2.7355(7)	Ag(2)–I(2)	2.8451(7)
Ag(2)–P(1)	2.4108(18)	I(2)–Ag(1)–I(1i)	102.21(2)
I(2i)–Ag(1)–I(1)	104.30(2)	P(2)–Ag(2)–I(1)	106.93(2)
P(2)–Ag(2)–I(1)	138.21(5)	I(2)–Ag(1)–I(1i)	180.0(15)
Cl(1)–Pt(1)–Se(1)	84.93(8)	P(1)–Ag(2)–I(2)	114.81(5)

Symmetry transformations used to generate equivalent atoms: #1 -x+1,-y+1,-z+1.

Complexes **(12)** consist of ligand **(1)** acting as a bidentate ligand. The P-atoms of **(1)** are bonded to four Ag(I) atoms centers in a bridging structure to construct the Ag_4 core. The complex have a centrosymmtric center of rotation along the Ag_4 core. The two Ag(I) metal centers are four coordinated with three iodide ligands and one P-atom of the ligand **(1)** to create a tetrahedral

coordination geometry, whereas the remaining two Ag(I) metal centers are three coordinate with two iodide species and one P atom to generate a trigonal planar coordination geometry. Complex **(12)** is a staircase tetranuclear cubane-type cluster and consist of two DMF solvates which co-crystallized with the molecule. One of the DMF molecules was distorted over two locations along one end of the methyl group. The DMF solvates' origin is the crystal growing solvent.

Table 4.1.2.12. Selected bond distances (Å) and angles (deg) of **10**-**12** for discussion.

Distances (Å) and Angles (°)	**10 (X = Cl)**	**11(X = Br)**	**12 (X = I)**
Distances (Å)			
Ag···Ag	3.52	3.39	3.78 and 3.42
Ag-P	2.41	2.42	2.45
Ag-X	2.72	2.91	2.95
Angles (°)			
Ag-X-Ag	82.14	73.88	79.91
X-Ag-X	97.86	106.11	104.44
P-Ag-P	138.83	136.46	-
X-Ag-P	113.74	115.47	127.62 and 107.44

For bond lengths and bond angles discussion that follows, see Table 4.1.2.12. The difference between complexes **(10)** and **(11)** are in the bond angles of Ag-X-Ag, X-Ag-X and P-Ag-P and their Ag···Ag distances of interactions in the rhombic unit. The angles of Ag-X-Ag, X-Ag-X and P-Ag-P for complexes **(10)** and **(11)** are {82.14(2), 97.86(2) and 138.83(2)°} for **(10)** and {73.888(7), 106.114(7) and 136.474(18)}° for **(11)**}. This is due to the increase in atomic radius of the halogens from Cl to Br and electronegativity. The atomic radius increases in size with an increase of electronic energy levels, therefore this lessens the attraction for valence electrons of other atoms, decreasing their reactivity. This decrease occurs because electronegativity decreases down a group, therefore there is less electron attraction. The size of halogen atoms influence the interactive Ag···Ag distances of complexes **(10)** and **(11)**. The argentophilic Ag···Ag interaction distances are 3.515 and 3.391Å for **(10)** and **(11)**, respectively. The P-Ag and Ag-Cl bond distances are in the range {2.4158(7)-2.4184(7) and 2.6318(7)-2.7182(7) Å for **(10)**}, respectively and the P-Ag and Ag-Br bond lengths are in the range {2.4175(5)-2.4259(5) and 2.7223(3)-2.9143(3) Å for **(11)**, respectively, which are in agreement with the literature reports.[28, 34, 35] For complexes **(10)** and **(11)** the non-bonding N atoms in the *peri*-

positions have distances that range from 2.775-2.795 Å. The bond distances for P-Ag and Ag-I of the complex **(12)** ranges from {2.4108(18)-2.4505(18) and 2.7355(7)-2.9573(7) Å, respectively. The bond angles surrounding the metal center for complex **(12)** can be viewed in three different ways, Ag-I-Ag, I-Ag-I and P-Ag-I and these are in the ranges: {73.63-79.91, 100.99-102.21 and 114.79-138.23 Å}, respectively. The complex is characterized by two weak Ag···Ag interactions. The core Ag···Ag interaction distance is 3.782 Å and terminal (outer) Ag···Ag interaction is 3.426 Å. The bond distances of P-Ag and Ag-I for tetranuclear complexes have been reported[36-38] for a core complex similar to **(12)**. There is a slight variation observed when compared to cubanes of M_4X_4 core reported by Churchill *et al.*[39] and Toe and co-workers[40]. Complexes **(12)** have a non-bonding N-atoms interaction distance of 2.781Å in the *peri*-position. This interaction is the same with distances observed in complexes **(10)** and **(11)**.

Strong intramolecular hydrogen bonding was observed between the H atoms on adjacent amines in the *peri*-position, which possibly contribute in stabilizing the molecular structure. The N atoms also interact with the opposite H atoms of the phenyl rings *via* intramolecular bonding. The DMF molecules occupies the voids within the crystal structure to further aid in stabilization of the molecule. The crystal packing is not supported by the π-π* stacking of the adjacent electron rich rings of the naphthalene, rather each molecule arranges itself in a unique manner *via* π interaction, see Figure 4.1.2.13.

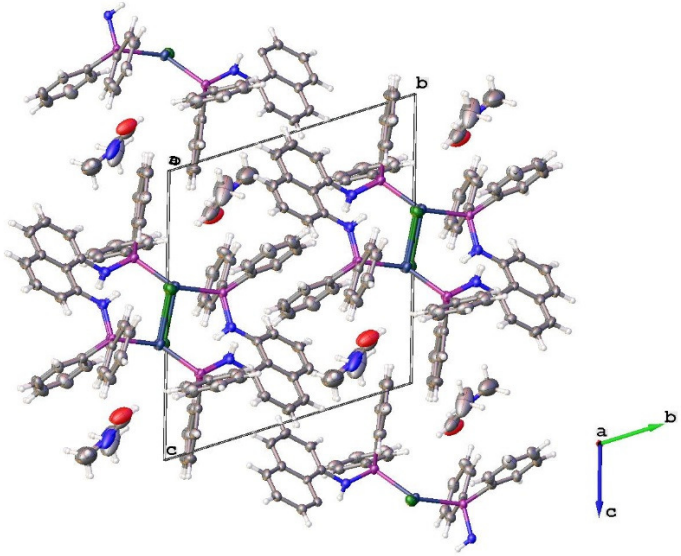

Figure 4.1.2.13. Molecular packing (portion of crystal structure) of **(3)** drawn at 50% probability.

Figure 4.1.1.1 shows selected coordination modes displayed by Ag(I) metal centers. Formation of coordination types (**a)** and (**b)** is due to the spacer of the ligand between the donor atoms, see section 4.1.1. Such coordination geometries are observed for bidentate ligands 1,5-bis(diphenylphosphino)pentane[41] and bis[(diphenylphosphino)ethyl]sulfide[42]. The metal centers in the complexes have a tetrahedral configuration with an Ag_2X_2 core geometry. The bridging format is attributed to the relative bond length strengths, i.e. Ag-halides > Ag-P donor atom > Ag···Ag weak anion interactions. These bond strengths are sustained by mild reaction conditions and the geometry is driven by the choice of the reaction medium.

Although, it was state that the bond lengths of the reported complexes are similar to those reported in literature, it is also good to account for the variation observed at the second decimal of the bond length values. For instance, complex **(11)** Ag-(P2) = 2.4175(5) and Ag-P(1) = 2.4249(5). These values are different at the second decimal, the same with halides, even more 2.7223(3) for Ag(1)-Br(1ii) vs. 2.9143(3). The similar behavior was observed for Cu(I) complexes which might be due to John-Teller effect.

4.1.2.5 Synthesis of Copper P-O-P Complexes of Type $[Cu_4(\mu_3\text{-}X)_2(\mu_2\text{-}X)_2(O\{PR_2\}_2)_2]$, (R = Phenyl for X = Cl and R = *iso*-Propyl for X = I)

Reactions that lead to P-O-P type bridging bis(phosphinites) ligands are shown in Scheme 4.1.2.4. Complex **(6.1)** of the type $[Cu_2(\mu\text{-}I)_2\{C_{10}H_6(1,8\text{-}NHPPh_2)_2\}_2]$, is an iodine analogue of complex **(6)** of the type $[Cu_2(\mu\text{-}Cl)_2\{C_{10}H_6(1,8\text{-}NHPPh_2)_2\}_2]$. Complex **(6.1)** was synthesized similarly to complex **(6)** but not reported in this work due to reproducibility issues. Complex **(3)** was treated with $PhI\cdot Cl_2$ in an attempt to oxidize Cu(I) to Cu(II) and thus open the ring to form a large metallacycle. However, it would appear as though $PhI\cdot Cl_2$ never served its original function because in the presence of air/moisture, the ligand fragmented by an undetermined mechanism and produced the P-O-P type ligand upon isolation and characterization. Thus, $[Cu_4(\mu_3\text{-}Cl)_2(\mu_2\text{-}Cl)_2(O\{PPh_2\}_2)_2]$ **(8)** was obtained from **(3)** in the presence of air. The rupture of P-N bonds in the ligands prepared in this study, seems to be easy to accomplish. The oxidation presumably occurred due to dissolved moisture or air (oxygen) in the reaction medium (THF). Complex **(3)** was then treated with few drops of water in an aerial atmosphere and complex **(8)** formed, proving the reproducibility of the reaction. The ^{31}P NMR confirms the formation of **(8)**. Following the same pattern, complex $[Cu_4(\mu_3\text{-}I)_2(\mu_2\text{-}I)_2(O\{P[CH(CH_3)_2]_2\}_2)_2]$ **(9)** was prepared from complex **(6.1)**, see Scheme 4.1.2.4. The complexes were obtained in good yield, i.e. 68-82%.

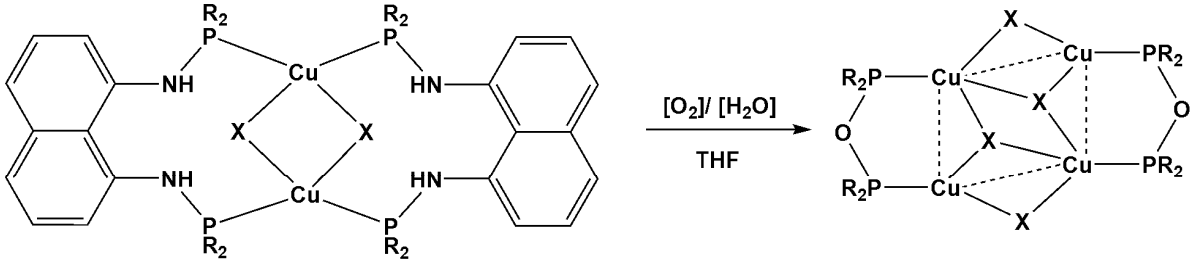

R = Ph, X = Cl (3)
R = $[(CH_3)_2CH]_2$, X = I (6.1)

R = Ph, X = Cl (8)
R = $[(CH_3)_2CH]_2$, X = I (9)

Scheme 4.1.2.4. Reaction of Cu-P-O-P complexes as a result of oxidation addition.

4.1.2.6 Characterisation: Spectroscopic Analysis ^1H, ^{13}C, and ^{31}P NMR

The phenyl-H atoms in the ^1H NMR of **(8)** were easily identified. The ^1H NMR for **(8)** integrated to a total of 40H (all phenyl) and complex **(9)** integrated to 56H (all iso-propyl). The ^{31}P NMR shows that the P atoms are chemically equivalent in solution and hence the peaks

resonate as singlets. Complexes **(8)** and **(9)** showed singlets at 34.6 and 62.5 ppm, respectively. The ^{31}P NMR of the P-O-P complexes resonate in those regions of the spectra as reported in litereature[43, 44]

4.1.2.7 Ligation Oxidative Addition and the Formation of P-O-P Bonds from P-N Bonds

Naktode *et al*.,[43] reported similar reactions to that prepared here in the P-O-P work. They treated a tetrameric Cu(I) complex with dichloromethane and water in 10:1 molar ratio for 12 hours to yield a P-O-P complex. Simulating their reaction, but in "wet THF" gave an oxidative addition product of the complexes **(3)** and **(6.1)**. The bulk purities of complexes were satisfactory as determined by mass spectrometry. A mechanism was proposed which favours the formation of **(8)** and **(9)**, it suggested that water solvent provided a nucleophilic attack on a P-atom of the phosphine which resulted in hydrolytic cleavage of the P-N bond. Water is an amphiprotic molecule and these P-N bonds are sensitive to trace amounts of acid/base contaminations, as also observed by Balakrishna.[45] Cleaving the P-N bonds **(3)** and **(6.1)** by water produces intermediate compounds. The OH moiety performed a second nucleophilic attack on the adjacent P-atom which breaks the P-N bond to form P-O-P bonds. This process eliminate the free *1,8*-diaminonaphthalene and isolate complexes **(8)** and **(9)**. It is possible, as indicated by Newton[46] and Burrows,[47] that during complexation reactions with metal salts, the P-N bonds can undergo cleavage. The cleavage in this case has resulted in a tetra-nuclear Cu(I) complex **(8)** and **(9)** which are demonstrative in Scheme 4.1.2.5.

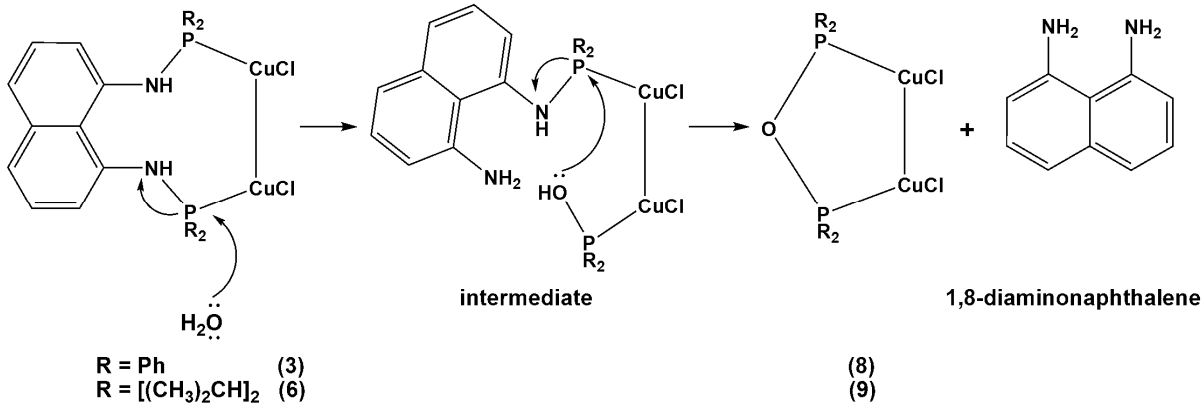

Scheme 4.1.2.5. A proposed mechanism towards the formation of **(8)** and **(9)**.

4.1.2.8 Molecular Structures of Copper P-O-P Complexes

The X-ray structures of the two representative complexes **(8)** and **(9)** were obtained and described herein. Single crystal X-ray structure data were obtained to determine the molecular structures of complexes **(8)** and **(9)**. Figure 4.1.2.14-15 shows the molecular structures of complexes **(8)** and **(9)** at different temperatures, see Table 4.1.2.13. The quality single X-ray crystals of **(8)** and **(9)** were obtained by slow diffusion of dichloromethane: hexane (50:50).

Table 4.1.2.13. Crystallographic data for **(8)** and **(9)**.

	8	**9**
Formula	$C_{48}H_{40}Cl_4Cu_4O_2P_4$	$C_{24}H_{56}I_4Cu_4O_2P_4$
M_r	1168.64	1261.37
Space group	$P2_1/n$	$P2_1/n$
a, Å	10.7203(5)	11.6641(3)
b, Å	16.1291(8)	13.6810(4)
c, Å	13.452(7)	12.7737(4)
α, deg	90	90
β, deg	95.068(17)	99.0470(10)
γ, deg	90	90
V, Å^3	2316.9(2)	2013(10)
Z	4	2
ρcalcd, g cm^{-3}	1.675	2.083
M, mm^{-1}	2.220	5.331
T, K	100(2)	100(2)
Reflections collected	30962	16563
Independent reflections	5724	4981
R_{int}	0.0341	0.0246
Final *R* indices [I > 2σ(*I*)][a]	*R*1 = 0.0280 w*R*2 = 0.0611	*R*1 = 0.0192, w*R*2 = 0.0433
R indices (all data)	*R*1 = 0.0388 w*R*2 = 0.0649	*R*1 = 0.0228 wR2 = 0.0450
Largest diff. peak and hole, e / Å	0.437 and -0.376	0.479 and -0.670

[a] $R1 = \Sigma \mid\mid F_o \mid - \mid F_c \mid\mid / \Sigma \mid F_o \mid$. [b] $wR2 = \{\Sigma [w(F_o^2 - F_c^2)^2] / \Sigma [w(F_o^2)^2]\}^{1/2}$

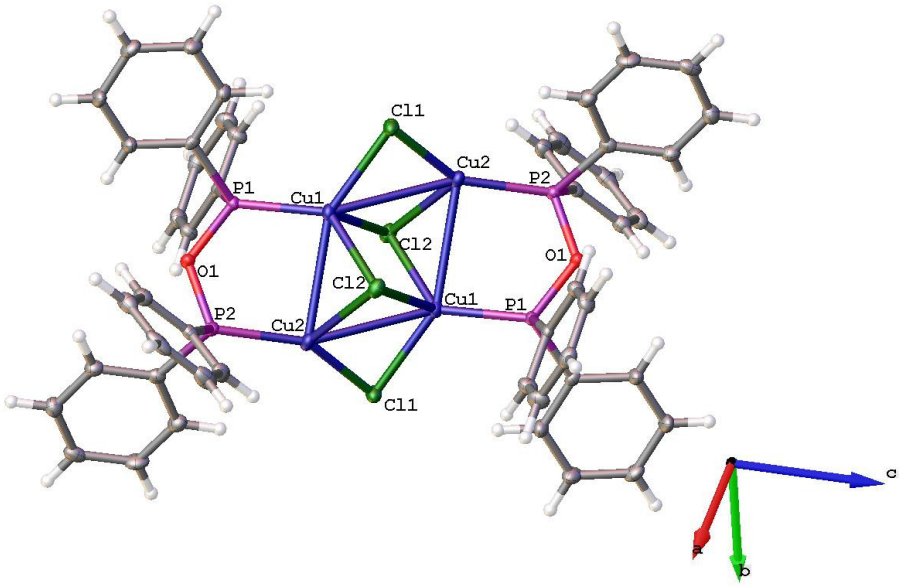

Figure 4.1.2.14. Molecular structure of **(8)** drawn at 50% probability with OLEX2.

Table 4.1.2.14. Selected bond distances (Å) and angles (deg) for **8** with esd's in parentheses.

Compound **8**			
O(1)–P(2)	1.6439(13)	O(1)–P(1)	1.6503(13)
P(1)–Cu(1)	2.1751(5)	P(2)–Cu(2i)	2.1639(5)
Cl(1)–Cu(2)	2.2363(5)	Cl(1)–Cu(1)	2.3694(5)
Cu(2)–Cu(1i)	2.3563(5)	Cl(1)–Cu(2i)	2.3563(5)
Cu(1)–Cu(2)	3.0108(3)	Cu(2)–P(2i)	2.1639(5)
Cu(2)–Cu(1i)	2.8953(3)	P(2)–O(1)–P(1)	123.71(8)
O(1)–P(1)–Cu(1)	118.58(5)	O(3)–P(1)–Cu(1)	114.56(6)
O(1)–P(2)–Cu(2i)	113.01(5)	Cu(2)–Cl(1)–Cu(1)	81.588(17)
Cu(1i)–Cl(2)–Cu(2)	75.606(16)	Cu(2)–Cl(2)–Cu(1)	75.471(15)
P(1)–Cu(1)–Cl(2i)	128.16(2)	P(1)–Cu(1)–Cl(1)	122.230(19)
Cl(2i)–Cu(1)–Cl(1)	101.187(18)	P(1)–Cu(1)–Cl(2)	109.214(19)
Cl(1)–Cu(2)–Cl(2)	99.390(19)		

Symmetry transformations used to generate equivalent atoms: #1 -x,-y,-z.

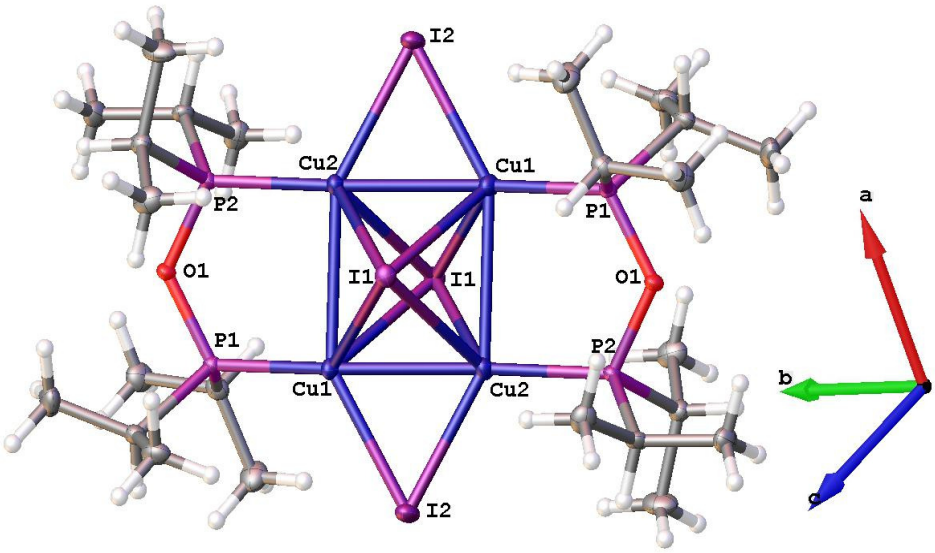

Figure 4.1.2.15. Molecular structure of **(9)** drawn at 50% probability with OLEX2.

Table 4.1.2.15. Selected bond distances (Å) and angles (deg) for **9** with esd's in parentheses.

Compound **9**			
O(1)–P(2)	1.6494(16)	P(1)–Cu(1)	2.2073(6)
P(2)–Cu(2)	2.1988(10)	Cu(1)–Cu(2i)	2.5736(4)
Cu(1)–I(2i)	2.6212(3)	Cu(1)–Cu(2)	2.8816(4)
Cu(1)–I(1)	2.9434(4)	Cu(2)–Cu(1i)	2.5736(4)
Cu(2)–I(1)–Cu(1)	59.341(9)	Cu(2i)–I(1)–Cu(1)	54.120(9)
Cu(2i)–I(1)–Cu(2)	86.286(10)	I(1)–Cu(2)–Cu(1)	61.479(10)
I(2)–Cu(2)–I(1)	98.417(11)	Cu(2)–Cu(1)–I(1)	92.179(10)
I(2i)–Cu(1)–I(1)	101.514(11)	P(2)–O(1)–P(1)	124.79(10)
O(1)–P(1)–Cu(1)	116.61(6)		

Symmetry transformations used to generate equivalent atoms: #1 -x+1,-y,-z+2 where (i = #1).

In complexes **(8)** and **(9)**, the P-O-P moieties of the ligand $[(O\{PPh_2\}_2)]$ and $[(O\{P[CH(CH_3)_2]_2\}_2)]$ was bound to four of the Cu atoms of the complex in a manner that bridges the Cu_4 core. The two Cu atoms are coordinated in a tetrahedral geometry. The two Cu atoms are 4-coordinate with the three chlorides and one P-donor atom from the ligand in **(8)**.

The same coordination characteristics are observed in **(9)** with iodides. The molecular structures of **(8)** and **(9)** are located on the center of symmetry and they have a tetrahedral and trigonal planar geometry, respectively. The complexes are isostructural (monoclinic, same space group), but have significantly different cell dimensions. Complexes **(8)** and **(9)** have four and two molecules in one unit cell, respectively.

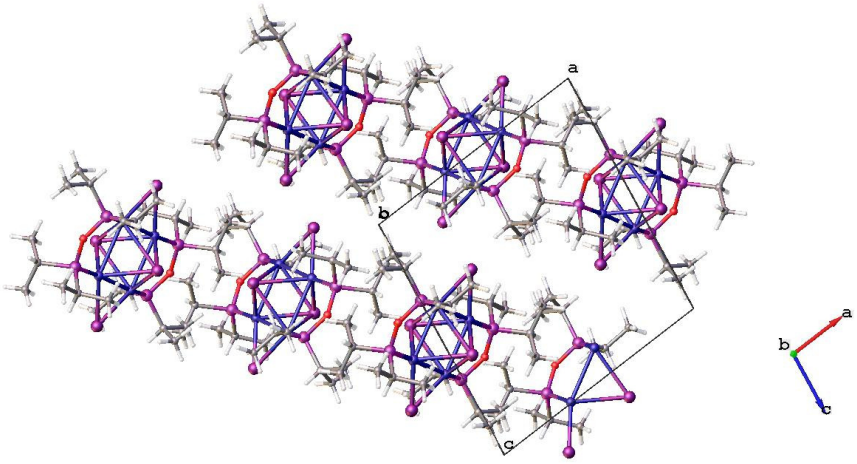

Figure 4.1.2.16. Crystal structure and molecular packing of **(9)**.

Figure 4.1.2.16 shows the molecular packing of **(9)** which is a complicated molecular packing with the metal center showing a clustered core. The complexes **(8)** and **(9)** were characterized by intramolecular hydrogen bonding with no intermolecular interactions. The molecules arranged themselves in a parallel fashion to each other.

Table 4.1.2.16. Selected bond distances (Å) and angles (deg) of complexes **8**-**9** for discussion.

Distances (Å) and Angles (°)	**8 (X = Cl)**	**9 (X = I)**
Distances (Å)		
Cu···Cu	3.01 and 3.30	2.57 and 2.88
Cu-·P	2.26	2.20
Cu-X	2.40-2.43	2.62-291
Angles (°)		
Cu-X-Cu	93.97	54.12-164.66
X-Cu-X	89.60	98.42
P-Cu-P	141.56	-
X-Cu-P	96.79-110.57	103.75-120.67

Table 4.1.2.14-15 and Table 4.1.2.16 list bond distances and angles of both complexes **(8)** and **(9)**, where the P-O bond distance for complex **(8)** is around 1.65 (13) Å and that of **(9)** is 1.69(16) Å, see above. The bond length for P-Cu is 2.26(5) Å for **(8)** and 2.20(6) Å for **(9)**. There is a large difference in the bond distances of Cu-halides. Complex **(8)** Cu-Cl are in the range ~2.40-2.43 Å. The range result from two different coordination geometry possessed by the halides around the Cu center. In complex **(9)** the Cu-I bond lengths are in the range ~ 2.6-2.9 Å. The bond lengths and angles agree with those reported.[44]

4.1.2.9 Synthesis of Complexes from the Ligands of the Type $[C_{10}H_6(NHPPh_2E)_2]$

Scheme 4.1.2.6 shows the synthesis method followed for complexes **(17)** and **(19)** of the type $[Ag\{C_{10}H_6(1,8\text{-}NHPPh_2E)_2\}_2]CF_3SO_3$ where E = S **(17)** and E = O **(19)**. The reaction of compound **(15)** with $AgCF_3SO_3$ in (1:1) molar equivalence resulted in the homoleptic complex **(17)** with a yield of 41%. Complex **(19)** was prepared similar to **(17)** starting from **(14)** in 39% yield.

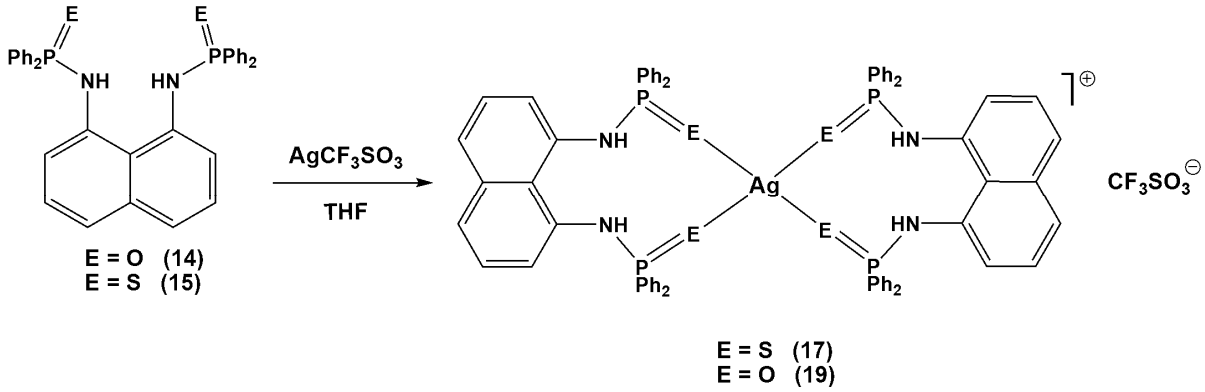

Scheme 4.1.2.6. The synthesis of **(17)** and **(19)** using silver triflate.

In an attempt to prepare different anion derivatives of complex **(17)** using AgX {X = BF_4, ClO_4, CF_3COO and PF_6} salts in THF, complex $[Ag_2(\mu\text{-}S)_2\{C_{10}H_6(1,8\text{-}NHPPh_2S)\}_2]$ **(18)** was formed from all the silver salts. In the crystal growth of complex **(18)** derivatives in dimethylformamide, yellow crystals were obtained. The reactions of AgX with ligand **(15)** generates HX acids and form an off-white to light brown stable precipitate of complex **(18)** in 52% yield. The abstraction of the anime proton by an anion X^- resulted in a delocalization of

the electrons from N-P-S bonds. This is evident from the shorter P=S bond which is 1.98 Å and the delocalized P-S bond which is 2.02 Å.

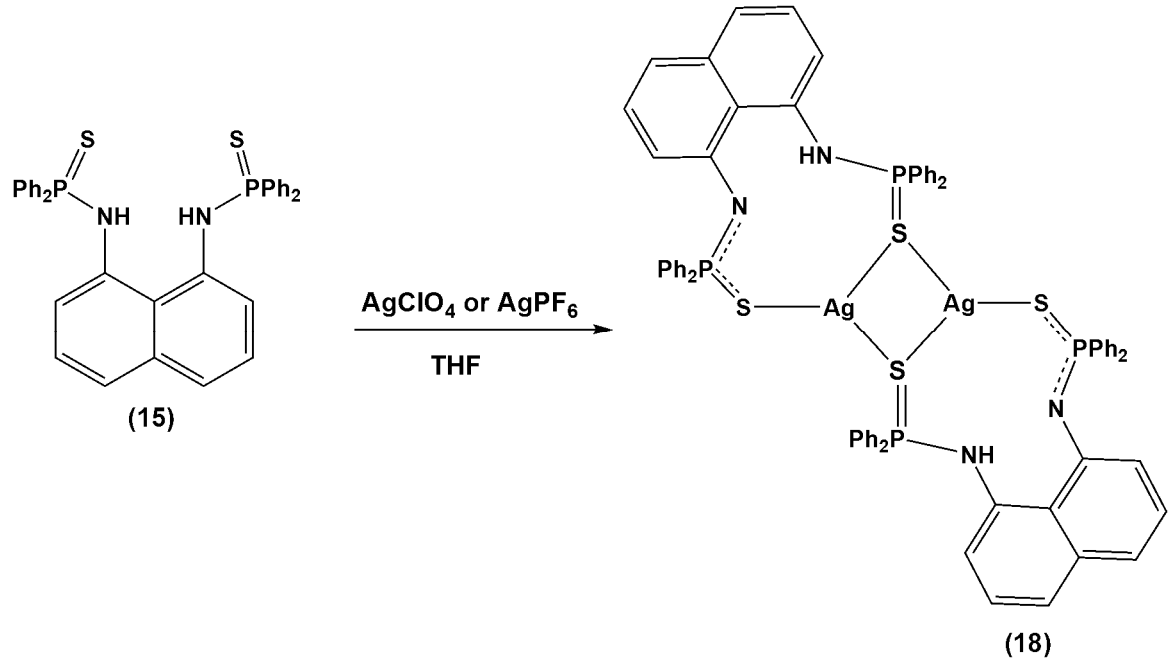

Scheme 4.1.2.7. Synthesis of **(15)** using $AgClO_4$ and $AgPF_6$.

When ligand **(15)** is treated with Cu-halides under reflux for 12 hours in chloroform, mononuclear complexes **(20)**-**(22)** of the type $[Cu\{C_{10}H_6(1,8\text{-}NHPPh_2O)_2\}_2\{X\}]$ where X = Cl, Br and I were produced. The percentage yields of the complexes range from 54-73%.

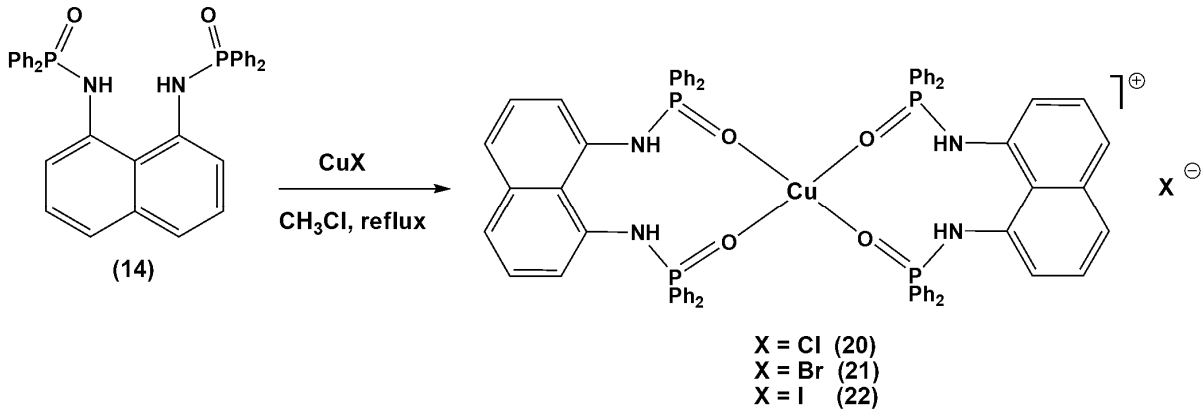

Scheme 4.1.2.8. A synthetic scheme for complexes **(20)-(22)** using copper halides.

The formation of the complexes was confirmed *via* solution and solid state spectroscopy, i.e. ^{1}H NMR and FTIR. The bulk purity analysis of the complexes was by mass spectrometer, see Chapter 2.

4.1.2.10 Characterisation: ^{1}H, ^{13}C, ^{31}P NMR and IR

The ^{1}H NMR for complex **(17)** showed resonating peaks at 9.42-6.65 ppm which are attributed to the protons of the phenyl-H and naphthalene. The position of the protons in the phenyl-H and naphthalene-H moieties are in the same chemical shift with the protons for **(3)**-**(5)** and **(10)**-**(12)**. The ^{31}P NMR indicated that the P-donor atoms are in the same chemical environment in solution and hence a singlet was observed at 58.3 ppm for **(17)**, see experimental section for ^{1}H, ^{31}P and ^{13}C NMR of the complexes **(19)**-**(21)**. The ^{31}P peak for **(17)** is a singlet and it supports the position of the P donor atoms of the proposed structure, see Figure 4.1.2.17.

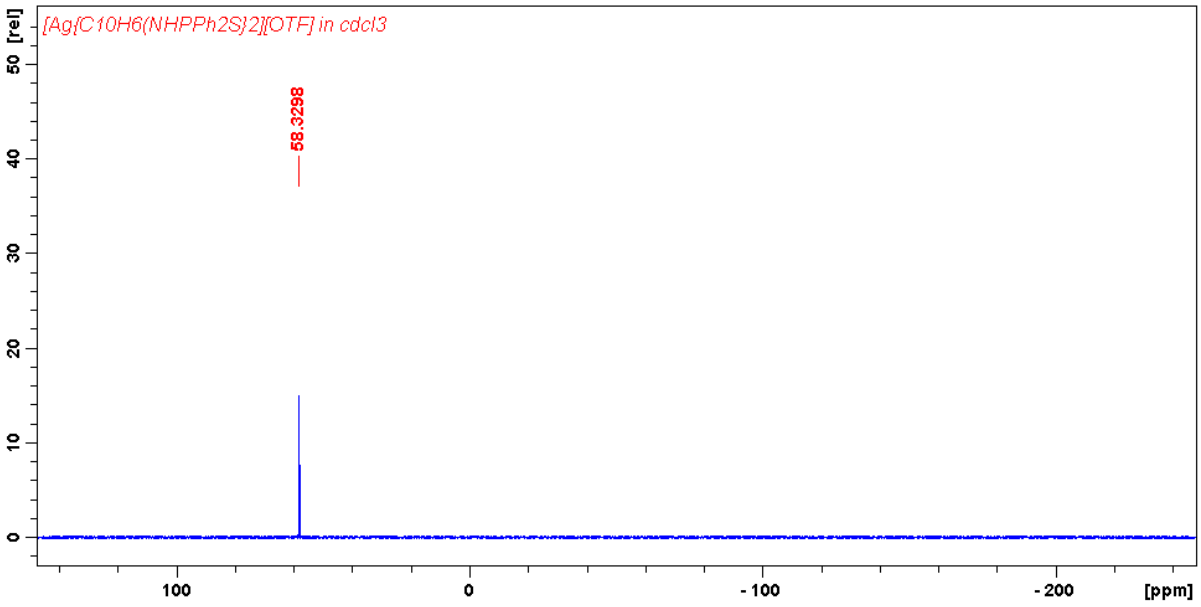

Figure 4.1.2.17. ^{31}P NMR spectrum of **(17)**.

For the ^{1}H NMR spectrum of complex **(18)**, the proton peaks for naphthalene and phenyl-H are shifted downfield in a region of 6.64-7.83 ppm. The ^{31}P NMR of complex **(18)** showed two peaks at 69.4 and 58.5 ppm. The ^{31}P NMR spectrum for complex **(18)** showed an observable chemical shift in the P atoms attached to the non-bridging S-atoms compared to the bridging S-donor atoms attached to the P-atoms. The P-donor atoms attached to the bridging S-donor

atoms are chemically shifted upfield at 69.4 ppm, whereas the P donor atoms attached to the S donor atoms which do not bridge the Ag species, resonates at 58.5 ppm. The non-bridging P=S unit has a similar value compared to compound **(15)** at 57.1-57.9 ppm. Integration of the spectrum support the formation of complex **(18)**. The amine protons in the ^{1}H NMR for ligands are overlapping in the aromatic region. The protons of **(18)** are defined in the region of 9.02-9.42 ppm, see appendix. Complex **(20)** have a similar spectrum to that of ligand **(14)**. Complex **(20)** was prepared from ligand **(14)**. The ^{1}H NMR spectra for complexes **(21)**-**(22)** showed broadened peaks. The EPR spectra for complexes **(21)**-**(22)** was determined to examine the broad peaks, see Figure 4.1.2.27. In FT-IR spectra of compound **(1)**, the ν(P=O) band stretches at 1282-1177 cm^{-1}, ν(PN) at 894, 721 cm^{-1}, ν(NH) at 3053 cm^{-1} and phenyl-H and naphthalene ν(C=C) were seen vibrating in the range 1581-1421 cm^{-1}. In complex **(17)**, the ν(NH) frequencies are observed resonating at 3057 cm^{-1}, ν(P=S) at 687 cm^{-1}, ν(PN) at 817, 752-723 cm^{-1} and naphthalene and phenyl-H at ν = 1574-1414 cm^{-1}. The chemical frequencies of complex **(18)** for ν(NH) are at 3200 cm^{-1}, ν(PN) at 860, 746 cm^{-1}, ν(P=S) at 619-598 cm^{-1} and aromatic ν(C=C) is at 1650-1414 cm^{-1}. The IR spectrum of **(19)** show vibrational peaks of ν(NH) at 3077 cm^{-1}, ν(PN) at 754-726 cm^{-1}, ν(P=O) at 690 cm^{-1} and the aromatic ν(C=C) at 1587 cm^{-1}. The FT-IR for complexes **(20)**-**(22)** for the band stretches of ν(NH), ν(PN), ν(P=O) and the aromatic ν(C=C) are in the range 3053-3054 cm^{-1}, 985-822 cm^{-1}, 691-690 cm^{-1} and 1646-1581 cm^{-1}, respectively. These IR show a vibrational shift compared to the IR of ligands **(14)** and **(15)**. The most important peaks due to ν(Cu-O) for **(20)**-**(22)** lie in the region, 519-410 cm^{-1}. The peaks due to ν(Ag-O) for **(19)** at 540-518 cm^{-1} and ν(Ag-S) for **(17)** at 514-500 cm^{-1} also reveals the presence of coordinated metal to O/ S-donor atoms in all these complexes. The detailed NMR are outlined in the experimental sections. All these values are similar to those observed in the literature.[48]

4.1.2.11 Molecular Structures of Type [Ag{$C_{10}H_6$(1,8-NHPPh_2E)$_2$}$_2${CF_3SO_3}] (17) and [Ag_2(μ-S)$_2${$C_{10}H_6$(1,8-NHPPh_2S)}$_2$] (18)

The molecular structures of complexes **(17)** and **(18)** are shown in Figure 4.1.2.18-19 and the selected bond lengths and angles are shown in Table 4.1.2.18-19. The single crystal X-ray structures unambiguously confirms the formation of a mononuclear complex **(17)** and a binuclear complex **(18)**. Good quality single crystals for complex **(17)** were obtained by slow diffusion of dichloromethane: hexane solution whereas, those of complex **(18)** were obtained *via* slow evaporation in dimethylformamide solvent.

Table 4.1.2.17. Crystallographic data for **(17)** and **(18)**.

	17	**18**
Formula	$C_{71}H_{60}AgCl_4F_3N_4O_3P_4S_5$	$C_{68}H_{52}Ag_2N_4P_4S_2$
M_r	1608.08	1393.00
Space group	*P*c	*P*-1
a, Å	11.0891(11)	11.1195(16)
b, Å	11.4790(11)	12.8067(19)
c, Å	28.103(3)	13.0373(19)
α, deg	90	61.868(2)
β, deg	91.0500(10)	65.197(2)
γ, deg	90	77.641(2)
V, Å^3	3576(6)	1485.9(4)
Z	2	1
ρcalcd, g cm^{-3}	1.493	1.557
M, mm^{-1}	0.724	0.954
T, K	173(2)	173(2)
Reflections collected	28970	15277
Independent reflections	12981	5417
R_{int}	0.0381	0.0514
Final *R* indices [I > 2σ(*I*)][a]	*R*1 = 0.0435, w*R*2 = 0.0935	*R*1 = 0.0488, w*R*2 = 0.01079
R indices (all data)	*R*1 = 0.0545 wR2 = 0.0999	*R*1 = 0.0863 w*R*2 = 0.1275
Largest diff. peak and hole, e / Å	0.921 and -0.894	0.903 and -0.375

[a] $R1 = \Sigma \mid\mid F_o \mid - \mid F_c \mid\mid / \Sigma \mid F_o \mid$. [b] $wR2 = \{\Sigma [w(F_o^2 - F_c^2)^2] / \Sigma [w(F_o^2)^2]\}^{1/2}$

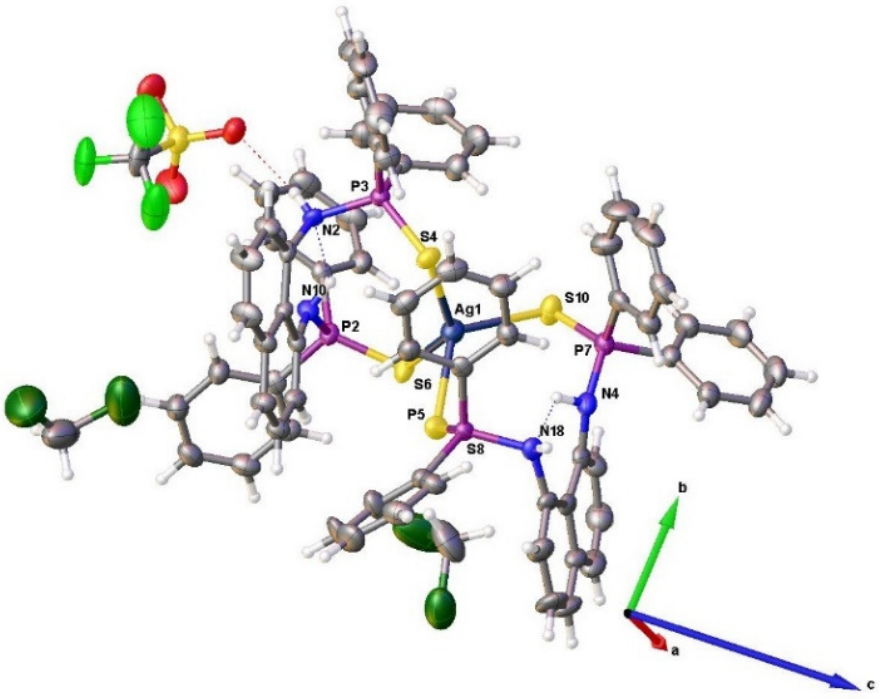

Figure 4.1.2.18. Molecular structure of **(17)** drawn at 50% probability with OLEX2.

Table 4.1.2.18. Selected bond distances (Å) and angles (deg) for **17** with esd's in parentheses.

Compound **17**			
Ag(1)–S(4)	2.5514(18)	Ag(1)–S(6)	2.6041(18)
Ag(1)–S(8)	2.6406(18)	Ag(1)–S(10)	2.619(2)
P(2)–S(6)	1.967(2)	P(2)–N(10)	1.653(5)
P(3)–S(4)	1.952(2)	P(3)–N(2)	1.686(6)
P(5)–S(8)	1.957(2)	P(7)–S(10)	1.974(3)
P(7)–N(4)	1.657(6)		
P(7)–S(10)–Ag(1)	103.67(9)	S(4)–Ag(1)–S(6)	134.96(6)
S(4)–Ag(1)–S(8)	103.65(6)	S(4)–Ag(1)–S(10)	110.36(6)
S(6)–Ag(1)–S(8)	92.20(6)	S(6)–Ag(1)–S(6)	119.55(6)
N(10)–P(2)–S(6)	117.6(2)	N(2)–P(3)–S(4)	112.9(2)
P(3)–S(4)–Ag(1)	115.92(9)	N(8)–P(5)–S(8)	111.6(2)
N(4)–P(7)–S(10)	118.3(2)	P(2)–S(6)–Ag(1)	102.92(8)

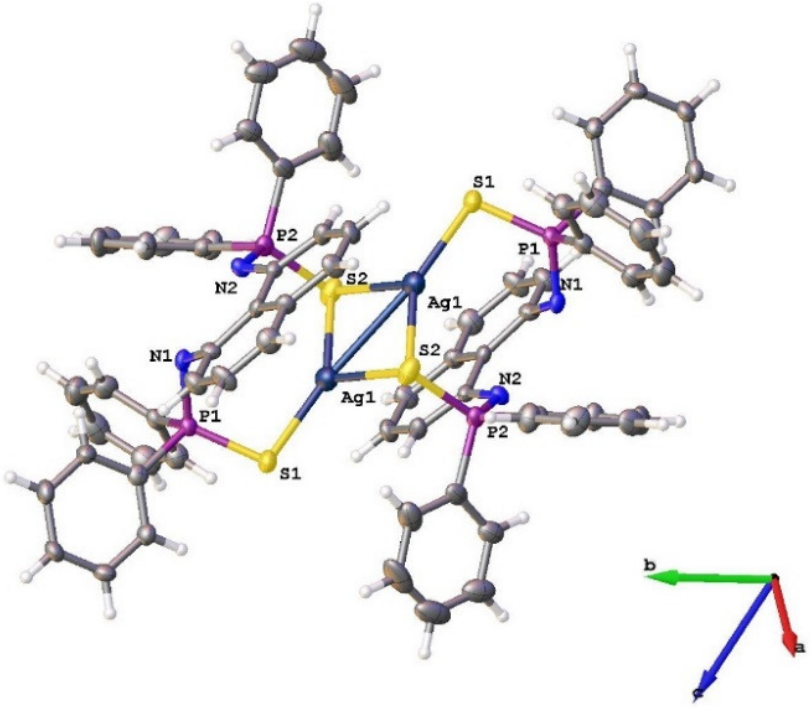

Figure 4.1.2.19. Molecular structure of **(17)** drawn at 50% probability with OLEX2.

Table 4.1.2.19. Selected bond distances (Å) and angles (deg) for **18** with esd's in parentheses.

Compound **18**			
Ag(1)–S(1)	2.4839(13)	Ag(1)–S(2)	2.5223(14)
Ag(1)–S(2ii)	2.7517(14)	Ag(1)–Ag(1ii)	3.0013(9)
N(1)–P(1)	1.668(4)	N(2)–P(2)	1.604(4)
P(1)–S(1)	1.9865(16)	P(2)–S(2)	2.0228(10)
S(2)–Ag(1ii)	2.7517(14)		
S(1)–Ag(1)–S(2)	146.99(5)	S(1)–Ag(1)–S(2ii)	100.21(5)
S(2)–Ag(1)–S(2ii)	110.79(4)	S(1)–Ag(1)–Ag(1)	150.15(4)
S(2)–Ag(1)–Ag(1ii)	59.00(3)	S(2)–Ag(1)–Ag(1ii)	51.79(3)
P(1)–S(1)–Ag(1)	100.92(6)	P(2)–S(2)–Ag(1)	98.38(6)
P(2)–S(2)–Ag(1ii)	101.70(6)	Ag(1)–S(2)–Ag(1ii)	69.21(4)

Symmetry transformations used to generate equivalent atoms: #1 -x+2,-y+1,-z+.

Complexes **(17)** and **(18)** crystallized in two different space group, monoclinic Pc and triclinic P-1, respectively. Complex **(17)** have a centrosymmetric at Ag whereas complex **(18)** have a centrosymmetric center of inversion coinciding with the midpoint of the Ag···Ag vector.

A brief description of the molecular structures of complexes **(17)** and **(18)** is given herein. Homoleptic complex **(17)** consist of two molecules in the unit cell with two dichloromethane solvates filling the voids between the closely packed molecular complexes. The complex is counter balanced by one triflate ion in the counter coordination sphere. Complex **(17)** is mononuclear and the two S-atoms of ligand **(15)** chelate to the Ag ion *via* a coordinative dative bond in a bridging fashion causing the Ag(I) center to have a tetrahedral coordination geometry. The bond distances of Ag-S are in the range 2.6401(18)-2.551(18) Å for **(17)**. The bond angles of S-Ag-S are in the range 92.20(6)-134.96(6)° for **(17)**. These are in agreement with literature values.[49-51]. The distance between the *peri*-N atoms of the complex **(17)** is 2.779 Å. This is slightly smaller than that of compound **(15)** which is 2.926 Å, presumably due to Ag(I) centers drawing the S-atoms of the molecule closer. This forces the ring of the naphthalene to move

out of the plane and therefore twisting the *peri*-N atoms closer to each other. Therefore, the non-bonding distances becomes smaller than that of the free ligand **(15)**. The molecular structure of complex **(17)** is stabilized by intermolecular π-interaction of both the adjacent triflate molecule and the H atoms of the adjacent molecular structure. Complex **(18)** is binuclear having ligand **(15)** bridging the Ag(I) center *via* the S-atoms in $\{Ag_2(\mu\text{-}S)_2\}$ core rhombus of the structural unit. It contains two molecules in the crystallographic unit cell, see Table 4.1.2.17. The other S-atoms is monodentate and coordinated to the Ag(I) center causing both silver(I) centers to have a trigonal planar geometry.

Table 4.1.2.20. Selected bond distances (Å) and angles (deg) of complexes **15-18** for discussion.

Distances (Å) and Angles (°)	**15**	**16**	**17**	**18**
Distances (Å)				
Ag···Ag	-	-	-	3.00
Ag-S	-	-	2.55-2.66	2.48 and 2.75
P=S	1.96	-	1.96	1.98-1.99 and 2..02
P-S	-	-	-	2.75 (delocalized)
P=O	-	1.49	-	-
P=Se	-	2.10	-	-
Angles (°)				
Ag-S-Ag	-	-	-	69.21
S-Ag-S	-	-	92.20-134.96	110.79-146.99

For the bond lengths and bond angles discussion that follows, see Table 4.1.2.20. The two Ag metal centers bridged by two S-atoms at a distance of 2.5223(14)-2.7517(14) Å confirms that $\{Ag_2(\mu\text{-}S)_2\}$ core unit forms a parallelogram for complex **(18)**. The non-bridging Ag-S bonds are 2.4839(15) Å. Complex **(18)** have a Ag···Ag interaction at a distance of 3.001 Å. The *peri*-non-bonding N atoms distance of complex **(18)** are 2.647 Å and are relatively smaller than that of compounds **(15)** and **(17)**. Comparable values were found in the complexes $[Ag_2(\mu\text{-}Br)_2(\kappa^1\text{-}S\text{-}Httsc\text{-}NMe)_2(Ph_3P)_2]$[52] and $[Ag\{\kappa^2(S,S')\text{-}(CH_2)_n[P\{=NP(=S)(OEt)_2\}Ph_2]_2\}][SbF_6]$[53], n= 1 in the literature. Surprisingly, weaker Ag···Ag distances was 3.138(2) Å and this is longer than seen in complex **(18)**. The bond angles around each Ag(I) centered core varies and were in the range 69.21-110.79°. The bond angle of S-Ag-S around the terminal edges of the molecule are in the range 100.21-146.99° which varies slightly to those reported in the literature.[53, 54]. The

molecular packing of complex **(18)** shows that the structures are held together by Ag-S interaction, interacting with the H-atoms of the adjacent naphthalene ring leading to a dimeric centrosymmetric molecular structure which is observed in the solid-state crystal analysis. The bond length and angles are listed in Table 4.1.2.18 and Table 4.1.2.20. The molecule arranges itself in a unique "zig-zag" fashion with the core centers lying planar.

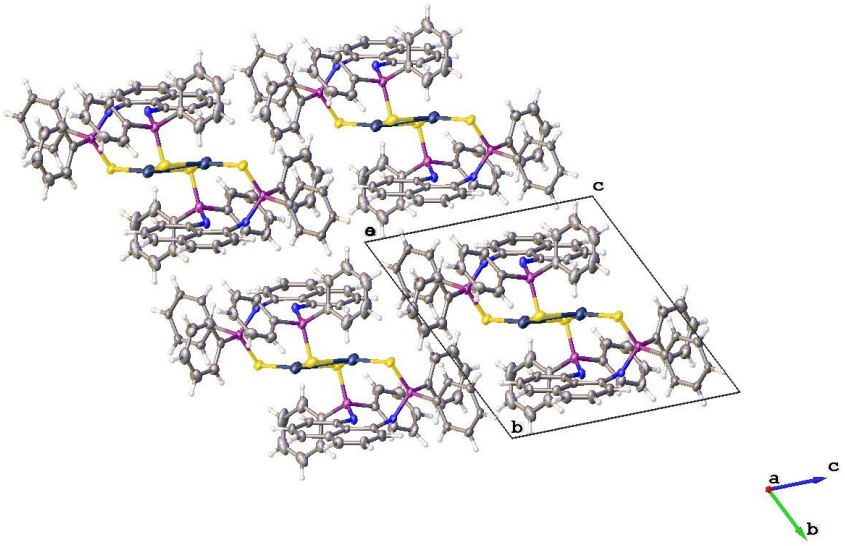

Figure 4.1.2.20. Molecular packing of **(18)**.

4.1.2.12 UV-Vis Spectroscopic Analysis of Complexes

UV-Vis spectroscopy of complexes (**3**)-(**5**) and (**7**)-(**8**) are shown in Figure 4.1.2.21 which shows the longest wavelength absorption band at ~230 nm close to 380 nm. These are due to π-π* transition which arises from the naphthalene moiety. Variation of halides on the Cu ions do not show any influence in the alteration of the wavelength absorption. The spectra in Figure 4.1.2.21 shows that complexes are blue shifted. The domination of the red shifted absorption band is not observed in these complexes. Hence, the absence of the red shifted bands does not influence any change in the emission. The molar extinction coefficient at λ_{max} for the complexes are reported in Table 4.1.2.21.

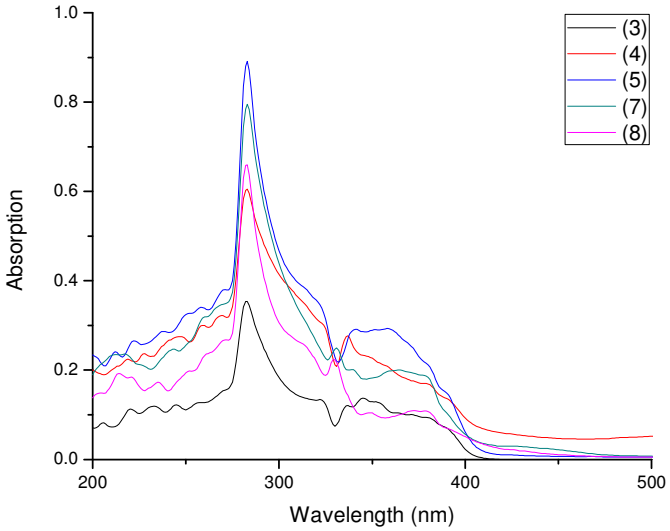

Figure 4.1.2.21. Typical UV–vis absorption spectra of complexes **(3)-5** and **(7)-(8)**.

Note that a study on possible luminescence behaviour of complexes (**3**)-(**5**) and (**8**) were conducted in both solid state and liquid (solution) at the maximum wavelength absorption of ~230 and ~386nm. Complex **(6)** and **(9)** UV-Vis emission was insignificant as the complexes contain sigma bonds (σ) diisopropylphosphine which act like normal alkanes. The amount of energy required to excite the electrons in the σ-bonds is high wavelength in the UV-Vis. When the complexes were excited at these wavelengths, no luminescence for the complexes were observed. In principle, fluorescence quenching occurs in the solid state due to the close packing which then result in energy transfer and reabsorption of fluorescence.[55-57] As stated by van de Weert,[58] addition of a compound to a solution containing fluorescent macromolecule may alter its emission through different mechanisms.

Table 4.1.2.21 shows molar extinction coefficient of **(3)**-**(5)** and **(7)**-**(8)**. Complexes **(6)** and **(9)** molar extinction could not be calculated because the complexes showed no emission, presumably due to the σ-bonds only. The molar extinction coefficient of **(3)**-**(5)** and **(7)**-**(8)** are in the range 8357-19097 $M^{-1}cm^{-1}$ which were assigned to the intraligand L→L* transitions.

Table 4.1.2.21. Molar extinction coefficient data of compounds **(3)-(9)**.

Compounds	λ_{abs}[a] (nm)	ε_{max}[b] ($M^{-1}cm^{-1}$)
3	283	8357
4	283	15047
5	283	14593
6	-	-
7	283	19097
8	284	15344
9	-	-

[a] Longest wavelength absorption maximum recorded in dichloromethane [b] Molar extinction coefficient at the longest wavelength absorption maximum. These were calculated at 4.006 $x10^{-5}$M.

The experimental UV-Vis absorption for complexes (**10**)-(**13**) spectra are presented in Figure 4.1.2.22. Although the experimental spectra for the complexes are similar, it is noteworthy that the ratio for the absorption intensity in the visible region for the complexes having the same concentration are different by only a very small margin. The maximum wavelength for all the complexes was observed at ~235 and ~350 nm. The absorption at this wavelength are attributed to π···π* transition of the naphthalene. The absorption of the *d-d* transition band are caused by the energy and electron transfer processes between the P- and N-donor atom as noted; P-donor atoms either act as electron pulling from the Ag(I) center and electron donation for the N-donor atoms.

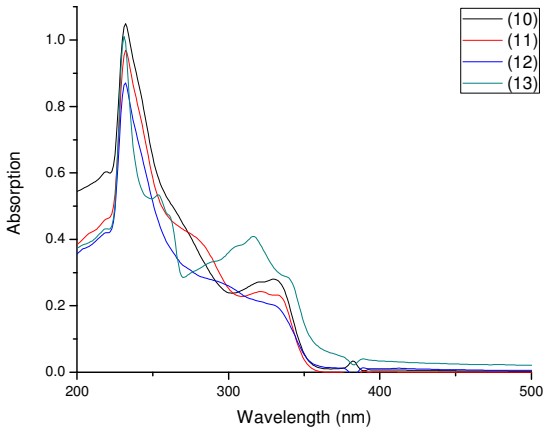

Figure 4.1.2.22. Representative UV–vis absorption spectra for complexes **(10)-(13)** in chloroform.

Similar to the Cu(I) complexes, the Ag(I) complexes do not show any luminescence properties either in solid state or solution. This might be caused by energy transfer and reabsorption of fluorescence and therefore causes luminescent quenching. The molecular structures of **(10)**-**(13)** also exhibits an inductive-resonance effect. The negative inductive effect various from one halogen to another in the following sequence: Cl > Br > I.

Table 4.1.2.22. The molar extinction coefficient data of compounds (**10)-(13)**.

Compounds	λ_{abs}[a] (nm)	ε_{max}[d] ($M^{-1}cm^{-1}$)
10	235, 325	2144, 839
11	235, 325	2749, 456
12	235, 325	2434, 727
13	235, 322	2069, 840

[a] Longest wavelength absorption maximum recorded in dichloromethane. The calculations are performed at a concentration of $3.723x10^{-4}$ M.

Table 4.1.2.22, shows the molar absorptivity of the compounds and this demonstrates the intrinsic property of the compounds to absorb visible light. The value is large and this means the electronic transition of the compounds is effective.

The electronic UV-Vis spectra for compounds **(17)**-**(22)** and their molar absorptivity coefficient are shown in Figure 4.1.2.23 and Table 4.1.2.23, respectively. The solution behaviour of all the compounds were performed in dry chloroform. Complexes **(17)**-**(22)** also exhibits a small band at ~474 nm attributed to MLCT. For the two prominent absorption bands in the spectra of complexes **(17)**-**(22)** which are assigned to the intraligand L→L* transitions, the first band is slightly shifted upon coordination only in complexes by 11 nm to the left (to 216 nm), while the second band are also blue shifted by 53 nm. For complexes these intraligand L→L* transitions are almost superimposable.

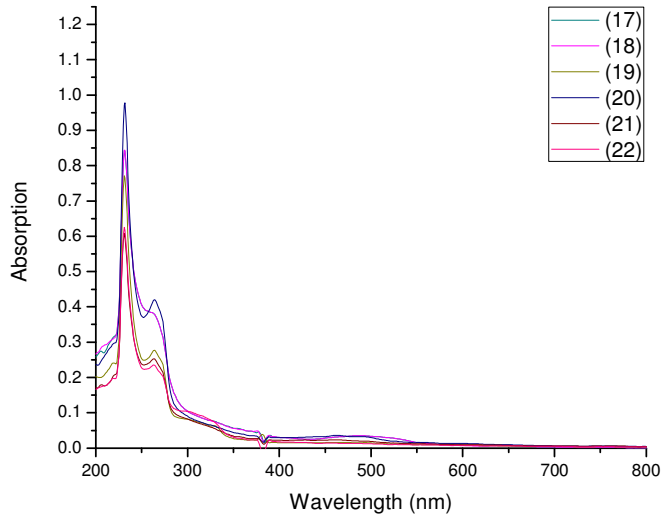

Figure 4.1.2.23. UV-Vis spectra of compounds **(17)**-**(22)**.

Concerning the molar extinction coefficient of complexes it is seen that the Cu(I) (oxygen) oxidized aminophosphines absorbs lower than those containing Ag(I). Where sulfur is used as an oxidant to the aminophosphines, the Ag(I) complexes absorbs stronger than those of complexes where oxygen is an oxidant atom, see Table 4.1.2.23.

Table 4.1.2.23. Molar extinction coefficient of compounds **(17)**-**(22)**.

Compounds	λ_{max}[a](nm)	ε[b] ($M^{-1}cm^{-1}$)
17	231, 261, 497	9130, 4276, 378
18	230, 260, 495	9327, 4344, 386
19	231, 264, 472	12349, 8622, 180
20	230, 265	11130, 4701
21	230, 263	6811, 2866
22	231, 265	7027, 2664

[a] wavelength, [b] Molar extinction coefficient

4.1.2.13 Thermogravimetric Analysis data of Complexes

The thermogravimetric analysis curves for complexes **(3)**-**(5)** and **(7)**-**(8)** from 25 °C to 100 °C are given in Figure 4.1.2.24. The graph portrays the weight loss of complexes with an increase in temperature. The complexes **(3)**-**(5)** were stable at room temperature up to ~150 °C which was then followed by a steady decompositions at ~325 °C for **(3)**, ~337 °C for **(4)** and ~350 °C for **(5)**. The decomposition residual weights were observed at ~600 °C for **(3)**, ~790°C for **(4)** and ~900 °C for **(5)**. The significant change in the weight loss of complexes **(3)**-**(4)** are due to a 'halide effect' as a result of atomic radius increase from Cl < Br and < I. Complex **(7)** is thermal stable until a slight degradation of the complexes occurs at ~150-170°C followed by a steady decomposition until the residual weight occurs at ~400 °C. Complex **(8)** had a steady decomposition and reach its decomposition maximum temperature at ~315 °C and further decomposition is observed at ~450 °C until the residual weight loss occurs at ~625 °C.

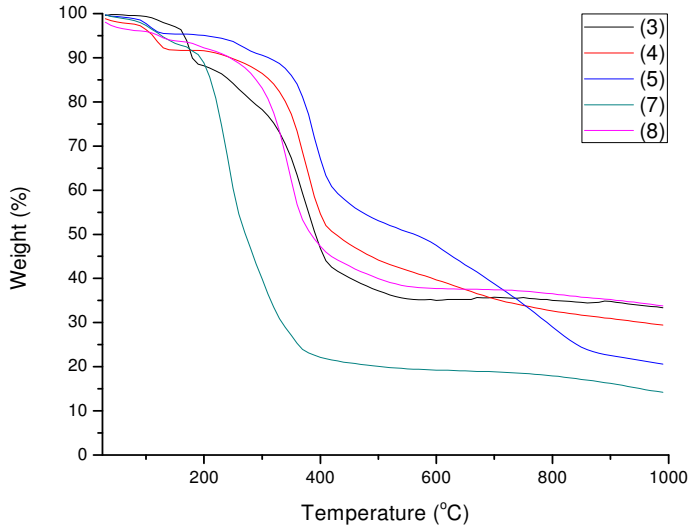

Figure 4.1.2.24. TGA curves of complexes **(3)-(5)** and **(7)-(8)**.

Complexes **(6)** and **(9)** TGA results are attached on the appendix. The profile graphs are similar to that of **(3)** for **(6)** and **(8)** for **(9)**.

Figure 4.1.2.25, demonstrate the thermogravimetric analysis (TGA) curves for complexes **(10)**-**(13)**. The curves show the steady decomposition of complexes from room temperature to 1000 °C. Complexes **(10)** and **(11)** possessing Ag_2X_2 manifold followed the same weight loss trend,

the complexes appears to be stable until they start to steadily decompose at ~150°C and ~350°C and reached their residual weights at ~550°C.

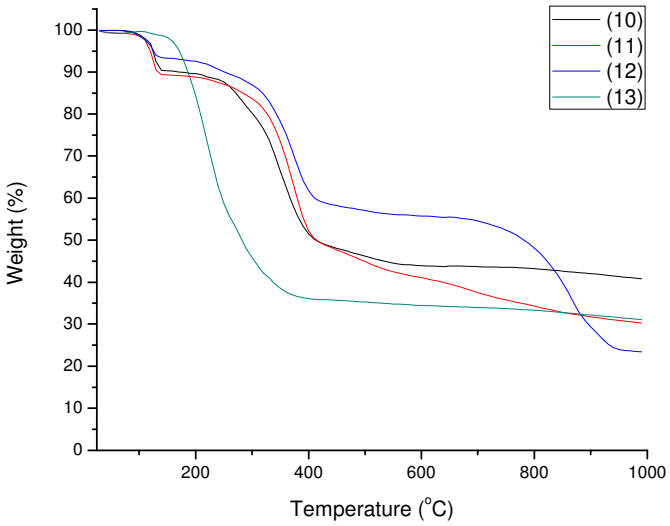

Figure 4.1.2.25. TGA curves of complexes **(10)**-**(13)**.

Complex **(12)** undergoes decomposition at three different weight loss temperatures, namely ~150, 350 and 800 °C until reaching residual weight at ~950 °C. The robustness of complex **(12)** compared to **(10)**-**(11)** and **(13)** is possibly due to its stair stepped Ag_4I_4 core motif. Complex **(13)** is stable at room temperature until it start to decompose at ~200 °C and reaches its residual weight at ~400 °C.

Thermogravimetric analysis curves for complexes **(17)-(22)** were recorded from room temperature to 1000 °C, as shown in Figure 4.1.2.26. Due to the differences in coordination modes of the Ag(I) center to the S-atoms, decomposition profile curves are different at the temperature range of ~150-250 °C. Complex **(17)** is stable at room temperature up to ~215 °C where a steady decline is noted at ~250 °C due to weight loss of the triflate ion until a complete degradation of the complex is observed at ~310 °C. Complex **(17)** reaches its residual weight loss at ~500 °C.

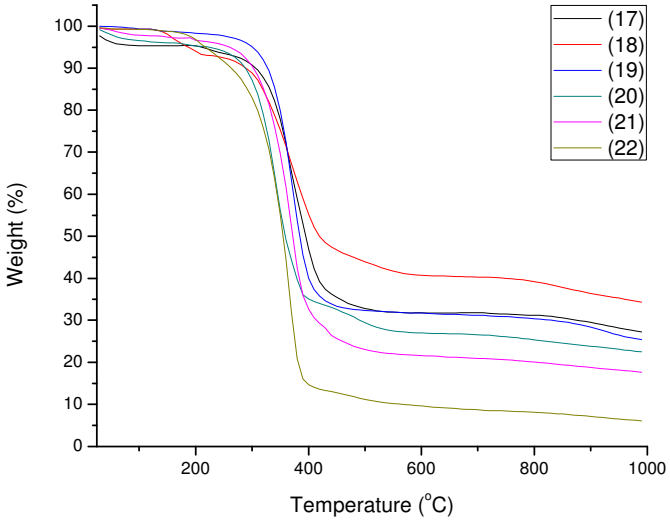

Figure 4.1.2.26. TGA decomposition curves of complexes **(17)**-**(22)**.

The thermal stability curve of complex **(18)**, shown in Figure 4.1.2.26, exhibits similar characteristics that are observed with complex **(17)**. The graph shows that at room temperature the complex is stable until temperatures reach 150 °C where there was a slight decline on the profile curve to about 215 °C. A massive decomposition of the complex **(18)** was seen at 310 °C until reaching residual weight at ~500 °C.

4.1.2.14 Electron Paramagnetic Resonance Spectroscopy (EPR)

The ^{1}H NMR spectra for **(20)**-**(22)** were not fully resolved as they show a slight overlap and broadening of the peaks in the aromatic region. Three combined EPR spectra of complexes **(20)**-**(22)** labelled **[A]**, **[B]** and **[C]**, respectively, are shown in Figure 4.1.2.27 and it summarizes the X-band EPR spectra found to examine the chemical species of the unpaired electrons of **(20)**-**(22)**. The complexes do not display the hyperfine multiplet pattern which normally appears due to spin-orbital coupling, instead the complexes spectrum appears sharpened and smooth.

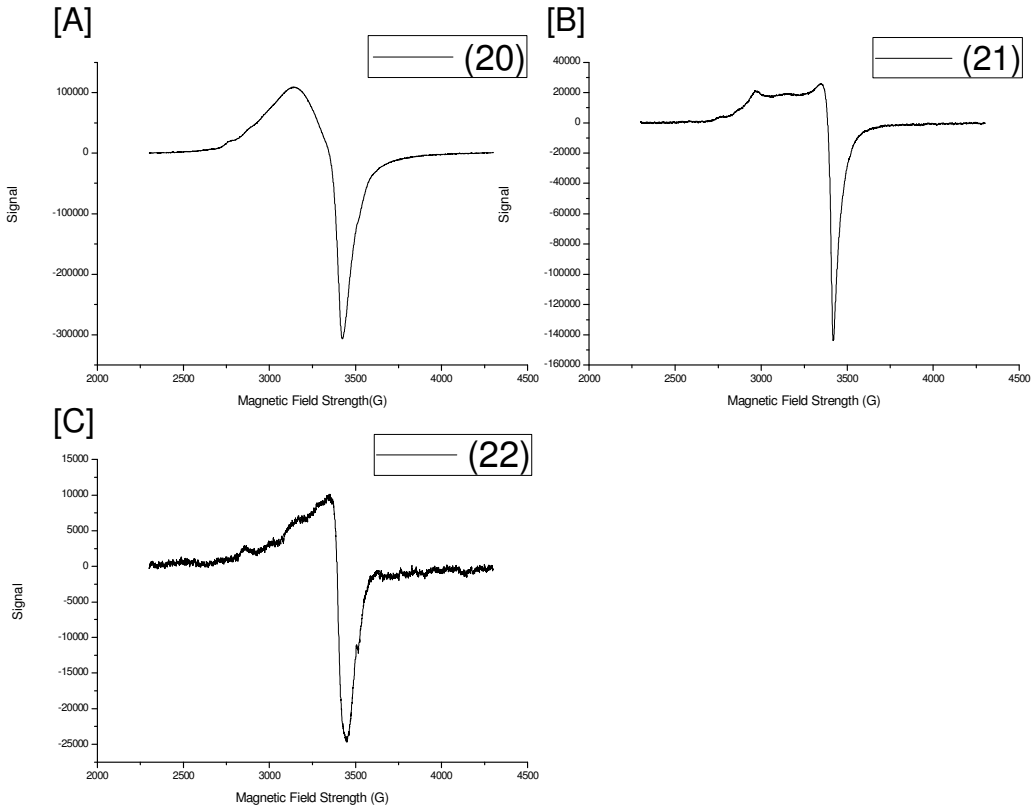

Figure 4.1.2.27. EPR spectra of complexes **(20)**, **(21)** and **(22)** shown in **[A]**, **[B]** and **[C]**, respectively. Complexes **(20)**-**(22)** shows atypical S = ½ EPR spectra in the absence of hyperfine coupling. The frequency dispersion is caused only by a g tensor with axial symmetry. The first derivative line-shape, as detected by EPR is dominated by the singularities that arise at the principal axis direction.

4.2 Synthesis of Perimidine Complexes, Spectroscopic Data and Crystal Structures

4.2.1 Background

The study of perimidine complexes is of ongoing focus in the field of inorganic and organometallic chemistry. The interest in coordination chemistry of heterocyclic compound is at the heart of many research endeavours because cyclic and acyclic compounds that contains nitrogen, oxygen and sulphur donor atoms provide different coordination modes to different metal centers, which lead to different properties and thus applications. Examples of such heterocyclic ligands were reported by Farghaly and Mahmoud,[59] although complexes of these ligands have not yet been reported. As the present study can attest, it is challenging to synthesize complexes of perimidine especially with cheap metal salts. Azam *et al*.,[60] have shown that organopalladium complexes of perimidines are very unstable in solution because of the coordination induced by the NH bond; the amine proton can easily be removed in solution. The chemistry of organo palladium complexes has established that organic moieties such as N-H and C-H proton can undergo metalation with formation of nitrogen-metal and carbon-metal bond. In cyclometallation chemistry, activation of the C–H σ-bond stabilized by the additional coordination of metal to a heteroatom may form transition metal complexes.[61-64] These C-H bonds are unreactive and robust if they are not functionalized. The inability of the C-H to react easily can be attributed to strong, localized, and unpolarized bonds. Transition metal catalysis or lithiating reagent can be used to assist in easing C-H bond to become more reactive towards the formation of carbon-metal bonds that can subsequently be functionalized to afford the desired complex. In most cases, the intramolecular activation of the C-H bond comes about with N-containing ligands, the metal quite often being palladium.[60] This study established that formation of the perimidine complexes with diamines undergo similar behaviour.

4.2.2 Results and Discussion

4.2.2.1 Synthesis of Perimidine Complexes

The starting perimidine aminals **(23)**-**(28)** were prepared as previously reported on Chapter 3.2. Unfortunately, the reaction of these simple perimidines with metal salts such as Cu(I), Cu(II)

and Ag(I) could not yield the desired product as the formed products decomposed in solution. Synthesis of $[C_{10}H_6(1,8\text{-}NH)_2{\cdot}Fe(C_5H_4)_2\{COCH_3\}_2]$, **(29)** follows the preparation route of aminals **(23)**-**(28)**. Compound **(29)** was an attempt to synthesis a perimidinyl ferrocene compound by treating *1,8*-diaminonaphthalene with 1,1′-diacetylferrocene, but instead a co-crystallization product of the two starting compounds formed. The naphthalene moiety in *1,8*-diaminonaphthalene is rigid and therefore cannot accommodate two 1,1′-diacetylferrocene due a steric hindrance caused by the bulkiness of the two starting compounds. Additionally, the rotation of the 1,1′-diacetylferrocene *Cp*-rings cause the instability to form the product similar to **(23)**-**(28)**. The reaction favours formation of **(29)**.

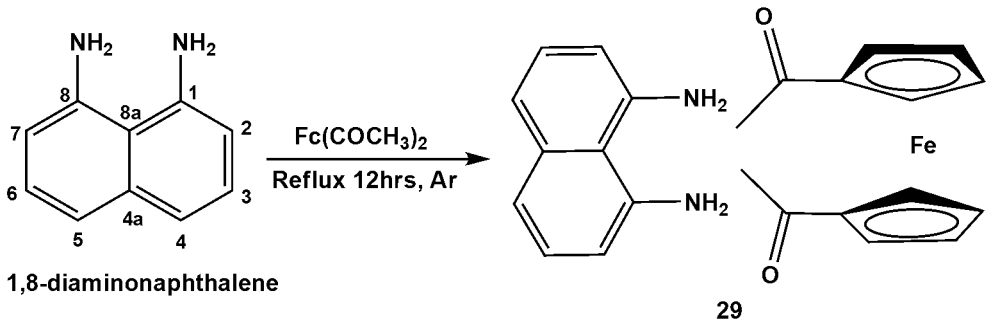

Scheme 4.2.2.1. Synthesis of **(29)**.

Complexes **(29)** and **(31)** were isolated as solids in satisfactory yields of 85% and 99%, respectively. The aim here was to prepare a derivative of perimidine complex containing an N or P donor atom. The approach was to either deprotonate the amine protons, then add a metal salt; or to react the amine without deprotonating with the aim to introduce a metal center to further develop the coordination chemistry. The complexes of perimidines are not easy to achieve and crystalize, and reports are rare. For example, direct metal attachment to compounds **(23)**-**(28)** lead to decomposition. Reaction of PPh_2Cl with simple perimidines compounds **(23)**-**(28)** was unsuccessful. Treatment of the phosphine derivatized ligand *in situ* with metal center leads to side products which could not be isolated due to instability of the products.

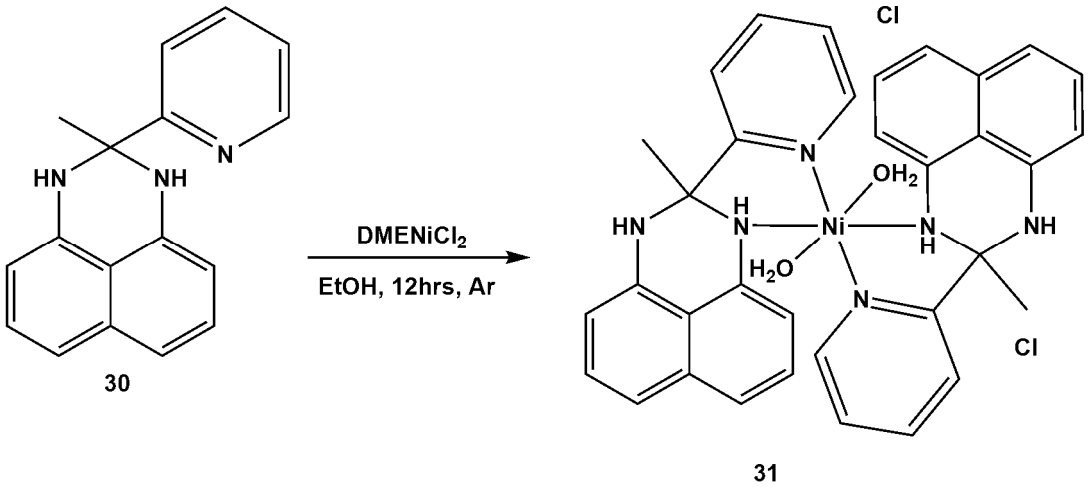

Scheme 4.2.2.2. Synthesis of **(31)**.

It was decided to synthesize compound **(30)** in high purity and then introduce a metal center to study the coordination chemistry. Compound **(30)** was treated with DME▪$NiCl_2$ in EtOH for 12 hrs in ratio (1:1) to yield the complex $[Ni(H_2O)_2\{C_{10}H_6(1,8\text{-}NH)_2(CH_3)(C_5H_4N)\}_2]2Cl$, **(31)** which was isolated in 88.6% yield. Complexes $[ZnCl_2\{C_{10}H_6(1,8\text{-}NH)_2(CH_3)(C_5H_4N)\}_2]$ and $[CdI_2\{C_{10}H_6(1,8\text{-}NH)_2(CH_3)(C_5C_4N)\}_2]$, **(32)** and **(33)** were prepared similar to **(31)** from **(30)** using $ZnCl_2$ and CdI_2, respectively, in good yields, i.e. 89.95% **(32)** and 71.91% **(33)**. The bulk purity of the complexes was in agreement with the microanalysis, although the MS peaks appeared fragmented. The peaks on the MS spectrum for the complexes was assigned to confirm the structures: MS (positive): (m/z) = 574 (4%) $[M+H+2Cl]^+$, 635 (6%) $[M+H\text{-}O]^+$, 262 (100%) $[M+C_{19}H_{21}N_3NiO_2]^+$ **(31)**, ESI-MS (positive): (m/z) = 183 (15%) $[M+C_{17}H_{15}C_{l2}N_3Zn]^+$, 262 (30%) $[M+C_{17}H_{15}Cl_2N_3Zn]^+$, 449 (100%) $[M+Na+C_{12}H_{12}N_2]^+$ **(32)** and ESI-MS (positive): (m/z) = 761 (1%) $[M+H+I]^+$, 135 (75%) $[M+C_{27}H_{23}CdI_2N_3]^+$, 102 (100%) $[M+C_{29}H_{28}CdI_2N_4]^+$ **(33)**.

4.2.2.2 Characterisation: Spectroscopic Analysis ^1H, ^{13}C NMR and FTIR

For ^1H NMR discussion that follows, see Scheme 4.2.2.1 for the key to assigning proton positions. The ^1H NMR for compound **(29)** shows that the protons resonate further downfield for the naphthalene backbone and are very different from the perimidine compounds because the *1,8*-diaminonaphthalene co-crystallized with 1,1′-diacetylferrocene. Therefore each compound maintained its NMR profile footprint. The ^1H NMR for compound **(29)** resonate in

the range 6.61-6.58 ppm for the protons at positions {7 and 2} as doublets, the protons at positions {6 and 3} and {4 and 3} are in the range 7.27-7.15 ppm resonating as multiplets. The 1,1′-diacetylferrocene have the Cp protons which resonate at 4.78-4.77 ppm and 4.52-4.51 ppm as doublets with a CH_3 resonating further upfield at a frequency of 2.36 ppm appearing as a singlet. The protons are observed in their respective positions, see Figure 4.2.2.1 for **(29)**. The ^{1}H NMR of **(31)** is paramagnetic. The difference in the ^{1}H NMR spectra of **(30)** to that of **(32)** and **(33)** lies in the NH chemical shift, i.e. **(30)** is 5.33 ppm and **(32)** and **(33)** is 7.14 ppm.

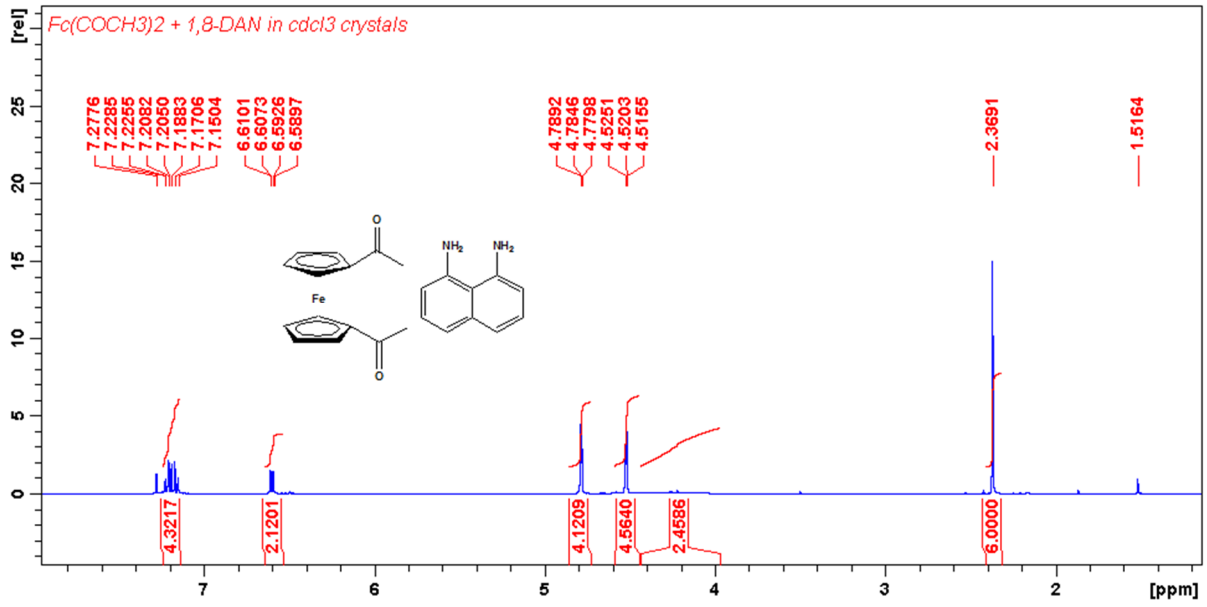

Figure 4.2.2.1. ^{1}H NMR spectrum of **(29)**.

The vibrational bands of *1,8*-diaminonaphthalene for ν(NH) and aromatic regions, i.e. ν(C=C) appear at 3385- 3295 and 1598-1402 cm^{-1}, respectively. Compound **(29)** shows a distinct broad peak of ν(NH) at 3339 cm^{-1} and the peak for CH_3 of 1,1′-diacetylferrocene at 3042 cm^{-1}. The characteristic sharp peaks for the naphthalene backbone in **(29)** for ν(C=C) appears at 1580 and 1452 cm^{-1}. The Cp peaks are observed at 1651 cm^{-1}. The FTIR absorption bands for compound **(30)** and complex **(31)** are different from each other. Compound **(30)** shows vibration peaks at 3372 and 3243 cm^{-1} for ν(NH), 2982 and 1922 cm^{-1} for ν(N=C) of the perimidinyl moiety of the ligand. The IR bands for ν(C=C), ν(C-C) of naphthalene are at 1697, 1623, 1588, 1598, 1510, 1467, 1423 cm^{-1}. Complex **(31)** FTIR spectrum consists of a broad peak at 3196 cm^{-1} corresponding to an overlap of ν(NH) peaks and ν(OH) of the water groups coordinated to the

metal center. Other prominent peaks which showed on the spectrum were attributed to the ν(C=C), ν(C-C) of the naphthalene at 1655, 1629, 1599, 1400, 1378 cm^{-1}. The ν(Ni-N) peak is seen at 424 cm^{-1} and this stretch supports the formation of the complex. The IR vibrational bands for ν(M-N) of **(32)** and **(33)** were observed in the region of 401 cm^{-1} and 403 cm^{-1}, respectively. Complexes **(32)** and **(33)** are closely related to **(31)** except that there are no observed peaks of ν(OH) for any traces of water. This suggests that there is no OH group from water coordinated or forming waters of crystallization.

4.2.2.3 Molecular Structures of Perimedine Complexes

The single crystal X-ray structures for compounds **(29)** and **(31)** were determined. The crystallographic data is shown in Table 4.2.2.1. The selected bond lengths and angles of the molecular structure are presented in Table 4.2.2.2. For compound **(29)** single-crystals were obtained by slow diffusion of dichloromethane and hexane, while **(31)** was grown in ethanol.

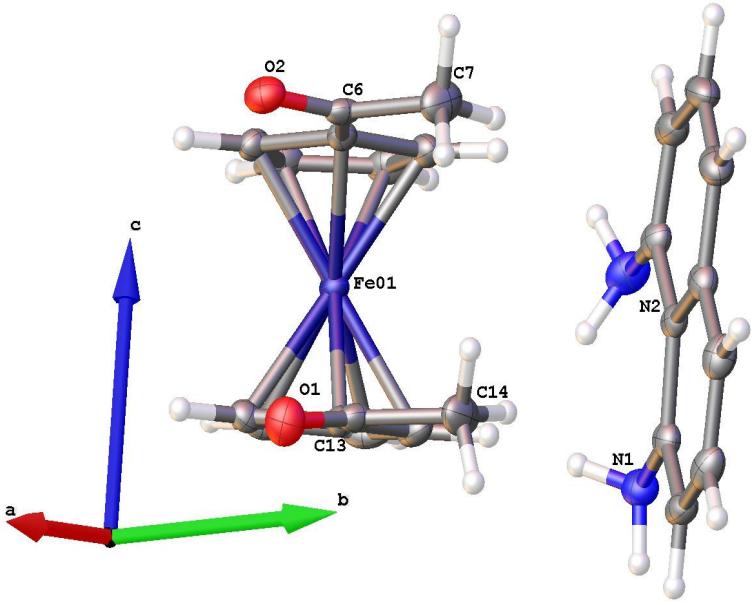

(29)

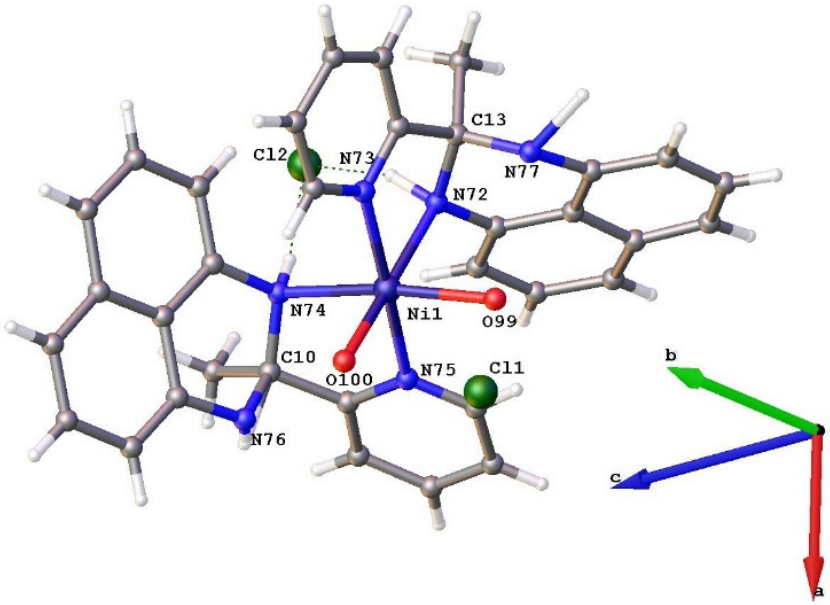

(31)

Figure 4.2.2.2. Molecular structures of (**29)** and **(31)** drawn at 50% probability using OLEX 2. The hydrogens of the water molecules were omitted for clarity.

Compound **(29)** exhibits a centrosymmetric center of inversion on the Ni(II) metal center. The molecular structure crystallized in a monoclinic $P2_1/c$ space group. There are four molecular structures of **(29)** contained in one unit cell. With a lone pair on each of the N-donor atoms, they are anticipated to assume a pyramidal geometry with a single bond between the carbon and N-donor atoms of the naphthalene ring. Complex **(31)** crystalized in a space group $P2_1/n$. The complex contain four molecules within the asymmetric unit, see Figure 4.2.2.3. Complex **(31)** has a centrosymmetric center of inversion. Complex **(31)** co-crystalized with chloride in the outer coordination sphere. The hygroscopic nature of the Ni(II) precursor allowed moisture condensation to replace chloride from the metal center during the reaction. The electron density of the Q peaks and data refinement indeed suggest that chlorides do not coordinate to metal center in the complex. Figure 4.2.2.2 shows that this complex consist of two bidentate ligands of compound **(30)** coordinating the Ni(II) center through the N-atoms of the pyrimidinyl NH ring and N-atom of the phenyl ring. The metal center is coordinated by two water molecules and counter balanced by two Cl^--ions. The coordination geometry around the metal center is octahedral.

Table 4.2.2.1. Crystallographic data for compound **(29)** and **(31)**.

	29	**31**
Formula	$C_{24}H_{24}FeN_2O_2$	$C_{34}H_{30}Cl_2N_7NiO_2$
M_r	428.30	684.23
Space group	$P2_1/_C$	$P2_1/n$
a, Å	9.661(5)	11.982(6)
b, Å	14.014(5)	16.2036(8)
c, Å	14.894(5)	19.902(1)
α, deg	90	90
β, deg	102.138(5)	90.155(3)
γ, deg	90	90
V, Å^3	1971.4(14)	3836.6(3)
Z	4	4
ρcalcd, g cm^{-3}	1.443	1.272
M, mm^{-1}	0.788	0.627
T, K	173(2)	293(2)
Reflections collected	55180	58006
Independent reflections	4697	7979
R_{int}	0.263	0.0426
Final *R* indices [I > 2σ(*I*)][a]	*R*1 = 0.0362 w*R*2 = 0.1088	*R*1 = 0.1645 w*R*2 = 0.4945
R indices (all data)	*R*1 = 0.0395 w*R*2 = 0.1123	*R*1 = 0.1866 w*R*2 = 0.5107
Largest diff. peak and hole, e / Å	0.835 and -0.783	5.308 and -1.812

[a] $R1 = \Sigma \mid\mid F_o \mid - \mid F_c \mid\mid / \Sigma \mid F_o \mid$. [b] $wR2 = \{\Sigma [w(F_o^2 - F_c^2)^2] / \Sigma [w(F_o^2)^2]\}^{1/2}$

The distance between the non-bonding N···N in the *peri*-position of compounds **(29)** and **(31)** is 2.751 and 2.358 Å, respectively. The distance between $N_{(pyridine)}$-$N_{(naph)}$ of compound **(30)** and **(31)** is 2.790 and 2.679 Å, respectively. These values are in agreement with literature values.[65] The bond angles for compounds **(30)** and **(31)** of N(2)-C(5)-C(6) and N(74)-C(10)-C(7) are 112.04(9) and 108.8(7)°, respectively. This shows that ligand **(30)** in complex **(31)** is bent to accommodate the metal center. The bond distances of C-N for the ligand **(30)** and complex **(31)** are within the range of the typical known C-N bonds previously observed.[65, 66] Table 4.2.2.2 shows the bond lengths and angles of **(29)** and that the C-N bond has distance of 1.389 Å which is similar to the reported bonds lengths of related compounds in the literature.[67] The non-bonding *peri*-N atoms of **(29)** is shorter than that of **(30)** because the free 1,8-diaminonaphthalene non-bonding *peri*-N atoms did not bend too much to relief the strain, while in **(30)**, the *peri*-N atoms are bent away from the naphthalene ring to create room for larger atoms. The bond angles and bond lengths of compound **(31)** are shown in Table 4.2.2.2 to further support the distorted octahedral nature of complex **(31)**.

Table 4.2.2.2. Selected bond distances (Å) and angles (deg) for **8** and **9** with esd's in parentheses.

Compound **29**			
C(21)–N(1)	1.389(3)	C(21)–C(20)	1.444(3)
N(2)–C(15)–C(20)	120.78(18)	N(2)–C(21)–C(20)	122.81(18)
Compound **31**			
Ni(1)–N(75)	2.032(7)	Ni(1)–N(73)	2.041(8)
Ni(1)–O(100)	2.059(7)	Ni(1)–O(99)	2.105(6)
Ni(1)–N(72)	2.160(7)		
N(75)–Ni(1)–C(73)	173.2(3)	N(75)–Ni(1)–O(100)	91.4(3)
N(73)–Ni(1)–O(100)	93.9(3)	N(75)–Ni(1)–O(99)	93.2(3)
N(73)–Ni(1)–O(99)	91.1(3)	O(100)–Ni(1)–O(99)	87.8(3)
N(75)–Ni(1)–N(72)	95.7(3)	N(73)–Ni(1)–N(72)	79.2(3)
O(100)–Ni(1)–N(72)	171.9(3)	O(99)–Ni(1)–N(73)	88.1(3)
N(75)–Ni(1)–N(74)	79.0(3)	N(73)–Ni(1)–N(74)	96.7(3)
O(100)–Ni(1)–N(74)	91.5(3)	O(99)–Ni(1)–N(74)	172.(2)
N(72)–Ni(1)–N(74)	95.4(3)		

Symmetry transformations used to generate equivalent atoms: #1 x-1,y,z **(29)**.

This indicates that the larger the substituent occupying the *peri*-positions, the more the molecule bend out of the plane to relief stress. The molecules are held together by intermolecular hydrogen bonding of NH interacting with the π electrons of the adjacent naphthalene rings and the CH_2 of the adjacent alkyl group and **(31)** is held by intermolecular interaction of the chlorine atoms. There are no observed π-π stacking centroid-centroid distances which stabilizes the crystal structure in the crystal lattice.

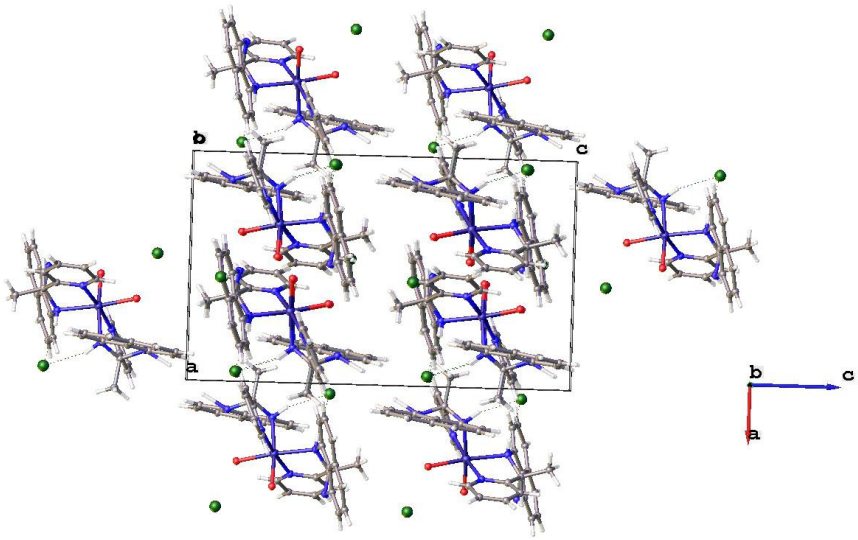

Figure 4.2.2.3. Molecular packing of **(31)**.

The symmetry codes for the crystal structures report herein Chapter 4 are provided in the Supporting Information of this work in the appendix. Some structures don not have symmetry transformations used to generate equivalent atoms.

4.3 References

1. A. Tsuboyama, K. Kuge, M. Furugori, S. Okada, M. Hoshino and K. Ueno, *Inorg. Chem.*, 2007, 46, 1992-2001.
2. R. Peng, M. Li and D. Li, *Coord. Chem. Rev.*, 2010, 254, 1-18.
3. K. Tsuge, *Chem. Lett.*, 2013, 42, 204-208.
4. M. A. Rawashdeh-Omary, M. A. Omary and H. H. Patterson, *J. Am. Chem. Soc.*, 2000, 122, 10371-10380.
5. E. C. Alyea, G. Ferguson and A. Somogyvari, *Inorg. Chem.*, 1982, 21, 1369-1371.
6. M. Camalli, F. Caruso, S. Chaloupka, L. Chaloupka and L. M. Venanzi, *Helv. Chim. Acta*, 1988, 71, 703-711.
7. W. Marty, P. N. Kapoor, H. B. Bürgi and E. Fischer, *Helv. Chim. Acta*, 1987, 70, 158-170.
8. B.-K. Teo and J. C. Calabrese, *Inorg. Chem.*, 1976, 15, 2474-2486.
9. B.-K. Teo and J. C. Calabrese, *Inorg. Chem.*, 1976, 15, 2467-2474.
10. A. Cassel, *Acta Crystallogr. Sect. B*, 1979, 35, 174-177.
11. S. Attar, N. W. Alcock, G. A. Bowmaker, J. S. Frye, W. H. Bearden and J. H. Nelson, *Inorg. Chem.*, 1991, 30, 4166-4176.
12. G. A. Bowmaker, Effendy, J. V. Hanna, P. C. Healy, B. W. Skelton and A. H. White, *J. Chem. Soc., Dalton Trans.*, 1993, 1387-1397.
13. M. Camalli, F. Caruso, S. Chaloupka, P. N. Kapoor, P. S. Pregosin and L. M. Venanzi, *Helv. Chim. Acta*, 1984, 67, 1603-1611.
14. A. Cassel, *Acta Crystallogr. Sect. B*, 1976, 32, 2521-2523.
15. A. Cassel, *Acta Crystallogr. Sect. B*, 1975, 31, 1194-1196.
16. E. Tiekink, *Acta Crystallogr. Sect. C: Cryst. Struct. Commun.*, 1990, 46, 235-238.
17. D. M. Ho and R. Bau, *Inorg. Chem.*, 1983, 22, 4073-4079.
18. R. Meijboom, R. J. Bowen and S. J. Berners-Price, *Coord. Chem. Rev.*, 2009, 253, 325-342.
19. S. J. Lippard and J. M. Berg, *Principles of Bioinorganic Chemistry, University Science Books, Mill Valley, CA*, 1994.
20. R. R. Conry, in *Encyclopedia of Inorganic Chemistry*, John Wiley & Sons, Ltd, 2006.
21. N. Farrell, *Transition Metal Complexes as Drugs and Chemotherapeutic Agents, Kluwer, Dordrecht*, 1980.
22. H. G. Petering, *Pharmacol. T her. A*, 1976, 1, 127-130.
23. C. L. Foxand and S. M. Modak, *Antimicrob. Agent Chemother.*, 1974, 5, 582-588.
24. H. Firouzabadi, P. Salehi and I. Mohammadpour-Baltork, *Bull. Chem. Soc. Jpn.*, 1992, 65, 2878-2880.
25. T. G. Hill, R. C. Haltiwanger, T. R. Prout and A. D. Norman, *Inorg. Chem.*, 1989, 28, 3461-3467.
26. Ö. Sarıöz, O. Serindağ and M. İ. Abdullah, *Phosphorus, Sulfur Silicon Relat. Elem.*, 2009, 184, 1785-1795.
27. C. Fliedel, A. Ghisolfi and P. Braunstein, *Chem. Rev.*, 2016, 116, 9237-9304.
28. F. Caruso, M. Camalli, H. Rimml and L. M. Venanzi, *Inorg. Chem.*, 1995, 34, 673-679.
29. M. Trivedi, R. Nagarajan, A. Kumar, N. P. Rath and P. Valerga, *Inorg. Chim. Acta*, 2011, 376, 549-556.
30. F. R. Knight, A. L. Fuller, A. M. Z. Slawin and J. D. Woollins, *Dalton Trans.*, 2009, 8476-8478.
31. F. De Angelis, S. Fantacci, A. Sgamellotti, E. Cariati, R. Ugo and P. C. Ford, *Inorg. Chem.*, 2006, 45, 10576-10584.
32. S. Perruchas, C. Tard, X. F. Le Goff, A. Fargues, A. Garcia, S. Kahlal, J.-Y. Saillard, T. Gacoin and J.-P. Boilot, *Inorg. Chem.*, 2011, 50, 10682-10692.

33. A. Kobayashi, K. Komatsu, H. Ohara, W. Kamada, Y. Chishina, K. Tsuge, H.-C. Chang and M. Kato, *Inorg. Chem.*, 2013, 52, 13188-13198.
34. V. Saboonchian, G. Wilkinson, B. Hussain-Bates and M. B. Hursthouse, *Polyhedron*, 1991, 10, 737-739.
35. L. Pauling, *The Nature of the Chemical Bond, 3rd Ed.; Cornell University Press: Ithaca, NY*, 1960, 260.
36. B. Liu, G.-W. Zhou, M.-L. Fu, L. Xu, G.-C. Guo and J.-S. Huang, *Notes*, 2004, 25, 1937.
37. B.-K. Teo and J. C. Calabrese, *Inorg. Chem.*, 1976, 15, 2474-2486.
38. G. A. Bowmaker, R. Hart, J. Kildea and A. White, *Aust. J. Chem.*, 1997, 50, 653-670.
39. M. R. Churchill and B. G. DeBoer, *Inorg. Chem.*, 1975, 14, 2502-2507.
40. B.-K. Teo and J. C. Calabrese, *J. Am. Chem. Soc.*, 1975, 97, 1256-1257.
41. A. Cassel, *Acta Crystallogr.* , 1976, B32, 2521-2523.
42. A. Cassel, *Acta Crystallogr.*, 1975, B31, 1194-1196.
43. K. Naktode, R. K. Kottalanka, H. Adimulam and T. K. Panda, *J. Coord. Chem.*, 2014, 67, 3042-3053.
44. Y. Sun, V. Lemaur, J. I. Beltrán, J. r. m. Cornil, J. Huang, J. Zhu, Y. Wang, R. Fröhlich, H. Wang and L. Jiang, *Inorg. Chem.*, 2016, 55, 5845-5852.
45. M. S. Balakrishna, B. D. Santarsiero and R. G. Cavell, *Inorg. Chem.*, 1994, 33, 3079-3084.
46. M. Newton, R. King, M. Chang and J. Gimeno, *J. Am. Chem. Soc.*, 1978, 100, 1632-1634.
47. A. D. Burrows, M. F. Mahon, M. T. Palmer and M. Varrone, *Inorg. Chem.*, 2002, 41, 1695-1697.
48. Ö. Sarıöz, S. Öznergiz and F. Kandemirli, *Synth. React. Inorg. Met.-Org. Nano-Metal Chem.*, 2013, 43, 185-195.
49. S. Gremler and M. Scheer, *Z. Anorg. Allg. Chem.*, 1993, 619, 466-470.
50. H. Liu, M. J. Calhorda, M. G. B. Drew and V. Félix, *Inorg. Chim. Acta*, 2003, 347, 175-180.
51. M. G. Drew, R. J. Hobson, P. P. Mumba and D. A. Rice, *Inorg. Chim. Acta*, 1988, 142, 301-303.
52. T. S. Lobana, R. Sharma and R. J. Butcher, *Polyhedron*, 2009, 28, 1103-1110.
53. V. Cadierno, J. Díez, J. García-Álvarez and J. Gimeno, *Dalton Trans.*, 2007, 2760-2769.
54. T. S. Lobana, S. Khanna, R. Sharma, G. Hundal, R. Sultana, M. Chaudhary, R. Butcher and A. Castineiras, *Cryst. Growth Des.*, 2008, 8, 1203-1212.
55. C. Kitamura, Y. Tanigawa, T. Kobayashi, H. Naito, H. Kurata and T. Kawase, *Tetrahedron*, 2012, 68, 1688-1694.
56. A. Dreuw, J. Plötner, L. Lorenz, J. Wachtveitl, J. E. Djanhan, J. Brüning, T. Metz, M. Bolte and M. U. Schmidt, *Angew. Chem. Int. Ed.*, 2005, 44, 7783-7786.
57. H. Langhals, T. Potrawa, H. Noeth and G. Linti, *Angew. Chem., Int. Ed. Engl.*, 1989, 28, 478-480.
58. M. Van de Weert and L. Stella, *J. Mol. Struct.*, 2011, 998, 144-150.
59. T. Farghaly, E. Abbas, K. Dawood and T. El-Naggar, *Molecules*, 2014, 19, 740.
60. M. Azam, I. Warad, S. I. Al-Resayes, N. Alzaqri, M. R. Khan, R. Pallepogu, S. Dwivedi, J. Musarrat and M. Shakir, *J. Mol. Struct.*, 2013, 1047, 48-54.
61. B. Garcia, F. J. Hoyuelos and S. Ibeas, *Chem. Asian J.*, 2010, 5 2530-2540.
62. B. Garcia, F. J. Hoyuelos and S. Ibeas, *Phys. Chem.* , 2006, A 113 9115-1923.
63. J. A. Labinger and J. E. Bercaw, *Nature* ,2002, 417, 507-517.
64. R. H. Crabtree, *Chem. Rev.*, 198, 85 245-269.
65. M. Elena Cucciolito, B. Panunzi, F. Ruffo and A. Tuzi, *Tetrahedron Lett.*, 2013, 54, 1503-1506.
66. S. Maloney, A. M. Z. Slawin and J. D. Woollins, *Acta Crystallogr. E*, 2013, 69, o246-o246.
67. A. S. Batsanov, J. C. Collings, J. A. K. Howard and T. B. Marder, *Acta Crystallogr. E*, 2001, 57, o950-o952.

Chapter 5

Density Functional Theory of Bis(amino)phosphines and Perimidines, and Antimicrobial Studies

5.1 Study of Electronic Properties of Bis(amino)phosphine Complexes

5.1.1 Background

When theory combines with single crystal X-ray data, the type and amount of information gained can be quite powerful in understanding molecular structure and bonding. For example Bader have shown that the topological analysis of the electron density derived from theoretical calculations can be a useful tool in finding valuable information about the chemical bonding and the properties of atoms in the compounds.[1] This information is vital because the topological analysis can be extended to electron densities experiments attained by X-ray diffraction.[2] The data gained by the X-ray diffraction experiment offer information on the electron density averaged over the thermal motions in the crystal at the given temperature. Consequently, it is essential to deconvolute the thermal motion of atoms to get the static electron density, which can be exposed by topological analysis and related to results from theoretical calculations. Should the thermal motion be successfully deconvoluted, then it is possible to obtain identical atomic multipole parameters from refinements of accurate, high-order X-ray diffraction data irrespective of the conditions especial temperature.[3]

The P(III)-N bonds are interesting in inorganic chemistry because of their various structural features. For example, the coordination chemistry of $(Me_2N)PF_2$ was studied comprehensively and it was concluded that the compound was a ligand with base strength that lies between PF_3 and Me_3N.[4-6] It was also suggested that both N- and P-donor atoms could coordinate depending on the nature of the metal. The X-ray structure of $(Me_2N)PF_2$ was determined to prove that P-donor atoms alone has the capability of coordinating to the metal. The N-donor atom was found

to have a planar geometry, as shown by Morris and co-workers, this then laid foundation for a large number of theoretical studies.[7] X-ray structural investigations of P(III)-N bonded systems have thus aided a great deal in understanding this bonding. It has been broadly accepted that the P(III)-N bond would be even better understood by means of theoretical and computational studies on new and more complicated P(III)-N model compounds.

Halogenated copper(I) and other d^{10} coinage metal salts are known to form complexes with ligands which contains the N-and P-atoms because of their affinity of lone pairs which form diverse complexes with mono-, di-, and tetranuclear discrete units. These can also form halogenato-bridged coordination oligomers depending on the ligand incorporated into the reaction mixture. [8] The following coordination modes have been observed when bulky ligands are used $[Cu_2X_2L_3]$ or $[Cu_2X_2L_2]$. Often, Cu(I) metal centers afford an assumed trigonal coordination geometry. The dimeric units, $\{Cu_2(\mu\text{-}X)_2$, have been studied as the structural units of metal-organic frameworks (MOFs)[9] and intermediates of some catalytic reactions.[10,11,12]

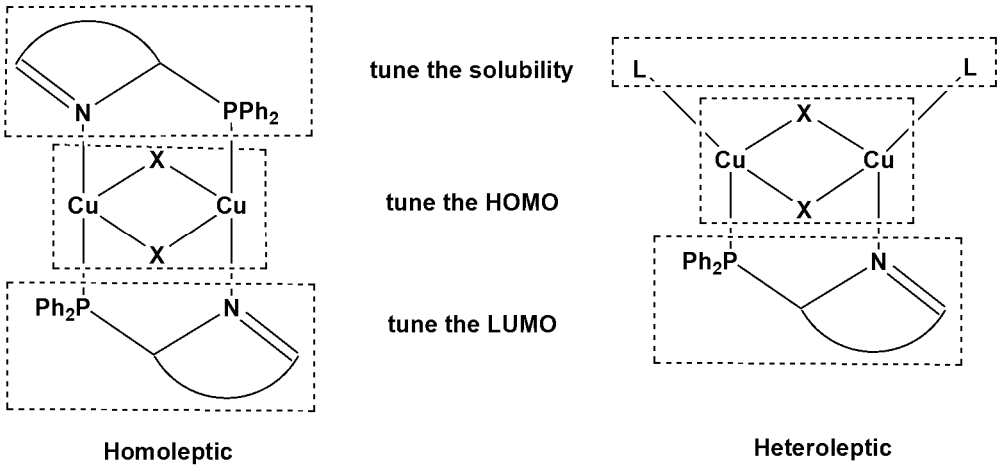

Figure 5.1.1.1. Homoleptic and heteroleptic PyrPHOS CuX complexes.[13]

In a homoleptic dinuclear CuX complex, ligands of a similar type can be used to tune the emission colour because they provide the modification of the LUMO. The same strategy may be applied for heteroleptic complexes, see Figure 5.1.1.1. Phosphines such as PPh_3 and different diphenylphosphinepyridine-derivatives (NHetPHOS) led to series of materials with different emission energies (colour), depending on the nature of the NHetPHOS ligands.[14] Addition of different substituents to the NHetPHOS ligands enhance the solubility in solvents

like toluene. In a slightly different approach, tuning of solubility and colour was done by modifying different sections of the molecule, see Figure 5.1.1.1. The monodentate ligands have a lower influence on the HOMO energy than the bridging NHetPHOS ligand when varied systematically.[13] Similar comparison studies can be made with Ag(I) complexes.[15]

The molecular orbital (MO) calculations for some of the aminophosphines were performed in order to study the i) stereochemistry at phosphorus centre, ii) nature of P-N torsional process, and iii) conformational effects of stabilizing and destabilizing orbital interactions between the N- and P-donor atoms.[16-18]

5.1.2 Results and Discussion

5.1.2.1 Cu(I) Complexes Electronic Properties

The geometries were optimized using the Becke3LYP[19, 20] functional and LANL2DZ basis sets[21-24] for three complexes. Figure 5.1.1.2 shows the environment of the frontier electronic levels in the ground state that shed light on the nature of the excited states in the absorption spectra. The energies involved in the frontier MO diagram of the three complexes are summarized in Table 5.1.1.1. The calculated bond distances and angles of all three complexes **(3)**-**(5)** are in complete agreement with those obtained experimentally by X-ray diffraction.

For Cu(I) complexes, the HOMO is most likely located on a Cu(I)X core, whereas the LUMO is located on the ligands with low-lying π^* orbitals, as reported.[25,26] Subsequently, these transitions are classified as metal-halide-to-ligand charge-transfer transitions [(M+X) LCT. This signify that electron density is shifted from the metal-halide unit to the ligands upon excitation. Figure 5.1.1.2 shows the HOMO and LUMO for complexes **(3)**-**(5)** which are concentrated around the naphthalene rings. There is no observed flow of electron density energy from $Cu_2(\mu\text{-}X)_2$ core to the ligands. Changing the halides ligand of Cu(I) complexes, i.e. lowering / raising the HOMO and the ligands, i.e. lowering / raising the LUMO, affect the colours of the complexes, see Chapter 2, experimental. This also means that moving from the chloride to the iodide results in a larger band gap, which is accompanied by blue a shift. Table 5.1.1.1 shows that the band gaps for the complexes report herein are constant and this cannot change the behaviour of the excitation of the molecules and non-luminescence. This trend is observed when moving from electron-poor to electron rich ligands.

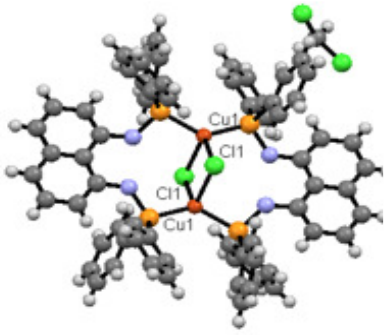

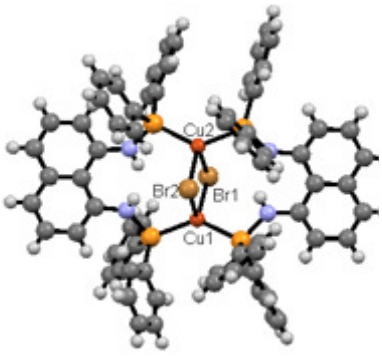

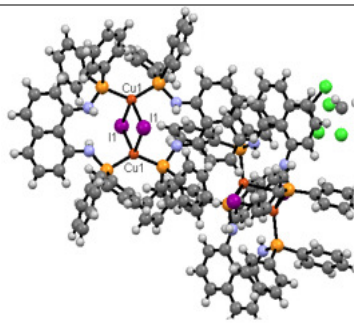

Cu···Cu: 3.376Å (3) | **Cu···Cu: 3.303Å (4)** | **Cu···Cu: 3.421Å (5)**

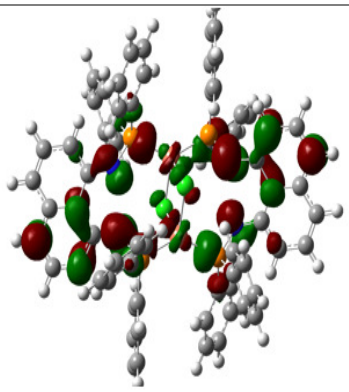

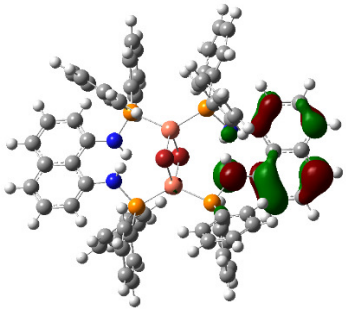

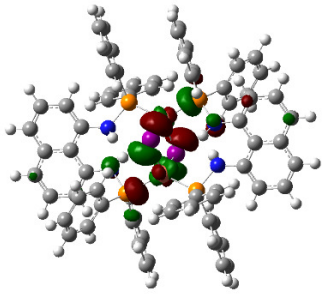

HOMO | HOMO | HOMO

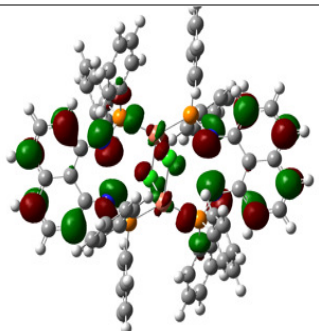

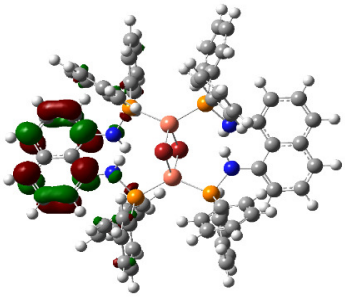

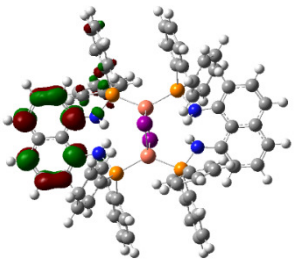

LUMO | LUMO | LUMO

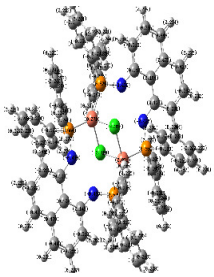

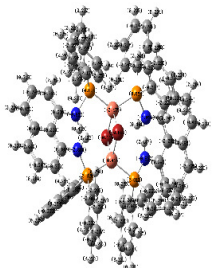

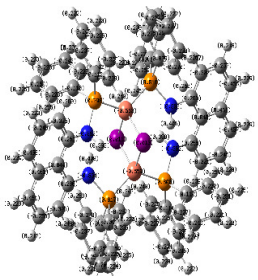

Charge density | Charge density | Charge density

Figure 5.1.1.2. The geometry-optimized molecular structures and schematic MO diagram of complexes **(3)**-**(5)** in the ground state from left to right, respectively. MO diagrams of one complexes are recorded vertically.

Figure 5.1.1.2 shows complex **(3)** $Cu_2(\mu\text{-}Cl)_2$ core where the HOMO mainly consists of the lone pairs of electrons of the NH (amine group), the lone pairs of electrons on the P atom and half of the molecule of the naphthalene moiety. The LUMO comprises almost all of the atoms building-up the naphthalene moiety and the lone pairs of the NH. The energy is highly circulating on the C-atoms of naphthalene. Complex **(4)** with the $Cu_2(\mu\text{-}Br)_2$ core reveals that HOMO comprises of a lone pair on the NH (amino group) and fully concentrated on the naphthalene π^* orbitals of C_1-C_2, C_3-C_4, C_5-C_6 and C_7-C_8, whereas the LUMO is mainly on the naphthalene moiety on the C_2-C_3, C_6-C_7 and solely on C_1, C_4, C_6 and C_8. It is observed that in both the HOMO and LUMO diagrams, the PPh_2 π^* orbitals are not involved in the electronic contribution of the molecule. Complex **(5)** display an interesting behaviour in its HOMO and LUMO orbitals and is very different from **(3)** and **(4)**. The HOMO consist mainly of its $Cu_2(\mu\text{-}I)_2$ core and partial localized on the P atoms of PPh_2 and NH (amine group). The LUMO of complex **(5)** are localized only on the naphthalene moieties. The nature in which the molecule packs itself affects the M···M interaction of the rhombus core. The charge electron densities of all three complexes showed the halides play an important role in distributing energies of the metal involved in coordination chemistry. Distinctive energies are comparable with the UV-Vis spectra. Table 5.1.1.1 confirms the behaviour observed in Figure 5.1.1.2 as to why weak HOMO and LUMO energies are involved in complex **(3)** compared to **(4)** and **(5)**. The absorption of the complexes **(3)** and **(4)** is influenced by $\pi\cdots\pi^*$ as opposed to **(5)** which is influenced by [(M+X) LCT.

Table 5.1.1.1. DFT Calculated Orbital Energies[a] (in eV) of the HOMO and LUMO levels in complexes **(3)-(5)** as well as their energy difference ($\Delta E_{H\text{-}L}$).

Compounds	**3**	**4**	**5**
$\mathbf{E_{HOMO\ (eV)}}$	-4.60768	-4.92728	-4.95176
$\mathbf{E_{LUMO\ (eV)}}$	-0.982464	-1.08637	-1.0423
$\mathbf{E_{HOMO\text{-}LUMO\ (eV)}}$	3.62522	3.840912	3.909456

[a]B3LYP/def2-SV(P) HOMO and LUMO orbital energies (in eV, 1 eV ≙ 8067 cm^{-1}) at the ground-state geometry.

The energy gaps between the HOMO and the LUMO of complexes are recorded as the change in energy difference as seen in Table 5.1.1.1. The HOMO/LUMO gap observed in **(3)**-**(5)** is

very small and hence excitation energy becomes low. This is due to inductive resonance effect of the molecules which might cause the statically quenching of the molecules.

5.1.2.2 Ag(I) Complexes Electronic Properties

Similar to the Cu(I) complexes, the Ag(I) complexes were typically characterized as luminescent complexes. The NMR spectra and the X-ray diffraction showed that the Ag(I) complexes reported herein have a broad variety of coordination modes through the P and S donor atoms which could be extended to other donor atoms like N, O, Se, As and C. Silver is better stabilised upon coordination with soft atoms. To understand the electronic effects of the reported complexes and the reasons why it is important to study the P(III)-N, DFT calculations were performed on several halide bridged Ag(I) complexes which leads to the delocalization of the frontiers orbitals, partly caused by the cooperative effects that coinage metal complexes possesses. The geometries of the Ag(I) complexes are optimized using the same basis set as Cu(I) complexes. Figure 5.1.1.3 and Table 5.1.1.2 summarizes that results obtained of the complexes **(10)**-**(12)**.

The MO diagrams of the homoleptic dinuclear Ag(I) complexes in Figure 5.1.1.3 shows that the LUMO resides on the naphthalene rings and PPh_2 for **(10)**-**(12)**, respectively. The HOMO is located mainly on the naphthalene rings and lone pairs of NH for **(10)** and **(11)**. The orbital energies extends to the P-donor atoms of the phosphines for **(11)**. The HOMO energies were located on the Ag_4I_4 for **(12)**. This behaviour is rare for these types of systems. Because the HOMO is tuned mainly on the metal halides while the LUMO is adjusted on the ligands, this will determine whether the groups in the ligands are electron rich or poor. In general, luminescence depend on the change in energies of the S1 (high lying singlet state)-T1 (thermal energy state) caused by an exchange in integral of S1 and T1, which is approximated by the exchange integral between HOMO and LUMO. The MO diagrams of the complexes also shows that the alternation of the HOMO and LUMO on the naphthalene may lead to a small overlap between the energies of the frontier orbitals and this reduces the mix of the states and therefore leads to a minimized change in S1-T1, which also corresponds to a minimized distortion upon excitation. For excitation to take place the HOMO and LUMO should be well separated as this provide enough overlap to enable a transition to occur. With the MO diagrams presented herein

the energies of the HOMO and LUMO are slightly overlapping. This could be one of many reasons which reduces or quenches luminescence properties of these complexes.

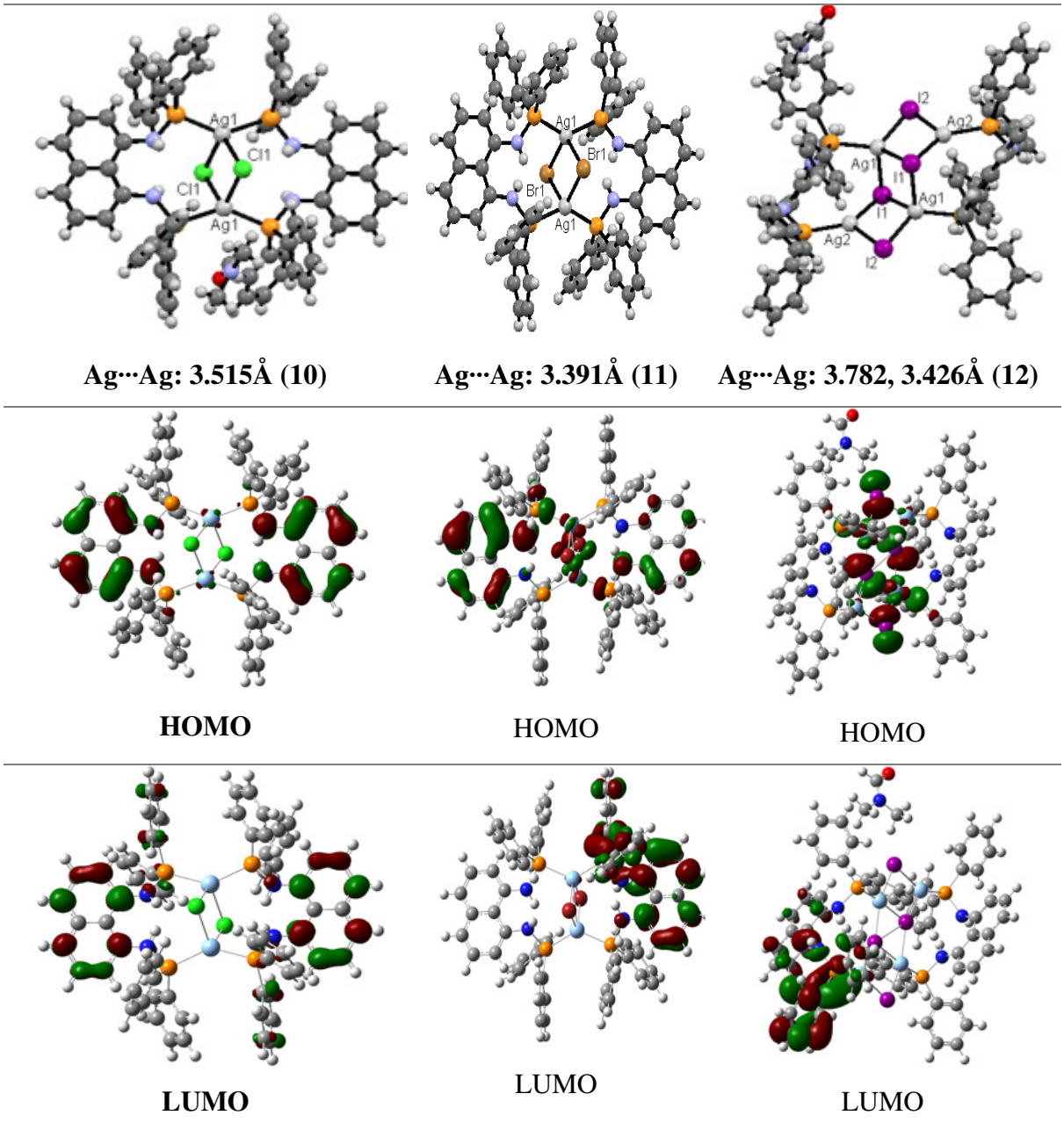

Figure 5.1.1.3. The geometry-optimized molecular structures and schematic MO diagram of complexes **(10)**-**(12)** in the ground state from left to right, respectively. MO diagrams of one complexes are recorded vertically.

Introducing chalcogenides to a molecule increase the electron density of the compound. Figure 5.1.1.4 shows the HOMO/ LUMO of **(17)** and **(18)**. The pictorial view shows that the HOMO of **(17)** are focused on the naphthalene and the lone pair of the NH group, while the LUMO are located both on the naphthalene and the PPh_2 group.

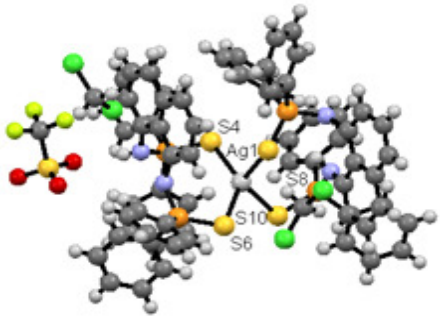

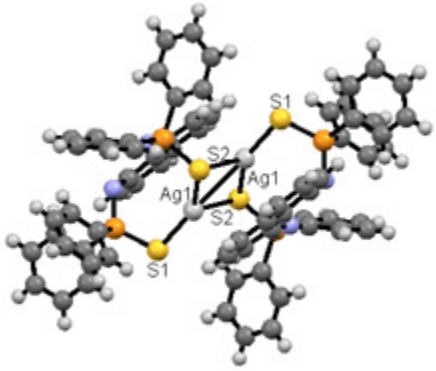

(no)Ag···Ag for (17) **Ag···Ag:3.001Å (18)**

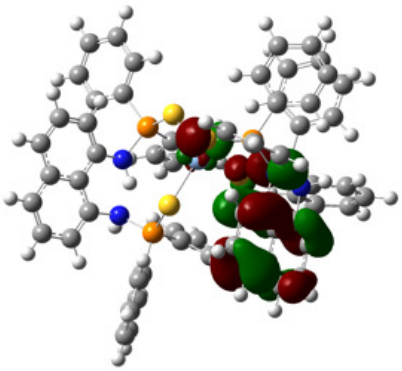

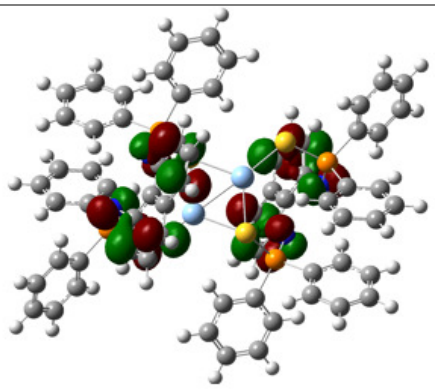

HOMO HOMO

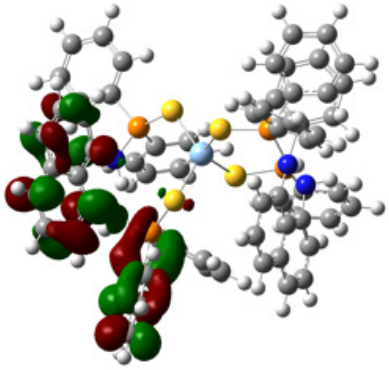

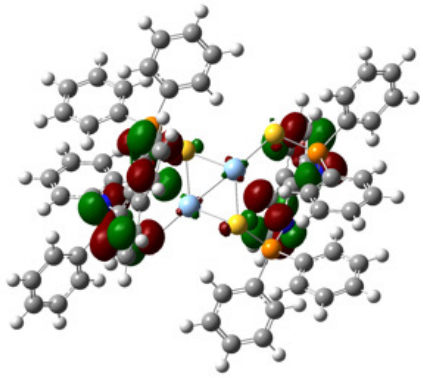

LUMO LUMO

Figure 5.1.1.4. The geometry-optimized molecular structures and schematic MO diagram of complexes **(17)** and **(18)** in the ground state from left to right, respectively. MO diagrams of one complexes are recorded vertically.

Complex **(17)** is a mononuclear compound and the Ag(I) center do not participate in the HOMO because there is less energy propagated to the sulfur atoms and further to the metal center Complex **(18)** show similar behaviour to that portrayed on **(17)**. The HOMO / LUMO are distributed along the ligands backbone, i.e. naphthalene moiety.

Ligand (1)	**Ligand (14)**
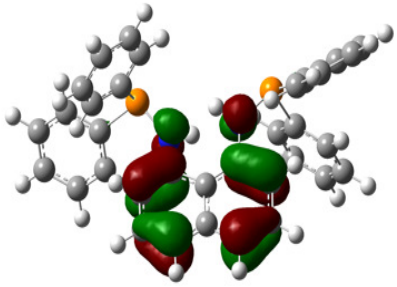	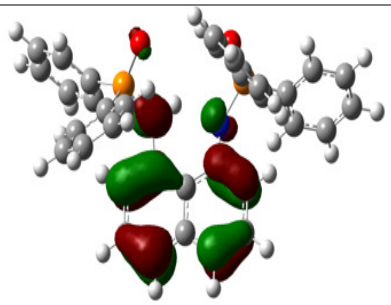
HOMO	HOMO
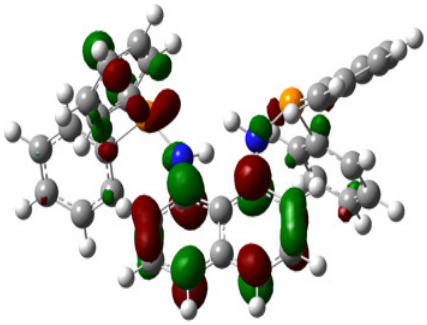	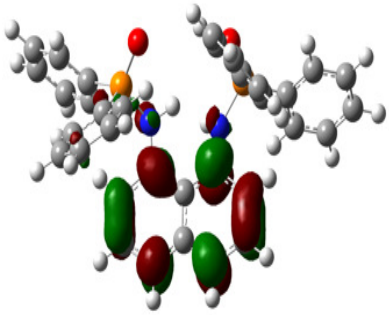
LUMO	LUMO

Figure 5.1.1.5. The geometry-optimized molecular structures and schematic MO diagram of ligands **(1)** and **(14)**, respectively. MO diagrams of one ligands are recorded vertically. The crystal structures of these ligand could not be isolated.

Figure 5.1.1.5 shows the environment of the electrons through the geometry-optimized molecular structures. Ligand **(1)** is used in the preparation of complexes **(3)**-**(5)** and **(10)**-**(12)** above, while ligand **(14)** is used to prepare **(19)**-**(22)**. The complexes prepared from **(14)** were not successfully in growing single crystals. Ligands **(1)** and **(14)** were compared to gain a better understanding on the effect of the P(III)-N bond compared to the P(V)-N bond in complexes. Ligand **(1)** have HOMO located on the naphthalene and the LUMO on both the naphthalene and lone pair of the P-donor atoms. Ligand **(14)** shows the HOMO/ LUMO on the naphthalene rings. Introduction of oxygen on ligand **(1)** did not change the distribution of the electron density on the molecule **(14)**.

The distribution of the electrons on **(1)** compared to **(3)**-**(5)** and **(10)**-**(11)** was similar, except on **(12)**. The HOMO of **(1)** and **(12)** are different. For **(1)** the HOMO was located on naphthalene and on **(12)** shared amongst the Ag_4I_4 unit This also indicated that stair-case type complexes typically luminesces better compared to cubanes, except that with the present complexes the luminescence got quenched.

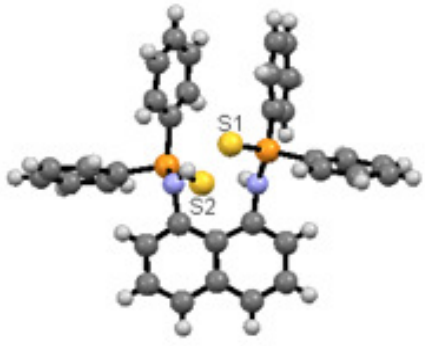

Ligand (15)

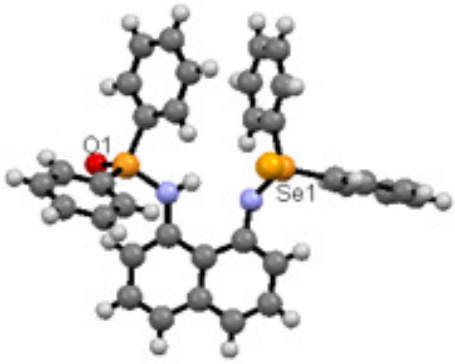

Ligand (16)

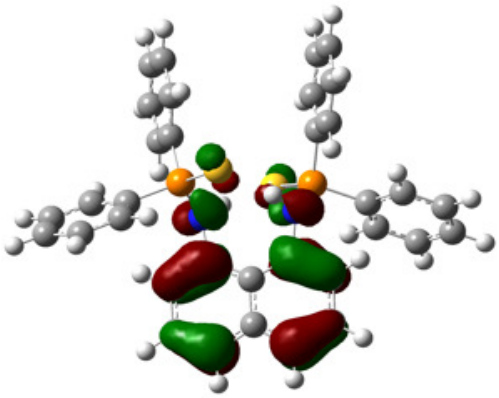

HOMO

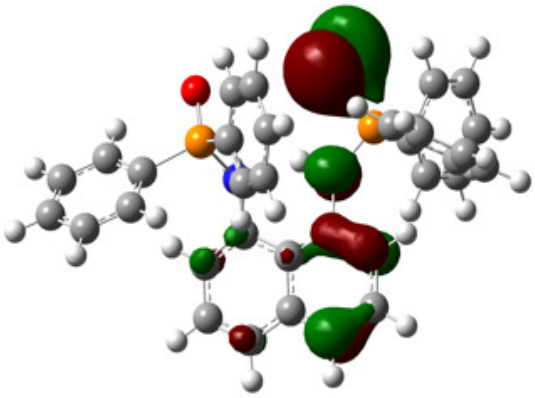

HOMO

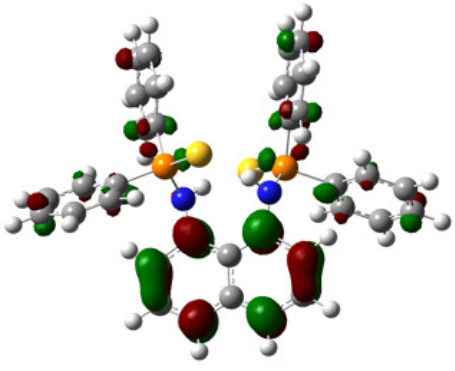

LUMO

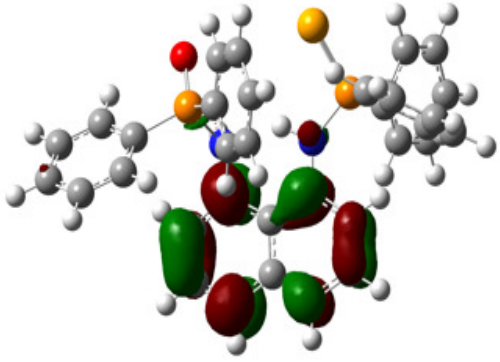

LUMO

Figure 5.1.1.6. The geometry-optimized molecular structures and schematic MO diagram of ligands **(15)**-**(16)**, respectively. MO diagrams of one ligands are recorded vertically.

The MO orbital diagrams of ligand **(15)** in Figure 5.1.1.6 is the same as that of **(1)** and **(14)**. Complex **(15)** illustrates a similar behaviour shown by **(1)** on **(3)**-**(5)** and **(10)**-**(12)**. The HOMO/ LUMO on **(15)** is arranged in the same way as its complexes **(17)** and **(18)**. The Se-atom in **(16)** appears to be more electron rich compared to the O-atom attached on the adjacent P-atoms.

The MO diagrams all represented molecules in the section showed that in most of the complexes, the photoluminescent properties could not have occurred due to a mix of HOMO/ LUMO excitation states which reduced movement of electrons from the ligands to the metal centers.

Table 5.1.1.2. DFT Calculated Orbital Energies[a] (in eV) of the HOMO and LUMO levels in complexes **(10)-(12)** as well as their energy difference (ΔE_{H-L}).

Compounds	**10**	**11**	**12**
$\mathbf{E_{HOMO\ (eV)}}$	-5.10408	-4.97216	-3.90701
$\mathbf{E_{LUMO\ (eV)}}$	-1.01456	-1.04067	-1.38693
$\mathbf{E_{HOMO\text{-}LUMO\ (eV)}}$	4.08952	3.931488	2.52008

[a]B3LYP/def2-SV(P) HOMO and LUMO orbital energies (in eV, 1 eV ≙ 8067 cm^{-1}) at the ground-state geometry.

Table 5.1.1.3. DFT Calculated Orbital Energies[a] (in eV) of the HOMO and LUMO levels in complexes **(17)** and **(18)** as well as their energy difference (ΔE_{H-L}).

Compounds	**17**	**18**
$\mathbf{E_{HOMO\ (eV)}}$	-4.06531	-4.78557
$\mathbf{E_{LUMO\ (eV)}}$	-3.732384	-1.42637
$\mathbf{E_{HOMO\text{-}LUMO\ (eV)}}$	7.797696	3.3592

[a]B3LYP/def2-SV(P) HOMO and LUMO orbital energies (in eV, 1 eV ≙ 8067 cm^{-1}) at the ground-state geometry.

The HOMO-LUMO gap is the molecular equivalent to the band gap in bulk materials. It refers to the potential energy difference between the highest occupied molecular orbital (HOMO) and the lowest unoccupied molecular orbital (LUMO).

Table 5.1.1.4. DFT calculated orbital energies[a] (in eV) of the HOMO and LUMO levels in complexes **(1)** and **(14)-(16)** as well as their energy difference (ΔE_{H-L}).

Compounds	E_{HOMO} (eV)	E_{LUMO} (eV)	$E_{HOMO-LUMO}$ (eV)
1	-4.90144	-0.76051	4.140928
14	-5.20962	-0.95717	4.252448
15	-5.11877	-1.16661	3.95216
16	-5.46856	-1.14784	4.32072
▪	-4.89845	-1.25256	3.645888

[a]B3LYP/def2-SV(P) HOMO and LUMO orbital energies (in eV, 1 eV ≙ 8067 cm^{-1}) at the ground-state geometry. ▪ The selenium version of compound **(15)**.

Tables 5.1.1.2-3 shows the energy gaps required to stabilize the HOMO/LUMO of the molecules. The ligands and complexes have similar large energy gaps ~4eV, except **(12)** with a gap of ~2eV. The larger band gap shows that it is not possible to excite the molecules.

The MO orbital diagrams of the compounds that consist of amines and phosphines have been reported.[27, 28] Literature describes the copper-iodide characters to be similar to Ag-iodine species. This shows that the absorption bands in the UV-Vis regions can be ascribed to the π···π* of the naphthalene moiety and not the transitions within the cluster units. The M···M also contributes in the length of the band gap as reported.[29] The DFT also showed that the molecular structures have an inductive-resonance effect. The amine groups behaved as an electron withdrawing moiety by inductive effect and electron donating moiety *via* the lone pairs by positive resonance effect, making the resonance effect stronger than the negative inductive effect. The overall net results is that the NH_2 group donates electrons more to the naphthalene moiety rather than the P-donor atom of the phosphine. The involvement of the halogens in the complexes proved that the idea of inductive effect is stronger than the resonance effect. There are no delocalization of electrons around the halogens and hence no activity in the core units of the structures. All the electron densities are channeled to the naphthalene.

To further understand the information of the ligands and complexes provided by the molecular orbital (MO) calculations on the modelled compounds, the P(III)-N bonds of the models were compared along with single crystal X-ray structures. The bonding in aminophosphines which

contain P(III)-N bonds made of trivalent P–N species, was to describe the environment of the P-N bonds. With a lone pair on each of the donor atoms, they are anticipated to undertake a pyramidal geometry with a two-electron covalent bond (single bond) between N- and P-donor atoms and the lone pair resided in a more or less an *sp*3 hybridized orbital. The MO diagrams have revealed a very different and an interesting pictorial bonding nature. The study propose explanations regarding the shortened P-N bonds and planar to near-planar geometry around N-donor atoms: (a) π-bond formation [$N_{p\pi} \rightarrow P_{d\pi}$] involving nitrogen lone pair of electrons and a vacant phosphorus *d*-orbital, (b) electron transfer from phosphorus to nitrogen (inductive electron release) promoted by the electronegativity difference between them and (c) negative hyperconjugative effect [n(N)$\rightarrow\sigma^*$(P-based)]. The three alternatives can take into account the possible influence of substituents on both phosphorus and nitrogen on the nature of the P–N bond. Examples which provide similar logical explanation to this are reported.[30, 31]

5.2 Electronic Properties and Luminescence of Perimidine Compounds

5.2.1 Results and discussion

5.2.1.1 Electronic Properties of Permidines

Theoretical calculations of compounds **(23)**-**(28)** and **(30)** using density functional theory (DFT) with functionals BP86 and B3LYP were investigated. The frontier orbitals for the investigations of the compounds are represented in Figure 5.2.1.1. The results of the frontier electronic levels in the ground state shed light on the nature of the excited states in the absorption spectra are reported in Table 5.2.1.1.

Table 5.2.1.1. DFT Calculated Orbital Energies[a] (in eV) of the HOMO and LUMO levels in compounds **(23)**-**(28)** as well as their energy difference (ΔE_{H-L}).

Compounds	**23**	**24**	**25**	**26**	**27**	**28**	**30**
$\mathbf{E}_{HOMO\ (eV)}$	-4.90443	-4.88594	-4.8979	-4.94306	-4.90362	-4.91558	-4.6833
$\mathbf{E}_{LUMO\ (eV)}$	-0.70883	-0.68299	-0.69931	-0.74446	-0.70774	-0.71835	-0.89542
$\mathbf{E}_{HOMO-LUMO}$ (eV)	4.1956	4.202944	4.198592	4.198592	4.195872	4.197232	3.787872

[a]B3LYP/def2-SV(P) HOMO and LUMO orbital energies (in eV, 1 eV ≙ 8067 cm^{-1}) at the ground-state geometry.

There is a similar trend observed for all seven compounds with the impact being more pronounced for HOMO than for LUMO. The HOMO is largely localized on the naphthalene than two amine (NH) groups. As shown in Table 5.2.1.1, the modification of the alkane group affect mainly the LUMO energies, whereas the HOMO energies remain stabilized around -4.91eV. The molecules are stabilized by the (ΔE_{H-L}) gap which is around ~4.19 (eV). The electron transition characters might have emerged due to π-π* stacking orbitals. The HOMO energies are occupied in position $\mathbf{C}_1$-$\mathbf{C}_2$ and $\mathbf{C}_7$-$\mathbf{C}_8$. The LUMO levels is basically localized on the ring occupied in the naphthalene on $\mathbf{C}_2$-$\mathbf{C}_3$ and $\mathbf{C}_5$-$\mathbf{C}_6$. The charge density distribution on the NH group decreases with an increase in alkane moiety and remain constant on one NH group when the molecule remain symmetrical. The methyl group is more electron donating than a hydrogen, and an ethyl group is more electron donating that a methyl group. The effect drops off with distance, and generally a pentyl group is considered no more donating than a butyl group. The reason a methyl group is more electron donating than a hydrogen is the carbon atom has a slightly higher electronegativity than hydrogen, polarizing the bond. This increased electron density near the carbon, which increases its electron donation positive inductive (I+) ability. The mechanism of a similar types of compounds formed was reported by Anga and co-workers[32] on the structural and mechanistic insights of substituted perimidine whereby a detailed experimental and computational study was done. The process proceed in two steps which involves a common transition state which take place through the lone pair attack by one nitrogen atom on the carbonyl carbon of the ketone and intermediate state which occurs as a result of the interaction between the involved amine and the carbonyl group of the ketone leading to the formation of a strong N-C covalent bond and proton transfer when the compounds get formed.

(23)	(24)
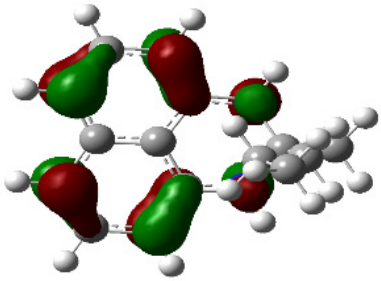	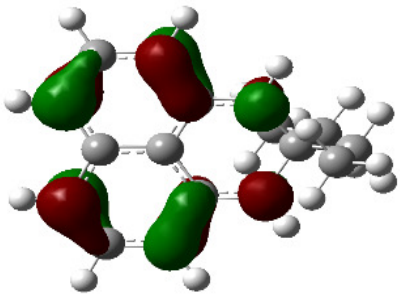
HOMO	HOMO
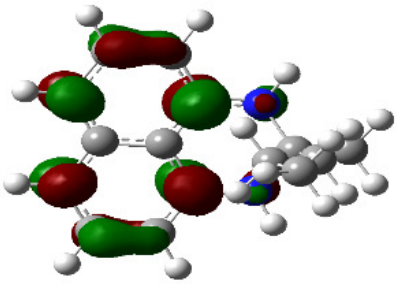	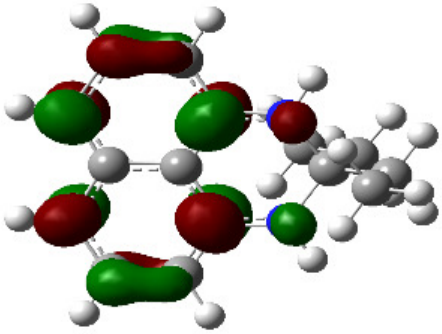
LUMO	LUMO
(25)	**(26)**
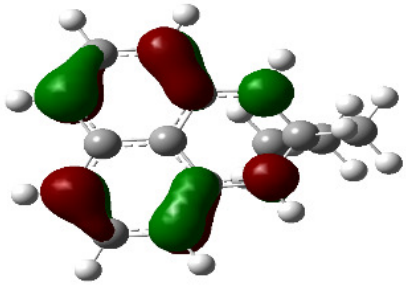	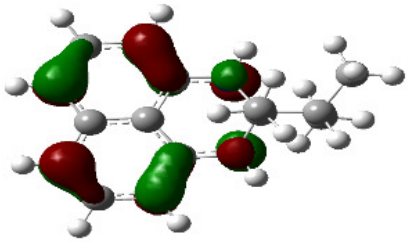
HOMO	HOMO
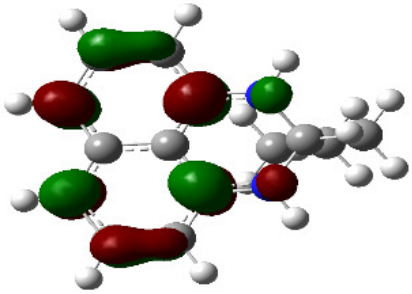	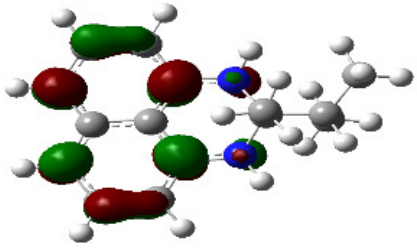
LUMO	LUMO

(27)	(28)
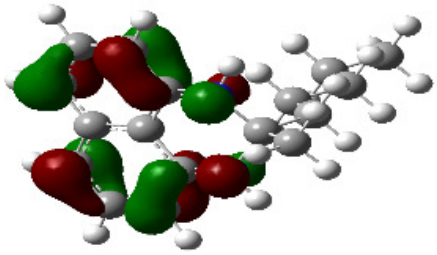	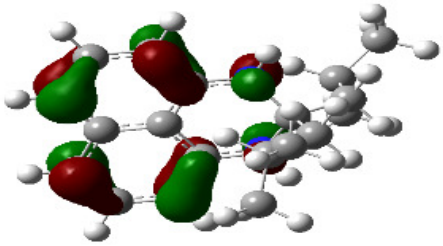
HOMO	HOMO
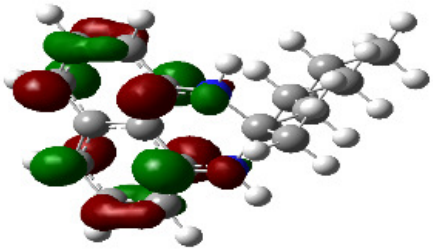	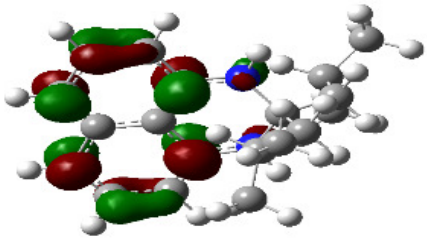
LUMO	LUMO
(30)	
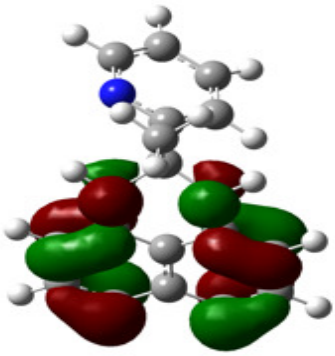	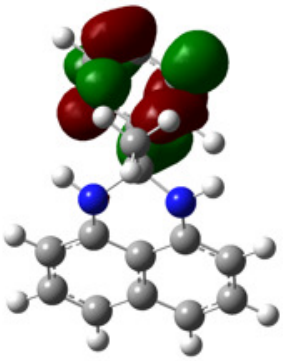
HOMO	LUMO

Figure 5.2.1.1. HOMO and LUMO frontier orbital plots of compounds **(23)**-**(28)** and **(30)** based on DFT calculations in the ground state. The localization of the HOMO (left), LUMO (center) and optimized molecular geometry of the compounds (right).

The frontier MO diagrams of **(30)** showed a different behavior to that of **(23)**-**(28)**. The HOMO of compound **(30)** are more located and localized around the naphthalene ring due to the π* orbitals, where the LUMO are distributed around the pyridinyl ring due to the π-orbitals around the N-atom. The MO also shows that the perimidines consists of nitrogen which have lone pairs that can play a role of π-systems of the molecules by transferring electron density from the heterocyclic ring moiety to the naphthalene rings.

5.3 Antimicrobial Studies of Bis(amino)phosphine and Perimidine Compounds

5.3.1 Background

Microorganisms such as viruses, bacteria, fungi, protozoa, etc. which exist in our environment may parasitize animals and humans. Bacteria such as *Micrococcus*, *Staphylococcus*, *Bacillus*, and *Pseudomonas* are naturally found in the environment. Bacteria enter human bodies through the eyes, nose, mouth, or urogenital openings, or through wounds or bites that breach the skin barrier and *via* contact. Some bacteria survive with humans and animals *via* mutualistic symbiotic relationship. Symbiotic refers to host-parasite relationship when both members benefit. For example bacteria, e.g. gut *Flora* and *Escherichia coli*, in the human intestines provide various vitamins which are important in the stimulation of specific immune responses. Nonetheless, many host-parasite relationships are dangerous and many microorganisms are pathogenic to human or animals. They cause various diseases initiating extensive morbidity and mortality. Diseases in humans or animals could cause upper respiratory tract infections (URTI) such as acute otitis media and sinusitis, lower respiratory tract infections (LRTI) such as pneumonia and bronchitis, skin and soft tissue infections (SSI), surgical wound infections (SWI), urinary tract infections (UTI), gastrointestinal tract infections, sexually transmitted diseases, endocarditis, septicaemia and sepsis, and Lyme disease. Discovery of penicillin led pharmaceutical companies to produce more than 100 antibacterial agents/antibiotics to fight a wide diversity of bacterial infections. The major classes of antibacterial agents are β-lactams which include (penicillins, cephalosporins, monobactams, carbapenems) aminoglycosides, tetracyclines, sulfonamides, macrolides (e.g. erythromycin), quinolones, and glycopeptides (e.g. vancomycin).

By the 1980s, with the use of antibacterial agents, improved sanitary conditions, and the extensive refrigeration of food, it was assumed that industrialized nations had won the war against pathogenic microbes.[33] However, in the past several years, the fast development of bacterial resistance to antibiotics has been detected. The wide use (and misuse) of antibiotics has provided powerful forces for the choice of microbes that either carried mutations conferring resistance or had the enhanced ability to mutate to resistance in the face of the antibiotic. Bacteria have mutated or have acquired new genes producing novel machinery to overcome the action of many antibiotics. Over the years, many new antibiotic-resistant strains have been

isolated from patients throughout the world. Development of bacterial resistance to a number of antimicrobial agents such as β-lactams antibiotics, macrolides, quinolones, and vancomycin is attracting a major universal health problem.[34, 35]

The vital problem in clinical practice is the increase in the isolation of methicillin-resistant *Staphylococcus aureus* (MRSA) strains. In addition to resistance to β-lactams antibiotic, multiply resistant MRSA are also resistant to macrolides, tetracyclines, aminoglycosides, and fluoroquinolones. Nowadays, the only active treatment for multiply resistant MRSA infections is vancomycin. The minimum inhibitory concentration (MIC) for vancomycin against some MRSA isolates has been increasing, leading to a condition where standard doses of vancomycin may not be effective for deep seated infections.[36]

There is a crucial need to develop new agents to treat patients infected with these multidrug resistant bacteria. Though antibacterial compounds have been recognised to a diverse group of intracellular compounds, the large majority of those that have been established into drugs are targeted to inhibit the synthesis of one or more components of the bacterial cell wall or to an event involved in macromolecular (DNA, RNA, or protein) biosynthesis.

Escherichia coli (known as *E. coli*) is a gram-negative, facultatively anaerobic, rod-shaped, coliform bacterium of the genus *Escherichia* that is commonly found in the lower intestine of warm-blooded organisms (endotherms).[37] Most *E. coli* strains are harmless, but some serotypes can cause serious food poisoning in their hosts.[38] The harmless strains are part of the normal flora of the gut, and can benefit their hosts by producing vitamin K_2. *Escherichia coli* is a common cause of life-threatening bloodstream infections[39, 40] and other common infections, like urinary tract infections. Antibiotic resistance rates in *E. coli* are rapidly rising, particularly with regard to fluoroquinolones and third- and fourth-generation cephalosporins. Amazingly, most of these multidrug-resistant strains are attained in the community rather than in healthcare settings[41, 42]

Drug-resistant *E. coli* are freely acquired *via* the diet such as food and water, and there is a major turnover of drug-resistant *E. coli* each day. When people eat sterile food, there is a rapid and substantial fall in the numbers of drug-resistant *E. coli* these people carry[43]. What remains unclear is where the drug-resistant *E. coli* in our food are coming from. Are they mainly human strains that contaminate our resources, e.g. food and water, or are these strains mainly derived from food animals? *Staphylococcus aureus* is anon pathogenic gram positive, round-shaped bacterium that is a member of the Firmicutes. It is found in the nose, respiratory tract, and on

the skin. *S. aureus* is a common cause of skin infections such as a skin abscess, respiratory infections such as sinusitis, and food poisoning.[44] *Klebsiella pneumoniae* is similar to *Escherichia coli* except that this bacteria is naturally found in the soil and it's pathogenic.[45]

Literature shows limited information on the biological activities of aminophosphine compounds in general regarding these bacteria. Starosta *et al*, reported that aminophosphines complexes could be tested for antimicrobial studies and the result could be compared with those of other tested drugs or compounds. The screening of phosphines and copper(I) complexes for their *in-vitro* antibacterial and antifungal activity against *Escherichia coli*, *Pseudomonas aeruginosa*, *Staphylococcus aureus* strains and *Candida albicans* is an achievable study. Starosta *et al*., further showed that the copper complexes exhibit significant antibacterial activity against *Staphylococcus aureus* strains. The activity of 1,10-phenanthroline complexes is higher than 2,2'-bipyridine complexes.[46] These are monodentate complexes and reports on bidentate complexes are scarce.

The antibiotics were discovered in the 20th century and brought assistance to humans to begin fighting a large number of life threatening diseases.[47] Nearly a century later, extreme and unselective usage of antibiotics has led to the rise of multiple drug resistant (MDR) bacterial strains.[48] The need to develop new approaches to fight these MDR strains "kicking off" to assist reducing the escalating mortality rate cause by these infectious diseases.[49, 50]. It is relevant to highlight that of all the infectious diseases, at least 65 % are linked to the bacterial communities which multiply by forming biofilms i.e. is any group of microorganisms in which cells stick to each other and often these cells adhere to a surface. These adherent cells are frequently embedded within a self-produced matrix of extracellular polymeric substance (EPS).[51] Bacterial behaviour within biofilms is regulated by the phenomenon of quorum sensing (QS), where bacteria release chemical signals and express virulence genes in a cell density dependent manner.[52-55] In simple terms, QS is a system of stimuli and response correlated to population density. Many species of bacteria use quorum sensing to coordinate gene expression according to the density of their local population.

Bacteria act as single cellular organisms at low cell densities; but they may change their behaviour to 'multicellular' type by sensing that their population density has reached a threshold level. Thereafter, they communicate through small signalling molecules, which

enable them to express genes for different phenotypes, especially those responsible for their infectious behaviour. Cunning pathogens like *Pseudomonas aeruginosa* prefer to lie "dormant" and defer their virulent phenotype until their population size has grown large enough to overpower the host's defence mechanisms. This phenomenon termed as bacterial QS operates through a wide range of signals such as: (I) Oligopeptides (5–10 amino acid cyclic thiolactone), (II) N-acyl homoserine lactones (AHLs), (III) Furanosyl borate (Autoinducer-2, AI-2), (IV) Hydroxyl-palmitic acid methylester, and (V) Methyl dodecanoic acid.[56, 57] The two most widely studied QS signals are: (1) (AHLs) produced by more than 70 species of Gram-negative bacteria, which diffuse across the cell membrane and bind to regulatory proteins within the cell and (2) peptide based QS system in Gram-positive bacteria, which operate through membrane bound receptor histidine kinases.[55, 58] QS-based bacterial behaviours have great economic impacts in food spoilage, aquaculture, water purification, ship industry, etc.[59-62]

Determinations to disrupt biofilms have allowed the identification of molecules produced by prokaryotes and eukaryotes with abilities to quench the QS system, termed as quorum quenching (QQ). The different mechanisms are used to disrupt QS: (1) reducing the activity of AHL cognate receptor protein or AHL synthase, (2) inhibiting the production of QS signal molecules, (3) degradation of the AHL, and (4) imitating the signal molecules primarily by using synthetic compounds as analogues of signal molecules. The enzymatic degradation of QS signal molecules (AHLs) has been appreciated and applied the most in controlling bacteria.[63-65] Antibodies and decoy receptors to inhibit QS signals have been suggested as a novel approaches for anti-infective therapy. Furthermore, synthetic compounds have also been found to be effective in regulating QS.[66-69] These quorum sensing inhibitors (QSIs) can competitively inhibit QS signalling system, providing an chance to develop new drugs against these targets to fight pathogens.[70, 71]

Structure Activity Relationships (SAR) studies give understandings to the molecular properties triggering receptors affinity and selectivity. The behavioural nature of the compounds may be ascribed to the substitutions at the hydrophobic domain. The perimidines structure had electron withdrawing and donating groups at the *ortho*, *meta* and *para* position of the hydrophobic aryl ring. The substituted derivatives of perimidines are more active than the other derivatives due to fact that the substituted derivatives are better fitted into the receptor site. Figure 5.3.1.1,

shows a comprehensive explanation of the pioneering experiments of the important core fragments of perimidines. These are defined by presence of hydrogen donor/acceptor unit (HAD), hydrophobic domain (A) (aryl ring substituted/unsubstituted) and electron donor atom (D). These common features were found in the structures of well-established pyrimidine drugs.[72, 73]

Figure 5.3.1.1, is a perimidinyl structure showing SAR of the compound. The substitution of a five membered saturated heterocyclic ring leads to anticancer and antiviral activities. Position B shows that insertion of a substituent on C-2 of a six or five membered saturated heterocyclic ring leads to anthelmintic, antiparkinsonism expectorant and treatment of growth inhibition (GI) disturbance and peripheral neuropathies. Position B of C-2 and C-4 indicates that keto group substitution or amino substitution or mixed keto, amino groups' substitution leads to anticancer, antiviral, antibacterial, antifungal, and treatment of respiratory tract infection and liver disorder. Position C of C-5 shows that insertion of halogen or substituted amine or saturated distal heterocyclic ring leads to antibacterial and anticancer activities. Position D arrows point to C-5 and C-6 showing that heterocyclic ring and *o*, *m*, *p* substituted distal aryl ring substitution leads to anticancer, antiviral, antibacterial, vasodilation and treatment of urinary tract infection

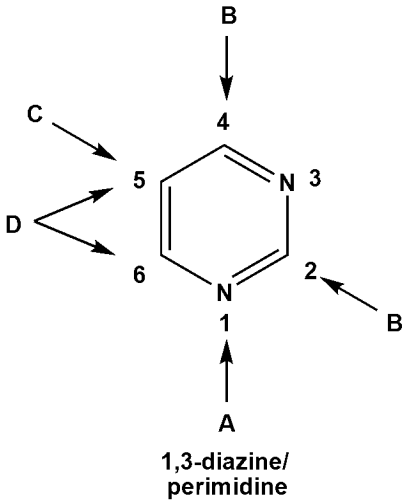

Figure 5.3.1.1. Structure activity relationships of perimidines.[74]

5.3.2 Evaluation of Antimicrobial Activity by Agar-Well Diffusion Assay

Compounds **(1)**-**(33)** were subjected to antibacterial screening using the agar-well diffusion method (CLSI, 2012). Stock solutions of compounds **(1)**-**(33)** (25 mg) were prepared in DMSO (1 mL). Four Gram-negative (*Chromobacterium violaceum* ATCC 12472, *Escherichia coli* ATCC 25922, *E. coli* ATCC 35218, and *Pseudomonas aeruginosa* ATCC 27853) and two Gram-positive (*Staphylococcus aureus* ATCC 29213 and *S. aureus* ATCC 43300) bacterial isolates, grown overnight on TSA agar plates, were re-suspended in sterile distilled water and the turbidity of cell suspensions adjusted equivalent to that of a 0.5 McFarland standard. Inocula were used to swab Mueller-Hinton (MH) agar plates. Wells (6 mm) punched into the swabbed agar surface were loaded with 5 µL (125 µg), 10 µL (250 µg), 20 µL (500 µg) and 40 µL (1000 µg), respectively. Two standard antimicrobial agents (Oxoid, UK), i.e., ampicillin (AMP10, 10 µg per disc) and tetracycline (TE30, 30 µg per disc) as well as a negative control (DMSO-impregnated discs) were also assessed. The following zone diameter criteria were used to assign susceptibility or resistance to tested compounds: Susceptible (S) ≥ 15 mm, Intermediate (I) = 11-14 mm, and Resistant (R) ≤ 10 mm (Chenia, 2013)[75]. The criteria for assigning susceptibility or resistance to AMP10 was as follows: (S) ≥ 17 mm, (I) = 14–16 mm, (R) ≤ 13 mm, while those for TE30 were: (S) ≥ 19 mm, (I) = 15–18 mm, (R) ≤ 14 mm (CLSI, 2012).

5.3.3 Quorum Sensing (QS) Inhibition Assay

Seven compounds **(2)**, **(12)**, **(13)**, **(16)**, **(29)**, **(30)** and **(31)**, which had demonstrated quorum sensing inhibitory effects against *C. violaceum* ATCC 12472 in antimicrobial susceptibility assay, were evaluated for their anti-QS activity using the qualitative agar-overlay diffusion assay[75]. This assay employs the biomonitor strain, *C. violaceum* ATCC 12472. Molten Luria-Bertani (LB) agar (0.5% w/v, 5 mL) was inoculated with 50 µL of the violacein (purple pigment)-producing strain, *C. violaceum* 12472 grown overnight in LB broth at 30 °C with agitation. The agar-culture solution was then poured over the surface of pre-warmed LB agar plates. Varying volumes (5 µL, 125 µg; 10 µL, 250 µg; 20 µL, 500 µg and 40 µl, 1000 µg) were added to 6 mm wells punched into solidified agar plates, incubated overnight at 30 ºC and then examined for violacein production. A known anti-quorum sensing agent, (Z-)-4-bromo-5-(bromomethylene)-2(5H)-furanone (20 µg) was used as a QSI-positive control. The inhibition

of QS, indicated by a colourless, opaque but viable halo around the disc, was estimated by measuring the diameter of the transparent and opaque zones for growth inhibition (GI) and quorum sensing inhibition (QSI), respectively.

Testing:

The following bacteria were tested:

Sensitive *E. coli* and QC organism ATCC 25922

B-lactam resistant *E. coli* ATCC 35218

Multidrug resistant *P. aeruginosa*

Sensitive *S. aureus* ATCC 29213

Methicillin-resistant *S. aureus* ATCC 43300

1. ***Susceptible (S):*** A bacterial strain is said to be susceptible to a given antibiotic when it is inhibited *in-vitro* by a concentration of this drug that is associated with a high likelihood of therapeutic success.
2. ***Intermediate (I):*** The sensitivity of a bacterial strain to a given antibiotic is said to be intermediate when it is inhibited *in-vitro* by a concentration of this drug that is associated with an uncertain therapeutic effect.
3. ***Resistant (R):*** A bacterial strain is said to be resistant to a given antibiotic when it is inhibited *in-vitro* by a concentration of this drug that is associated with a high likelihood of therapeutic failure.

5.3.4 Results and Discussion

5.3.4.1 Preliminary Antimicrobial Activity of Bis(amino)phosphine and Perimidine Compounds

The antimicrobial results are shown in Table 5.3.1.1, Table 5.3.1.2 and Table 3.3.1.3 for compounds **(1)**-**(33)**. All compounds shows better activity against *C.violaceum* ATCC 12472. *C.violaceum* ATCC 12472 is a sensitive organism and is only tested to identify a potential quorum sensing effect, not any antimicrobial activity. The compounds have shown positive quorum sensing effect against both Gram-positive and Gram-negative bacteria. There was limited antibacterial activity against Gram-negative *E.coli* and *P.aeruginosa,* Table 5.3.1.2. Compound **(2)** is the only promising candidate with antibacterial activity against sensitive *E.coli* ATCC 25922 at ≥ 500µg, compound **(13)**, susceptibility was observed at 100µg. For *E.coli* ATCC 35218, compound **(2)** was effective only at > 1000µg. Compound **(2)** was better than ampicillin in terms of its antibacterial activity. Compounds did not demonstrate any good antimicrobial activities against *P.aeruginosa* ATCC27853. Compounds shows weak activity against *E.coli 25922* and *E.coli* ATCC 35218, except compounds **(2)**, **(8)**-**(11)**, **(13)**, **(17)**, **(19)** and **(33)**.

Table 5.3.1.3 shows that twelve compounds demonstrated antibacterial properties against the sensitive *S.aureus* ATCC 29213, while nine compounds demonstrated antibacterial properties against the methicillin-resistant *S.aureus* ATCC 43300. Compounds **(25)** and **(26)** were most effective against *S.aureus* ARCC 29213 at 125µg, followed by compounds **(2)**, **(24)**, **(23)**, **(13)**, **(32)** and **(33)**. Compound **(2)** was effective against the MRSA strain, followed by compounds **(25)**, **(9)**, **(26)**, **(29)**, **(28)**, **(13)**, **(8)** and **(32)**. Compound **(2)** was effective against both sensitive and resistant *S. aureus* following exposure to ≥ 250µg. Compounds **(24)-(26)** are also promising in terms of their activity.

The compounds are divided into two categories, **(1)**-**(22)** are aminophosphines and **(23)**-**(33)** are perimidines. The results in Table 5.3.1.1, Table 5.3.1.2 and 5.3.1.3 indicates that incorporation of halides and different d^{10} coinage metal centers [Cu(I) and Ag(I)] into an aminophosphine ligands **(1)** and **(2)** increases activity in Gram-positive bacteria, see Table 5.3.1.3, while the activity reduces in Gram-negatives bacteria, see Table 5.3.1.1 and Table 5.3.1.2. The promising results were observed for compound **(2)** due to the incorporation of the isopropyphosphine moiety into the diaminonaphthalene. Ligand **(1)** is inactive against bacteria strains compared to ligand **(2)**. Incorporation of chalcogenides into ligand **(1)** influences the behaviour of compounds activities towards two different bacteria stains. Compounds **(17)**–**(21)** shows activity against Gram negative *C.violanceum* ATCC 12472 and *E.coli* 25922, but the same compounds are inactive against *S.aureus* ATCC 29213 and *S.aureus* ATCC 43300. In comparison, the Ag(I) complexes showed high antibacterial activity against Gram-negative bacteria than the Cu(I) complexes, see Table 5.3.1.1. Table 5.3.1.3 showed that the Cu(I) complexes have high antimicrobial activities against Gram-positive bacteria compare to Ag(I) complexes.

Perimidine compounds (**23)-(28)** consisted of alkyl substituent groups, **(29)** co-crystallization of *1,8*-diaminonaphthalene and 1,1′-diacetylferrocene, **(30)** consisted of aryl pyridinyl substituent group and **(31)-(33)** are Ni(II), Zn(II) and Cd(II) metal complexes of **(30)**. The results showed that the perimidines do not inhibit bacterial growth against Gram-negative bacteria, but they inhibit the growth of Gram-positive bacteria. Surprisingly, compound **(30)** on its own shows no activity at all against both Gram-negative and Gram-positive bacteria. In addition, the presence metal centers like Ni(II), Zn(II) and Cd(II) that are incorporated in ligand **(30)** increases the antimicrobial activity against Gram-positive bacteria. The same metal complexes shows no activity on Gram-negative bacteria.

Table 5.3.1.1. The activity of compounds **(1)**-**(33)** against Gram-negative bacteria.

	***C. violaceum ATCC* 12472**				***E. coli* 25922**			
Sample	**125**	**250**	**500**	**1000**	**125**	**250**	**500**	**1000**
1	-	-	-	-	-	-	-	-
2	-	-	-	-	-	11(I)	15(S)	22(S)
3	-	-	-	-	-	-	-	-
4	-	-	-	-	-	-	-	-
5	-	-	-	-	-	-	-	-
6	14(I)	14(I)	16(S)	18(S)	-	-	-	-
7	-	-	-	11(I)	-	-	-	-
8	-	-	11(I)	14(I)	-	-	-	-
9	-	-	-	12(I)	-	-	-	9(R)
10	-	10(I)	11(I)	14(I)	-	-	-	11(I)
11	-	-	-	-	-	-	-	10(R)
12	-	-	-	-	-	-	-	-
13	-	12(I)	25(S)	-	-	-	-	20(S)
14	-	-	-	-	-	-	-	-
15	-	-	-	-	-	-	-	-
16	-	-	-	-	-	-	-	-
17	11(I)	11(I)	11(I)	15(S)	-	-	-	-
18	-	12(I)	12(I)	14(I)	-	-	-	
19	11(I)	12(I)	15(S)	16(S)	-	-	10(R)	12(I)
20	-	-	-	-	-	-	-	-
21	-	-	-	11(I)	-	-	-	-
22	-	-	-	-	-	-	-	-
23	-	-	-	-	-	-	-	-
24	-	-	-	-	-		-	-
25	-	-	-	-	-	-	-	-
26	-	-	-	-	-	-	-	-
27	-	-	-	-	-	-	-	-
28	-	-	-	14(I)	-	-	-	-
29	-	-	-	-	-	-	-	-
30	-	-	-	-	-	-	-	-
31	-	-	-	-	-	-	-	-
32	-	-	-	-	-	-	-	-
33	-	-	-	-	-	-	-	13(I)
DMSO	-	-	-	-	-	-	-	-
Ampicillin			Not tested				20(S)	
(AMP10)-10µg								
Ciprofloxacin (CIP5)-5µg			Not tested				35(S)	
Tetracycline (TE30)-30µg			Not tested				27(S)	

Table 5.3.1.2. The activity of compounds **(1)**-**(33)** against Gram-negative bacteria.

	***E. coli* ATCC 35218**				***P. aeruginosa ATCC 27853***			
Sample	**125**	**250**	**500**	**1000**	**125**	**250**	**500**	**1000**
1	-	-	-	-	-	-	-	-
2	-	-	-	16(S)	-	-	-	-
3	-	-	-	-	-	-	-	-
4	-	-	-	-	-	-	-	-
5	-	-	-	-	-	-	-	-
6	-	-	-	-	-	-	-	-
7	-	-	-	-	-	-	-	-
8	-	-	-	10(R)	-	-	-	-
9	-	-	-	11(I)	-	-	-	-
10	-	-	-	-	-	-	-	-
11	-	-	-	-	-	-	-	-
12	-	-	-	-	-	-	-	-
13	-	-	-	10(R)	-	-	-	-
14	-	-	-	-	-	-	-	-
15	-	-	-	-	-	-	-	-
16	-	-	-	-	-	-	-	-
17	-	-	10(R)	12(I)	-	-	-	10(R)
18	-	-	-	-	-	-	-	-
19	-	-	-	11(I)	-	-	-	-
20	-	-	-	-	-	-	-	-
21	-	-	-	-	-	-	-	-
22	-	-	-	-	-	-	-	-
23	-	-	-	-	-	-	-	-
24	-	-	-	-	-		-	-
25	-	-	-	-	-	-	-	-
26	-	-	-	-	-	-	-	-
27	-	-	-	-	-	-	-	-
28	-	-	-	-	-	-	-	-
29	-	-	-	-	-	-	-	-
30	-	-	-	-	-	-	-	-
31	-	-	-	-	-	-	-	-
32	-	-	-	-	-	-	-	-
33	-	-	-	13(I)	-	-	-	-
DMSO	-	-	-	-	-	-	-	-
Ampicillin			0(R)				0(S)	
(AMP10)-10µg								
Ciprofloxacin (CIP5)-5µg			30(S)				35(S)	
Tetracycline (TE30)-30µg			23(S)				15(I)	

Table: 5.3.1.3. The activity of compounds **(1)-(33)** against Gram-positive bacteria.

	***S. aureus* ATCC 29213**				***S. aureus* ATCC 43300**			
Sample	125	250	500	1000	125	250	500	1000
1	-	-	-	-	-	-	-	-
2	14(I)	18(S)	24(S)	26(S)	14(I)	18(S)	20(S)	26(S)
3	-	-	-	14(I)	-	-	-	-
4	-	-	12(I)	14(I)	-	-	-	-
5	-	-	-	-	-	-	-	12(I)
6	-	-	9(R)	9(R)	-	-	-	-
7	-	-	-	-	-	-	-	-
8	-	-	10(R)	15(S)	-	-	10(R)	15(S)
9	-	-	-	9(R)	-	-	15(S)	17(S)
10	-	-	-	12(I)	-	-	-	-
11	-	-	-	-	-	-	-	-
12	-	-	-	-	-	-	-	-
13	-	9(R)	14(I)	19(S)	-	-	12(I)	15(S)
14	-	-	-	-	-	-	-	-
15	-	-	-	-	-	-	-	-
16	-	-	-	9(R)	-	-	-	-
17	-	-	-	11(I)	-	-	-	-
18	-	-	-	-	-	-	-	
19	-	-	-	-	-	-	-	-
20	-	-	-	-	-	-	-	14(I)
21	-	-	-	-	-	-	-	-
22	-	-	-	-	-	-	-	-
23	10(R)	14(I)	15(S)	18(S)	-	-	-	-
24	14(I)	16(S)	17(S)	20(S)	10(R)	12(I)	16(R)	16(R)
25	16(S)	18(S)	20(S)	23(S)	-	14(I)	17(S)	20(S)
26	17(S)	19(S)	21(S)	24(S)	12(I)	14(I)	15(S)	17(S)
27	10(R)	11(I)	12(I)	16(S)			10(R)	10(R)
28		13(I)	14(I)	16(S)		11(I)	13(I)	15(S)
29	-	-	-	-	-	-	-	-
30	-	-	-	-	-	-	-	-
31	-	-	-	12(I)	-	-	-	-
32	-	-	11(I)	16(S)	-	-	-	15(S)
33	-	-	13(I)	15(S)	-	-	-	-
DMSO	-	-	-	-	-	-	-	-
Ampicillin			25(S)				20(S)	
(AMP10)-10µg								
Ciprofloxacin (CIP5)-5µg			27(S)				28(S)	
			28(S)				36(S)	
Tetracycline (TE30)-30µg								

5.4 References

1. R. F. W.Bader, *Atoms in Molecules: A Quantum Theory; Oxford University Press: New York*, 1994.
2. P. Coppens, *X-ray Charge Densities and Chemical Bonding; Oxford University Press: New York*, 1997.
3. J. Oddershede and S. Larsen, *J. Phys. Chem. A*, 2004, 108, 1057-1063.
4. T. Nowlin and K. Cohn, *Inorg. Chem.*, 1971, 10, 2801-2803.
5. G. TerHaar, M. A. Fleming and R. W. Parry, *J. Am. Chem. Soc.*, 1962, 84, 1767-1767.
6. M. Bennett and T. Turney, *Aust. J. Chem.*, 1973, 26, 2335-2348.
7. E. D. Morris Jr and C. Nordman, *Inorg. Chem.*, 1969, 8, 1673-1676.
8. R. Peng, M. Li and D. Li, *Coord. Chem. Rev.*, 2010, 254, 1-18.
9. R. Peng, S.-R. Deng, M. Li, D. Li and Z.-Y. Li, *CrystEngComm*, 2008, 10, 590-597.
10. G. Hattori, K. Sakata, H. Matsuzawa, Y. Tanabe, Y. Miyake and Y. Nishibayashi, *J. Am. Chem. Soc.*, 2010, 132, 10592-10608.
11. S. Diez-Gonzalez, E. C. Escudero-Adan, J. Benet-Buchholz, E. D. Stevens, A. M. Z. Slawin and S. P. Nolan, *Dalton Transactions*, 2010, 39, 7595-7606.
12. K. Tsuge, *Chem. Lett.*, 2013, 42, 204-208.
13. D. Volz, D. M. Zink, T. Bocksrocker, J. Friedrichs, M. Nieger, T. Baumann, U. Lemmer and S. Brase, *Chem. Mater.*, 2013, 25, 3414-3426.
14. D. M. Zink, D. Volz, T. Baumann, M. Mydlak, H. Flugge, J. Friedrichs, M. Nieger and S. Brase, *Chem. Mater.*, 2013, 25, 4471-4486.
15. F. Endrizzi, P. Di Bernardo, P. L. Zanonato, F. Tisato, M. Porchia, A. Ahmed Isse, A. Melchior and M. Tolazzi, *Dalton Trans.*, 2017, 46, 1455-1466.
16. A. H. Cowley, D. J. Mitchell, M.-H. Whangbo and S. Wolfe, *J. Am. Chem. Soc.*, 1979, 101, 5224-5231.
17. I. G. Csizmadia, A. H. Cowley, M. W. Taylor and S. Wolfe, *J. Chem. Soc., Chem. Commun.*, 1974, 432-433.
18. A. H. Cowley, *Phosphorus Sulfur Silicon Relat. Elem.*, 1976, 2, 283-300.
19. A. D. Becke, *J. Chem. Phys.*, 1993, 98, 5648-5652.
20. C. Lee, W. Yang and R. G. Parr, *Phys. Rev. B*, 1993, 37, 785–789.
21. P. J. Hay and W. R. Wadt, *J. Chem. Phys*, 1985, 82, 299-310.
22. W. R. Wadt and P. J. Hay, *J. Chem. Phys.*, 1985, 82, 284-298.
23. P. J. Hay and W. R. Wadt, *J. Chem. Phys.*, 1985, 82, 270-283.
24. J. D. T. H. and P. J. Hay, *In Methods of Electronic Structure Theory; Schaefer, H. F., III, Ed.; Modern Theoretical Chemistry; Plenum: New York*, 1977, 3, 1-28.
25. M. Wallesch, D. Volz, D. M. Zink, U. Schepers, M. Nieger, T. Baumann and S. Bräse, *Chem. Eur. J.*, 2014, 20, 6578-6590.
26. D. Volz, M. Nieger, J. Friedrichs, T. Baumann and S. Brase, *Inorg. Chem. Commun.*, 2013, 37, 106-109.
27. P. Aslanidis, P. Cox, S. Divanidis and A. C. Tsipis, *Inorg. Chem.*, 2002, 41, 6875-6896.
28. M. Vitale, C. K. Ryu, W. E. Palke and P. C. Ford, *Inorg. Chem.*, 1994, 33, 561-566.
29. V. W.-W. Yam and K. K.-W. Lo, *Chem. Soc. Rev.*, 1999, 28, 323-334.
30. I. Csizmadia, A. Cowley, M. Taylor, L. M. Tel and S. Wolfe, *J. Chem. Soc., Chem. Commun.*, 1972, 1147-1148.
31. A. Cowley and J. Schweiger, *J. Chem. Soc. D*, 1970, 1492-1493.
32. S. Anga, S. Biswas, R. K. Kottalanka, B. S. Mallik and T. K. Panda, *Can Chem Trans.*, 2014, 2, 72-82.
33. D. T. W. Chu, J. J. Plattner and L. Katz, *J. Med. Chem.*, 1996, 39, 3853-3874.
34. E. Rubinstein, *Science*, 1994, 264, 360-393.
35. M. L. Cohen, *Trends in microbiology*, 1994, 2, 422-425.

36. *Major Unmet Needs in Bacterial Infection Therapy. Infectious Disease, A Pharmacor Service*, 1992.
37. P. S. Singleton, *Bacterias: en biología, biotecnología y medicina/Bacteria in biology, biotechnology and medicine*, Acribia, 1999.
38. R. L. Vogt and L. Dippold, *Public health reports*, 2005, 120, 174-178.
39. S. Hudault, J. Guignot and A. Servin, *Gut*, 2001, 49, 47-55.
40. K. J. Kennedy, J. L. Roberts and P. J. Collignon, *Med. J. Aust.*, 2008, 188, 209-213.
41. K. B. Laupland, D. L. Church, J. Vidakovich, M. Mucenski and J. D. Pitout, *J. Infect.*, 2008, 57, 441-448.
42. R. J. Mesa, V. Blanc, A. R. Blanch, P. Cortés, J. J. González, S. Lavilla, E. Miro, M. Muniesa, M. Saco and M. T. Tórtola, *J. Antimicrob. Chemother.*, 2006, 58, 211-215.
43. J. R. Johnson, J. S. McCabe, D. G. White, B. Johnston, M. A. Kuskowski and P. McDermott, *Clinical Infectious Diseases*, 2009, 49, 195-201.
44. M. Masalha, I. Borovok, R. Schreiber, Y. Aharonowitz and G. Cohen, *J. Bacteriol.*, 2001, 183, 7260-7272.
45. M. H. Kifle and M. D. Laing, *Frontiers in plant science*, 2016, 6, 1225.
46. R. Starosta, F. Magdalena, J. Kro´l, M. Puchalskaa and A. Kochela, *New J. Chem.*, 2010, 34, 1441-1449.
47. V. C. Kalia, A. Rani, S. Lal, S. Cheema and C. Raut, *Expert Opin Drug Discov.*, 2007, 2, 211-224.
48. N. Bagge, M. Hentzer, J. B. Andersen, O. Ciofu, M. Givskov and N. Høiby, *Antimicrob. Agents Chemother.*, 2004, 48, 1168-1174.
49. T. Bjarnsholt, P. Ø. Jensen, T. B. Rasmussen, L. Christophersen, H. Calum, M. Hentzer, H.-P. Hougen, J. Rygaard, C. Moser and L. Eberl, *Microbiology*, 2005, 151, 3873-3880.
50. T. B. Rasmussen, T. Bjarnsholt, M. E. Skindersoe, M. Hentzer, P. Kristoffersen, M. Köte, J. Nielsen, L. Eberl and M. Givskov, *J. Bacteriol.*, 2005, 187, 1799-1814.
51. K. Lewis, *Nature Rev. Microbiol.*, 2007, 5, 48-56.
52. N. Bhargava, P. Sharma and N. Capalash, *Crit. Rev. Microbio.*, 2010, 36, 349-360.
53. M. B. Miller and B. L. Bassler, *Annu. Rev. Microbiol.*, 2001, 55, 165-199.
54. M. Romero, L. Acuña and A. Otero, *Recent Pat Biotechnol.*, 2012, 6, 2-12.
55. C. M. Waters and B. L. Bassler, *Annu. Rev. Cell Dev. Biol.*, 2005, 21, 319-346.
56. Y.-H. Dong and L.-H. Zhang, *J. Microbiol.*, 2005, 43, 101-109.
57. D. McDougald, S. A. Rice and S. Kjelleberg, *Anal. Bioanal. Chem*, 2007, 387, 445-453.
58. N. Amara, B. P. Krom, G. F. Kaufmann and M. M. Meijler, *Chem. Rev.*, 2010, 111, 195-208.
59. M. S. Ammor, C. Michaelidis and G.-J. E. Nychas, *J. Food Prot.*, 2008, 71, 1510-1525.
60. E. Martinelli, M. Suffredini, G. Galli, A. Glisenti, M. E. Pettitt, M. E. Callow, J. A. Callow, D. Williams and G. Lyall, *Biofouling*, 2011, 27, 529-541.
61. M. Schultz, J. Bendick, E. Holm and W. Hertel, *Biofouling*, 2011, 27, 87-98.
62. P. N. Skandamis and G.-J. E. Nychas, *Appl. Environ. Microbiol.*, 2012, 78, 5473-5482.
63. V. C. Kalia and H. J. Purohit, *Crit. Rev. Microbiol.*, 2011, 37, 121-140.
64. V. A. Dembitsky, A. A. Quntar and M. Srebnik, *Chem. Rev.*, 2011, 111, 209-237.
65. G. F. Kaufmann, R. Sartorio, S.-H. Lee, J. M. Mee, L. J. Altobell, D. P. Kujawa, E. Jeffries, B. Clapham, M. M. Meijler and K. D. Janda, *J. Am. Chem. Soc.*, 2006, 128, 2802-2803.
66. G. D. Geske, R. J. Wezeman, A. P. Siegel and H. E. Blackwell, *J. Am. Chem. Soc.*, 2005, 127, 12762-12763.
67. J. C. Janssens, H. Steenackers, S. Robijns, E. Gellens, J. Levin, H. Zhao, K. Hermans, D. De Coster, T. L. Verhoeven and K. Marchal, *Appl. Environ. Microbiol.*, 2008, 74, 6639-6648.
68. M. Rasch, T. B. Rasmussen, J. B. Andersen, T. Persson, J. Nielsen, M. Givskov and L. Gram, *J. Appl. Microbiol.*, 2007, 102, 826-837.

69. M. Rasch, C. Buch, B. Austin, W. J. Slierendrecht, K. S. Ekmann, J. L. Larsen, C. Johansen, K. Riedel, L. Eberl and M. Givskov, *Syst. Appl. Microbiol.*, 2004, 27, 350-359.
70. E. Drenkard, *Microb. Infect.*, 2003, 5, 1213-1219.
71. Z. Zeng, L. Qian, L. Cao, H. Tan, Y. Huang, X. Xue, Y. Shen and S. Zhou, *Appl. Microbiol. Biotechnol.*, 2008, 79, 119.
72. L. Bruno-Blanch, J. Galvez and R. Garcia-Domenac, *Bioorg. Med. Chem. Lett.*, 2003, 13, 2749-2754.
73. E. Estrada and A. Pena, *Bioorg. Med. Chem.*, 2000, 8, 2755-2770.
74. T. P. Selvam, C. R. James, P. V. Dniandev and S. K. Valzita, *Research in Pharmacy*, 2015, 2.
75. H. Y. Chenia, *Sensors*, 2013, 13, 2802-2817.

Chapter 6

Conclusion

6.1 Conclusion and Future Perspectives

6.1.1 Conclusion

This thesis reported on bis(amino)phosphine ligands **(15)** and **(16)** being isolated and characterized, by single crystal X-ray crystallography out of a series of five ligands. Ligands of the type $[C_{10}H_6(1,8\text{-}NHPR_2)_2]$ (R = Ph **(1)** and $(CH_3)_2(CH)_2$ **(2)**), and $[C_{10}H_6(1\text{-}NHPPh_2O)(8\text{-}NHPPh_2Se)]$ **(16)** were isolated as unstable air products in comparison to ligands $[C_{10}H_6(1,8\text{-}NHPPh_2E)_2]$ (E = O **(14)** and S **(15)**). The ligands gave satisfactory yields in the range (50**-**75%). The ^{31}P NMR spectroscopic analysis of the ligands gave a single peak which confirmed that the P-donor atoms were chemically equivalent in solution. The IR showed that the ligands absorption bands for the ν(NH), ν(C=C) and ν(P-N) were in the wavelengths ranges 3050-3052, 1641-1474 and 891-835 cm^{-1}, respectively. The absorption bands for ν(P=S), ν(P=O) and ν(P=Se) were observed in the range 629-627, 1177-1263 and 555-542 cm^{-1}, respectively. The UV-Vis spectroscopy of the ligands showed that the two absorption bands in the range ~230-318 nm which are slightly red-shifted compared with *1,8*-diaminonaphthalene were due to the intraligand $L \rightarrow L^*$ transitions. Thermogravimetric analysis showed that ligand **(1)** undergo readily decomposition compared to ligands **(14)**-**(16)**. The DFT calculations showed that the HOMO and LUMO were located on the naphthalene rings. The correlation of the DFT and single crystal X-ray structures confirmed that the N atoms in **(15)** and **(16)** possesses a pyramidalization phenomenon, whereby the N-donor atoms undergo a deformation of a trigonal planar molecule into a tetrahedral arrangement which make the whole ligand structure chiral. The ligands have a (*R, R*) conformation around the N-atoms. The antimicrobial activity of the ligands *in-vitro* were very poor and only ligand **(2)** produced exceptional results.

The complexes **(3)**-**(6)** and **(10)**-**(11)** of the type $[M_2(\mu\text{-}X)_2\{C_{10}H_6(1,8\text{-}NHPR_2)_2\}_2]$, where M = Cu(I) and Ag(I), respectively, were synthesized from ligands **(1)**, except **(6)** which was

prepared form **(2)**. The halide counter ions were [X = Cl **(3)**, Br **(4)**, I **(5)**, Cl **(6)**, Cl **(10)**, Br **(11)** and I **(12)**]. The molecular formula of complex **(12)** consisted of iodide step bridged cubane of the type[$Ag_4(\mu_3\text{-}I)_2(\mu_2\text{-}I)_2\{C_{10}H_6(1,8\text{-}NHPPh_2)_2\}_2$]. Complexes **(7)** and **(13)** of the type [$M\{C_{10}H_6(1,8\text{-}NHPPh_2)_2\}_2$]$PF_6$, where M = Cu(I) and Ag(I), respectively, were prepared from ligand **(1)** and [$M(CH_3CN)_4$]PF_6 (M = Cu(I) or Ag(I)), respectively. Oxidation of ligand **(1)** to ligands **(14)** and **(15)** and further treating them with Ag(I) and Cu(I) salts produced complexes of the type [$M\{C_{10}H_6(1,8\text{-}NHPPh_2E)_2\}_2$]X. Ligand **(14)** produced complexes of **(19)**-**(22)** and ligand **(15)** produced complexes of **(17)** and **(18)**. The isolation of these complexes was enabled by covalently linking kinetically labile P-N bonds from the bis(amino)phosphine ligands. The complexes gave moderate to good yields (20-45%). The complexes were characterized spectroscopically by NMR, IR, MS and microanalysis technique. The ^{31}P NMR spectra for complexes **(3)**-**(6)** were singlet peaks in solution confirming that the P-donor atoms of the complexes were chemically equivalent and the ^{31}P NMR spectra for complexes **(10)**-**(11)** were doublet of doublets. The naturally occurring isotopes of silver (^{107}Ag, 51.82% and ^{109}Ag, 48.18%) both have a nuclear spin I = ½ and although their magnetogyric ratios are similar in magnitude (~10^7 rad $T^{-1}s^{-1}$) {$\gamma(^{109}Ag)/\gamma(^{107}Ag)$ = 1.15} the scalar coupling is proportional to the gyromagnetic ratio of the nuclei and the number for ^{109}Ag and ^{107}Ag is *different*. The ^{31}P NMR spectra for complexes **(7)** and **(13)** consisted of singlet peaks which resonated in the different chemical environment and the PF_6 ions which appeared in the same chemical environment for both complexes. Complexes **(17)**, **(19)**-**(22)** showed a singlet peak for their ^{31}P NMR spectrum, respectively. The ^{31}P NMR spectrum of complex **(18)** showed two peaks of the P-donor atoms which suggested that these were not chemically equivalent in solution. The IR spectra showed that the absorption bands for ν(NH), ν(C=C) and ν(P-N) for all complexes where in the range 3057-3371, 1645-1413, and 817-872 cm^{-1}, respectively. The absorption bands for ν(P=S), ν(P=O), ν(Ag-S), ν(Ag-O), ν(Cu-O), ν(Cu-P) and (Ag-P) for complexes were observed in the range 687-598, 691-690, 514-500, 540-518, 519-410, 515-473 and 543-522 cm^{-1}, respectively. The MS and microanalysis confirmed the bulk purity of the complexes. Complexes **(8)** and **(9)** of the type [$Cu_4(\mu_3\text{-}X)_2(\mu_2\text{-}X)_2(O\{PR_2\}_2)_2$] were synthesized from complex **(6)** and an iodide analogue of **(6)** 68.6 and 82.5%, respectively. Complexes **(3)**-**(6)**, **(8)**-**(9)**, **(10)**-**(12)** and **(17)**-**(18)** were isolated and characterized, by single crystal X-ray crystallography. The single crystal X-ray structures of **(3)**-**(6)**, **(10)**-**(12)** and **(17)** contains a rhombus {$M_2(\mu\text{-}X)_2$} core units bridged by halogens and chelated by two bis(amino)phosphine ligands which coordinated *via* the P-donor atoms, except for complex **(17)** where the Ag(I) metal centers were bridged by S-donor atoms

of the ligands. The metal centers coordinated the ligands in a tetrahedral geometry. Complex **(17)** was coordinated to four S-donor atoms forming a Ag(I) complex balanced by a triflate counter ion. The single crystal X-ray structures showed that the bis(amino)phosphine ligands contained P- and N- donor atoms and the metal center where bonded *via* the P-donor atoms. The UV-Vis spectra of complexes suggested that the π-π* transition which arises were due to the naphthalene moiety in the complexes. The thermogravimetric analysis showed that the complexes were stable at room temperature and steadily decomposed in a range ~150-350°C and finally reached their residual peaks in a temperature range ~480 - ~600°C. The complexes showed a wide range of antimicrobial activity against Gram-positive and a limited range for Gram-negative bacteria.

Furthermore, the thesis reported perimidine compounds which were isolated and characterized by single crystal X-ray crystallography and other spectroscopic analysis such as NMR, IR and MS. Perimidine compounds of the formula $[C_{10}H_6(1,8\text{-}NH)_2(CH_3)\{(CH_2)_2CH_3\}]$ $[C_{10}H_6(1,8\text{-}NH)_2(CH_2CH_3)_2]$, $[C_{10}H_6(1,8\text{-}NH)_2(CH_3)(CH_2CH_3)]$, $[C_{10}H_6(1,8\text{-}NH)_2(CH_3)\{CH(CH_3)_2\}]$, $[C_{10}H_6(1,8\text{-}NH)_2(CH_3)\{(CH_2)_4CH_3\}]$, $[C_{10}H_6(1,8\text{-}NH)_2(CH_3)\{CH_2CH(CH_3)_2\}_2]$, $[C_{10}H_6(1,8\text{-}NH)_2{\cdot}Fe(C_5H_4)_2\{COCH_3\}_2]$, and $[C_{10}H_6(1,8\text{-}NH)_2(CH_3)(C_5H_4N)]$, **(23)-(30),** respectively were prepared by condensation reaction of *1,8*-diaminonaphthalene and the corresponding liquid alkyl and aryl ketones. The percentage yields were good (85-99%). The ^{1}H NMR spectra of compounds showed that the proton peaks of the naphthalene were shifted downfield while the methyl protons of the compounds were shifted further upfield. The IR spectra of compounds showed that the ν(NH) and ν(C=C) absorption bands occurred in the range 3388-3295 and 1702-1406 cm^{-1}, respectively. Compound **(25)** and **(26)** were characterized by a single crystal X-ray crystallography. The molecules crystalized in a space group groups tetragonal ($P\text{-}42_1c$) and monoclinic (Pn), respectively. The UV-Vis spectra showed that the σ-electron rich six membered heterocyclic perimidine ring resulted in n···π*transitions and the molecular spectra also showed that the compounds contained unsaturated naphthalene moieties with shoulders due to ligand centered (LC) π···π*transitions. Thermogravimetric analysis showed that the compounds decomposed at ~310°C. The compound showed a wide range of antimicrobial activity against Gram-positive and a very poor range for Gram-negative bacteria.

Isolated of compound **(30)** led to the synthesis of complexes $[Ni(H_2O)_2\{C_{10}H_6(1,8\text{-}NH)_2(CH_3)(C_5H_4N)\}_2]2Cl$, **(31)** which was isolated in 88.6% yield. Complexes

$[ZnCl_2\{C_{10}H_6(1,8\text{-}NH)_2(CH_3)(C_5H_4N)\}_2]$ and $[CdI_2\{C_{10}H_6(1,8\text{-}NH)_2(CH_3)(C_5C_4N)\}_2]$, **(32)** and **(33)** were prepared similar to **(31)** from **(30)** using $Zn(II)Cl_2$ and $Cd(II)I_2$, respectively, in good yields, i.e. 89.95% **(32)** and 71.91% **(33)**. The ^1H NMR for complex **(31)** was paramagnetic whereas, complexes **(32)-(33)** spectra were well integrated. The imported IR vibration bands were indicated by the ν(M-N) at 401-424 cm^{-1}. Compound **(29)** was an attempt to synthesis a ferrocenyl perimidine compound by treating *1,8*-diaminonaphthalene with 1,1′-diacetylferrocene, but instead a co-crystallization of the two starting compounds formed. DFT, to extract the information about the electron density which have an influence on the molecular orbital frontiers of the complexes. It was found that the HOMO and LUMO are localized around the naphthalene and that there is no electronic communication between the metals and the naphthalenes. The complexes showed a promising result of antimicrobial activity against Gram-positive and a very poor result for Gram-negative bacteria.

6.1.2 Future Perspectives

Bis(amino)phosphine ligands can be functionalized further *via* the amine groups by either reacting the ligands with chloro-alkyl/ aryl groups in the presence of a base or by condensation reactions. The resulting products can be treated with metal centers to form new complexes *via* the P-donor atoms.

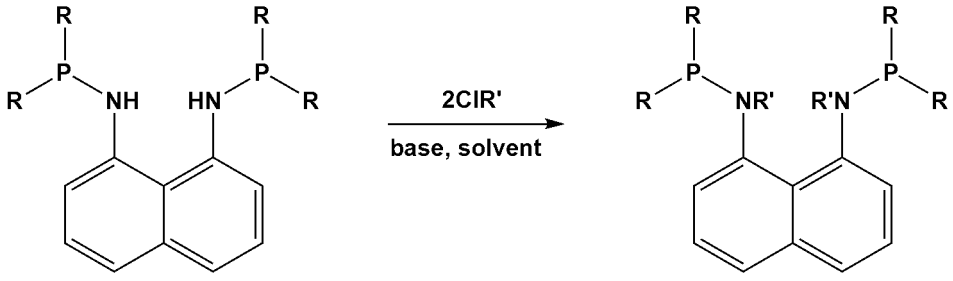

Scheme 6.1.2.1. Functionalization of $[C_{10}H_6(1,8\text{-}NHPR_2)_2]$ ligands.

The Cu(I) and Ag(I) complexes of the type $[M_2(\mu\text{-}X)_2\{C_{10}H_6(1,8\text{-}NHPR_2)_2\}_2]$, $[M\{C_{10}H_6(1,8\text{-}NHPPh_2)_2\}_2]PF_6$ and $[M\{C_{10}H_6(1,8\text{-}NHPPh_2E)_2\}_2]X$ contains amine functional groups which can be deprotonation to further react with metal center.

The Cu(I) complexes of the type $[M_2(\mu\text{-}X)_2\{C_{10}H_6(1,8\text{-}NHPR_2)_2\}_2]$ can undergo oxidative addition reaction, provided that the reaction of the complexes with Br_2 or I_2 or $Ph{\cdot}Cl_2$ oxidize Cu(I) to Cu(II) metal center in the process of forming a macrocyclic complex.

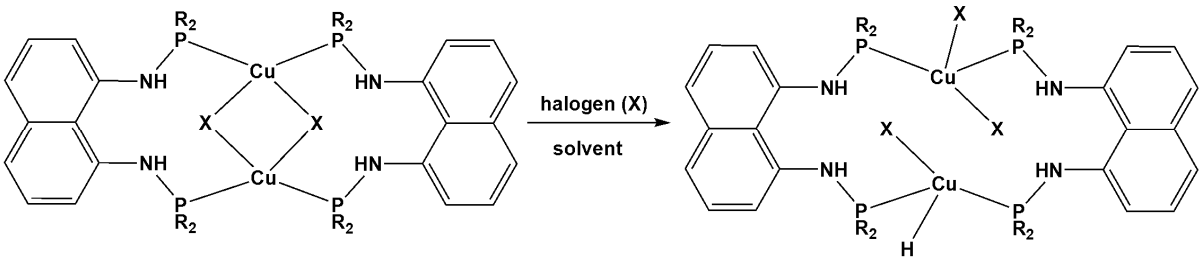

Scheme 6.1.2.2. Formation of macrocyclic complex from $[M_2(\mu\text{-}X)_2\{C_{10}H_6(1,8\text{-}NHPR_2)_2\}_2]$.

The ^{31}P NMR spectra of Ag(I) complexes of the type $[M_2(\mu\text{-}X)_2\{C_{10}H_6(1,8\text{-}NHPR_2)_2\}_2]$ gave a doublet of doublets at room temperature. Alteration of ^{31}P NMR temperature will determine whether the peaks can adjust to the configurations of the Ag nuclei presented in Figure 6.1.2.1.

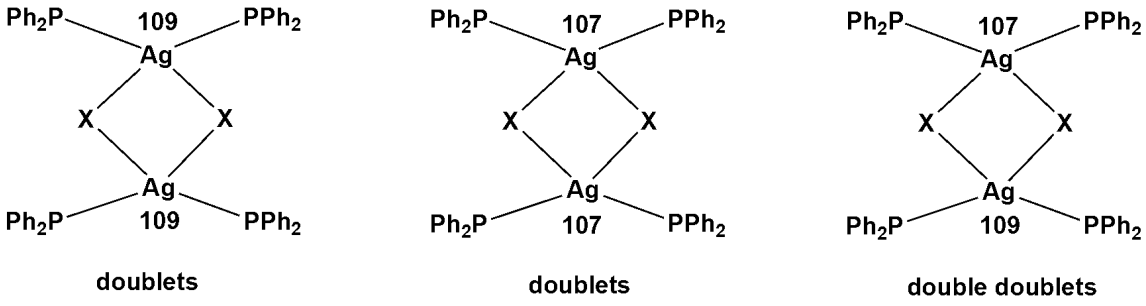

Figure 6.1.2.1. ^{31}P NMR configuration for complexes $[Ag_2(\mu\text{-}X)_2\{C_{10}H_6(1,8\text{-}NHPR_2)_2\}_2]$.

The mechanism which produced complexes **(8)** and **(9)** need to be well established. The reaction is reproducible, but it is not clear which path the products took form.

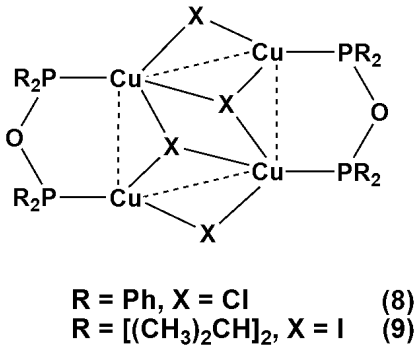

Figure 6.1.2.2. P-O-P copper complexes

It will be interesting to synthesis the P-O-P ligands and react them with different M(I) halide salts to examine the end product, i.e. whether the same or different products will form.

Complexes of perimadines that contains *1,8*-diaminonaphthalene backbone are scares in literature and therefore the preparation of perimidine compounds similar to those reported herein might give a chance for better development of chemistry for such complexes. The two amines in such perimidine compounds could be functionalized with substituents that contains donor atoms which can easily coordinate metal centers.

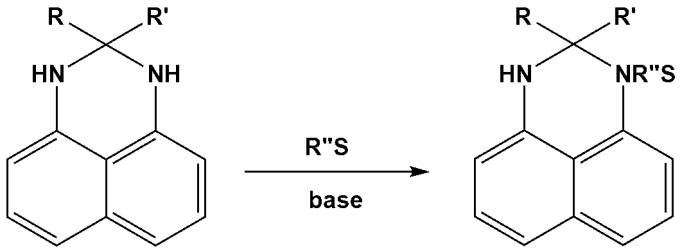

Figure 6.1.2.3. Possible functionalized perimidine ligands with donor atoms.

Complex **(31)** reported herein contains pyridinyl substituent and by extending the alkyl chain length between the σ-electron-rich, six-membered heterocyclic ring and the pyridinyl substituent could provide better flexibility for chelation.

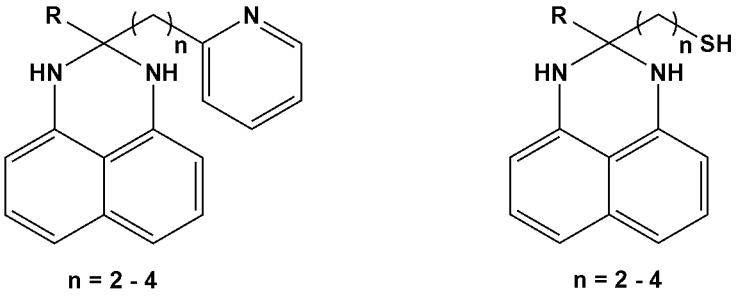

Figure 6.1.2.4. Examples of potential perimidine ligands containing donor atoms.

The examples above shows that there is room for improvement in this field of chemistry. The development could come from the synthesis part or applications of the compounds. The compounds showed impressive quorum sensing results which is an on-going progress.

Attachments on the disk contains supporting information of the thesis.